Development of Novel Thin Membrane Electrode Assemblies (MEAs) for High-Efficiency Energy Storage

A Dissertation Presented for the

Doctor of Philosophy

Degree

The University of Tennessee, Knoxville

Zhenye Kang

May 2018

Copyright © 2018 by Zhenye Kang.

All rights reserved.

ACKNOWLEDGEMENTS

I would like to express my most sincere gratitude to my academic advisor, Dr. Feng-Yuan Zhang for his support, patience and guidance throughout my entire doctoral study. I would like to thank Dr. Matthew M. Mench, Dr. Zhili Zhang and Dr. Lloyd M. Davis for serving on my committee and giving me valuable advice towards my research.

I would also like to thank the NanoHELP group - Dr. Jingke Mo, Dr. Bo Han, Gaoqiang Yang, Yifan Li, Shule Yu, Dr. Qiang Yang, Derrick A Talley, Yeshi Dohrmann, Stuart M. Steen III, William Barnhill, - it has been my privilege working amongst you. I'd also like to thank Dr. Lei Shi, Dr. Zhongren Yue, Rong Chen, Douglas Warnberg, Alexander Terekhov, Kathleen Lansford, Dr. Lee Leonard, Dr. Lino Costa, and Natallia Kaptur, for their countless help on my research.

I also want to express my appreciation to Dr. Scott T. Retterer, Dr. David A. Cullen, Dr. Todd J. Toops, Dr. Michael P. Brady, Dr. Ryan R. Dehoff, Dr. William H. Peter, Dayrl Briggs, Dale Hensley, Kevin C. Lester, Dr. Bernadeta R. Srijanto from ORNL, and Dr. Johney B. Green Jr., Dr. Guido Bender, Dr. Bryan S. Pivovar from NREL for the guidance, advice and help for my research.

My friends and family have been extremely helpful throughout my doctoral work. Finally, I wish to thank my parents, Wenlong Kang and Shuli Han, and my wife Jing Lian for their unconditional love and support, and their belief in me to succeed. I also thank my lovely daughter Katherine Xiyue Kang, who has made my life full of happiness and love. They all always support me to pursue my dreams.

I also greatly appreciate the support from U.S. Department of Energy's National Energy Technology Laboratory under Award DE-FE0011585, and National Renewable Energy Laboratory under Award DE-AC36-08GO28308.

ABSTRACT

Hydrogen is a ‘zero-emission’ energy carrier, which could be an important part of environment-friendly solutions to the global energy crisis via energy storage without producing greenhouse gases. The proton exchange membrane electrolyzer cell (PEMEC) is one of the most practical and energy efficient methods for producing high purity hydrogen from renewable sources, such as wind, hydro and solar energy. Since the wide commercialization of PEMECs is still hindered by their performance, cost and durability, superior performance PEMECs with low-cost and high-efficiency are strongly desired. The membrane electrode assembly (MEA), which consists of liquid/gas diffusion layers (LGDLs), catalyst layers (CLs) and membrane, is the core component of the PEMECs. LGDLs play an important role in enhancing the performance of PEMECs. They are expected to transport electrons, heat, and reactants/products simultaneously with minimum electrical, thermal, interfacial, and fluidic losses. CLs are mainly formed by noble metals or their oxides, which has great impact on PEMEC performance, durability and cost. The objective of this research is to develop novel MEAs coupled with the titanium-based thin/tunable LGDLs (TT-LGDLs) that has the well-controlled pore morphologies. The main achievements of this research include: (a) The TT-LGDLs can achieve superior performance due to the remarkably reduced ohmic and activation losses, and the effects of pore morphologies have been identified. (b) The gold electroplating is a promising method for the PEMEC performance enhancement by surface modifications. (c) The microporous layers (MPLs) offer some improved PEMEC performance under specific conditions, but

may not be required for optimum TT-LGDLs. (d) The novel GDEs with ultra-low Pt catalyst loadings have been developed, which has obtained an acceptable performance with a significantly improved catalyst mass activity. (e) The theoretical analysis is adopted to study the true electrochemical reaction mechanism in PEMECs, and a model is developed, which is used to simulate the PEMEC performance and optimize the parameters of the electrodes. The novel thin MEAs developed in this research point out a promising direction for future MEA development, and can be a guide for the high-efficiency and large scale energy storage.

TABLE OF CONTENTS

LIST OF TABLES

LIST OF FIGURES

CHAPTER I

INTRODUCTION

1.1 Overview

Renewable energy sources, including solar, wind, hydro, biomass and geothermal power, produce electricity in sustainable ways, while most of these renewable sources are variable and often produce electricity intermittently (e.g., only when the sun is up or the wind is blowing), which presents a major challenge to delivering consistent power to grid. In addition, the current electrical grid has limited ability to digest the fluctuation from renewable energy sources. Therefore, a sustainable, high-efficiency, and robust electrochemical energy storage/conversion or a hybrid system to accommodate daily or even hourly changes of energy demand becomes more critical [1-6].

Hydrogen is a 'zero-emission' energy carrier which could be an important part of environmentally friendly solutions to the global energy crisis via combustion or transformation into electricity through fuel cells without producing any greenhouse gases and pollutants. However, hydrogen is not an energy source, and it doesn't exist in nature in elemental or molecular form. Therefore, hydrogen must be produced or generated. An advanced proton exchange membrane electrolyzer cell (PEMEC), which is a reverse PEM fuel cell (PEMFC), has been considered as an very attractive energy storage method by producing hydrogen/oxygen from water splitting as shown in Equation 1 [7], especially when it is coupled with renewable energy sources, because it has several advantages, such

as distinguished efficiency, high purity products, compact design, large capacity, quick response, and low maintenance activities. It effectively connects renewable electricity supply and multiscale energy demand, including stationary, transportation, and portable applications [8-12]. When renewable energy resources are available, it can be stored in hydrogen through PEMECs. Later, hydrogen can be converted back to water and electricity with a PEMFC, when more energy demand, as shown in Figure 1. Additionally, surplus electricity in electric grids during off-peak periods can also be stored via the PEMEC. This entire portfolio will make hybrid energy systems able to provide renewable and reliable energy at different scales whenever/wherever needed. More importantly, its key features of high efficiency, large capacity, quick startup, hazard free and low maintenance make PEMECs coupled with renewable energy source more attractive [13-16].

$$\boldsymbol{H_2O + 237.2\frac{kJ}{mol}(Electricity) + 48.6\frac{kJ}{mol}(Heat) \xrightarrow{Catalysts} H_2 + \frac{1}{2}O_2} \quad \textbf{Equation 1}$$

But, the wide commercialization of PEM electrolyzer cells is still hindered by their performance, cost and durability. For the performance assessment, the polarization curves are widely used, which is one of the most important parameter for PEMEC. Superior performance of water splitting in PEMECs with low cost and high efficiency are strongly desired for hydrogen production. Membrane electrode assembly (MEA), which consists of liquid/gas diffusion layers (LGDLs), catalyst layers (CLs) and membrane, is the core component of the PEMECs. It can significantly affect the cost, performance and efficiency of the PEMECs. Therefore, this research is to develop a kind novel thin MEAs with high efficiency and low cost.

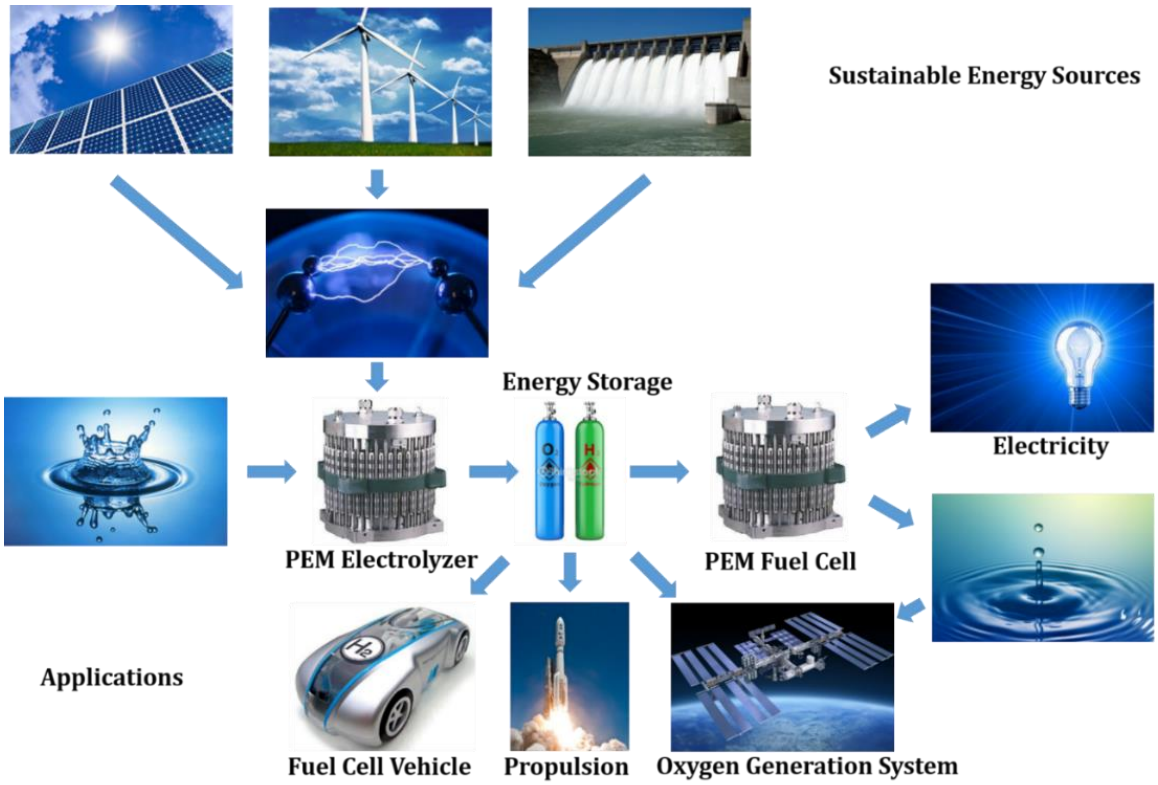

Figure 1. Schematic of applications of PEMECs and PEM fuel cells coupled with sustainable energy sources.

1.2 Background

A PEM electrolyzer cell mainly consists of a catalyst-coated membrane (CCM) sandwiched by anode and cathode electrodes, as shown in Figure 2. Each electrode includes a catalyst layer (CL), a liquid/gas diffusion layer (LGDL), and a bipolar plate (BP), which also acts as the current distributor (CD) and the flow field. After electricity is applied, water is split into molecular oxygen, protons, and electrons at the anode side, as shown in Figure 2.

Di-oxygen, as one product on the anode CLs, is ideally transported from the CL through the LGDL back to the flow field to avoid blocking the LGDL, which can hinder the reaction. Electrons, which are also generated at anode CLs, pass through the LGDL, anode BP, and external circuit. Meanwhile, protons diffuse through the membrane to the cathode and react with electrons which come from the external circuit to form di-hydrogen. H_2/O_2 will be produced and stored continuously as long as water and electricity are supplied. Thus, not only should the water be supplied continuously, but also the oxygen and hydrogen should be effectively removed through the LGDLs.

The anode of PEMECs resides in a harsh environment, which is highly corrosive due to the high overpotential, oxygen enrichment and high humidity. The LGDLs, which are located between the CL and BP, play an important role in enhancing the performance of water splitting in PEMECs. They are expected to transport electrons, heat, and reactants/products simultaneously with minimum voltage, current, thermal, interfacial, and fluidic losses.

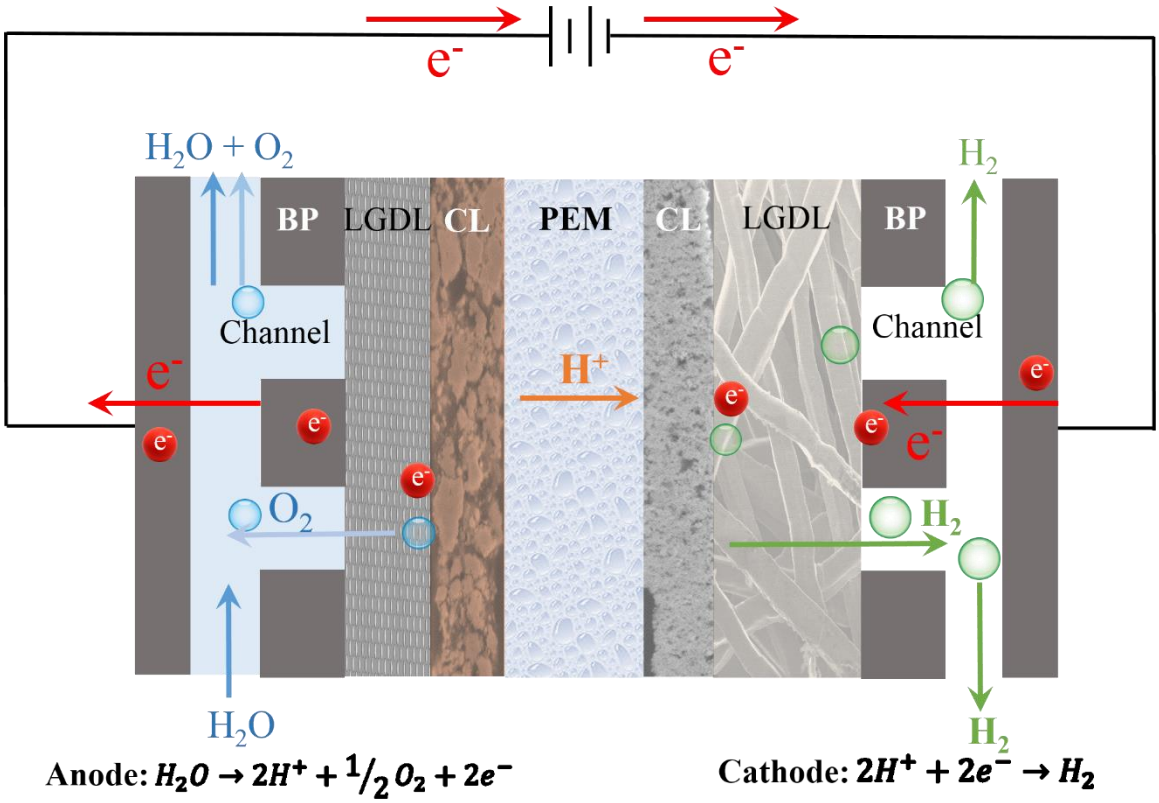

Figure 2. Schematic of the general working process of a PEMEC at cross-section view.

Carbon materials (like carbon paper or carbon cloth), which are typically used in PEMFCs, are unsuitable on this side of the PEMECs due to the high potential of the oxygen electrode [17-24]. Ideal anode LGDLs should have good conductivity, high corrosion resistance, good two-phase transport capability and mechanical strength. Metallic LGDLs and bipolar plates, including titanium, have attracted more interest in both PEMECs and PEMFCs due to their high conductivity, rapid production, and low cost [25-29].

Grigoriev et al. conducted an optimization of porous current collectors. The optimum porosity and mean pore size value were investigated of porous titanium plates formed by thermal sintering of spherically particles. According to his research, the mean pore size of the particles and the thickness of the titanium plates have a significant effect on current-voltage performances. They pointed out that the optimum spherical particle sizes are 50 - 75 µm and the optimum pore size value is 12 - 13 µm. Whereas, the porosity (between 0.35 - 0.40) and gas permeability of the porous titanium plates don't have a significant influence on electrolysis efficiency [30]. Millet et al. noted that it is necessary to reduce the ohmic resistance between the separator plates and current collectors in order to improve the performance of the PEMECs, which can be achieved by smoothing the contact between different components [31]. Ma et al. investigated some factors including LGDL's thickness iridium catalyst loading, membrane thickness and operating temperature, which may have an effect on the performance of water electrolyzer. They concluded that a thinner carbon paper used as anode LGDL will improve the PEMEC performance due to its better gas diffusion property and smaller resistance [32].

Oh et al. introduced a pore size gradient structure inside LGDL in order to improve the performance of a PEMFC which takes the reverse process of a PEMEC. They concluded that the pore size gradient structure can enhance the steady-state and transient response of a PEMFC [33]. Lettenmeier et al. have also developed a novel pore-graded LGDLs for PEMECs via the vacuum plasma spraying method. The pore radius in the layers of the GDL close to the BP is about 10 μm, while those in contact with the CL are just in the range of 5 μm. The pore-graded LGDLs achieved PEMEC performances comparable to those of the state-of-the-art sintered plates and far superior than those of meshes. [34]. Hwang et al. made MPL by loading titanium powder over titanium felt for PEMECs to promote interfacial contacts [35]. And they also investigated titanium felt LGDL of the anode electrode. The effect of pore properties and PTFE content for titanium felt LGDL on performance were examined [36]. Ito et al. carried out PEMEC experiment focusing on the porosity and pore diameter of titanium felt current collectors. Their results showed that the electrolysis performance can be improved with decreasing the MPD of the porous current collector when the MPD was larger than 10 μm. And they also pointed out that the porosity had insignificant effect on the electrolysis performance if the porosity was larger than 0.5 [37]. In another study, the influence of porosity and pore diameter of current collectors on PEMEC performance was also conducted. The results showed that the oxygen bubble produced at anode may block the LGDL when the MPD is less than 50 μm [38]. Borgardt et al. have investigated the mechanical characterization and durability of sintered porous LGDLs in PEMECs. They fabricated the titanium based LGDLs from tape casting

method and analyzed its mechanical stability *ex-situ* via tensile tests and *in-situ* in a PEMECs with a differential pressure of 50 bar. They concluded that the flow field width should be limited to 3 mm in order for a LGDL with a thickness of 500 μm and porosity above 25% to be able to withstand 50 bar pressure difference in a cell [39]. Mo et al. have studied the effect of parameters of titanium felt LGDLs in a PEMEC, and they found that the thickness of LGDLs have a large impact on the EPMEC performance [40].

The main efforts in the previous studies so far have focused on investigating conventional titanium LGDLs, including felts, woven meshes, or foams. Their thicknesses are larger than 0.3 mm with significant electrical conductive path and fluidic resistance. In addition, their fiber/foam-based pore morphologies result in large interfacial contact resistance. More importantly, random and complicated structures in conventional titanium LGDLs make it impossible to control the liquid/gas/electron/thermal distribution. Novel structures of LGDLs for good interfacial contact and well controllable pore morphologies are expected.

Titanium based LGDLs are widely used as anode LGDL due to their good bulk conductivity, high corrosion resistivity, and excellent mechanical strength. The conventional Ti based LGDLs, including Ti felt, Ti mesh, and sintered Ti powers, have been widely used and investigated in PEMECs [24, 35, 37, 38, 41, 42]. However, resistance to corrosion in such systems is achieved by surface oxide formation, which can increase surface electrical resistivity and detrimentally impact cell performance [43].

Hwang *et al*. tested titanium felt by loading titanium powder or polytetrafluoroethylene (PTFE) in the PEMECs. They investigated the effects of pore properties and PTFE content on the PEMEC performance [36]. Ioroi *et al*. investigated the wettability of the titanium mesh by loading TiO_2 powder and PTFE. They concluded that the LGDL with hydrophilic property showed better performance than the hydrophobic one [44]. Mo *et al*. have also studied the effect of parameters of Ti felt and Ti mesh LGDLs in a PEMEC. They also conducted surface treatments such as thermal nitridation and sputter coating, which can improve the PEMEC performance significantly [40]. Omrani et al. have reviewed the GDL modifications and treatments for improving the performance of PEMECs and PEMFCs. They said that the main focus of the modifications was on water management and reactant delivery improvement. The typical modifications include the hydrophobisation, structural modification and micro porous layer (MPL) [45]. It has been found that an optimum amount of coating on GDLs, such as polytetrafluoroethylene (PTFE), or fluorinated ethylene propylene (FEP), can improve the water management, but this methods are mainly contributed to PEMFC performance enhancement. [46-51] For the structural modification of GDLs, thin metal GDLs, GDL with groove and perforation, and porosity graded GDLs were mostly widely used [45]. Some researchers have investigated the effects of GDL perforation, and forming a water removal path by some advanced methods, such as electric discharge machining, laser perforation, or micro drilling [52-55]. But very few studies have been worked on the effect of using perforated thin metal sheets as GDLs in both PEMFCs and PEMECs [16, 25, 56-60].

Previous efforts have investigated different kinds of titanium based LGDLs, and modification methods to improve their performance. We have developed the TT-LGDLs with straight-through pores that was fabricated using advanced micro/nano manufacturing techniques [25, 61, 62]. By using the surface modifications or treatments, the interfacial contact resistance of the TT-LGDLs is expected to be reduced, and it is also anticipated that the performance can be improved further [63]. In addition, Based on our previous discoveries, the oxygen evolution reaction (OER) sites can be identified by the formation of oxygen bubble nucleation sites, which only occur at the rim of the TT-LGDL pores due to the large in-plane electrical resistance of the CL and the difficult two-phase transport under the TT-LGDL land area [16, 64]. Therefore, it seems that large amounts of catalyst located in the middle of the pore area and under the TT-LGDL land area is inactive or underutilized to some extent. By introducing the MPLs between the CLs and TT-LGDLs, it is anticipated that more OER sites will be accessible and the PEMEC performance can be improved compared with TT-LGDLs without a MPL.

It is well known that the noble metal or their oxides are required for water splitting and hydrogen generation by PEMECs, but its drawback is the high cost of the platinum-group metals (PGM) as electrocatalysts. [65, 66]. It is due to the harsh environment in PEMECs, where there is an acidic environment and only PGM can withstand especially under high operating voltages. Water can be split into oxygen and hydrogen through the electrochemical reactions under the catalytic effect at low temperature with catalysts which are typical IrRuOx at anode and PtB at cathode in PEMECs. The high cost of catalysts is

not a big problem in PEMECs at small scale, but it can increase greatly when the PEMECs are applied to industrial usage which has huge hydrogen producing rate [67]. So how to decrease the cost of catalysts in PEMECs is a critical problem before its wide commercialization.

Typical and conventional methods of manufacturing membrane electrode assemblies for PEMECs including painting, spraying, or printing of catalyst inks, which contain a content of electrolyte like Nafion solution or carbon supported catalysts, onto the Nafion membrane. Many new fabrication techniques have been used to produce extremely low catalyst loading electrodes, such as sputter deposition, reactive spray deposition techniques (RSDT), core-shell catalyst structure fabrication, platinum nano cages, etc.[68-70]. The polyol method has been considered as an easy method to fabricate nano sized Ir or Ru colloids [71]. The Adams fusion method is also an attracting way to prepare fine metal oxides powders for electrocatalysts [72]. Sputter deposition with its advantages of low cost and easily operation, has been investigated to fabricate electrodes in different type of fuel cells, and many of which could have an improved performance and catalyst utilization compared to conventional CCM.

Andrew T. Haug and O'Hayre et al. have found that catalysts deposited directly on the membrane didn't exhibit better performance than deposited on gas diffusion layers (GDLs) [70, 73]. Sputter depositing a single layer of platinum on the GDL provided better performance (0.28 A/cm^2 at 0.6 V) than sputtering the platinum directly onto a Nafion membrane (0.065 A/cm^2 at 0.6 V). Shen-Yu Fang et al. have used SEM to examine the

coated titanium on GDL. They have investigated the performance of the PEMFCs with titanium coated GDLs as anode at different operating temperatures of 25^0C, 45^0C and 65^0C. The results showed that the MEAs with titanium coated GDLs were superior to that of the MEAs without titanium coating [74].

Theoretical analysis and PEMEC modeling is one of the promising methods to optimize PEMEC designs and operating conditions due to its precisely predicting results, time saving, and low cost. In the past years, lots of experimental studies have been conducted to investigate PEM electrolyzer cell performance under different conditions, but there are only a few papers regarding PEM electrolyzer cell modeling [43, 75-78]. Choi et al. introduced a simple mathematical model of solid polymer electrolyte water electrolysis. In the model, the cell voltage was calculated by the sum of open circuit voltage, electrode overpotential, ohmic overpotential due to the membrane and interfacial resistances [79]. Gorgun introduced the first dynamic model of PEM electrolyzer cells. This model included water transport phenomenon through the membrane due to electro-osmotic drag and diffusion [80]. Lebbal et al. conducted a dynamical model including a steady state electrical model and a dynamic thermal model to monitor the PEM electrolysis safety and efficiency. In the model, the total relationship of voltage and current density was expressed as four parts: open circuit voltage, activation overpotential, diffusion overpotential and ohmic overpotential. The diffusion overpotential was related to the values of current due to the effects of gas and water transport and the ohmic loss was given by an empirical relation [81]. Grigoriev et al. developed mathematical models in order to evaluate the

electrochemical performance of atmosphere and high pressure (up to 130 bars) PEM electrolyzer cells. To evaluate and optimize electrolyzer efficiency and performance, different operating conditions including pressure, temperature, current density, membrane thickness are discussed [30, 82]. Marangio et al. also conducted a detailed theoretical model to analyze characteristics of a high pressure PEM electrolyzer cell. In their model, the Gibbs free energy was used to calculate the open circuit voltage under non-standard temperature and pressure conditions [83]. Water flow inside the electrolyzer cell included several parts: water inlet and outlet flow in the anode and cathode, water transport due to concentration difference, water transport due to the electroosmotic drag, water transport due to pressure difference across the membrane, and water consumed by the electrochemical reaction. The ohmic resistance was calculated by the sum of electrodes, plates, membrane resistance and interfacial contact resistance between them. A series of modeling polarization curves of PEM electrolyzer cells was obtained and then compared with the experimental results. Our group has also established a model which fully consider the effects of various operating conditions and design parameters on the cell performance based on the porous LGDLs. Based on the above reviews, since existing models did not fully consider the effects of various operating conditions and design parameters on the cell performance, a comprehensive model for better correlating the effects of both design parameters and operating conditions with PEM electrolyzer cell performance is strongly desired.

1.3 Objectives

The objective of this research is to develop novel thin MEAs coupled with the titanium based novel thin/well-tunable LGDLs (TT-LGDLs) for electrolyzer cells with the help of micro/nano technology, thermal fluid science, and novel materials. The main tasks include: (a) The experimental investigation of TT-LGDLs, including study the effects of pore size, porosity, pore shape, and temperature etc.; (b) The performance enhancement with surface modified TT-LGDLs by both direct surface modifications and indirectly MPLs; (c) The development and investigation of novel thin gas diffusion electrodes; (d) The theoretical analysis to study the true electrochemical reaction mechanism in PEMECs, and to establish a model to simulate the performance, current distribution and optimize the parameters of electrodes.

The novel TT-LGDLs have the advantages of low weight and thickness, well-controllable pore morphologies such as pore shape, pore size, pore distribution, and therefore porosity and permeability. Successful development of a TT-LGDL, which is more reliable and reusable, will reduce the cost, thickness, and weight of the LGDL itself and the system as a whole. Therefore, this study will comprehensively investigate the effects of the TT-LGDL parameters. A high-speed and micro-scale visualization systems (HMVS) will be used to reveal the true electrochemical reaction (HER and OER) mechanism in PEMECs, which helps to investigate the effects of the TT-LGDLs and catalysts.

For PEMEC performance enhancement, the direct surface modification methods, such as sputter deposition and electroplating, will be used. In addition, indirect method that is the

addition of MPLs, will also be adopted. The effects of MPL particle size and thickness will be investigated *in-situ* and *ex-situ* comprehensively, and their effects will be visualized and investigated by the HMVS.

Based on the previous discoveries, a novel thin and tunable GDE with a catalyst layer thickness of tens of nano meters and a total thickness of about 25 μm has been proposed and developed. By using sputter deposition, the novel thin GDEs with ultra-low catalysts loading can be achieved without losing good performance. The activities of catalysts are analyzed comprehensively by HMVS, and the novel thin GDEs can significantly improve the electrocatalysts mass activity in PEMEC.

A comprehensive computational model for the PEMECs with TT-LGDLs at anode side will be established, and MATLAB/Simulink is adopted to develop this novel model. A new ohmic loss submodel for PEMECs, including the interfacial contact resistances between the CLs and TT-LGDLs, has been proposed. Furthermore, the roughness factor in the Butler-Volmer equation, which is used to calculate the activation overpotential, can greatly influence the PEMEC performance by pore morphology of the TT-LGDLs, and its relation has been embedded in the comprehensive computational model. The influence of the operating conditions and TT-LGDL pore diameter and porosity on PEMEC performance can be investigated precisely. More importantly, a novel two-dimensional (2D) CL resistance model, which consists of both in-plane and through-plane resistance models, is also developed to predict the current distribution on the CLs.

References

[1] Turner JA. A realizable renewable energy future. *Science*. 1999;285:687-9.

[2] Turner JA. Sustainable hydrogen production. *Science*. 2004;305:972-4.

[3] Rausch B, Symes MD, Chisholm G, Cronin L. Decoupled catalytic hydrogen evolution from a molecular metal oxide redox mediator in water splitting. *Science*. 2014;345:1326-30.

[4] Isherwood W, Smith JR, Aceves SM, Berry G, Clark W, Johnson R, Das D, Goering D, Seifert R. Remote power systems with advanced storage technologies for Alaskan villages. *Energy*. 2000;25:1005-20.

[5] Chen X, Li C, Grätzel M, Kostecki R, Mao SS. Nanomaterials for renewable energy production and storage. *Chem Soc Rev*. 2012;41:7909-37.

[6] Ager JW, Shaner MR, Walczak KA, Sharp ID, Ardo S. Experimental demonstrations of spontaneous, solar-driven photoelectrochemical water splitting. *Energ Environ Sci*. 2015;8:2811-24.

[7] Mo J. Fundamental Studies of Electrochemical Reactions and Microfluidics in Proton Exchange Membrane Electrolyzer Cells. 2016.

[8] Debe M, Hendricks S, Vernstrom G, Meyers M, Brostrom M, Stephens M, Chan Q, Willey J, Hamden M, Mittelsteadt CK. Initial performance and durability of ultra-low loaded NSTF electrodes for PEM electrolyzers. *J Electrochem Soc*. 2012;159:K165-K76.

[9] Javadekar A, Jayakumar A, Gorte RJ, Vohs JM, Buttrey D. Energy storage in electrochemical cells with molten Sb electrodes. *J Electrochem Soc*. 2012;159:A386-A9.

[10] Shapiro D, Duffy J, Kimble M, Pien M. Solar-powered regenerative PEM electrolyzer/fuel cell system. *Sol Energy*. 2005;79:544-50.

[11] Ramasamy RP, Kumbur EC, Mench MM, Liu W, Moore D, Murthy M. Investigation of macro-and micro-porous layer interaction in polymer electrolyte fuel cells. *Int J Hydrogen Energ*. 2008;33:3351-67.

[12] Pekula N, Heller K, Chuang P, Turhan A, Mench M, Brenizer J, Ünlü K. Study of water distribution and transport in a polymer electrolyte fuel cell using neutron imaging. *Nuclear Instruments and Methods in Physics Research Section A: Accelerators, Spectrometers, Detectors and Associated Equipment*. 2005;542:134-41.

[13] Baxter J, Bian Z, Chen G, Danielson D, Dresselhaus MS, Fedorov AG, Fisher TS, Jones CW, Maginn E, Kortshagen U. Nanoscale design to enable the revolution in renewable energy. *Energ Environ Sci*. 2009;2:559-88.

[14] Gorensek MB, Forsberg CW. Relative economic incentives for hydrogen from nuclear, renewable, and fossil energy sources. *Int J Hydrogen Energ*. 2009;34:4237-42.

[15] Liu C-j, Burghaus U, Besenbacher F, Wang ZL. Preparation and characterization of nanomaterials for sustainable energy production. *Acs Nano*. 2010;4:5517-26.

[16] Kang Z, Mo J, Yang G, Retterer ST, Cullen DA, Toops TJ, Green Jr JB, Mench MM, Zhang F-Y. Investigation of thin/well-tunable liquid/gas diffusion layers exhibiting superior multifunctional performance in low-temperature electrolytic water splitting. *Energ Environ Sci*. 2017;10:166-75.

[17] Jung H-Y, Huang S-Y, Popov BN. High-durability titanium bipolar plate modified by electrochemical deposition of platinum for unitized regenerative fuel cell (URFC). *J Power Sources*. 2010;195:1950-6.

[18] Fall J, Humphreys D, Guo S. Design and testing of a unitized regenerative fuel cell. *J Fuel Cell Sci Tech*. 2009;6:031003.

[19] Chen G, Waraksa CC, Cho H, Macdonald DD, Mallouka TE. EIS Studies of Porous Oxygen Electrodes with Discrete Particles I. Impedance of Oxide Catalyst Supports. *J Electrochem Soc*. 2003;150:E423-E8.

[20] Bockris JOM. Hydrogen. *Materials*. 2011;4:2073-91.

[21] Nikiforov A, Petrushina I, Christensen E, Tomás-García A, Bjerrum N. Corrosion behaviour of construction materials for high temperature steam electrolysers. *Int J Hydrogen Energ*. 2011;36:111-9.

[22] Fuentes RE, Farell J, Weidner JW. Multimetallic electrocatalysts of Pt, Ru, and Ir supported on anatase and rutile TiO2 for oxygen evolution in an acid environment. *Electrochemical and Solid-State Letters*. 2011;14:E5-E7.

[23] Dihrab SS, Sopian K, Alghoul M, Sulaiman MY. Review of the membrane and bipolar plates materials for conventional and unitized regenerative fuel cells. *Renewable and Sustainable Energy Reviews*. 2009;13:1663-8.

[24] Mo J, Steen SM, Zhang F-Y, Toops TJ, Brady MP, Green JB. Electrochemical investigation of stainless steel corrosion in a proton exchange membrane electrolyzer cell. *Int J Hydrogen Energ*. 2015;40:12506-11.

[25] Zhang F-Y, Advani SG, Prasad AK. Performance of a metallic gas diffusion layer for PEM fuel cells. *J Power Sources*. 2008;176:293-8.

[26] Matsuura T, Kato M, Hori M. Study on metallic bipolar plate for proton exchange membrane fuel cell. *J Power Sources*. 2006;161:74-8.

[27] Arisetty S, Prasad AK, Advani SG. Metal foams as flow field and gas diffusion layer in direct methanol fuel cells. *J Power Sources*. 2007;165:49-57.

[28] Tawfik H, Hung Y, Mahajan D. Metal bipolar plates for PEM fuel cell—a review. *J Power Sources*. 2007;163:755-67.

[29] Wang H, Turner J. Reviewing metallic PEMFC bipolar plates. *Fuel Cells*. 2010;10:510-9.

[30] Grigoriev S, Millet P, Volobuev S, Fateev V. Optimization of porous current collectors for PEM water electrolysers. *Int J Hydrogen Energ*. 2009;34:4968-73.

[31] Millet P, Dragoe D, Grigoriev S, Fateev V, Etievant C. GenHyPEM: a research program on PEM water electrolysis supported by the European Commission. *Int J Hydrogen Energ*. 2009;34:4974-82.

[32] Ma L, Sui S, Zhai Y. Investigations on high performance proton exchange membrane water electrolyzer. *Int J Hydrogen Energ*. 2009;34:678-84.

[33] Oh H, Park J, Min K, Lee E, Jyoung J-Y. Effects of pore size gradient in the substrate of a gas diffusion layer on the performance of a proton exchange membrane fuel cell. *Appl Energ*. 2015;149:186-93.

[34] Lettenmeier P, Kolb S, Sata N, Fallisch A, Zielke L, Thiele S, Gago A-S, Friedrich K. Comprehensive investigation of novel pore-graded gas diffusion layers for high-performance and cost-effective proton exchange membrane electrolyzers. *Energ Environ Sci*. 2017;10:2521-33.

[35] Hwang CM, Ishida M, Ito H, Maeda T, Nakano A, Kato A, Yoshida T. Effect of titanium powder loading in gas diffusion layer of a polymer electrolyte unitized reversible fuel cell. *J Power Sources*. 2012;202:108-13.

[36] Hwang CM, Ishida M, Ito H, Maeda T, Nakano A, Hasegawa Y, Yokoi N, Kato A, Yoshida T. Influence of properties of gas diffusion layers on the performance of polymer electrolyte-based unitized reversible fuel cells. *Int J Hydrogen Energ*. 2011;36:1740-53.

[37] Ito H, Maeda T, Nakano A, Hwang CM, Ishida M, Kato A, Yoshida T. Experimental study on porous current collectors of PEM electrolyzers. *Int J Hydrogen Energ*. 2012;37:7418-28.

[38] Ito H, Maeda T, Nakano A, Kato A, Yoshida T. Influence of pore structural properties of current collectors on the performance of proton exchange membrane electrolyzer. *Electrochim Acta*. 2013;100:242-8.

[39] Borgardt E, Panchenko O, Hackemüller FJ, Giffin J, Bram M, Müller M, Lehnert W, Stolten D. Mechanical characterization and durability of sintered porous transport layers for polymer electrolyte membrane electrolysis. *J Power Sources*. 2018;374:84-91.

[40] Mo J, Steen SM, III BH, Kang Z, Terekhov A, Zhang F-Y, Retterer ST, Cullen DA. Investigation of titanium felt transport parameters for energy storage and hydrogen/oxygen production. 13th International Energy Conversion Engineering Conference. AIAA 2015-39142015. p. 3914.

[41] Carmo M, Fritz DL, Mergel J, Stolten D. A comprehensive review on PEM water electrolysis. *Int J Hydrogen Energ*. 2013;38:4901-34.

[42] Steen III SM, Mo J, Kang Z, Yang G, Zhang F-Y. Investigation of Titanium Liquid/Gas Diffusion Layers in Proton Exchange Membrane Electrolyzer Cells. *International Journal of Green Energy*. 2016.

[43] Toops TJ, Brady MP, Zhang F-Y, Meyer HM, Ayers K, Roemer A, Dalton L. Evaluation of nitrided titanium separator plates for proton exchange membrane electrolyzer cells. *J Power Sources*. 2014;272:954-60.

[44] Ioroi T, Oku T, Yasuda K, Kumagai N, Miyazaki Y. Influence of PTFE coating on gas diffusion backing for unitized regenerative polymer electrolyte fuel cells. *J Power Sources*. 2003;124:385-9.

[45] Omrani R, Shabani B. Gas diffusion layer modifications and treatments for improving the performance of proton exchange membrane fuel cells and electrolysers: A review. *Int J Hydrogen Energ*. 2017.

[46] Ferreira RB, Falcão D, Oliveira V, Pinto A. Experimental study on the membrane electrode assembly of a proton exchange membrane fuel cell: effects of microporous layer, membrane thickness and gas diffusion layer hydrophobic treatment. *Electrochim Acta*. 2017;224:337-45.

[47] Lin G, Van Nguyen T. Effect of thickness and hydrophobic polymer content of the gas diffusion layer on electrode flooding level in a PEMFC. *J Electrochem Soc*. 2005;152:A1942-A8.

[48] Moreira J, Ocampo A, Sebastian P, Smit MA, Salazar M, Del Angel P, Montoya J, Pérez R, Martí L. Influence of the hydrophobic material content in the gas diffusion electrodes on the performance of a PEM fuel cell. *Int J Hydrogen Energ*. 2003;28:625-7.

[49] Lim C, Wang C. Effects of hydrophobic polymer content in GDL on power performance of a PEM fuel cell. *Electrochim Acta*. 2004;49:4149-56.

[50] Liu C-H, Ko T-H, Shen J-W, Chang S-I, Chang S-I, Liao Y-K. Effect of hydrophobic gas diffusion layers on the performance of the polymer exchange membrane fuel cell. *J Power Sources*. 2009;191:489-94.

[51] Sow PK, Prass S, Kalisvaart P, Mérida W. Deconvolution of electrical contact and bulk resistance of gas diffusion layers for fuel cell applications. *Int J Hydrogen Energ*. 2015;40:2850-61.

[52] Manahan M, Mench M. Increased performance of PEFCs with engineered mass-transport pathways. *Ecs Transactions*. 2011;41:569-81.

[53] Manahan M, Hatzell M, Kumbur E, Mench M. Laser perforated fuel cell diffusion media. Part I: Related changes in performance and water content. *J Power Sources*. 2011;196:5573-82.

[54] Okuhata G, Tonoike T, Nishida K, Tsushima S, Hirai S. Effect of perforation structure of cathode GDL on liquid water removal in PEFC. *Ecs Transactions*. 2013;58:1047-57.

[55] Alink R, Gerteisen D, Mérida W. Investigating the water transport in porous media for PEMFCs by liquid water visualization in ESEM. *Fuel Cells*. 2011;11:481-8.

[56] Blanco M, Wilkinson DP, Wang H, Liu SZ. Engineered gas diffusion layers for proton exchange membrane fuel cells. *Ecs Transactions*. 2009;25:1507-18.

[57] Blanco M, Wilkinson DP, Wang H. Application of water barrier layers in a proton exchange membrane fuel cell for improved water management at low humidity conditions. *Int J Hydrogen Energ*. 2011;36:3635-48.

[58] Blanco M, Wilkinson DP, Wang H. Perforated metal sheets as gas diffusion layers for proton exchange membrane fuel cells. *Electrochemical and Solid-State Letters*. 2011;15:B20-B3.

[59] Mo J, Kang Z, Yang G, Retterer ST, Cullen DA, Toops TJ, Green JB, Zhang F-Y. Thin liquid/gas diffusion layers for high-efficiency hydrogen production from water splitting. *Appl Energ*. 2016;177:817-22.

[60] Kang Z, Mo J, Yang G, Li Y, Talley DA, Retterer ST, Cullen DA, Toops TJ, Brady MP, Bender G, Pivovar BS, Green Jr JB, Zhang F-Y. Thin film surface modifications of thin/tunable liquid/gas diffusion layers for high-efficiency proton exchange membrane electrolyzer cells. *Appl Energ*. 2017;206:983-90.

[61] Mo J, Steen SM, Retterer S, Cullen DA, Terekhov A, Zhang F-Y. Mask-Patterned Wet Etching of Thin Titanium Liquid/Gas Diffusion Layers for a PEMEC. *Ecs Transactions*. 2015;66:3-10.

[62] Zhang F-Y, Prasad AK, Advani SG. Investigation of a copper etching technique to fabricate metallic gas diffusion media. *J Micromech Microeng*. 2006;16:N23.

[63] Han B, Steen S, Mo J, Zhang F-Y. Modeling of interfacial resistance effects on the performance and efficiency for electrolyzer energy storage. 13th International Energy Conversion Engineering Conference2015. p. 3915.

[64] Mo J, Kang Z, Retterer ST, Cullen DA, Toops TJ, Green JB, Mench MM, Zhang F-Y. Discovery of true electrochemical reactions for ultrahigh catalyst mass activity in water splitting. *Science Advances*. 2016;2:e1600690.

[65] Rozain C, Mayousse E, Guillet N, Millet P. Influence of iridium oxide loadings on the performance of PEM water electrolysis cells: Part I–Pure IrO2-based anodes. *Applied Catalysis B: Environmental*. 2016;182:153-60.

[66] Rozain C, Mayousse E, Guillet N, Millet P. Influence of iridium oxide loadings on the performance of PEM water electrolysis cells: Part II–Advanced oxygen electrodes. *Applied Catalysis B: Environmental*. 2016;182:123-31.

[67] Ayers KE, Renner JN, Danilovic N, Wang JX, Zhang Y, Maric R, Yu H. Pathways to ultra-low platinum group metal catalyst loading in proton exchange membrane electrolyzers. *Catalysis Today*. 2016;262:121-32.

[68] Zhang L, Roling LT, Wang X, Vara M, Chi M, Liu J, Choi S-I, Park J, Herron JA, Xie Z. Platinum-based nanocages with subnanometer-thick walls and well-defined, controllable facets. *Science*. 2015;349:412-6.

[69] Witham C, Chun W, Valdez T, Narayanan S. Performance of Direct Methanol Fuel Cells with Sputter-Deposited Anode Catalyst Layers. *Electrochemical and solid-state letters*. 2000;3:497-500.

[70] Haug AT, White RE, Weidner JW, Huang W, Shi S, Stoner T, Rana N. Increasing proton exchange membrane fuel cell catalyst effectiveness through sputter deposition. *J Electrochem Soc*. 2002;149:A280-A7.

[71] Bonet F, Delmas V, Grugeon S, Urbina RH, Silvert P, Tekaia-Elhsissen K. Synthesis of monodisperse Au, Pt, Pd, Ru and Ir nanoparticles in ethylene glycol. *Nanostructured Materials*. 1999;11:1277-84.

[72] Siracusano S, Van Dijk N, Payne-Johnson E, Baglio V, Aricò A. Nanosized IrOx and IrRuOx electrocatalysts for the O2 evolution reaction in PEM water electrolysers. *Applied Catalysis B: Environmental*. 2015;164:488-95.

[73] O'Hayre R, Lee S-J, Cha S-W, Prinz FB. A sharp peak in the performance of sputtered platinum fuel cells at ultra-low platinum loading. *J Power Sources*. 2002;109:483-93.

[74] Fang S-Y, Teoh LG, Huang R-H, Hsueh K-L, Yang K-H, Chao W-K, Shieu F-S. Enhancement of proton exchange membrane fuel cell performance by titanium-coated anode gas diffusion layer. *Int J Hydrogen Energ*. 2014;39:21177-84.

[75] Grigoriev S, Porembsky V, Fateev V. Pure hydrogen production by PEM electrolysis for hydrogen energy. *Int J Hydrogen Energ*. 2006;31:171-5.

[76] Marshall AT, Sunde S, Tsypkin M, Tunold R. Performance of a PEM water electrolysis cell using IrxRuyTazO2 electrocatalysts for the oxygen evolution electrode. *Int J Hydrogen Energ*. 2007;32:2320-4.

[77] Marangio F, Pagani M, Santarelli M, Cali M. Concept of a high pressure PEM electrolyser prototype. *Int J Hydrogen Energ*. 2011;36:7807-15.

[78] Steen SM, Zhang F-Y. In-situ and ex-situ characterizations of electrode interfaces in energy storage electrolyzers. *Ecs Transactions*. 2014;59:95-102.

[79] Choi P, Bessarabov DG, Datta R. A simple model for solid polymer electrolyte (SPE) water electrolysis. *Solid State Ionics*. 2004;175:535-9.

[80] Görgün H. Dynamic modelling of a proton exchange membrane (PEM) electrolyzer. *Int J Hydrogen Energ*. 2006;31:29-38.

[81] Lebbal M, Lecœuche S. Identification and monitoring of a PEM electrolyser based on dynamical modelling. *Int J Hydrogen Energ*. 2009;34:5992-9.

[82] Grigoriev S, Kalinnikov A, Millet P, Porembsky V, Fateev V. Mathematical modeling of high-pressure PEM water electrolysis. *J Appl Electrochem*. 2010;40:921-32.

[83] Marangio F, Santarelli M, Cali M. Theoretical model and experimental analysis of a high pressure PEM water electrolyser for hydrogen production. *Int J Hydrogen Energ*. 2009;34:1143-58.

CHAPTER II

INVESTIGATION OF THIN/WELL-TUNABLE LIQUID/GAS DIFFUSION LAYERS EXHIBITING SUPERIOR MULTIFUNCTIONAL PERFORMANCE IN LOW-TEMPERATURE ELECTROLYTIC WATER SPLITTING

A version of this chapter was originally published by Zhenye Kang:

Zhenye Kang, Jingke Mo, Gaoqiang Yang, Scott T. Retterer, David A. Cullen, Todd J. Toops, Johney B. Green Jr, Matthew M. Mench, Feng-Yuan Zhang. "Investigation of thin/well-tunable liquid/gas diffusion layers exhibiting superior multifunctional performance in low-temperature electrolytic water splitting." *Energy & Environmental Science* 10(1), (2017): 166-175.

I am fully responsible for the work submitted in these publications.

2.1 Graphical Abstract

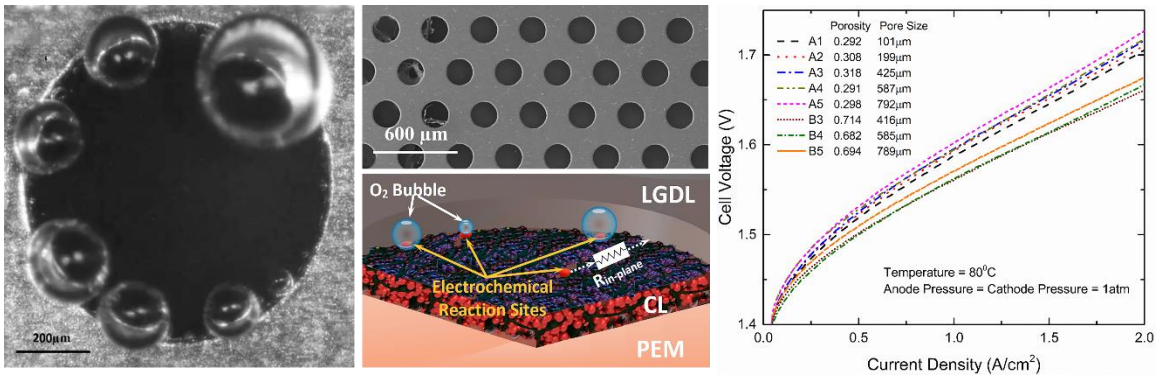

2.2 Abstract

Liquid/gas diffusion layers (LGDLs), which are located between the catalyst layer (CL) and bipolar plate (BP), play an important role in enhancing the performance of water splitting in proton exchange membrane electrolyzer cells (PEMECs). They are expected to transport electrons, heat, and reactants/products simultaneously with minimum voltage, current, thermal, interfacial, and fluidic losses. In this study, the novel thin titanium-based

LGDLs which are only 25 μm in thickness with straight-through pores and well-defined pore morphologies are comprehensively investigated for the first time. A thin titanium-based LGDL with a 400 μm pore size and 0.7 porosity achieved a best-ever performance of 1.66 V at 2 A/cm^2 and 80 ^{o}C, as compared to the published literature. The thin/well-tunable titanium based LGDLs remarkably reduce ohmic and activation losses, and it was found that porosity has a more significant impact on performance than pore size. In addition, an appropriate equivalent electrical circuit model has been established to quantify the effects of pore morphologies. The rapid electrochemical reaction phenomena at the center of the PEMEC are observed by coupling with high-speed and micro-scale visualization systems. The observed reactions contribute reasonable and pioneering data that elucidate the effects of porosity and pore size on the PEMEC performance. This study can be a new guide for future research and development towards high-efficiency and low-cost hydrogen energy.

2.3 Broader Context

Hydrogen is a ‘zero’ emission energy carrier which could be an important part of environmentally friendly solutions to the global energy crisis via combustion or transformation into electricity through fuel cells without producing any greenhouse gases and pollutants. Proton exchange membrane (PEM) water splitting is one of the most practical and high-efficiency methods to produce pure hydrogen from renewable sources like wind and solar energy. The wide commercialization of PEM electrolyzer cells is still hindered by their performance and durability. Successful development of a thin titanium

liquid/gas diffusion layer (LGDL) will reduce the cost, thickness, and weight of the LGDL itself and the system as a whole. This investigation demonstrates the ability to produce LGDLs with precise control of pore size, shape, distribution, and therefore overall porosity and permeability, which can aid in developing modeling routine or validating simulations. More importantly, thin titanium based LGDLs will lead to a manufacturing solution to couple the LGDL with the metallic bipolar plates, since they can be easily integrated together by top-down and bottom-up manufacturing process. Thus, one metallic part could function simultaneously as flow field, bipolar plate, current distributor/collector, and LGDL.

2.4 Introduction

Renewable energy sources, including solar, wind, hydro, biomass and geothermal power, produce clean electricity in sustainable ways. However, most of these renewable sources are variable and often produce electricity intermittently (e.g., only during daylight or when windy), which present major challenges to delivering consistent power to operate today's electrical grid. In addition, the current electrical grid has very limited ability to digest the fluctuation from renewable energy sources. Thereby, a sustainable, high-efficiency, and robust electrochemical energy storage/conversion or a hybrid system to accommodate daily or even hourly changes becomes more critical [1-9]. An advanced proton exchange membrane electrolyzer cell (PEMEC), which is a reverse PEM fuel cell (PEMFC), has been considered as a very attractive energy storage method for producing hydrogen/oxygen from water splitting when coupled with renewable energy sources. PEMECs have several

advantages, such as distinguished efficiency, compact design, large capacity, quick startup, and low maintenance activities, and effectively connect renewable electricity supply and multiscale energy demands including stationary, transportation, and portable applications [10-16]. When renewable energy resources are available, hydrogen/oxygen will be produced and stored with a PEMEC. Later, hydrogen/oxygen can be converted back to water and electricity with a PEM fuel cell (PEMFC), whether the renewable source is available or not. Additionally, surplus electricity in electric grids during off-peak periods can also be stored via the electrolyzer. This entire portfolio will make hybrid energy systems able to provide renewable and reliable energy at different scales whenever and wherever needed [17-22].

A PEM electrolyzer cell mainly consists of a catalyst-coated membrane sandwiched by anode and cathode electrodes, as shown in Figure 3. Each electrode includes a catalyst layer (CL), a liquid/gas diffusion layer (LGDL), and a bipolar plate (BP), which also acts as the current distributor (CD) and the flow field. After electricity is applied, water is split into molecular oxygen, protons, and electrons at the anode side, as shown in Figure 3. Di-oxygen, as one product on the anode CLs, is ideally transported from the CL through the LGDL back to the flow field to avoid blocking the LGDL, which can hinder the reaction. Electrons, which are also generated at anode CLs, pass through the LGDL, anode BP, and external circuit, and then back to the cathode side. Meanwhile, protons pass through the membrane to the cathode and react with electrons which come from the external circuit to form di-hydrogen. H_2/O_2 will be produced and stored continuously as long as water and

electricity are supplied. Thus, not only should the water be supplied continuously, but also the oxygen and hydrogen should be effectively removed through the LGDLs. This is especially important at high current density, where mass transport is a dominant limiting factor of PEMEC performance [23-25].

The anode resides in a harsh environment, which is highly corrosive due to the high overpotential and humidity. Carbon materials (like carbon paper or carbon cloth), which are typically used in PEMFCs, are unsuitable on this side of the PEMECs due to the high potential of the oxygen electrode [14, 26-32]. Ideal anode LGDLs should have good conductivity, high corrosion resistance, good two-phase transport capability and mechanical strength. Metallic LGDLs and bipolar plates, including titanium, have attracted more interest in both PEMECs and PEMFCs due to their high conductivity, rapid production, and low cost [33-37].

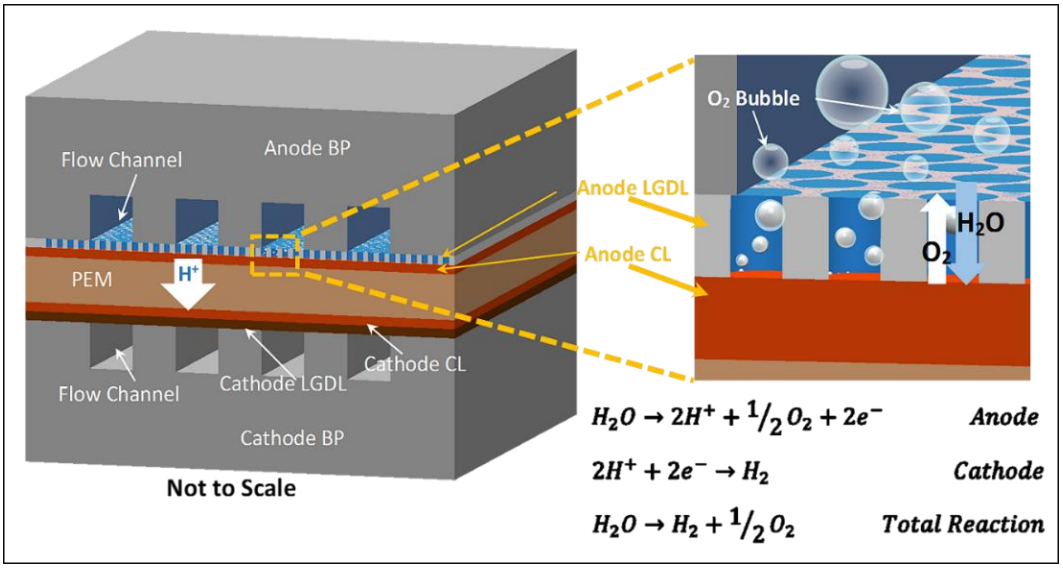

Figure 3. Schematic of thin titanium LGDL functions.

Grigoriev et al. conducted an optimization of porous current collectors. According to his research, the mean pore size of the particles and the thickness of the titanium plates have a significant effect on current-voltage performance. The study found that the optimum sphere particle sizes ranged from 50 to 75 μm and the optimum pore sizes were between 12 and 13 μm, whereas the porosity (between 0.35 - 0.40) and gas permeability of the porous titanium plates did not have a significant influence on electrolysis efficiency [38]. Millet et al. noted that it is necessary to reduce the ohmic resistance between the separator plates and current collectors in order to improve the performance of the PEMECs [39]. Ma et al. concluded that a thinner carbon paper used as an anode LGDL will improve the PEMEC performance due to its better gas diffusion properties and smaller resistance [40]. Hwang et al. made microporous layers (MPL) for PEMECs by loading titanium powder over titanium felt to promote interfacial contacts and they also investigated the effect of pore properties and PTFE content for titanium felt LGDL of the anode electrode [41, 42].

The main efforts in the previous studies, so far, have focused on investigating conventional titanium LGDLs, including felts, woven meshes, or foams [43-45]. The thickness of these LGDLs were larger than 200 μm with significantly longer electrically conductive path lengths and higher fluidic resistances. In addition, their fiber/foam-based pore morphologies result in not only nonuniform interfacial contacts, but random pore sizes and distributions. These random, nonuniform and complicated structures in conventional titanium LGDLs make it impossible to control the liquid/gas/electron/thermal distribution

precisely. Therefore, novel LGDLs with tunable and controlled pore morphologies are strongly desired.

In this study, by taking advantage of advanced micro/nano-manufacturing, a new thin, planar titanium LGDL with straight-through pores and well-tunable pore morphologies is developed. The well-controllable pore size and porosity help to systematically examine the effects of the pore morphology, and to characterize the two-phase transport through the LGDL. The effects of well-defined pore parameters (such as pore size and porosity) on the PEMEC performance are comprehensively investigated for the first time. Both the electro-potential performance and electrochemical impedance are evaluated with the novel LGDLs, and significant improvements have been achieved. Electrochemical impedance spectroscopy (EIS) is further analyzed by equivalent electrical circuit fitting which helps to identify the effect of each loss in the PEMEC. In addition, the LGDL thickness is reduced from greater than hundreds micrometers of conventional LGDLs to only 25 microns, which remarkably reduces the transport and ohmic resistances. More importantly, the development of thin/well-tunable LGDLs with straight pores permits direct visualizations of the electrochemical reactions, which facilitate better understanding of effects of the LGDL pore size and porosity. The impressive observation of the visualization reveals that the oxygen bubble only nucleate at the rim of the pores and we have established an appropriate assumption to analyze and explain the effects of the pore size and porosity for the first time.

2.5 Experimental Details

2.5.1 Nano-manufacturing of titanium thin/well-tunable LGDLs

The thin/well-tunable titanium LGDLs are manufactured lithographically - patterned resist masks and chemical wet etching of thin foils which is shown in Figure 11 [46, 47]. Figure 4 shows a typical scanning electron microscopy (SEM) image of thin/well-tunable LGDLs (Sample A1 and A2) used in this study. The thickness of all LGDLs was 25.4 µm. The pore shapes of the LGDLs were controlled to be circular and all the pores were distributed regularly and uniformly. The pore diameter and the distance between adjacent pore rims are defined as pore size and land length, which are represented by *D* and *L*, respectively. The pore morphology like pore size, pore shape, pore distribution and porosity can be well controlled through the mask design and/or etching conditions.

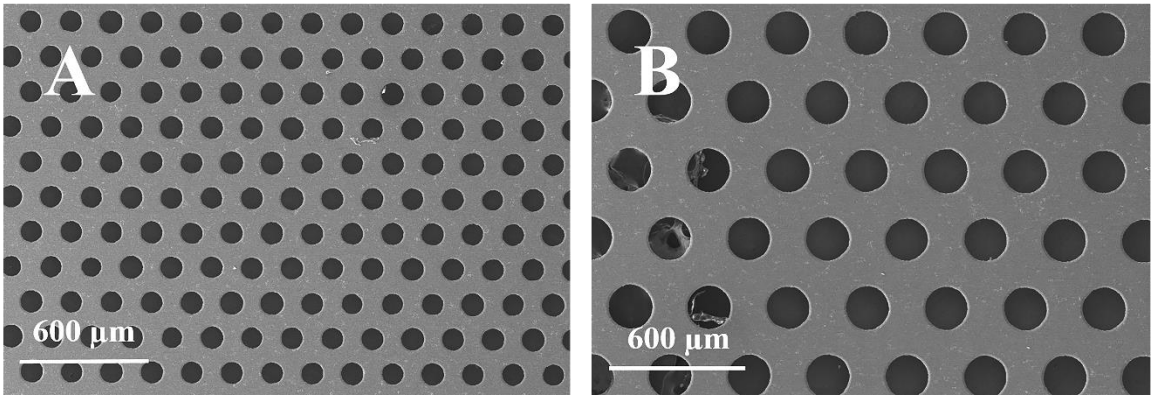

Figure 4. SEM images of typical thin/well-tunable titanium LGDLs: (A) Pore morphology and structure of Sample A1 with approximately 100 µm pore size and 0.30 porosity. (B) Pore morphology and structure of Sample A2 with approximately 200 µm pore size and 0.30 porosity.

The porosity of the LGDL ε, is defined as the total pore area, A_P, divided by the total area of the entity, A_H, which can be given as:

$$\boldsymbol{\varepsilon = \frac{A_P}{A_H} = \frac{\sqrt{3}}{6}\frac{\pi D^2}{(D+L)^2}} \qquad \textbf{Equation 2}$$

This mathematical method was used to design a set of LGDLs with different pore sizes and porosities. Due to the manufacturing error, the real parameters of each sample are measured before evaluation in PEMECs. The pore size and land length were measured under an optical microscope so that the actual porosity can be calculated. Each sample was measured five times and the parameters are the average of the measured data, as shown in Table 1. Eight samples with different parameters, including pore sizes and porosities, were used. Various pore sizes ranging from 100 - 800 μm with approximately 0.3 porosity were prepared to investigate the effects of the pore size (A samples). To study porosity, three additional LGDLs (B samples) were made with 0.7 porosity and pore sizes (about 400, 600, and 800 μm).

2.5.2 PEMEC and testing system

The thin/well-tunable LGDLs were tested in a conventional PEMEC. The two end-plates were made from commercial grade aluminum and designed to provide even compression pressure on the PEMEC. The cell was compressed by eight evenly distributed bolts which were tightened to 4.52 N·m of torque. A copper plate, which was inserted between the bipolar plate and end-plate at both the anode and cathode, was used to apply current to the PEMEC. The bipolar plates were made of graphite and fabricated with a parallel flow field

which was intended to introduce the reactants and products in and out of the PEMEC. Titanium thin film with 25 µm thickness and carbon paper (Toray 090 with 280 µm thickness and porosity of 0.78) were used as anode and cathode LGDLs, respectively. The catalyst-coated membrane (CCM) (Electrolyzer CCM from FuelCellsEtc, EZ-CCM) was comprised of a Nafion 115 membrane, a perfluorosulfonic polymer with a thickness of 125 µm, an anode catalyst layer with an $IrRuO_x$ catalyst loading of 3.0 mg/cm^2, and a cathode layer with a platinum black (PtB) catalyst loading of 3.0 mg/cm^2 with a 5 cm^2 working area. Table 2 shows the detailed characteristics and experimental conditions.

The PEMEC was attached to an electrolyzer control system with current range up to 100 A and voltage range up to 5 V. The hardware was connected to EC-Lab, an electrochemical analysis software from Bio-Logic, which was used to evaluate performance and perform electrochemical impedance spectroscopy (EIS). For controlling the flow, a system of tubing was connected to the PEMEC. While the cathode tubing was merely intended to safely exhaust hydrogen gas that formed during electrolysis, a diaphragm liquid pump from KNF Neuberger was used to supply de-ionized (DI) water at a constant volumetric flow rate of 20 ml/min to the anode. The water bath (General Purpose Water Baths of Model WB10 from PolyScience) was used to pre-heat the DI water to designed temperatures. Two heaters used to heat the PEMEC were inserted into the end-plates at both anode and cathode and two thermocouples used to measure the temperature were inserted into the bipolar plates at both anode and cathode. Both of the heaters and thermocouples were connected to a temperature control system (Multi-Zone controller from OMEGA).

Table 1. Parameters of the titanium thin LGDLs.

Index of the LGDL	Pore Size (D)[μm]	Land Length (L)[μm]	Pore Distance [μm]	Calculated Porosity (ε)
A1	101.06	77.07	178.13	0.29
A2	199.11	142.41	341.52	0.31
A3	424.64	292.91	717.55	0.32
A4	586.96	448.51	1035.47	0.29
A5	791.61	589.51	1381.12	0.30
B3	415.51	52.74	468.25	0.71
B4	585.46	89.91	675.37	0.68
B5	789.16	113.21	902.37	0.69

Table 2. PEM electrolyzer characteristics and experimental conditions.

Characteristics and conditions	Value
Membrane Type	Nafion® 115
Membrane Area	5 cm^2
Membrane Thickness	125 µm
Anode Catalyst Loading	3.0 mg/cm^2 ($IrRuO_x$)
Cathode Catalyst Loading	3.0 mg/cm^2 (PtB)
Anode LGDL	titanium thin film
Cathode LGDL	Toray 090 carbon paper
Operating Temperature	20, 40, 60, 80 ^oC
Operating Pressure	1 atm
Anode Water Flow Rate	20 ml/min

For performance evaluation, an increasing current density was applied to the PEMEC and the current was stepped up from a current density of 0.2 A/cm^2 to 2.0 A/cm^2 with a step of 10 mA/s. Galvanostatic electrochemical impedance spectroscopy (GEIS) was used to measure the impedance of the PEMEC at different operating conditions. In this method, the current is controlled as opposed to the potential. The test station was equipped with an operating current range of -100 A to +100 A and a voltage range of 0 V to 5 V. The current precision was 100 fA. The scanning frequency was varied from 15 kHz to 10 mHz, and recorded 20 points of data per decade. For analyzing impedance data, a Nyquist plot is normally used.

2.6 Results and Discussion

2.6.1 The impact of the pore size and porosity

All the titanium thin/well-tunable LGDLs were evaluated in a standard PEMEC. They were applied and tested as anode LGDLs. The performance of the PEMEC can be derived based on polarization curves of the current density and voltage. The lower voltage at a given current density indicates better PEMEC performance. Figure 5 shows the PEMEC performance results of all the eight LGDLs with different pore sizes and porosity under the same operating conditions. As is shown in Figure 5, increasing the pore size from 101 µm to 791 µm (A1 to A5 with the same porosity of about 0.3), the PEMEC performance decreases. The LGDL with a pore size of 791 µm (A5) results in the worst performance among these five LGDLs. For instance, at a fixed current density of 2 A/cm^2, the required

cell voltage increased from 1.705 V for the LGDL A1 to 1.726 V for A5, although this is still much better than conventional LGDLs [38, 41, 43, 45, 48-52]. The three LGDLs with a larger porosity of about 0.7 and smaller pore distances (B3, B4, and B5), show further improved performance over LGDLs with similar pore sizes but lower porosity/larger pore distance (A3, A4, and A5), and the voltages required at a current density of 2 A/cm^2 are just 1.661 V, 1.667 V, 1.675 V, respectively. With a lower porosity of about 0.3 and larger pore distances, the performance with LGDLs of A3, A4 and A5 were in the range of 1.713 - 1.726 V at 2 A/cm^2. It was noted that porosity had a greater impact on performance than pore size.

EIS is a very useful *in situ* method for analyzing PEMEC performance measuring the impedance of a system at different frequencies. In this study, EIS is conducted on PEMECs with different thin titanium LGDLs during performance testing at 80 ^{o}C and with a current density of 1.0 A/cm^2. The scan frequency is set from high to low frequency (15 kHz to 10 mHz). As shown in Figure 6, there are two x-intercepts: the left one (at the high frequency part) indicates the ohmic loss and the right one (at the low frequency part) is the sum of the resistance.[45, 53] The distance between the two intercepts indicates the sum of activation and mass transport losses.[53, 54] Therefore, the diameter of the first semicircle in Figure 6 mainly indicates the activation resistance.

It can be found that a second arc showed up, which is very small, indicating the limited mass transport losses. The titanium well-tunable LGDLs with straight pores are thin and very hydrophilic. The water contact angle on the thin titanium foil was measured to be

around 45^{o}, while the micro pore features on LGDLs cause a wettability change. For instance, the water contact angles with air-filled pores for samples A1, A4 and B4 are about 81^{o}, 63^{o} and 71^{o}, respectively. During the PEMEC operation, the anode LGDLs are immersed in liquid water, and the pores of LGDLs are water filled. Under these conditions, the LGDL contact angles were found to decrease greatly and liquid water transport through LGDLs very quickly during the measurements. These phenomena show that the titanium thin/well-tunable LGDLs exhibit very hydrophilic wettability, and significantly reduce the transport loss of liquid water from the flow field to the reaction sites in a PEMEC.

The frequency between the two arcs is about 500 mHz. The LGDL performance enhancement is closely related to the impedance changes. LGDLs with a porosity of 0.3 have larger ohmic resistance, and the value decreases with the increase of porosity. It can be seen that for LGDLs with the same porosity, the impedance spectra do not change significantly, which coincides with the result of the polarization curves. The ohmic loss decreases significantly from around 0.08 ohm*cm^2 for the LGDL with a porosity of 0.3 to less than 0.07 ohm*cm^2 for one with a porosity of 0.7.

It is also obvious that the 0.7 porosity LGDLs show smaller first and second arcs, which indicates that the activation and mass transfer losses decrease with increasing porosity. The sum of activation and mass transfer losses are reduced from about 0.046 ohm*cm^2 for 0.3 porosity LGDLs to 0.039 ohm*cm^2 for 0.7 porosity LGDLs. The total losses from EIS decreased by 14% when increasing porosity from 0.3 to 0.7. The detailed quantitative analysis of the EIS will be discussed.

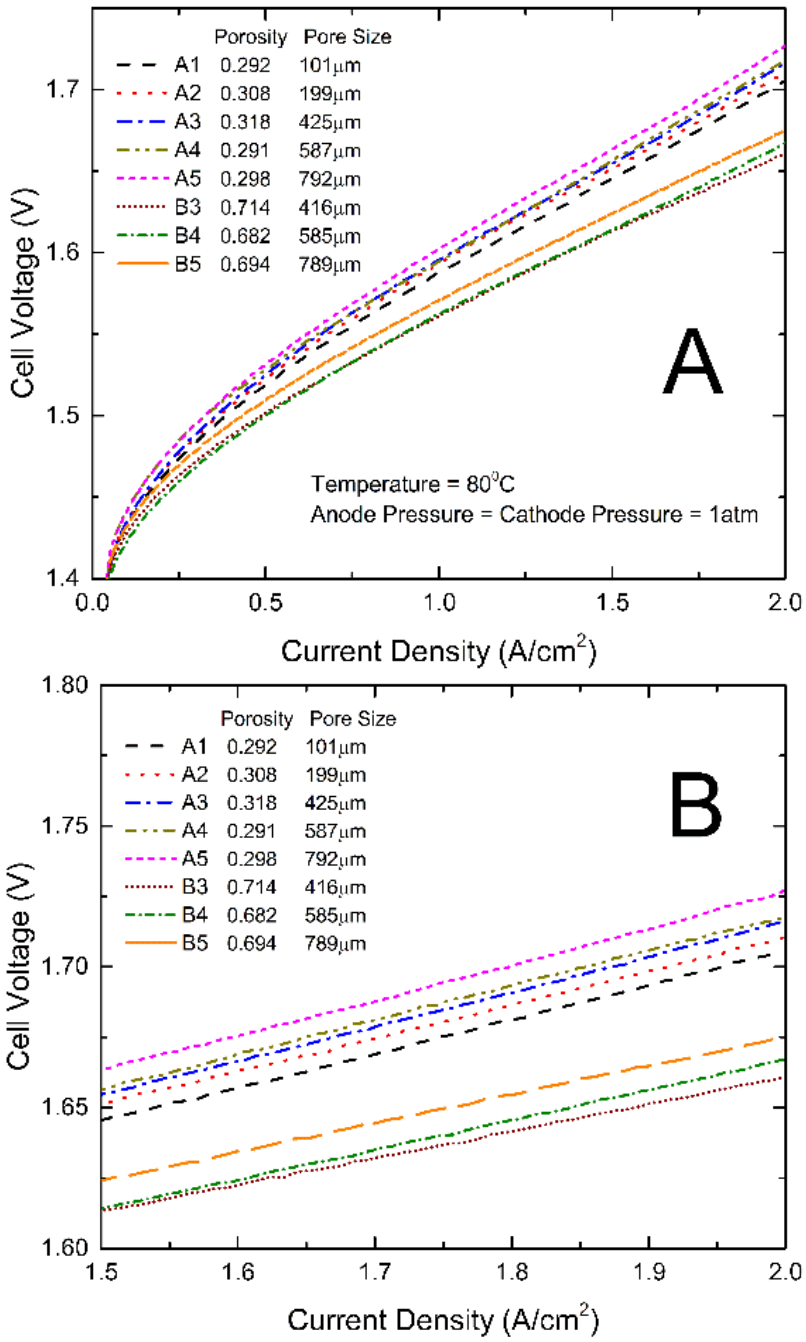

Figure 5. Performance comparison curves between different LGDLs. (A) performance with a current density range from 0 to 2 A/cm^2; (B) close-up of Figure 3A with a current density range from 1.5 to 2 A/cm^2.

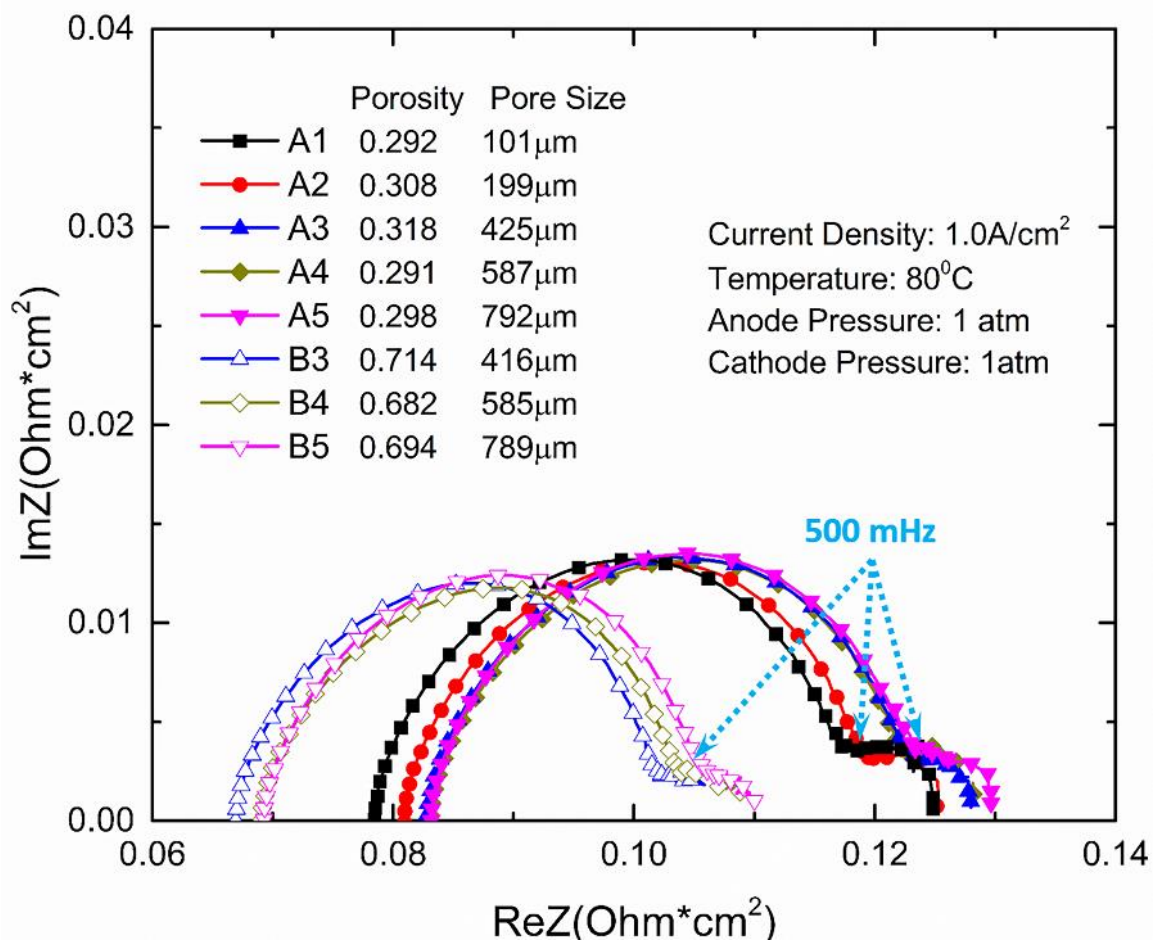

Figure 6. EIS comparison curves between different LGDLs.

2.6.2 Temperature impact

The open circuit voltage, membrane conductive and activation of a PEMEC have a close relation with temperature [25]. In order to get a full understanding of this effect on the thin titanium LGDL, the PEMEC performance and EIS were evaluated at different temperatures. It can be expected that the PEMEC operating temperature has a significant effect on the PEMEC performance. In this study, PEMEC operating temperature was varied from 20 ^{o}C to 80 ^{o}C.

Figure 7 illustrates the effect of operating temperature on the PEMEC performance and EIS. As shown in Figure 7(A), increasing the operating temperature results in a steady improvement in PEMEC performance. At a current density of 2.0 A/cm^2, the cell voltage of PEMEC assembled with LGDL A4 is reduced from 1.971 V at 20 ^{o}C to 1.715 V at 80 ^{o}C. Figure 7(B) shows that the ohmic loss decreases significantly with the increase of PEMEC operating temperature [23-25]. The ohmic loss of the PEMEC consists of the resistances of each component, including PEM, CLs, LGDLs, bipolar plates (BP), and interfacial resistances between components. With the increase of the temperature, the proton conductivity of the PEM and CLs will increase gradually, leading to decreased ohmic losses [55]. The interfacial contacts between components will improve at higher temperature, which will also reduce the ohmic loss of the PEMEC. The electrical resistivities of LGDL and BP materials do not change much with the temperature range from 20 to 80 ^{o}C, and their impacts on ohmic losses would be very limited.

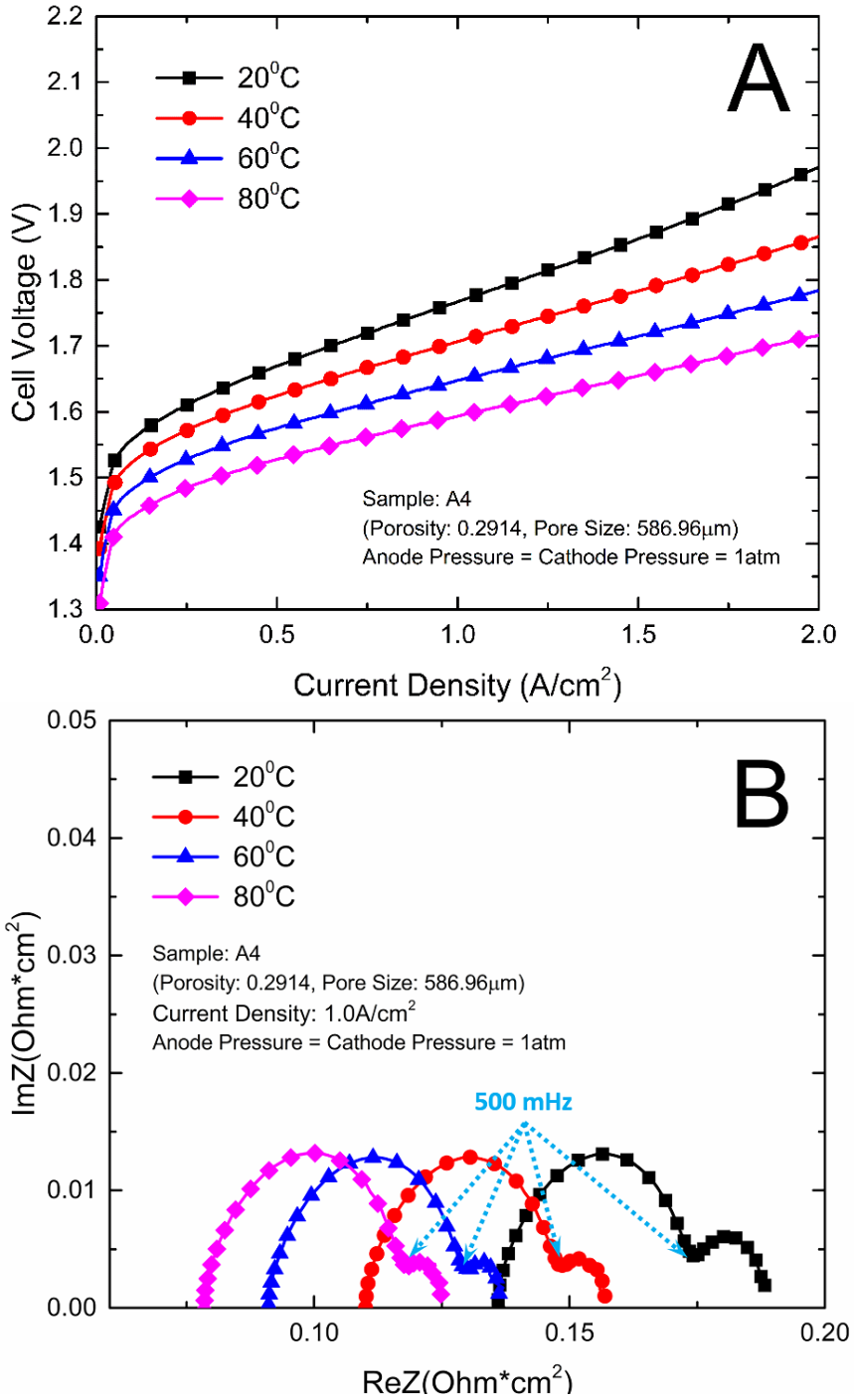

Figure 7. Impact of temperature change on PEMEC. (A) performance curves comparison at different temperature; (B) EIS curves comparison at different temperature.

In addition, the higher temperature will result in improved diffusion processes, catalytic activity and electrode kinetics, and promote oxygen and hydrogen evolution reactions. Both the catalytic transfer coefficient and exchange current density increase with the temperature [56]. The mass transport in PEMECs will also be enhanced at higher temperature. As shown in Figure 7(B), the second arc of the EIS becomes smaller at higher temperature. As a result, the PEMEC performance improves significantly with increasing temperature. Most importantly, it can be noted that the PEMEC with the new LGDLs has an impressive performance even at low temperature (20–40 ^{o}C) compared to the literature [57, 58], which demonstrates that PEMECs with thin/well-tunable LGDLs can operate at room temperature, an exciting possibility for further applications.

2.6.3 Correlation of pore size and porosity with electrochemical reaction mechanisms

The total losses in a PEMEC mainly compose of ohmic loss, activation loss, and mass transport loss. Using an equivalent electrical circuit (EEC) to model the EIS curves can separate each of these losses. Therefore, an electrical circuit model was developed based on the generalized Randles equivalent circuit to investigate the effect of each loss [59-61]. The EEC model is comprised by all the possible impact elements, including inductor (L), resistor of ohmic loss (R_{Ohm}), constant phase element (CPE), resistor of activation (R_2) and Warburg diffusion element (W_d), which is shown in Figure 8. R_{Ohm} mainly represents the ohmic losses of the whole PEMEC which is caused by membrane, CL, LGDLs, BP and all interfacial resistances between each component [62]. The inductance of all the conductors in the PEMEC is assumed as L. R_2 represents the activation losses, which are mainly related

to the kinetics of the reactions at both anode and cathode. CPE is a flexible element, which represents a combination of resistor, capacitor and inductor. The surface reactivity, surface roughness, electrode porosity and surface inhomogeneity could be effectively affected by the CPE [61, 63]. The resistance of the Warburg diffusion element (W_d) is expressed by diffusion resistance (R_d) and it is used to judge the effect of diffusion in the PEMEC [61, 64]. Figure 8 shows an example of EIS fitting of a LGDL. Dots are for test results, while solid line represents EEC model fitting curve. The EIS fitting parameters of all LGDLs in this study have been listed in Table 3.

From the Table 3, it can be seen that all the fitting error can be controlled within 0.5%, which means the fitting curve have a good coincidence with the experimental data and its feasibility is confirmed for the PEMECs with thin titanium LGDLs. For each electrical circuit element, the inductor parameters are very small and remain almost unchanged with different LGDLs. With the increase of porosity, the ohmic losses, activation losses and diffusion losses are all decreased, which lead to good performance of LGDLs. With the increase of pore size, the trend of the parameters is not obvious, which indicates that the effect of pore size is limited compared to porosity.

Table 4 shows the fitting parameters of EIS with LGDL A4 at different temperatures at a current density of 1.0 A/cm^2. It can be found that the inductor changed at different temperatures. With the increase of temperature, the ohmic losses and diffusion losses are decreased while the activation losses are increased. It should be noted that the ohmic losses dominate the losses which leads to better performance at high temperature.

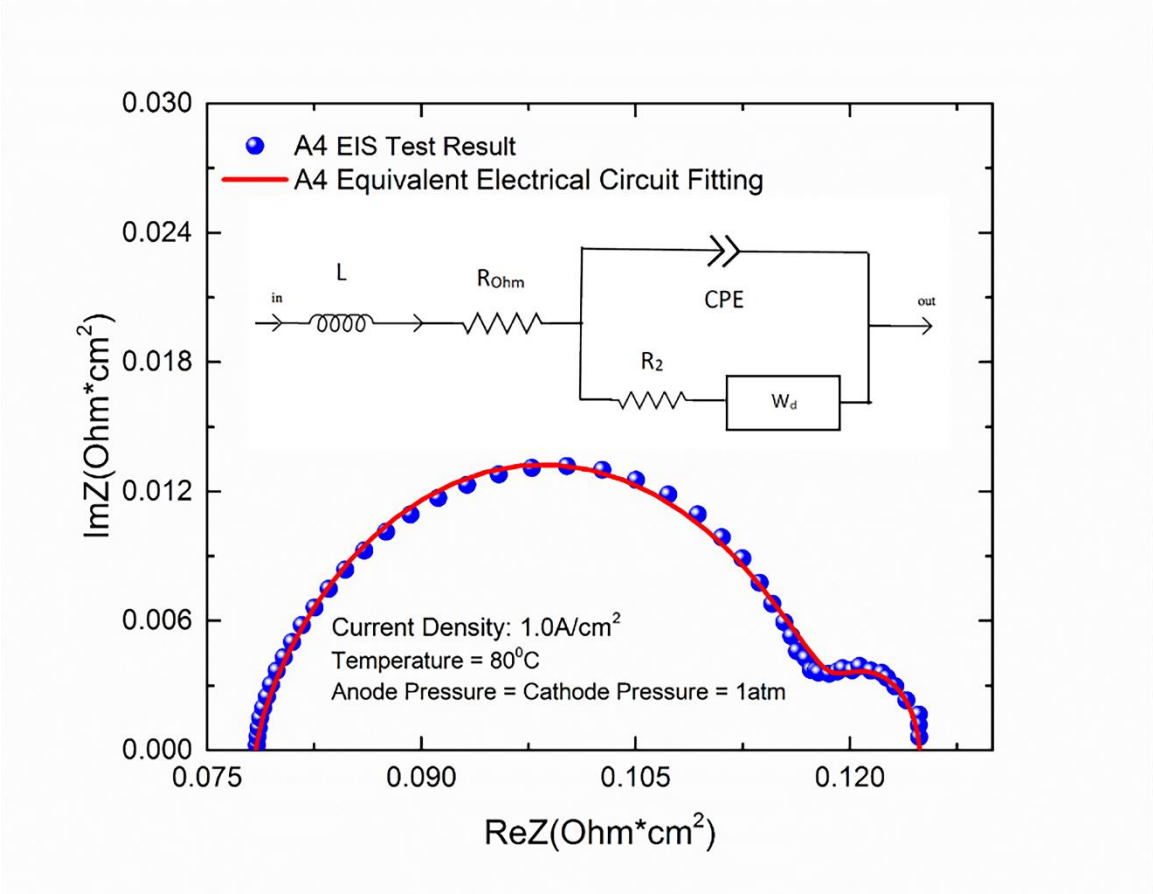

Figure 8. EIS results of sample A4 and its equivalent circuit fitting.

Table 3. The fitting parameters of EIS of different LGDLs at 1.0A/cm^2.

Sample	L_{Ind} [H]	R_{Ohm} [Ω*cm^2]	CPE_Q [F.s^(a-1)]	R_2 [Ω*cm^2]	R_d [Ω*cm^2]	ERROR [%]
A1	1.23E-08	0.0779	3.48	0.0406	0.006	0.31
A2	1.19E-08	0.0804	3.31	0.0410	0.005	0.29
A3	1.28E-08	0.0822	3.36	0.0411	0.004	0.23
A4	1.24E-08	0.0825	3.61	0.0418	0.004	0.31
A5	1.21E-08	0.0824	3.47	0.0420	0.004	0.20
B3	1.24E-08	0.0665	3.88	0.0363	0.003	0.45
B4	1.20E-08	0.0688	4.04	0.0365	0.003	0.48
B5	1.28E-08	0.0696	3.64	0.0381	0.002	0.33

Table 4. The fitting parameters of EIS of A4 with different temperatures at 1.0A/cm^2.

Temperature[^{o}C]	L_{Ind} [H]	R_{Ohm} [Ω*cm^2]	CPE_Q [F.s^(a-1)]	R_2 [Ω*cm^2]	R_d[Ω*cm^2]	ERROR [%]
20	2.73E-08	0.135	3.23	0.0390	0.014	0.22
40	2.15E-08	0.110	3.33	0.0391	0.008	0.26
60	1.73E-08	0.0905	3.46	0.0399	0.007	0.44
80	1.24E-08	0.0822	3.61	0.0418	0.004	0.31

In order to better understand the impacts of porosity and pore size on the resistance and performance of the PEMEC and help us to optimize the properties of LGDLs, the mechanism of the electrochemical reaction in PEMEC was analyzed. The high-speed and micro-scale visualization was introduced to observe the electrochemical reaction of a PEMEC with thin/well-tunable titanium LGDLs and the experiments were conducted in a transparent PEMEC. Figure 9(A) shows the visualization of the reaction which occurred in a typical pore which comes from the screenshot of a video. In the field of vision, the 791 μm pore located at the middle of the channel was focused and it is obvious that the electrochemical reaction happens only at the rim of the pore.

From the Figure 9, the bubble generation, growth and detachment can be observed clearly. Even under the current density of 2.0 A/cm^2, the type of two phase flow in microchannel is only bubbly, the bubble detachment diameter is much smaller than the pore size. All those visualization results demonstrate that the dynamics of bubble evolution didn't affect the mass transfer much, which means under the range of current density in this research,

the effect of dynamics of bubble on the performance of PEMEC can be ignored. This conclusion has been also verified in the EIS results in Figure 6. However, there is a very interesting phenomena in visualization results. All bubble are nucleating along the rim of pore, which also means that the triple phase boundary (TPB) sites are achieved only at the sites which are located at the rim of the pore. The sites that don't satisfy TPB conditions will not have electrochemical reaction, and the bubble will not generate and grow. As shown is Figure 9(B), there is an in-plane resistance between the sites and LGDL which are expressed as $R_{in\text{-}plane}$. The $R_{in\text{-}plane}$ closes to zero when the sites are located at the rim of the pore. Although the catalyst is expected to transport electrons, the $R_{in\text{-}plane}$ of the $IrRuO_x$ catalyst layer has been found to be more than 10,000 times larger than the thin titanium LGDL. The large in-plane ohmic losses in catalyst layers prevent the electrochemical reactions from occurring in the middle region of pores and act as an open circuit.

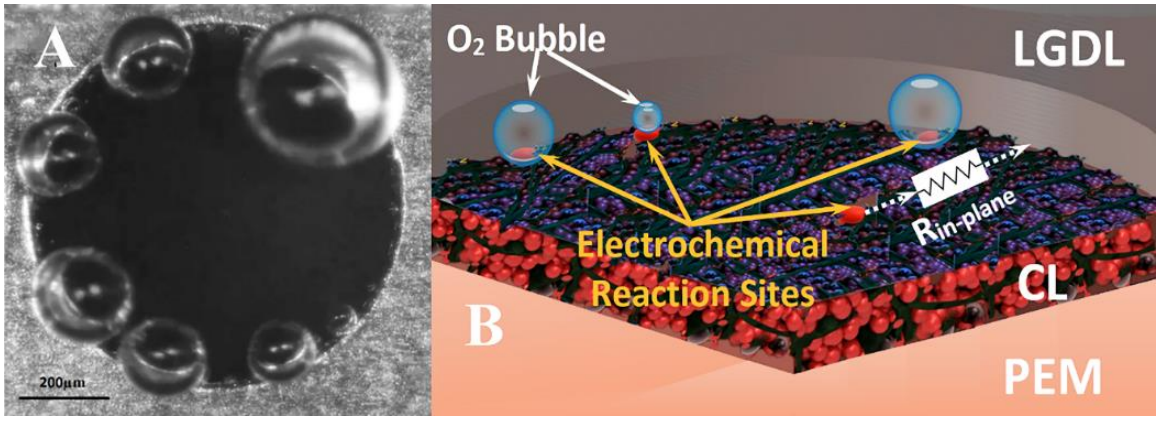

Figure 9. Visualization and schematic of the electrochemical reaction at 2.0 A/cm^2 at pore scale (A) Screenshot of visualization video shows the electrochemical reaction phenomenon in one pore. (B) Schematic of electrochemical reaction occurred at pore scale.

A Hitachi HF3300 scanning transmission electron microscope (STEM) equipped with a Bruker energy-dispersive X-ray spectrometer (EDS) and both high-angle annular dark-field (HAADF) and secondary electron (SE) detectors was used to image the morphology and composition of the different catalyst layers. Cross-sectional specimens were prepared by diamond-knife ultramicrotomy with a target thickness of 50 - 100 nm. Figure 10 shows the cross-section and top-view morphology of the CCMs which were examined by SEM and STEM, and it can be seen that both the anode and cathode catalyst particles ($IrRuO_x$ and Pt Black, respectively) form non-uniformly distributed agglomerates on the surface membrane [65]. The anode and cathode catalyst layers are roughly 20 μm and 15 μm thick, respectively, and the particle size of cathode PtB is smaller than anode. The membrane is observed above the anode, marked by the high fluorine signal in Figure 10(F). Fluorine was also present throughout the PtB cathode and is important for proton conduction throughout the electrode. The microstructures of the $IrRuO_x$ particles at the anode vary widely, which may cause different physical properties at a different point on the CL. At the anode electrode, water is split into electrons, protons and atomic oxygen at reaction sites. The TPB exists where water, good electron and proton conductivity and catalytically-active sites all meet. It can be assumed that not all of the sites on the CL yield electrochemical reactions; these are limited to sites where a TPB exist, which are distributed randomly on the CL.

From the above phenomena and conclusions, some assumptions are made to establish a model that could investigate the performance of PEMEC using titanium thin/well-tunable

LGDLs: (a) there are *n* reaction sites on each length *l* on the rim of the pore; (b) δR_m is the local resistance of the reaction site *m*, all reaction sites are in parallel with each other (The difference of resistance between each sites probably due to the non-uniformly distributed anode catalysts which can be seen in Figure 10.); (c) A_t is the active reaction area of the PEMEC which is 5 cm^2 in this study; (d) *D* and ε are the pore diameter and porosity of the thin LGDL, respectively; (e) *I* is the current of the PEMEC. So the total reaction sites *N* can be calculated by Equation 3.

$$\boldsymbol{N = 4A_t \times \frac{n}{l} \times \frac{\varepsilon}{D}} \qquad \textbf{Equation 3}$$

It can be found that with the increase of porosity or decrease of pore size, the total reaction sites will increase correspondingly. When the current, *I*, is kept constant, the hydrogen/oxygen production rate will remain unchanged according to Faraday's Law. So the production rate at each reaction sites will decrease when the number of reaction sites is increased in order to keep a constant total gas producing rate. For each local reaction site, the local voltage, $V_{m,}$ can be expressed as:

$$\boldsymbol{V_m = I_m \times \delta R_m \quad (m = 1, 2, 3 \cdots N)} \qquad \textbf{Equation 4}$$

Where, I_m is the local current at each reaction site and it has a relation with PEMEC current I.

$$\boldsymbol{I = \sum_{m=1}^{N} I_m} \qquad \textbf{Equation 5}$$

The V_m of different reaction sites will be the same due to the parallel relation between all the reaction sites. So the local current density may vary because of the different local resistance and area of each reaction site, which will cause different oxygen production rates

at different reaction sites; this phenomenon can be confirmed from the visualization video. When the current remains unchanged, the local current will decrease with the increase of total reaction sites N. As a result, the local voltage, $V_{m,}$ will decrease which will result in the decrease of the cell voltage.

So, it can be concluded that as the total reaction sites increases, the cell voltage of the PEMEC will decrease. It can also be found that with larger pore size, a large amount of catalyst sites located away from the rim will not behave normally due to the large in-plane resistance, which will result in worse performance and catalyst underutilization. By increasing the porosity or decreasing the pore size, the number of reaction sites can be increased and more catalysts are active. Meanwhile, the total ohmic losses can be decreased due to more parallel resistances which exist in the equivalent circuit, which will lead to better performance. On the other hand, the increase of the total reaction sites N means more active catalyst, which will impact the kinetics and decrease the activation loss. In the Butler-Volmer model of kinetics, the activation potential is related to many factors, such as reaction mechanism, catalyst morphology, operating parameters, species concentrations and so on [55]. The larger porosity LGDLs with more reaction sites will lead to a larger roughness factor which causes higher effective exchange current density and result in a smaller activation overpotential. It can be concluded that the smaller ohmic loss and activation loss are the two main reasons why larger porosity thin LGDLs can achieve better performance.

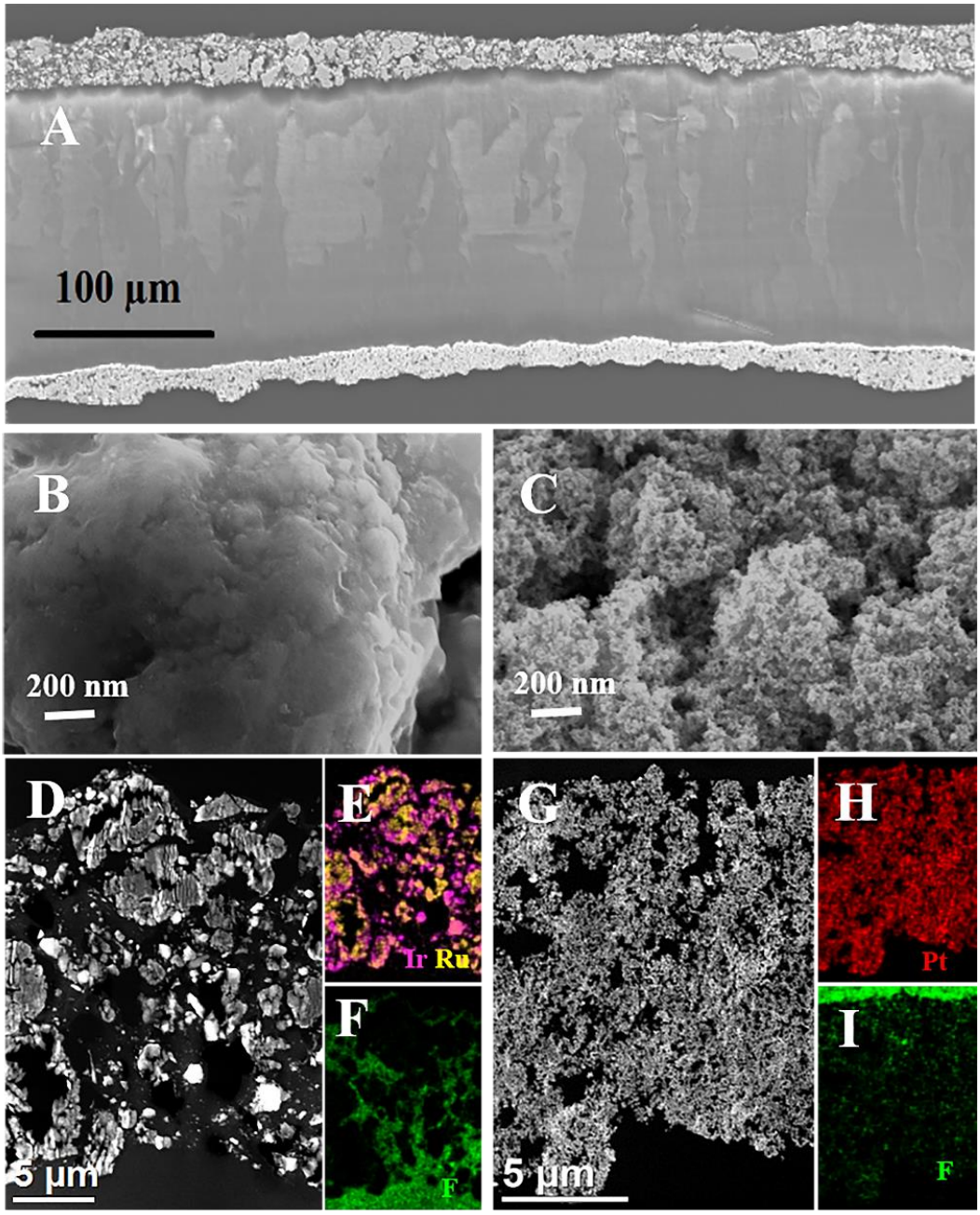

Figure 10. SEM and STEM images of catalyst coated membrane (A) SEM image of cross-section of catalysts coated membrane with $IrRuO_x$ anode at top side and PtB cathode at bottom side. (B) Top view images of catalyst particles for $IrRuO_x$. (C) Top view images of catalyst particles for PtB. (D) STEM image of $IrRuO_x$ at anode with complementary EDS spectrum images for (E) IrRu and (F) F. (G) STEM image of PtB at cathode with complementary EDS spectrum images for (H) Pt and (I) F.

2.7 Conclusion

In this study, a set of thin and planar titanium LGDLs with well-tunable pore morphologies are developed to promote PEMEC performance, and to precisely investigate the impacts of the LGDL pore size and porosity. The thin LGDLs have exhibited exceptional performance. At a current density of 2.0 A/cm^2 with a porosity of 0.7 and a pore size of 400 μm, the required voltage reaches 1.661 V, the lowest value that has been publicly reported so far. The PEMEC has a better performance with a larger porosity under a fixed pore size. It also can be found that the PEMEC performance decreases gradually with the increase of pore size from 100 to 800 μm, but pore-size impacts are not as significant as porosity. Additionally, operating temperatures also have a large impact on the PEMEC performance. The PEMEC performance is significantly improved when the temperature increased from 20 ^{o}C to 80 ^{o}C. For better understanding the performance mechanisms, EIS evaluations are conducted and comprehensive equivalent electrical circuits, including CPE and Warburg diffusion element, are established to quantify the ohmic, activation and transport losses, respectively. The ohmic and activation losses are found to play the dominant roles in promoting PEMEC performance. By taking advantage of the straight-through pores of the novel LGDLs, the direct visualizations of the electrochemical reaction were captured by a high-speed and micro-scale visualization system. The effect of pore size and porosity explained by the electrochemical reaction mechanism that is introduced in this study. The great observation reveals that the oxygen bubble only generated at the rim of the pores and the performance is closely related to the number of the reaction sites.

Larger porosity and smaller pore size can increase the reaction sites in the PEMEC which could help to decrease the total ohmic loss and activation loss, which are two dominant factors that impact PEMEC performance. Due to the thin feature of the novel LGDL, not only the thickness/volume/weight of the PEMEC stack can be reduced greatly, but also the materials used for LGDLs can be decreased which helps to reduce the cost. In addition, the well-tunable pore morphologies can facilitate the investigation of the two phase flow more easily and modeling the flow. Because all titanium thin LGDLs in this study have a better performance than the conventional ones (like titanium felt), they are expected to have many potential applications in energy and environmental engineering. More work will be performed to investigate the other parameters that may have affect the performance of PEMEC.

References

[1] Ager JW, Shaner MR, Walczak KA, Sharp ID, Ardo S. Experimental demonstrations of spontaneous, solar-driven photoelectrochemical water splitting. *Energ Environ Sci*. 2015;8:2811-24.

[2] Hong WT, Risch M, Stoerzinger KA, Grimaud A, Suntivich J, Shao-Horn Y. Toward the rational design of non-precious transition metal oxides for oxygen electrocatalysis. *Energ Environ Sci*. 2015;8:1404-27.

[3] Turner JA. A realizable renewable energy future. *Science*. 1999;285:687-9.

[4] Isherwood W, Smith JR, Aceves SM, Berry G, Clark W, Johnson R, Das D, Goering D, Seifert R. Remote power systems with advanced storage technologies for Alaskan villages. *Energy*. 2000;25:1005-20.

[5] Chen X, Li C, Grätzel M, Kostecki R, Mao SS. Nanomaterials for renewable energy production and storage. *Chem Soc Rev*. 2012;41:7909-37.

[6] Rodriguez CA, Modestino MA, Psaltis D, Moser C. Design and cost considerations for practical solar-hydrogen generators. *Energ Environ Sci*. 2014;7:3828-35.

[7] Hou Y, Lohe MR, Zhang J, Liu S, Zhuang X, Feng X. Vertically oriented cobalt selenide/NiFe layered-double-hydroxide nanosheets supported on exfoliated graphene foil: an efficient 3D electrode for overall water splitting. *Energ Environ Sci*. 2016.

[8] Lai X, Halpert JE, Wang D. Recent advances in micro-/nano-structured hollow spheres for energy applications: From simple to complex systems. *Energ Environ Sci*. 2012;5:5604-18.

[9] Tang H, Hessel CM, Wang J, Yang N, Yu R, Zhao H, Wang D. Two-dimensional carbon leading to new photoconversion processes. *Chem Soc Rev*. 2014;43:4281-99.

[10] Debe M, Hendricks S, Vernstrom G, Meyers M, Brostrom M, Stephens M, Chan Q, Willey J, Hamden M, Mittelsteadt CK. Initial performance and durability of ultra-low loaded NSTF electrodes for PEM electrolyzers. *J Electrochem Soc*. 2012;159:K165-K76.

[11] Javadekar A, Jayakumar A, Gorte RJ, Vohs JM, Buttrey D. Energy storage in electrochemical cells with molten Sb electrodes. *J Electrochem Soc*. 2012;159:A386-A9.

[12] Shapiro D, Duffy J, Kimble M, Pien M. Solar-powered regenerative PEM electrolyzer/fuel cell system. *Sol Energy*. 2005;79:544-50.

[13] Smith W. The role of fuel cells in energy storage. *J Power Sources*. 2000;86:74-83.

[14] Jung H-Y, Huang S-Y, Popov BN. High-durability titanium bipolar plate modified by electrochemical deposition of platinum for unitized regenerative fuel cell (URFC). *J Power Sources*. 2010;195:1950-6.

[15] Barbir F. PEM electrolysis for production of hydrogen from renewable energy sources. *Sol Energy*. 2005;78:661-9.

[16] Ha D-H, Han B, Risch M, Giordano L, Yao KP, Karayaylali P, Shao-Horn Y. Activity and stability of cobalt phosphides for hydrogen evolution upon water splitting. *Nano Energy*. 2016.

[17] Baxter J, Bian Z, Chen G, Danielson D, Dresselhaus MS, Fedorov AG, Fisher TS, Jones CW, Maginn E, Kortshagen U. Nanoscale design to enable the revolution in renewable energy. *Energ Environ Sci*. 2009;2:559-88.

[18] Gorensek MB, Forsberg CW. Relative economic incentives for hydrogen from nuclear, renewable, and fossil energy sources. *Int J Hydrogen Energ*. 2009;34:4237-42.

[19] Uzunoglu M, Onar O, Alam M. Modeling, control and simulation of a PV/FC/UC based hybrid power generation system for stand-alone applications. *Renew Energ*. 2009;34:509-20.

[20] Liu C-j, Burghaus U, Besenbacher F, Wang ZL. Preparation and characterization of nanomaterials for sustainable energy production. *Acs Nano*. 2010;4:5517-26.

[21] Oh H, Park J, Min K, Lee E, Jyoung J-Y. Effects of pore size gradient in the substrate of a gas diffusion layer on the performance of a proton exchange membrane fuel cell. *Appl Energ*. 2015;149:186-93.

[22] Qi J, Lai X, Wang J, Tang H, Ren H, Yang Y, Jin Q, Zhang L, Yu R, Ma G. Multi-shelled hollow micro-/nanostructures. *Chem Soc Rev*. 2015;44:6749-73.

[23] Han B, Mo J, Kang Z, Zhang F-Y. Effects of membrane electrode assembly properties on two-phase transport and performance in proton exchange membrane electrolyzer cells. *Electrochim Acta*. 2016;188:317-26.

[24] Han B, Mo J, Kang Z, Zhang F-Y. Modeling of interfacial resistance effects on the performance and efficiency for electrolyzer energy storage. 13th International Energy Conversion Engineering Conference. AIAA 2015-39152015. p. 3915.

[25] Han B, Steen SM, Mo J, Zhang F-Y. Electrochemical performance modeling of a proton exchange membrane electrolyzer cell for hydrogen energy. *Int J Hydrogen Energ*. 2015;40:7006-16.

[26] Fall J, Humphreys D, Guo S. Design and testing of a unitized regenerative fuel cell. *J Fuel Cell Sci Tech*. 2009;6:031003.

[27] Chen G, Waraksa CC, Cho H, Macdonald DD, Mallouka TE. EIS Studies of Porous Oxygen Electrodes with Discrete Particles I. Impedance of Oxide Catalyst Supports. *J Electrochem Soc*. 2003;150:E423-E8.

[28] Bockris JOM. Hydrogen. *Materials*. 2011;4:2073-91.

[29] Nikiforov A, Petrushina I, Christensen E, Tomás-García A, Bjerrum N. Corrosion behaviour of construction materials for high temperature steam electrolysers. *Int J Hydrogen Energ*. 2011;36:111-9.

[30] Fuentes RE, Farell J, Weidner JW. Multimetallic electrocatalysts of Pt, Ru, and Ir supported on anatase and rutile TiO2 for oxygen evolution in an acid environment. *Electrochemical and Solid-State Letters*. 2011;14:E5-E7.

[31] Dihrab SS, Sopian K, Alghoul M, Sulaiman MY. Review of the membrane and bipolar plates materials for conventional and unitized regenerative fuel cells. *Renewable and Sustainable Energy Reviews*. 2009;13:1663-8.

[32] Mo J, Steen SM, Zhang F-Y, Toops TJ, Brady MP, Green JB. Electrochemical investigation of stainless steel corrosion in a proton exchange membrane electrolyzer cell. *Int J Hydrogen Energ*. 2015;40:12506-11.

[33] Zhang F-Y, Advani SG, Prasad AK. Performance of a metallic gas diffusion layer for PEM fuel cells. *J Power Sources*. 2008;176:293-8.

[34] Matsuura T, Kato M, Hori M. Study on metallic bipolar plate for proton exchange membrane fuel cell. *J Power Sources*. 2006;161:74-8.

[35] Arisetty S, Prasad AK, Advani SG. Metal foams as flow field and gas diffusion layer in direct methanol fuel cells. *J Power Sources*. 2007;165:49-57.

[36] Tawfik H, Hung Y, Mahajan D. Metal bipolar plates for PEM fuel cell—a review. *J Power Sources*. 2007;163:755-67.

[37] Wang H, Turner J. Reviewing metallic PEMFC bipolar plates. *Fuel Cells*. 2010;10:510-9.

[38] Grigoriev S, Millet P, Volobuev S, Fateev V. Optimization of porous current collectors for PEM water electrolysers. *Int J Hydrogen Energ*. 2009;34:4968-73.

[39] Millet P, Dragoe D, Grigoriev S, Fateev V, Etievant C. GenHyPEM: a research program on PEM water electrolysis supported by the European Commission. *Int J Hydrogen Energ*. 2009;34:4974-82.

[40] Ma L, Sui S, Zhai Y. Investigations on high performance proton exchange membrane water electrolyzer. *Int J Hydrogen Energ*. 2009;34:678-84.

[41] Hwang CM, Ishida M, Ito H, Maeda T, Nakano A, Hasegawa Y, Yokoi N, Kato A, Yoshida T. Influence of properties of gas diffusion layers on the performance of polymer electrolyte-based unitized reversible fuel cells. *Int J Hydrogen Energ*. 2011;36:1740-53.

[42] Hwang CM, Ishida M, Ito H, Maeda T, Nakano A, Kato A, Yoshida T. Effect of titanium powder loading in gas diffusion layer of a polymer electrolyte unitized reversible fuel cell. *J Power Sources*. 2012;202:108-13.

[43] Ito H, Maeda T, Nakano A, Hwang CM, Ishida M, Kato A, Yoshida T. Experimental study on porous current collectors of PEM electrolyzers. *Int J Hydrogen Energ*. 2012;37:7418-28.

[44] Ito H, Maeda T, Nakano A, Kato A, Yoshida T. Influence of pore structural properties of current collectors on the performance of proton exchange membrane electrolyzer. *Electrochim Acta*. 2013;100:242-8.

[45] Mo J, Steen SM, III BH, Kang Z, Terekhov A, Zhang F-Y, Retterer ST, Cullen DA. Investigation of titanium felt transport parameters for energy storage and hydrogen/oxygen production. 13th International Energy Conversion Engineering Conference. AIAA 2015-39142015. p. 3914.

[46] Mo J, Steen SM, Retterer S, Cullen DA, Terekhov A, Zhang F-Y. Mask-Patterned Wet Etching of Thin Titanium Liquid/Gas Diffusion Layers for a PEMEC. *Ecs Transactions*. 2015;66:3-10.

[47] Zhang F-Y, Prasad AK, Advani SG. Investigation of a copper etching technique to fabricate metallic gas diffusion media. *J Micromech Microeng*. 2006;16:N23.

[48] Carmo M, Fritz DL, Mergel J, Stolten D. A comprehensive review on PEM water electrolysis. *Int J Hydrogen Energ*. 2013;38:4901-34.

[49] Marshall AT, Sunde S, Tsypkin M, Tunold R. Performance of a PEM water electrolysis cell using IrxRuyTazO2 electrocatalysts for the oxygen evolution electrode. *Int J Hydrogen Energ*. 2007;32:2320-4.

[50] Xu J, Liu G, Li J, Wang X. The electrocatalytic properties of an IrO 2/SnO 2 catalyst using SnO 2 as a support and an assisting reagent for the oxygen evolution reaction. *Electrochim Acta*. 2012;59:105-12.

[51] Xu J, Miao R, Zhao T, Wu J, Wang X. A novel catalyst layer with hydrophilic–hydrophobic meshwork and pore structure for solid polymer electrolyte water electrolysis. *Electrochem Commun*. 2011;13:437-9.

[52] Mo J, Kang Z, Yang G, Retterer ST, Cullen DA, Toops TJ, Green JB, Zhang F-Y. Thin liquid/gas diffusion layers for high-efficiency hydrogen production from water splitting. *Appl Energ*. 2016;177:817-22.

[53] Sun S, Xiao Y, Liang D, Shao Z, Yu H, Hou M, Yi B. Behaviors of a proton exchange membrane electrolyzer under water starvation. *Rsc Adv*. 2015;5:14506-13.

[54] Dale N, Mann M, Salehfar H, Dhirde A, Han T. Ac impedance study of a proton exchange membrane fuel cell stack under various loading conditions. *J Fuel Cell Sci Tech*. 2010;7:031010.

[55] Mench MM. Fuel cell engines: *John Wiley & Sons*; 2008.

[56] Bel'skaya EA, Kulyamina EY. Electrical resistivity of titanium in the temperature range from 290 to 1800 K. *High Temperature*. 2007;45:785-96.

[57] Su H, Linkov V, Bladergroen BJ. Membrane electrode assemblies with low noble metal loadings for hydrogen production from solid polymer electrolyte water electrolysis. *Int J Hydrogen Energ*. 2013;38:9601-8.

[58] Spurgeon JM, Lewis NS. Proton exchange membrane electrolysis sustained by water vapor. *Energ Environ Sci*. 2011;4:2993-8.

[59] Mainka J, Maranzana G, Dillet J, Didierjean S, Lottin O. Effect of oxygen depletion along the air channel of a PEMFC on the Warburg diffusion impedance. *J Electrochem Soc*. 2010;157:B1561-B8.

[60] Malevich D, Halliop E, Peppley BA, Pharoah JG, Karan K. Investigation of charge-transfer and mass-transport resistances in PEMFCs with microporous layer using electrochemical impedance spectroscopy. *J Electrochem Soc*. 2009;156:B216-B24.

[61] Ter Heijne A, Schaetzle O, Gimenez S, Fabregat-Santiago F, Bisquert J, Strik DP, Barriere F, Buisman CJ, Hamelers HV. Identifying charge and mass transfer resistances of an oxygen reducing biocathode. *Energ Environ Sci*. 2011;4:5035-43.

[62] Seo S-J, Woo J-J, Yun S-H, Lee H-J, Park J-S, Xu T, Yang T-H, Lee J, Moon S-H. Analyses of interfacial resistances in a membrane-electrode assembly for a proton exchange membrane fuel cell using symmetrical impedance spectroscopy. *Phys Chem Chem Phys*. 2010;12:15291-300.

[63] Jorcin J-B, Orazem ME, Pébère N, Tribollet B. CPE analysis by local electrochemical impedance spectroscopy. *Electrochim Acta*. 2006;51:1473-9.

[64] Jeong KM, Lee CK, Sohn HJ. Time-Averaged Current Distribution for a Rotating-Disk Electrode under Periodic Current Reversal Conditions. *J Electrochem Soc*. 1992;139:1927-31.

[65] Peron J, Shi Z, Holdcroft S. Hydrocarbon proton conducting polymers for fuel cell catalyst layers. *Energ Environ Sci*. 2011;4:1575-91.

Appendix

Nano-manufacturing of titanium thin/well-tunable LGDLs

A typical fabrication procedure for thin titanium LGDL begins with the design and fabrication of the photomasks, (as shown in Figure 11), which is the most important step to control the pore size, pore shape and porosity of LGDLs. A mask pattern was designed using commercially available CAD/VLSI software (LayoutEditor, layouteditor.net). The design pattern was imported into a Heidelberg DWL 66 laser lithography system and patterned on a soda-lime glass mask plate that is pre-coated with chromium and photoresist. After patterning, the masks were developed for 1 minute in Microposit® MF® CD-26 Developer (Shipley Company, Marlborough, MA), rinsed with DI water and dried in N_2. Masks were then submerged in chrome etchant for 2 minutes, rinsed with DI water and dried in N_2. The remaining resist was subsequently removed in a heated bath (70 ^oC) of N-methyl pyrolidone (NMP). The titanium thin film was placed on the resist-coated silicon wafer with special care due to its delicate features, and gently heated for 90 s at 115 ^oC. A second layer of adhesion promoter (MicroPrime MP-P20, ShinEtsuMicroSi) and MEGAPOSIT™ SPR™ 220 photoresist (MicroChem) was applied to the titanium foil under identical conditions, and then exposed to UV light using conventional contact photolithography. It was then developed in Microposit® MF® CD-26 developer (Shipley Company, Marlborough, MA), rinsed with DI water and dried in N_2. After patterning the photoresist mask on the foil, the patterned material was etched in HF. The photoresist was the removed, completing the processing of the thin titanium LGDL.

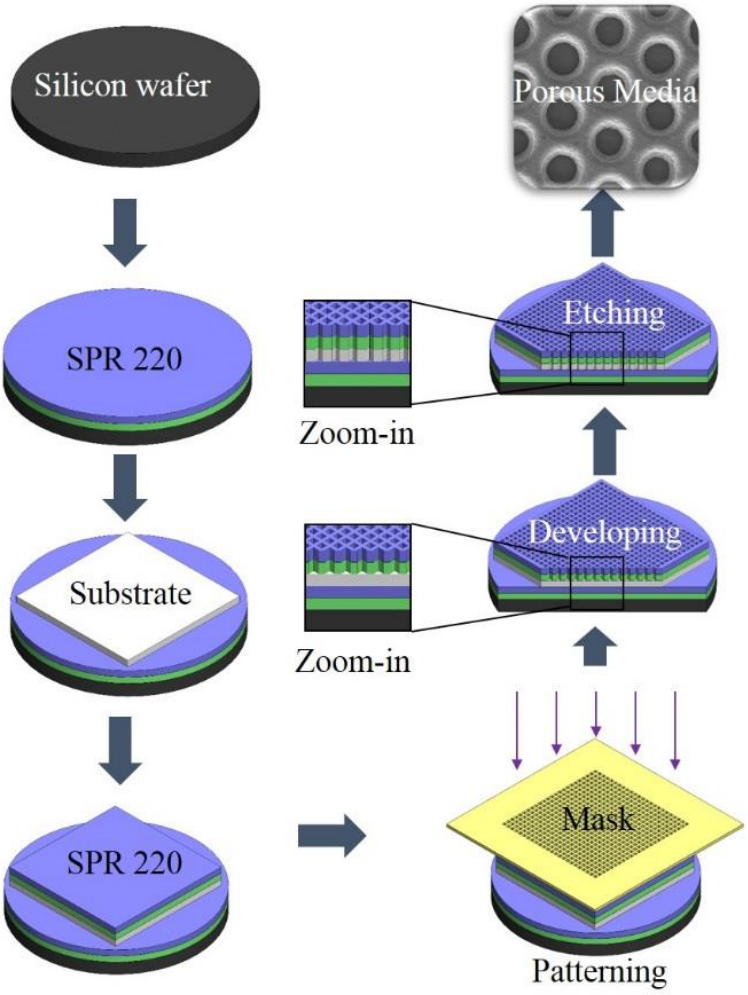

Figure 11. Typical fabrication process for thin titanium LGDLs.

Introduction of the high-speed and micro-scale visualization system

To observe the phenomena of electrochemical reaction inside an operation PEMEC, a high-speed and micro-scale visualization system (HMVS) was built and used with a transparent PEMEC by taking advantage of new LGDL development, which is shown in Figure 12. To get the visual image from inside of PEMEC, the following modifications were made to the conventional electrolyzer cells: (i) a rectangular hole was cut into the anode end plate as an observation window; (ii) the copper anode current distributor was removed; and (iii) the graphite anode bipolar plate with a parallel flow field was separated into two parts, one was a transparent block with flow-in hole, the other one was a thin titanium plate serving as the flow channel. In the transparent electrolyzers, the anode LGDL flow fields with current distributors were made chemically through etching titanium plates to form flow channels with lands for current distributions. They were capped by transparent plates and visually accessed through a rectangular window in the aluminum end plate. A 25 μm titanium thin film with 791 μm circular pores was installed as the LGDL during operation of PEM water electrolyzer. The channel width was 1061 μm. These changes allow for optical imaging of the anode. A high-speed micro-scale visualization system was possible using a high speed camera Phantom V711 and long-distance optical system (Infinity K2 DistaMax). With the V711, a maximum speed of 7530 frames-per-second at full resolution can be achieved. At reduced resolutions, the camera can deliver up to 680,000 frames-per-second or up to 1,400,000 fps with the FAST option. With all this equipment and design,

local O_2 formation can be monitored and analyzed based on micro-scale bubble formation in transparent/operational PEMECs by HMVS.

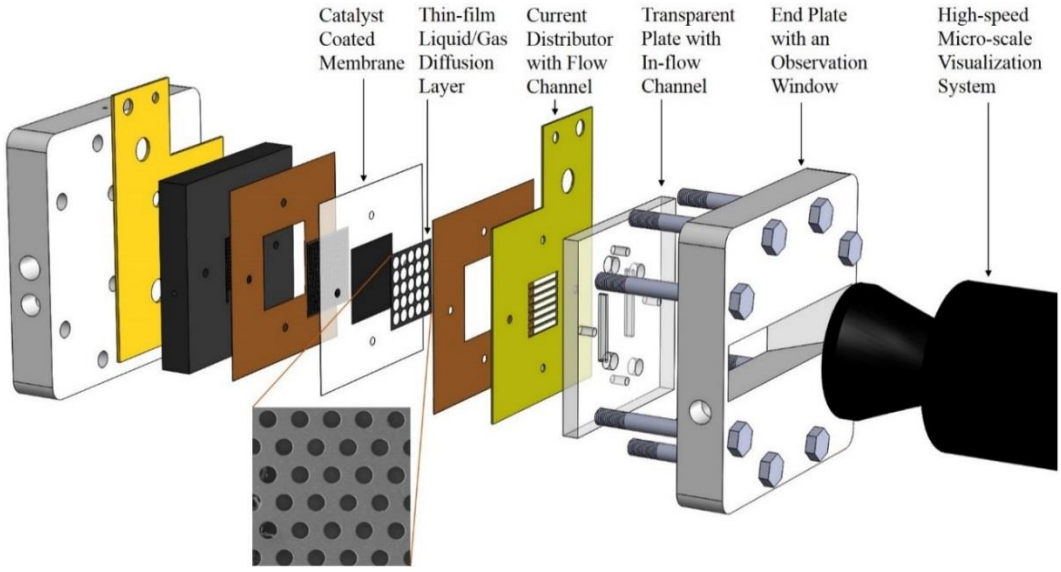

Figure 12. Schematic of high-speed micro-scale visualization system (HMVS) and transparent PEMEC with thin film/well tunable LGDL.

Nomenclature

BP	=	Bipolar Plate
CCM	=	Catalyst Coated Membrane
CD	=	Current Distributor
CL	=	Catalyst Layer
CPE	=	Constant Phase Element
DI	=	De-ionized
EDS	=	Energy Dispersive X-Ray Spectroscopy

EEC	=	Equivalent Electrical Circuit
EIS	=	Electrochemical Impedance Spectroscopy
F	=	Fluorine
HAADF	=	High Angle Annular Dark Field
Ir	=	Iridium
LGDL	=	Liquid/Gas Diffusion Layer
MG	=	Modular Galvanodynamic
ML	=	Microporous Layers
MPD	=	Mean Pore Diameter
MPL	=	Micro Porous Layer
PEM	=	Proton Exchange Membrane
PEMEC	=	Proton Exchange Membrane Electrolyzer Cell
PEMFC	=	Proton Exchange Membrane Fuel Cell
Pt	=	Platinum
Ru	=	Ruthenium
SE	=	Secondary Electron
SEM	=	Scanning Electron Microscopy
SOEC	=	Solid Oxide Electrolyzer Cell
STEM	=	Scanning Transmission Electron Microscopy
Ti	=	Titanium
TPB	=	Triple Phase Boundary

CHAPTER III

INVESTIGATION OF PORE SHAPE EFFECTS OF NOVEL THIN LGDLS FOR HIGH-EFFICIENCY HYDROGEN/OXYGEN GENERATION AND ENERGY STORAGE

A version of this chapter was originally published by Zhenye Kang:

Zhenye Kang, Jingke Mo, Gaoqiang Yang, Derrick A. Talley, Yifan Li, Feng-Yuan Zhang, Scott T. Retterer, David A. Cullen. "Investigation of Novel Thin LGDLs for High-Efficiency Hydrogen/Oxygen Generation and Energy Storage." *In 15th International Energy Conversion Engineering Conference*, p. 4873. 2017.

I am fully responsible for the work submitted in this publication.

3.1 Abstract

Proton exchange membrane electrolyzer cells (PEMECs) with its high efficiency even at low-temperature operating conditions, have received more attention for hydrogen/oxygen generation and energy storage. Liquid/gas diffusion layers (LGDLs), which are located between the catalyst layers (CLs) and bipolar plates (BPs), play an important role in enhancing the performance of water splitting in PEMECs. They are expected to transport electrons, heat, and reactants/products simultaneously with minimum voltage, current, thermal, interfacial, and fluidic losses. In this study, a set of novel planar titanium based thin LGDLs with straight-through pores and well-tunable pore morphologies, named as TT-LGDLs, is developed by taking advantage of advanced micro/nano manufacturing methods. The TT-LGDLs with different pore shapes have been in-situ tested in a regular PEMEC and the novel TT-LGDLs have achieved a superior performance, which is only 1.639 V at 2.0 A/cm^2 and 80 ^{o}C with a commercial catalyst coated membrane (CCM). This

novel TT-LGDLs can be a new guide for future research and development towards high-efficiency and low-cost hydrogen energy

3.2 Introduction

Sustainable energy sources, especially the solar energy, are very attractive in human space exploration, which can be used to generate power for the equipment in the space station/ship. In addition, the environment and life support system need to provide sufficient oxygen for the astronauts and sustain a comfortable living environment [1-4]. Therefore, a sustainable, high-efficiency, and robust electrochemical energy storage/conversion or a hybrid system to accommodate the space exploration becomes more critical.

An advanced proton exchange membrane electrolyzer cell (PEMEC), which is a reverse PEM fuel cell (PEMFC), has been considered as a very attractive energy storage method for producing hydrogen/oxygen from water splitting when coupled with renewable energy sources [5-10]. Due to the presence of ice on other planetary, as shown in Figure 13, the PEMECs coupled with solar energy sources can provide oxygen/hydrogen for future living and propulsion fuel [3]. A PEMEC mainly consists of a catalyst-coated membrane sandwiched by anode and cathode electrodes. Each electrode includes a catalyst layer (CL), a liquid/gas diffusion layer (LGDL), and a bipolar plate (BP), which also acts as the current distributor (CD) and the flow field [11], as shown in Figure 14.

After electricity being applied, water is split into oxygen, protons, and electrons at the anode side. Oxygen is ideally transported from the CL through the LGDL back to the flow

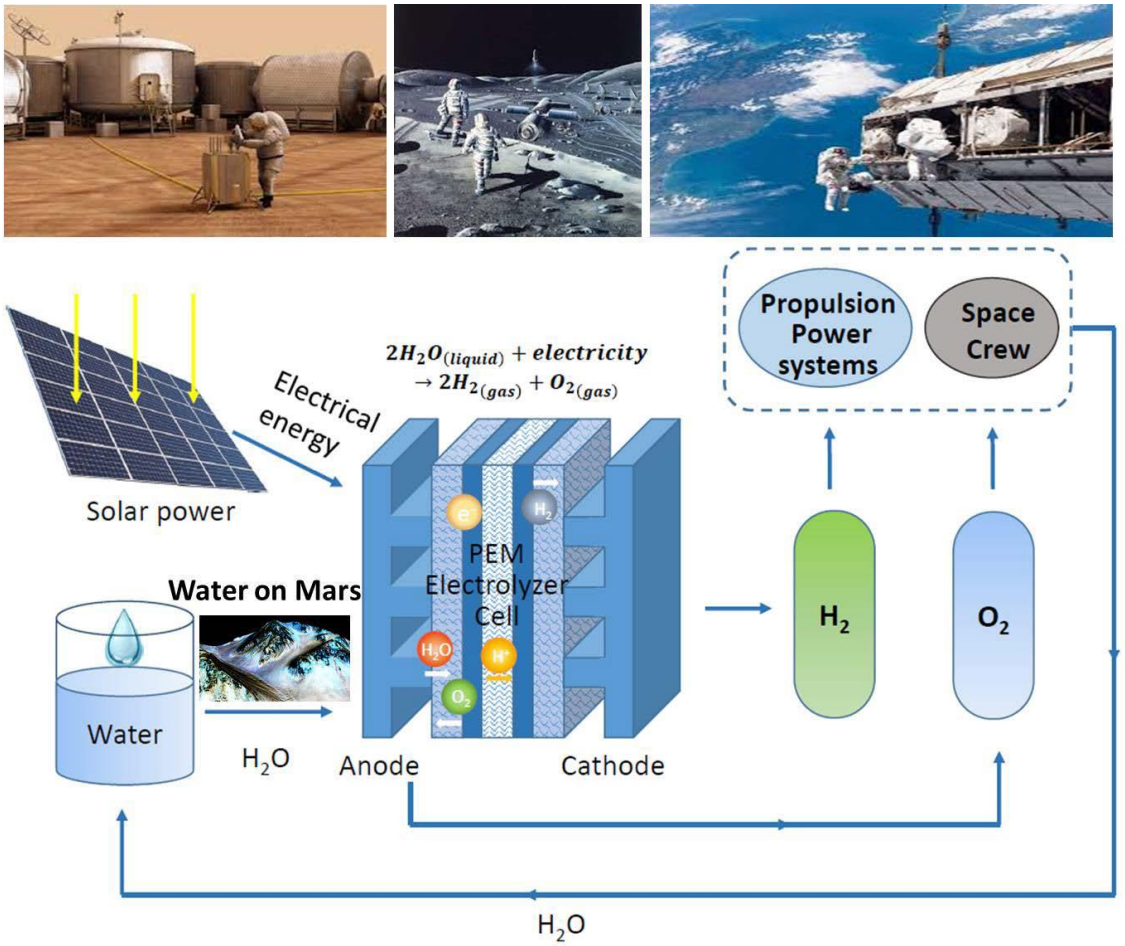

Figure 13. High-efficiency oxygen/hydrogen generation and energy storage in space applications.

field to avoid blocking the LGDL, and hindering the reaction. Electrons, which are also generated at anode CLs, pass through the LGDL, flow to the external circuit. Meanwhile, protons transport through the membrane to the cathode and react with electrons to form hydrogen. H_2/O_2 can be produced and stored continuously as long as water and electricity are supplied [12].

The anode resides in a harsh environment, which is highly corrosive due to the high overpotential and humidity [13-15]. Ideal anode LGDLs should have good conductivity, high corrosion resistance, good two-phase transport capability and mechanical strength [5]. The previous studies, so far, have focused on investigating conventional titanium LGDLs, including felts, woven meshes, or foams [4, 16-18]. The thickness of these LGDLs were hundreds of microns with significantly longer electrically conductive path lengths and higher fluidic resistances. In addition, their fiber/foam-based pore morphologies result in not only nonuniform interfacial contacts, but also random pore sizes and distributions. Therefore, novel LGDLs with tunable and controlled pore morphologies are strongly desired.

In this study, a novel thin titanium based LGDLs with planar surface, straight-through pores and well-tunable pore morphologies were developed and fabricated by photo-lithography and chemical wet etching. The novel thin/tunable LGDLs (TT-LGDLs) with different pore shapes and pore morphologies were investigated in a regular PEMEC, both the electro-potential performance and electrochemical impedance spectroscopy (EIS) were tested and analyzed.

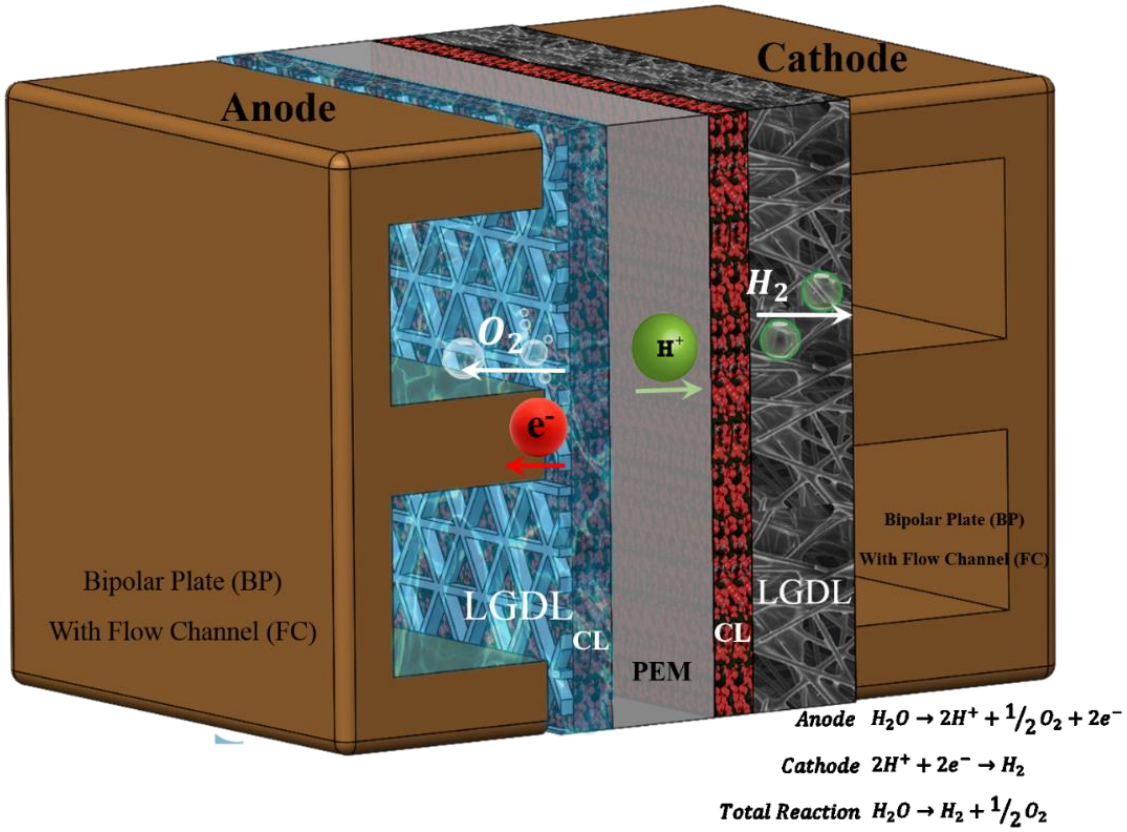

Figure 14. Schematic of PEMECs with TT-LGDLs at anode electrode.

3.3 Experimental Details

The fabrication procedure for the novel titanium TT-LGDLs begins with the design and fabrication of the photomasks, which is the most important step to control the pore size, pore shape, and porosity of LGDLs [11, 19]. A mask pattern was designed using commercially available CAD/VLSI software (LayoutEditor, layouteditor.net). The design pattern was imported into a Heidelberg DWL 66 laser lithography system and patterned on a soda-lime glass mask plate that is pre-coated with chromium and photoresist. After patterning, the masks were developed for 1 minute in Microposit® MF® CD-26 Developer (Shipley Company, Marlborough, MA), rinsed with DI water and dried in N_2. Masks were then submerged in chrome etchant for 2 minutes, rinsed with DI water and dried in N_2. The remaining resist was subsequently removed in a heated bath (70 ^oC) of N-methyl pyrolidone (NMP). The titanium thin film was placed on the resist-coated silicon wafer with special care due to its delicate features, and gently heated for 90 s at 115 ^oC. A second layer of adhesion promoter (MicroPrime MP-P20, ShinEtsuMicroSi) and MEGAPOSIT™ SPR™ 220 photoresist (MicroChem) was applied to the titanium foil under identical conditions, and then exposed to UV light using conventional contact photolithography. It was then developed in Microposit® MF® CD-26 developer (Shipley Company, Marlborough, MA), rinsed with DI water and dried in N_2. After patterning the photoresist mask on the foil, the patterned material was etched in HF. The photoresist was the removed, completing the processing of the TT-LGDL. Figure 15 shows the SEM image comparison

of conventional Ti felt LGDL and the novel TT-LGDL with a triangle pore and a pore length of 644 µm and a porosity of 0.59.

The novel TT-LGDLs were evaluated in a regular PEMEC, which was compressed by two end-plates that were made from aluminum. The current distributor, which was made from copper, was inserted between the bipolar plate and end-plate at both the anode and cathode. The bipolar plates, which were made from graphite materials, had 14 parallel flow channels on it and the dimension of each channel was 0.79 mm*0.79 mm*19.35 mm. The TT-LGDLs with 25.4 µm thickness and carbon paper (Toray 090 with 280 µm thickness and porosity of 0.78) were used as anode and cathode LGDLs, respectively.

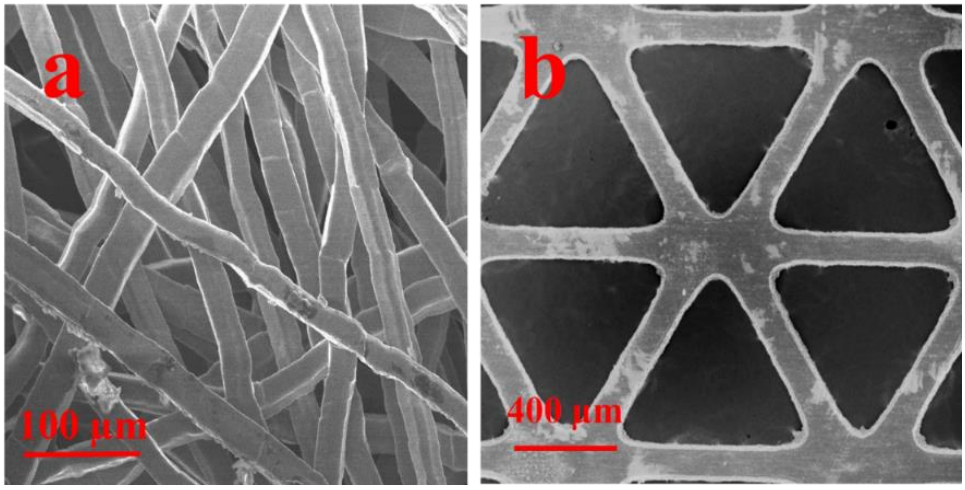

Figure 15. SEM image of the LGDLs. (a) Conventional Ti felt. (b) TT-LGDLs with triangle pore.

The catalyst-coated membrane (CCM) (Electrolyzer CCM from FuelCellsEtc, EZ-CCM) was comprised of a Nafion 115 membrane, which was made of a perfluorosulfonic polymer with a thickness of 125 µm, an anode catalyst layer with an IrRuOx catalyst loading of 3.0

mg/cm^2, and a cathode layer with a platinum black (PtB) catalyst loading of 3.0 mg/cm^2 with a 5 cm^2 working area. The detailed information was shown in Table 5. The PEMEC was attached to an electrolyzer control system with current range up to 100 A and voltage range up to 5 V. The hardware was controlled by EC-Lab, an electrochemical analysis software from Bio-Logic, which was used to evaluate performance and perform electrochemical impedance spectroscopy (EIS). For controlling the flow, a system of tubing was connected to the PEMEC. While the cathode tubing was merely intended to safely exhaust hydrogen gas that formed during electrolysis, a diaphragm liquid pump from KNF Neuberger was used to supply de-ionized (DI) water at a constant volumetric flow rate of 20 ml/min to the anode. The water bath (General Purpose Water Baths of Model WB10 from PolyScience) was used to preheat the DI water to designed temperatures. Two heaters were inserted into the end-plates at both anode and cathode to heat the PEMEC, and two thermocouples were inserted into the bipolar plates at both anode and cathode to measure the temperature. Both of the heaters and thermocouples were connected to a temperature control system (Multi-Zone controller from OMEGA).

3.4 Results and Discussion

The novel TT-LGDLs were tested in a standard PEMEC and the polarization curve and electrochemical impedance spectroscopy (EIS) were used to evaluate and analyze the performance of the PEMEC. Figure 16(a) shows the polarization curve and HFR of PEMECs with the TT-LGDL or Ti felt at anode side, which indicates the performance of the PEMECs. It can be seen that the voltage reaches only 1.6716 V at the operating

Table 5. PEMECs characteristics and experimental conditions.

Characteristics and conditions	Value
Membrane Type	Nafion® 115
Membrane Thickness	125 µm
Catalsyt Active Area	5 cm^2
Anode Catalyst Loading	3.0 mg/cm^2 ($IrRuO_x$)
Cathode Catalyst Loading	3.0 mg/cm^2 (PtB)
Anode LGDL	Titanium based TT-LGDLs
Cathode LGDL	Toray 090 carbon paper
Operating Temperature	80 ^oC
Operating Pressure	1 atm
Anode Water Flow Rate	20 ml/min

conditions of 2.0 A/cm^2 and 80 ^{o}C, which is much lower than the one with conventional Ti felt LGDLs. The HFR indicates the total ohmic resistance of the whole PEMEC, which mainly consists of the resistance of each components, including PEM, CLs, LGDLs, bipolar plate, etc. and interfacial resistances between each component. The main ohmic loss comes from the PEM and interfacial resistances. The planar surface of the TT-LGDLs improves the contacts between the CL/LGDL and LGDL/BP interfaces, which help to reduce the ohmic resistance.

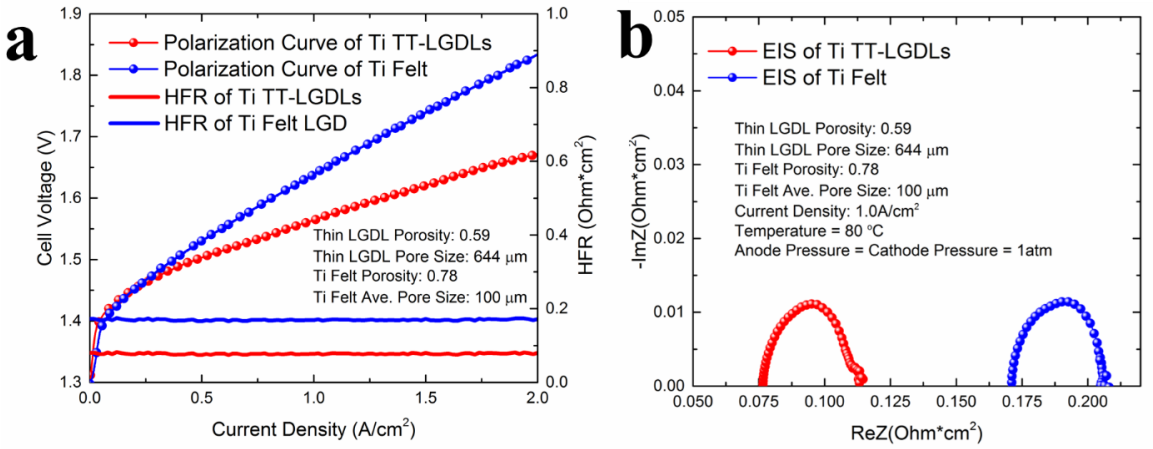

Figure 16. Comparison between conventional Ti felt and novel Ti based TT-LGDLs. (a) Performance and HFR. (b) EIS curves at 1.0 A/cm^2.

EIS is a very useful *in situ* method for analyzing PEMEC performance by measuring the impedance of a system at different frequencies. In this study, EIS is conducted on PEMECs with different titanium LGDLs during performance testing at 80 ^{o}C and with a current density of 1.0 A/cm^2. The scan frequency is set from high to low frequency (15 kHz to 10 mHz). A Nyquist plot of EIS result is shown in Figure 16(b). There are two x-intercepts:

the left one (at the high frequency part) indicates the ohmic loss and the right one (at the low frequency part) is the sum of the resistance. The distance between the two intercepts indicates the sum of activation and mass transport losses [5]. The diameter of the first semicircle mainly indicates the activation resistance. Thereby, the second semicircle indicates the mass transport loss. It can be seen that the right x-intercept is in accordance with the HFR in Figure 16(a), which all represent the ohmic resistance. The TT-LGDLs can achieve much smaller ohmic resistance than Ti felt, which contribute to the better performance of PEMECs.

The TT-LGDLs with different pore shapes and parameters were also investigated and the detailed parameters were listed in Table 6. Figure 17 shows the microscope images for the samples with different pore morphologies. It can be seen that the pore shapes are well controlled, the shapes can be circular, triangle, and square. In addition, the pore distributed uniformly on the TT-LGDLs according to the designed patterns. The pore size and distance between each pore can also be precisely controlled. The pore size was varied from ~200 μm to ~900 μm, and the porosity was in the range of 0.26 to 0.76, which is a wide range for the micro pore morphology.

All the 9 TT-LGDLs were *in-situ* tested in a PEMEC and the polarization curves were shown in Figure 18. From the previous studies, it has been found that the TT-LGDLs with circular pore shape can achieve superior performance, and the smaller pore size and large porosity help to improve the performance [5, 13]. Therefore, it is expected that the TT-LGDLs with triangle and square pore shapes would also follow this rule.

Table 6. TT-LGDLs parameters and cell voltage at 2.0 A/cm^2.

Index of the TT-LGDLs	Pore Shape	Pore Size [µm]	Hydraulic Diameter of the Pore [µm]	Porosity	Cell Voltage [V]
C1	Circular	220	220	0.55	1.678
C2		414	414	0.62	1.681
C3		632	632	0.76	1.681
T1	Triangle	176	117	0.26	1.672
T2		644	430	0.59	1.672
T3		882	588	0.76	1.663
S1	Square	215	215	0.50	1.649
S2		418	418	0.70	1.639
S3		623	623	0.76	1.655

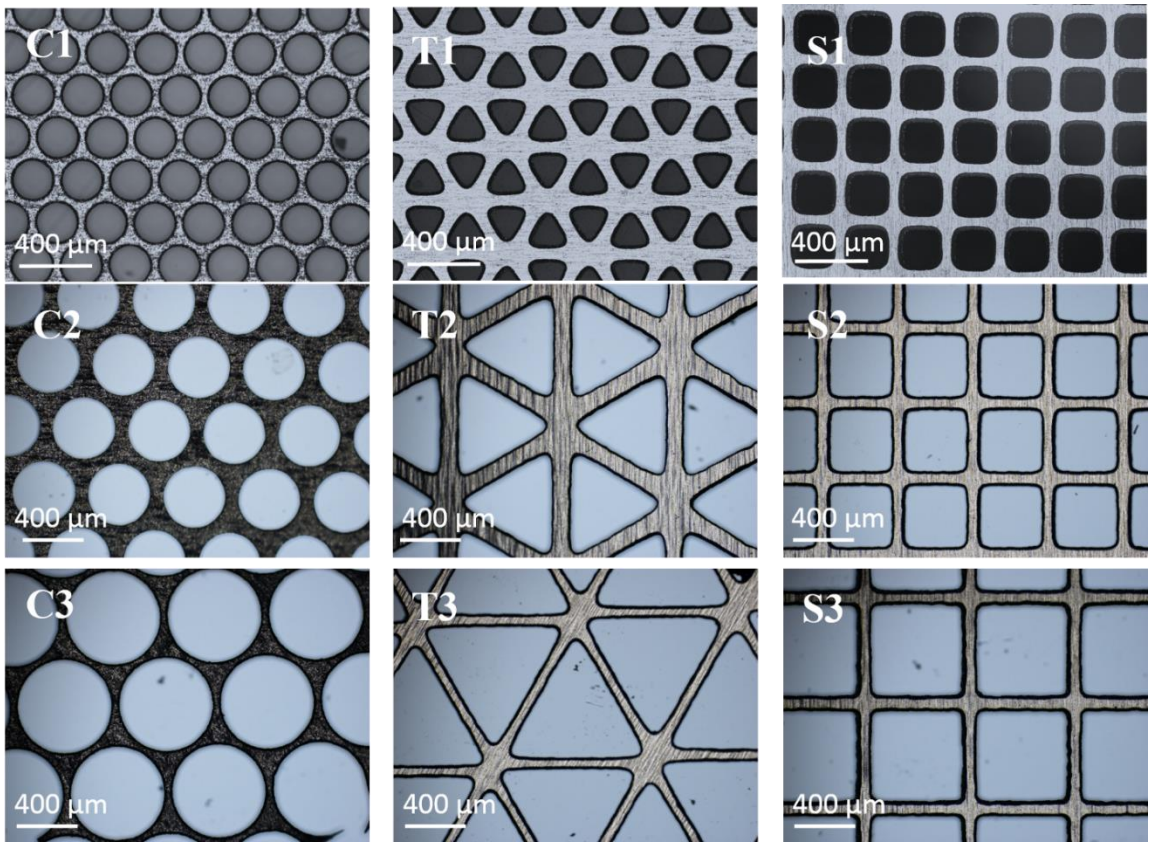

Figure 17. Microscope images of the TT-LGDLs with different pore shapes and parameters.

The samples were compared under similar parameters, such as pore size, hydraulic diameter, and porosity. From Figure 18(A), the TT-LGDLs with square pore shape and similar hydraulic diameter can get better performance than the one with triangle and circular pore shapes. It can be seen that the square TT-LGDLs has the largest porosity, which is a reason for the good performance. In order to eliminate the effects of porosity, Figure 18(B) shows the TT-LGDLs with the same porosity of 0.76 and similar hydraulic diameter of around 600 μm, and the square pore shape TT-LGDLs also achieve better performance than the other two samples. The performance of TT-LGDLs with similar pore sizes were shown in Figure 18(C) and (D), and the results had the same trend with (A) and (B): the performance of square TT-LGDLs is better than triangle TT-LGDLs, and the performance of triangle TT-LLGDL is better than circular TT-LGDLs. It should be noticed that the triangle TT-LGDLs has the better performance than circular TT-LGDLs, although the triangle TT-LGDLs has a much smaller porosity than circular TT-LGDLs, as shown in Figure 18(C) and (D). It can be concluded that the pore shape of the TT-LGDLs has some effects on the PEMEC performance: the square TT-LGDLs has the best performance, and the circular TT-LGDLs has the worst performance with a similar pore morphology.

Table 6 shows the cell voltage of the PEMECs at 2.0 A/cm^2 and 80 ^oC. It can be seen that the cell voltage of the square TT-LGDLs has the lowest range that is varied from 1.639 V to 1.655 V, the triangle TT-LGDLs has a higher range that is varied from 1.663 V to 1.672 V, and the circular TT-LGDLs has the highest range that is varied from 1.678 V to 1.681 V, which proves that the square pore shape can help to improve the PEMEC performance.

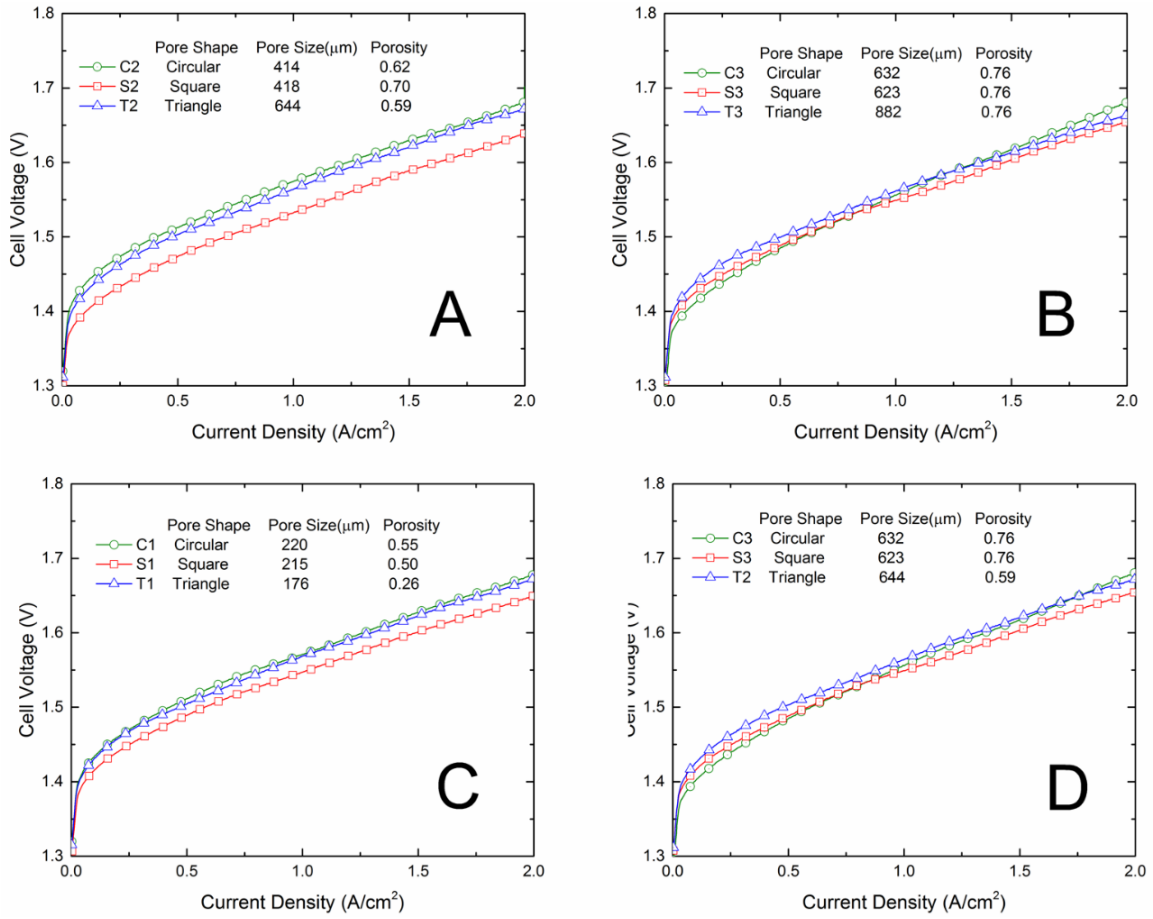

Figure 18. Performance of TT-LGDLs with different pore shapes. (A) Similar hydraulic diameter around 420 μm. (B) Same porosity of 0.76. (C) Similar pore size around 200 μm. (D) Similar pore size around 630 μm.

In addition, no matter what the pore shape is, the smaller pore size and larger porosity can enhance the PEMEC performance, which is accordance with our previous study [5]. The square TT-LGDLs with 418 μm pore size and 0.70 porosity has obtained an superior performance with a commercial CCM, compared with any public literatures, which is only 1.639 V at 2.0 A/cm^2 and 80 ^{o}C [2, 5, 20-22].

3.5 Conclusion

In this study, a set of titanium-based TT-LGDLs with different pore morphologies was fabricated and *in-situ* tested in a PEMEC. The novel TT-LGDLs have a planar surface, straight-through pores, thin thickness (only 25 μm) and well-tunable pore morphologies, which contribute to smaller interfacial contact resistance, two-phase transport losses, and better PEMEC performance. The TT-LGDLs can achieve much better performance than conventional Ti felt LGDL, which is a very thick porous media made of Ti fibers and has a random pore morphology. The superior performance (1.639 V at 2.0 A/cm^2 and 80 ^{o}C) has been achieved by a square TT-LGDLs with 418 μm pore size and 0.70 porosity. In addition, it has been found that the square is the best and the circular is the worst pore shape among the three different designs. The TT-LGDLs with square pore shape can achieve better PEMEC performance than triangle and circular TT-LGDLs with a similar pore morphology. In addition, the PEMEC performance can be further improved by TT-LGDLs with smaller pore size and larger porosity. Due to the thin features of the novel TT-LGDLs, not only the thickness/volume/weight of the PEMEC stack can be reduced greatly, but also the materials used for LGDLs can be decreased which helps to reduce the cost. The well-

tunable pore morphologies are extremely valuable to advance numerical modeling of electrochemical reactions and associated multiphase flow as well. Since all the TT-LGDLs in this study have a better performance than the conventional LGDLs, such as titanium felt and woven mesh, they are expected to have many potential applications in energy and environmental engineering.

References

[1] Ayers KE, Dalton LT, Anderson EB. (Invited) Efficient Generation of High Energy Density Fuel from Water. *Ecs Transactions*. 2012;41:27-38.

[2] Carmo M, Fritz DL, Mergel J, Stolten D. A comprehensive review on PEM water electrolysis. *Int J Hydrogen Energ*. 2013;38:4901-34.

[3] Mo J, Steen SM, III BH, Kang Z, Terekhov A, Zhang F-Y, Retterer ST, Cullen DA. Investigation of titanium felt transport parameters for energy storage and hydrogen/oxygen production. 13th International Energy Conversion Engineering Conference. AIAA 2015-39142015. p. 3914.

[4] Han B, Mo J, Kang Z, Zhang F-Y. Effects of membrane electrode assembly properties on two-phase transport and performance in proton exchange membrane electrolyzer cells. *Electrochim Acta*. 2016;188:317-26.

[5] Kang Z, Mo J, Yang G, Retterer ST, Cullen DA, Toops TJ, Green Jr JB, Mench MM, Zhang F-Y. Investigation of thin/well-tunable liquid/gas diffusion layers exhibiting superior multifunctional performance in low-temperature electrolytic water splitting. *Energ Environ Sci*. 2017;10:166-75.

[6] Ager JW, Shaner MR, Walczak KA, Sharp ID, Ardo S. Experimental demonstrations of spontaneous, solar-driven photoelectrochemical water splitting. *Energ Environ Sci*. 2015;8:2811-24.

[7] Turner JA. A realizable renewable energy future. *Science*. 1999;285:687-9.

[8] Hong WT, Risch M, Stoerzinger KA, Grimaud A, Suntivich J, Shao-Horn Y. Toward the rational design of non-precious transition metal oxides for oxygen electrocatalysis. *Energ Environ Sci*. 2015;8:1404-27.

[9] Han B, Steen S, Mo J, Zhang F-Y. Modeling of interfacial resistance effects on the performance and efficiency for electrolyzer energy storage. 13th International Energy Conversion Engineering Conference2015. p. 3915.

[10] Mo J, Kang Z, Retterer ST, Cullen DA, Toops TJ, Green JB, Mench MM, Zhang F-Y. Discovery of true electrochemical reactions for ultrahigh catalyst mass activity in water splitting. *Science Advances*. 2016;2:e1600690.

[11] Yang G, Mo J, Kang Z, III FAL, Green J, Babu SS, Zhang F-Y. Additive manufactured bipolar plate for high-efficiency hydrogen production in proton exchange membrane electrolyzer cells. *Int J Hydrogen Energ*. 2017. 10.1016/j.ijhydene.2017.04.100.

[12] Han B, Mo J, Kang Z, Yang G, Barnhill W, Zhang F-Y. Modeling of two-phase transport in proton exchange membrane electrolyzer cells for hydrogen energy. *Int J Hydrogen Energ*. 2017;42:4478-89. doi: 10.1016/j.ijhydene.2016.12.103.

[13] Mo J, Kang Z, Yang G, Retterer ST, Cullen DA, Toops TJ, Green JB, Zhang F-Y. Thin liquid/gas diffusion layers for high-efficiency hydrogen production from water splitting. *Appl Energ*. 2016;177:817-22.

[14] Mo J, Steen S, Zhang F-Y. High-speed and micro-scale measurements of flow and reaction dynamics for sustainable energy storage. 13th International Energy Conversion Engineering Conference. AIAA 2015-39132015. p. 3913.

[15] Steen III SM, Mo J, Kang Z, Yang G, Zhang F-Y. Investigation of Titanium Liquid/Gas Diffusion Layers in Proton Exchange Membrane Electrolyzer Cells. *International Journal of Green Energy*. 2016;14:162-70.

[16] Hwang CM, Ishida M, Ito H, Maeda T, Nakano A, Hasegawa Y, Yokoi N, Kato A, Yoshida T. Influence of properties of gas diffusion layers on the performance of polymer electrolyte-based unitized reversible fuel cells. *Int J Hydrogen Energ*. 2011;36:1740-53.

[17] Ito H, Maeda T, Nakano A, Hwang CM, Ishida M, Kato A, Yoshida T. Experimental study on porous current collectors of PEM electrolyzers. *Int J Hydrogen Energ*. 2012;37:7418-28.

[18] Ito H, Maeda T, Nakano A, Kato A, Yoshida T. Influence of pore structural properties of current collectors on the performance of proton exchange membrane electrolyzer. *Electrochim Acta*. 2013;100:242-8.

[19] Mo J, Steen SM, Retterer S, Cullen DA, Terekhov A, Zhang F-Y. Mask-Patterned Wet Etching of Thin Titanium Liquid/Gas Diffusion Layers for a PEMEC. *Ecs Transactions*. 2015;66:3-10.

[20] Xu J, Liu G, Li J, Wang X. The electrocatalytic properties of an IrO 2/SnO 2 catalyst using SnO 2 as a support and an assisting reagent for the oxygen evolution reaction. *Electrochim Acta*. 2012;59:105-12.

[21] Spurgeon JM, Lewis NS. Proton exchange membrane electrolysis sustained by water vapor. *Energ Environ Sci*. 2011;4:2993-8.

[22] Grigoriev S, Millet P, Volobuev S, Fateev V. Optimization of porous current collectors for PEM water electrolysers. *Int J Hydrogen Energ*. 2009;34:4968-73.

Appendix

Nomenclature

BP = Bipolar plate

CCM = Catalyst coated membrane

CD = Current distributor

CL = Catalyst layer

EIS = Electrochemical impedance spectroscopy

HFR = High frequency resistance

LGDL = Liquid/gas diffusion layer

PEM = Proton exchange membrane

PEMEC = Proton exchange membrane electrolyzer cell

PEMFC = Proton exchange membrane fuel cell

SEM = Scanning electron microscopy

TT-LGDL = Thin/tunable liquid/gas diffusion layer

CHAPTER IV

THIN FILM SURFACE MODIFICATIONS OF THIN/TUNABLE LIQUID/GAS DIFFUSION LAYERS FOR HIGH-EFFICIENCY PROTON EXCHANGE MEMBRANE ELECTROLYZER CELLS

A version of this chapter was originally published by Zhenye Kang:

Zhenye Kang, Jingke Mo, Gaoqiang Yang, Yifan Li, Derrick A. Talley, Scott T. Retterer, David A. Cullen, Todd J. Toops, Michael P. Brady, Guido Bender, Bryan S. Pivovar, Johney B. Green Jr, Feng-Yuan Zhang. "Thin film surface modifications of thin/tunable liquid/gas diffusion layers for high-efficiency proton exchange membrane electrolyzer cells." *Applied Energy* 206 (2017): 983-990.

I am fully responsible for the work submitted in this publication.

4.1 Abstract

A proton exchange membrane electrolyzer cell (PEMEC) is one of the most promising devices for high-efficiency and low-cost energy storage and ultrahigh purity hydrogen production. As one of the critical components in PEMECs, the titanium thin/tunable LGDL (TT-LGDL) with its advantages of small thickness, planar surface, straight-through pores, and well-controlled pore morphologies, achieved superior multifunctional performance for hydrogen and oxygen production from water splitting even at low temperature. Different thin film surface treatments on the novel TT-LGDLs for enhancing the interfacial contacts and PEMEC performance were investigated both in-situ and ex-situ for the first time. Surface modified TT-LGDLs with about 180 nm thick Au thin film yielded performance improvement (voltage reduction), from 1.6849 V with untreated TT-LGDLs to only 1.6328 V with treated TT-LGDLs at 2.0 A/cm2 and 80 °C. Furthermore, the hydrogen/oxygen

production rate was increased by about 28.2% at 1.60 V and 80 °C. The durability test demonstrated that the surface treated TT-LGDL has good stability as well. The gold electroplating surface treatment is a promising method for the PEMEC performance enhancement and titanium material protection even in harsh environment.

4.2 Introduction

Sustainable energy resources, including solar, wind, and tide, generate electricity intermittently, which leads to challenges in supplying continuous power to the electrical grid and a large amount of energy has been wasted due to this reason [1-8]. High-efficiency and robust electrochemical energy storage or conversion systems coupled with the sustainable energy resources would accommodate seasonal, daily or even hourly changes and it is promising for future smart grid [7-15]. Energy can be stored in the form of chemical, electrical, kinetic, potential or thermal devices and they can be used directly or indirectly via an energy conversion system. The ideal energy storage system should exhibit high performance and low cost to meet the certain requirements [16]. At present, battery is the most widely used method to store and mitigate the intermittent energy sources [17]. Hydrogen can also be an ideal energy carrier due to its high energy density and environment-friendly, which will not generate any greenhouse gases, like CO_2, during its usage [18-24]. Currently, there are many ways to produce hydrogen, such as steam reforming of hydrocarbons or alcohols, water electrolysis, and etc. [20]. Water electrolysis is the foremost technology for producing high purity hydrogen with its advantages of the ability to rapidly follow an intermittent load for grid-balancing that is caused by differences

in supply and demand for energy generation and consumption [25]. Proton exchange membrane electrolyzer cells (PEMECs), which act as a reverse proton exchange membrane fuel cells (PEMFCs), have been regarded as a very promising method of hydrogen production for energy storage by water splitting [26-33]. PEMECs also yield very high purity hydrogen gas, which is beneficial for storage and future energy production by multiple methods [34-37].

A typical PEMEC mainly consists of a catalyst coated membrane (CCM), which is sandwiched between two electrodes (anode and cathode). At the anode side, water is split into molecular oxygen, protons, and electrons, which leads to a harsh operating environment for the PEMEC components, i.e. high potential and humidity [22, 38]. Therefore, the components of the anode electrode, such as LGDL and bipolar plate (BP), require very high corrosion resistance. Titanium (Ti) based LGDLs are widely used as anode LGDL due to their good bulk conductivity, high corrosion resistivity, and excellent mechanical strength. The conventional Ti based LGDLs, including Ti felt, Ti mesh, and sintered Ti powers, have been widely used and investigated in PEMECs [37-42]. However, resistance to corrosion in such systems is achieved by surface oxide formation, which can increase surface electrical resistivity and detrimentally impact cell performance [22].

Ito et al. carried out PEMEC experiments focusing on the porosity and pore diameter of titanium felt LGDLs. Their results showed that the electrolysis performance can be improved by decreasing the mean pore diameter (MPD) of the LGDL when the MPD was larger than 10 μm. And they also pointed out that the porosity had no significant effect on

the electrolysis performance if the porosity was greater than 0.5 [41]. In another study, the influence of porosity and pore diameter of LGDLs on PEMEC performance was also conducted. The results showed that the oxygen bubbles produced at the anode may block the LGDL when the MPD is less than 50 µm [42]. Hwang *et al*. tested titanium felt by loading titanium powder or polytetrafluoroethylene (PTFE) in the PEMECs. They investigated the effects of pore properties and PTFE content on the PEMEC performance [43]. Grigoriev *et al*. experimentally optimized various parameters of the sintered titanium powder LGDLs. They found that the optimum titanium sphere particle sizes were from 50 to 75 µm, and the pore sizes were around 12 µm [44]. Ioroi *et al*. investigated the wettability of the titanium mesh by loading TiO_2 powder and PTFE. They concluded that the LGDL with hydrophilic property showed better performance than the hydrophobic one [45]. Millet *et al*. stated that the interfacial ohmic resistance between the LGDLs and BPs should be reduced in order to improve the performance of the PEMECs [46]. Oh et al. introduced a pore size gradient structure inside the LGDL in order to improve the performance of a PEMFC, concluding that the pore size gradient structure can enhance the steady-state and transient response [47]. Siracusano *et al*. used a novel short-side chain (SSC) perfluorosulfonic acid (PFSA) membrane to develop low catalyst loading membrane electrode assemblies (MEAs). They have achieved a high current density > 3.0 A/cm^2 with an efficiency >80% and the low catalyst loading MEAs had a very good durability [25]. Mo *et al*. have studied the effect of parameters of Ti felt and Ti mesh LGDLs in a PEMEC, and they found that the thickness of LGDLs have a significant impact on the PEMEC

performance. They also conducted surface treatments such as thermal nitridation and sputter coating, which can improve the PEMEC performance significantly [48].

Previous efforts have been focused on investigation of different kinds of titanium based LGDLs, and modification methods to improve their PEMEC performance. We recently reported a novel thin, planar titanium LGDL with straight-through pores and tunable pore morphologies that was fabricated using advanced micro/nano manufacturing techniques [49-51]. These novel thin/tunable LGDLs (TT-LGDLs) exhibited superior multifunctional performance with values of 1.66 V at 2.0 A/cm^2 and 80 ^{o}C, which to our knowledge exceed the best values reported in the open literature [1, 52]. The TT-LGDLs remarkably reduce ohmic and activation losses with its advantages of planar surface and thin thickness, which is totally different from the conventional Ti felt or foam LGDLs. The planar surface of the TT-LGDLs have already contribute to smaller interfacial contact resistance in PEMECs when compared with conventional LGDLs [1, 52]. There are no public literatures that study the TT-LGDLs surface treatment effects so far. By further reducing the interfacial electrical surface resistance of the TT-LGDLs using surface treatment with the mature and low cost micro/nano technologies, it is anticipated that the performance can be further improved [27].

In this study, different gold surface treatment methods were applied to TT-LGDLs in order to gauge the potential to improve the PEMEC performance for the first time. PEMEC performance was evaluated *in-situ* by polarization and EIS techniques, with microstructural characterization of the LGDLs pre/post testing performed by SEM and

EDS. Furthermore, the 100 hours test of the surface treated TT-LGDLs showed no obvious degradation.

4.3 Experimental Details

The circular pore shape TT-LGDLs with a pore diameter about 414 μm and porosity about 62%, as shown in Figure 19, were fabricated by a combination of conventional contact photolithography and chemical wet etching. The detailed fabrication procedure can be found in our previous work [49, 52]. It can be seen that the novel TT- LGDLs have a planar surface and straight-through pores, which is completely different from conventional LGDLs, such as titanium felt [1]. The TT-LGDLs can significantly improve the PEMEC performance by reducing the mass transport, ohmic and activation losses. The SEM of the TT-LGDL surface characteristics is shown in Figure 19(B) and it can be seen that the surface of the untreated titanium TT-LGDL is very smooth, which contribute to the smaller ohmic resistances in PEMEC compared with conventional Ti felt LGDLs.

The TT-LGDLs were used as a substrate for gold sputter deposition. Plasma modifications and sputter deposition augmentations were both completed using a BIO-RAD Polaron Division SEM Coating System E5150. A potential of 2.4 kV and a current of 20 mA was maintained to control the deposition for gold. The thickness of the coating was controlled by adjusting the operating time. The *in-situ* coated Ti foil was weighed before and after sputter deposition to determine coating thickness.

Gold electroplating was conducted mainly with three steps: electro-cleaning, electro-striking and electro-plating. First, the TT-LGDLs acted as cathode and was put into the 4%

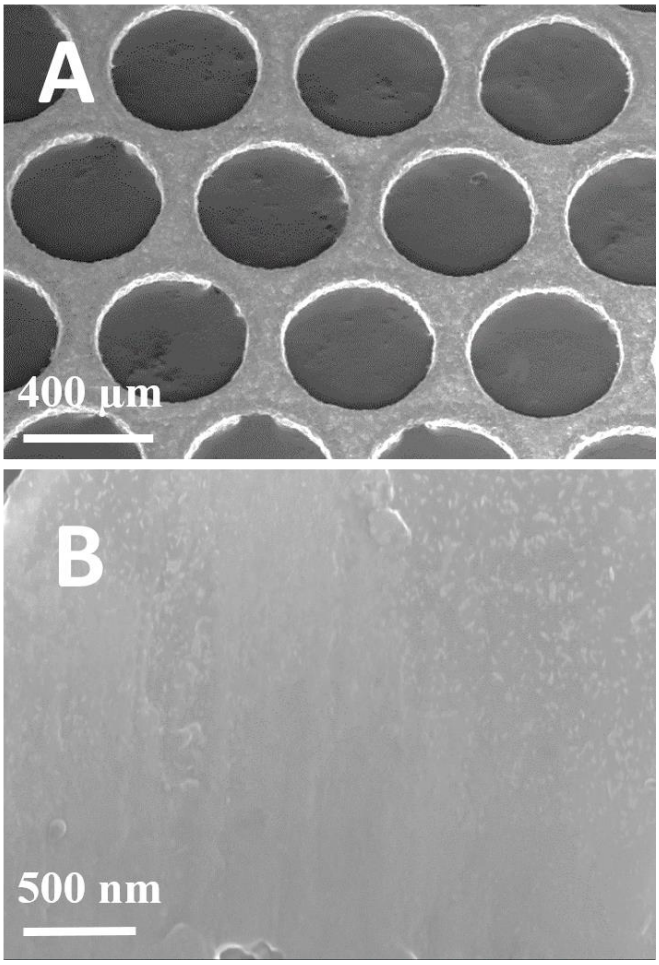

Figure 19. SEM images of the untreated TT-LGDLs (A) Low magnification for untreated TT-LGDLs with a pore diameter about 414 µm and porosity about 0.62 (B) High magnification surface characterization.

solution of sodium hydroxide. A negative potential of 6 V was applied for 45 s at 60 ^{o}C. It was used to clean the sample surface and provided hydrophilic surface properties. Second, the TT-LGDLs were immersed in 24K (also called pure gold or 100 percent gold) acid gold strike solution at room temperature, and a negative voltage of 7 V was applied for 25 s. Third, the TT-LGDLs were moved to the 24K bright gold plating solution at 38 ^{o}C and the time for electro-plating was controlled based on the desired gold thickness. It should be noted that the TT-LGDLs were thoroughly rinsed in DI water after each step.

Commercial CCM made from Nafion 115 (Electrolyzer CCM from FuelCellsEtc, EZ-CCM) with 3.0 mg/cm^2 $IrRuO_x$ at anode and 3.0 mg/cm^2 PtB at cathode was employed, and the working area of the CCM is 5 cm^2. The CCM was sandwiched by anode and cathode electrodes, and the whole cell was compressed by eight evenly distributed bolts which are tightened to 4.52 N m of torque. A fresh carbon paper (Toray 090 from FuelCellStore) with a 280 μm thickness and 78% porosity was used as a cathode LGDL for each test. Graphite plates with a parallel flow channel on it were used as both the anode and cathode bipolar plate. The PEMEC was connected to the control system (Potentiostat VSP/VMP3B-100 from Bio-Logic) with a current range up to 100 A and voltage range up to 5 V. In addition, a diaphragm liquid pump (KNF Neuberger) was used to supply deionized (DI) water at a constant volumetric flow rate of 20 ml/min to the anode. Water was pre-heated to the desired temperature in a water bath (WB10 from PolyScience) before being pumped into the PEMEC. Two heaters coupled with two thermocouples connected to a temperature control system (Multi-Zone controller from OMEGA), were inserted into

the anode and cathode to measure and control the cell temperature.

Each of the TT-LGDL is tested in a regular PEMEC. After the PEMEC is assembled, it is connected to the testing system and heated to 80 ^{o}C. Then the cell is tested at 80 ^{o}C with polarization curve and EIS, which is used to condition the cell. After the conditioning, the cell is cooled down to room temperature and then tested at 23 ^{o}C, 50 ^{o}C and 80 ^{o}C in sequence. After all these tests, the PEMECs are disassembled and the surface of the CCM anode are examined *ex situ* by SEM and EDS.

4.4 Results and Discussions

4.4.1 Effects of the different gold surface treatment methods

Figure 20(A) shows the SEM image of the Au sputter coated TT-LGDLs. The thickness of the Au layer is about 180 nm. It can be seen that the gold is uniformly distributed on the surface, but there are some cracks formed throughout the surface. Figure 20(B) and (C) show the SEM images for the thin LGDLs with different Au thicknesses (about 180 nm and 820 nm, respectively). It can be found that the gold is distributed uniformly around the surface and there are no cracks observed.

Figure 21 shows the EDS results of the untreated and surface treated TT-LGDLs. It can be seen that only titanium is examined with the untreated LGDL. Figure 21(B) and (C) show the EDS results of sputter coated TT-LGDL and electroplated TT-LGDL with the similar Au coating thickness of about 180 nm. The higher peak of Ti in Figure 21(B) is attributed to the cracks formed on the surface of Au thin film, while the Au distributed uniformly

throughout the surface with electroplated LGDLs, the Ti peak is very small in Figure 21(C) and (D).

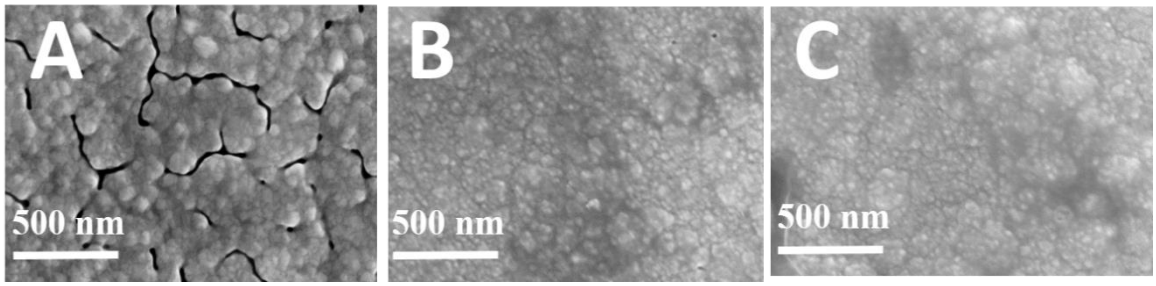

Figure 20. SEM images of the tested TT-LGDLs (A) 180 nm sputter coated thin film gold (B) 180 nm electroplated thin film gold (C) 820 nm electroplated thin film gold.

The performance of PEMECs using both the untreated and gold surface treated TT-LGDLs were evaluated. The polarization curves shown in Figure 22(A) exhibit the performance of the PEMECs. The PEMECs with the untreated TT-LGDLs achieve a voltage of 1.6849 V at 2.0 A/cm^2 and 80 ^{o}C, which is consistent with our previous work with this LGDL design [1, 52]. The performance of the PEMECs was improved to 1.6492 V with sputter coating 180 nm Au thin film on TT-LGDLs, and it can be further improved to 1.6328 V and 1.6382 V with the 180 nm and 820 nm Au electroplated TT-LGDLs, respectively, which exceeds values reported in the open literature [36, 37, 52-56]. It can be found that the different thickness of the electroplated Au layer had very limited effects on the performance of the PEMECs.

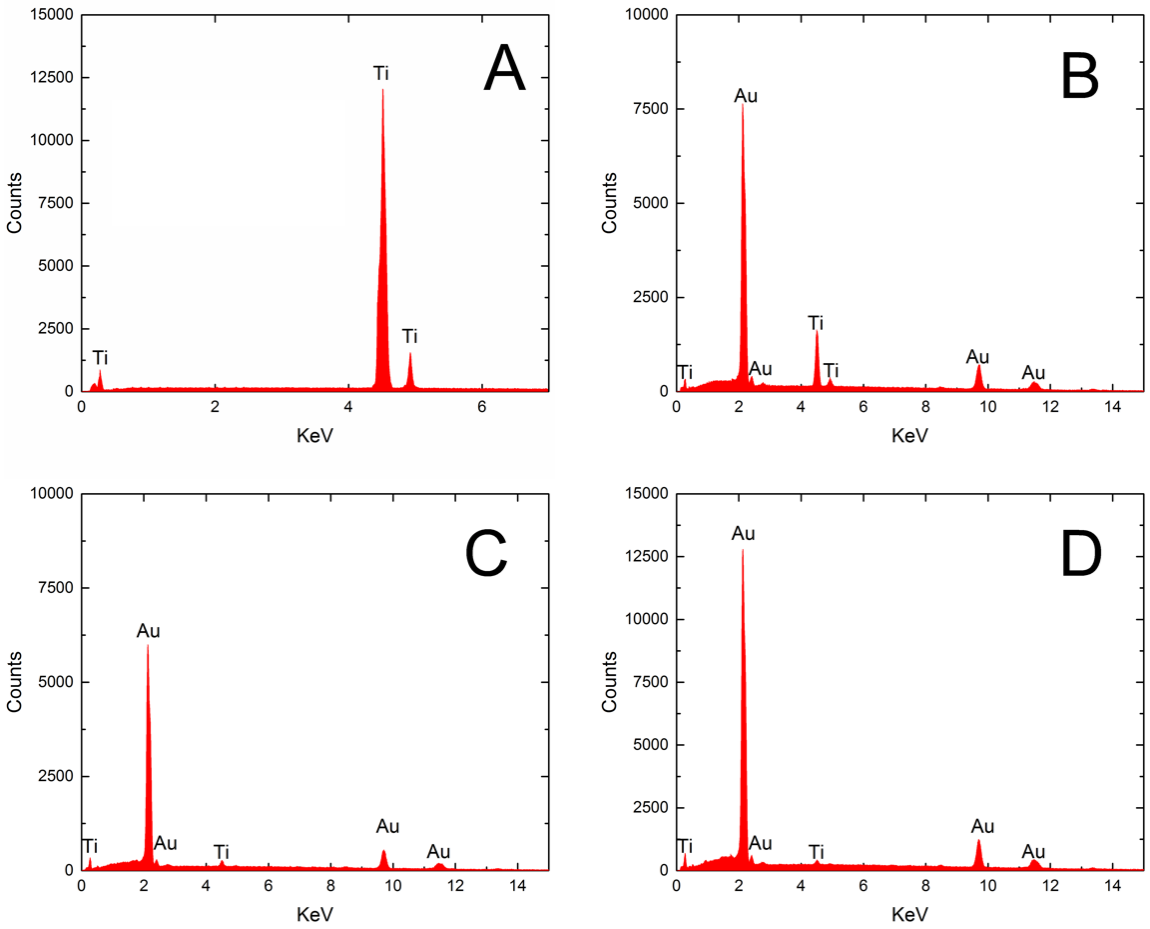

Figure 21. EDS results of the tested TT-LGDLs (A) Untreated titanium TT-LGDLs (B) 180 nm sputter coated TT-LGDL (C) 180 nm electroplated TT-LGDL (D) 820 nm electroplated TT-LGDL.

The hydrogen production rate and efficiency were also significantly improved with the gold surface treated TT-LGDLs. The hydrogen/oxygen production rate is directly related to the current density and working area of the PEMECs, which is shown in Equation 6 below.

$$\boldsymbol{n_{H_2} = \frac{iA}{zF}} \qquad \textbf{Equation 6}$$

Where n_{H_2} is the molar generation rate of hydrogen and the unit is mole/s, i is the current density, A is the active area of the membrane electrode assembly (MEA), z is equivalent electrons per mole of hydrogen which equals to 2 in this equation, F is the Faraday's constant which is 96,485 C/eq.

When the working area is a constant (5 cm^2 in this study), a larger current density indicates higher hydrogen/oxygen production rates according to the Faraday's law [29, 57]. From Figure 22(A), it can be seen that the current density of the untreated TT-LGDL, 180 nm sputter coated TT-LGDL, 180 nm and 820 nm Au electroplated TT-LGDLs is 1.317, 1.489, 1.688 and 1.610 A/cm^2 at a fixed cell voltage of 1.60 V. With only a 180 nm Au thin film on TT-LGDLs, the hydrogen/oxygen production rate was significantly increased by about 28.2% compared with the untreated titanium TT-LGDLs. Although the price of the Au is high, the 180 nm thickness or even thinner Au thin film on TT-LGDLs will be very cheap due to the minimal amount of Au required and mature manufacturing methods. The estimated cost of the Au electroplating is about \$0.014/cm^2 for the TT-LGDLs, and it only costs about \$0.07 to treat 5 cm^2 TT-LGDLs in this study with 180 nm Au thin film.

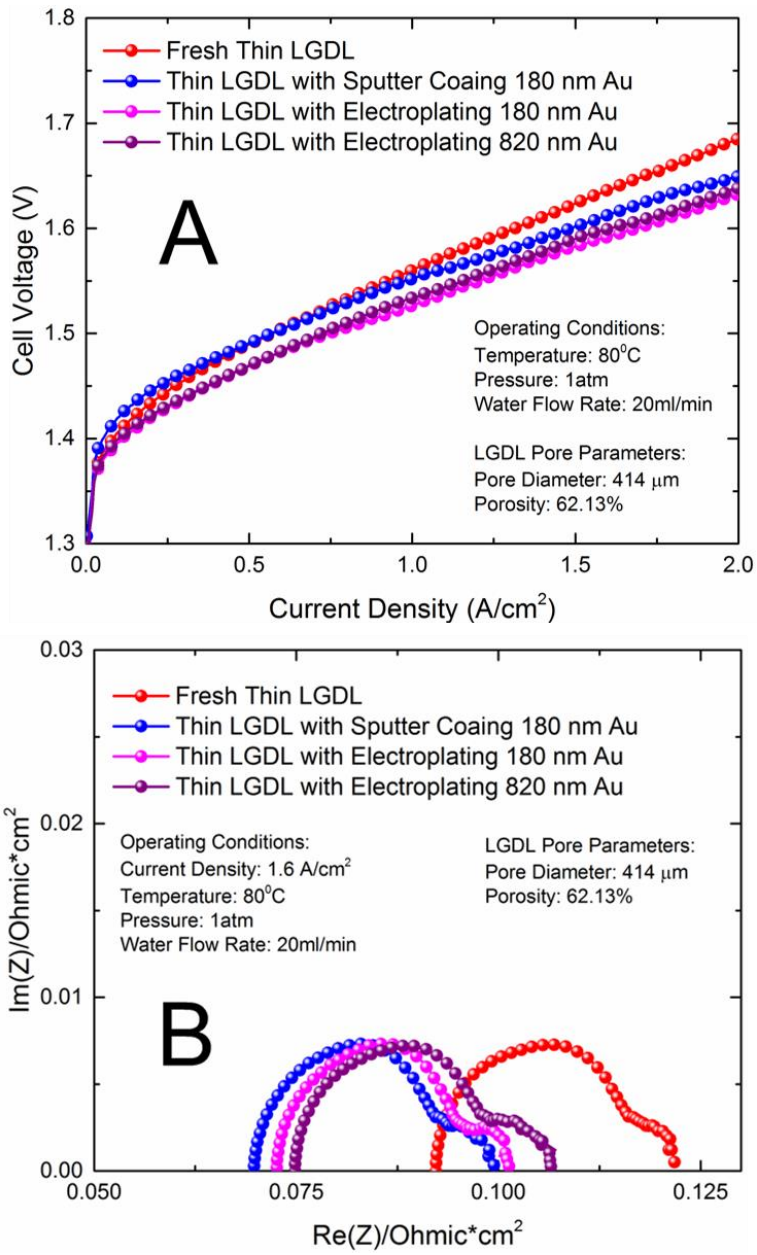

Figure 22. Polarization curve and EIS comparison between untreated and surface treated TT-LGDLs (A) Polarization curve (B) EIS results at 1.6 A/cm^2.

In addition, increasing the single cell hydrogen producing rate by 28.2% could reduce the numbers of single PEMEC when a constant volume of hydrogen are needed. It has been reported that the high cost of the PEMEC stacks are mainly caused by Nafion membrane, noble metal catalysts, bipolar plates, which contribute to more than 60% of the PEMEC stack costs [25, 37]. By reducing the number of PEMECs the quantity of bipolar plate, Nafion membrane, and metal catalyst will also be decreased, which will eventually reduce the cost of the PEMEC stack greatly as a whole.

Figure 22(B) shows the electrochemical impedance spectroscopy (EIS) results, which are conducted under 1.6 A/cm^2 at 80 ^{o}C. The left-most x-intercept of the EIS curves show the ohmic loss of the whole PEMEC, while the right-most x-intercepts indicate the total losses, including the ohmic loss, activation loss, and transport loss [58]. The EIS curves of the PEMECs often consist of two semicircles, the x-distance of the first one represents the activation loss; the x-distance of the second one represents the mass transport loss [52]. It can be seen that the second semicircles are very small at 1.6 A/cm^2, which indicates that the mass transport loss has limited effects on the PEMEC performance. It can be concluded that the TT-LGDLs promote the two-phase counter flow inside the PEMECs due to the small thickness, straight-through pores, and easy flow path. The ohmic loss of the untreated TT-LGDL is about 0.0925 Ω·cm^2, while it is reduced to only 0.0700, 0.0725 and 0.0750 Ω·cm^2 for the 180 nm sputter coated, 180 nm and 820 nm electroplated TT-LGDLs, respectively. Although the sputter coated TT-LGDL achieves smaller ohmic resistance than the electroplated TT-LGDLs, which also corresponds to the polarization curves. The

performance doesn’t get improved because of the higher activation overpotential at low current density range. This can be seen in Figure 22(A), where the polarization curve is higher at low current density. Thus, the electroplating is an optimal choice for surface treatment of TT-LGDLs.

4.4.2 Effects of temperature

The open circuit voltage (OCV), ohmic resistance of the cell, activation and transport effects have a very close relationship with temperature [59]. The untreated TT-LGDLs temperature effects have been investigated in previous work [52]. The surface treated TT-LGDLs are experimentally investigated and the results are shown in Figure 23.

It can be seen from Figure 23(A) that the performance of the PEMECs is gradually improved with increasing temperatures. The cell voltages of the PEMECs with Au sputter coated TT-LGDLs are1.947 V, 1.770 V and 1.649 V at 23 ^{o}C, 50 ^{o}C and 80 ^{o}C, respectively. While the voltages of the PEMECs with electroplating Au TT-LGDLs are 1.900 V, 1.753 V and 1.6328 V at 23 ^{o}C, 50 ^{o}C and 80 ^{o}C, respectively. The performance of the TT-LGDLs with electroplated Au is better than sputter coating at different temperatures.

The performance of the PEMECs is closely related to the ohmic loss, activation loss, mass transport loss, and open circuit voltage [19]. It can be seen in Figure 23(B) that the ohmic loss decreases significantly with the increase of PEMEC operating temperature. The ohmic loss of the PEMECs consists of the resistance of each component, including PEM, CLs, LGDLs, bipolar plate, etc., as well as the interfacial resistances between each component.

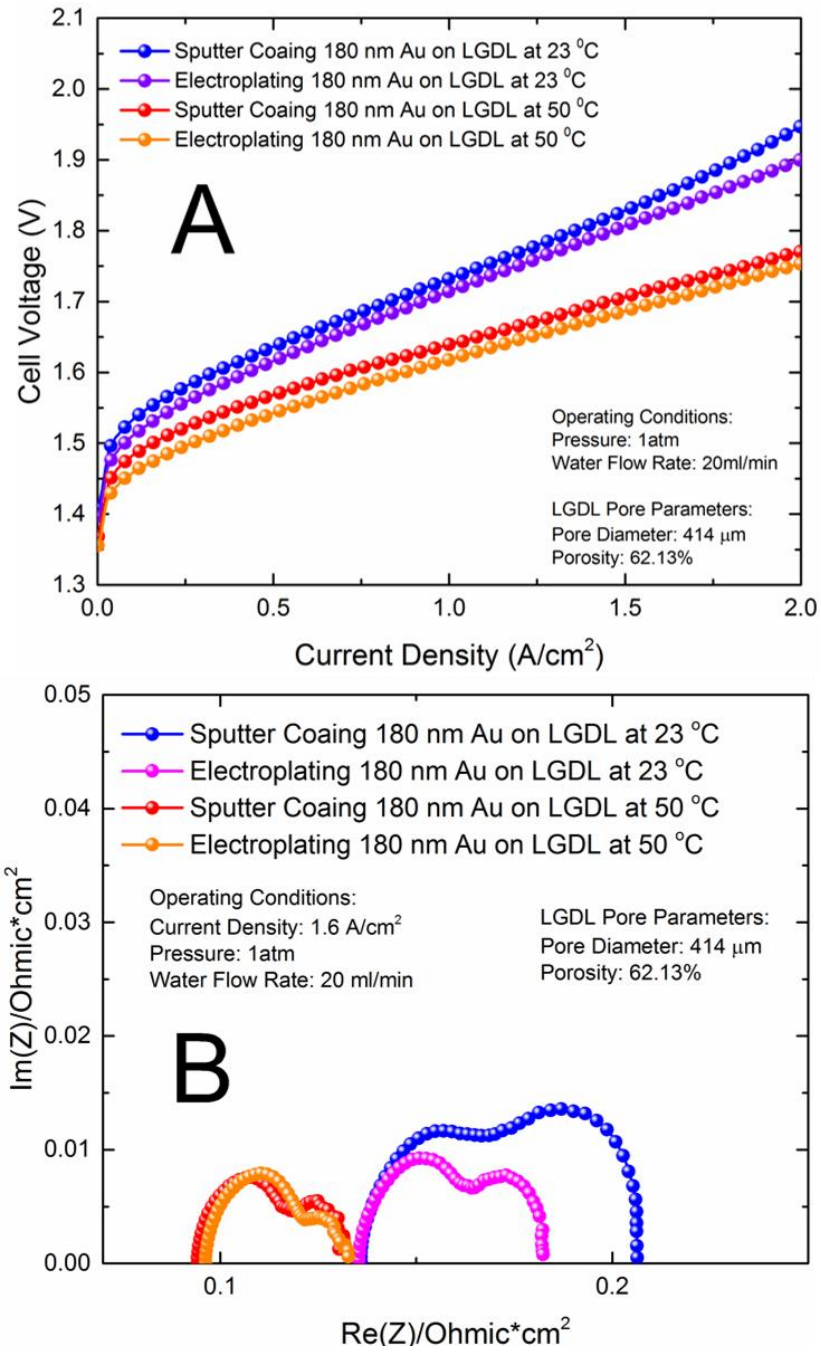

Figure 23. Polarization curve and EIS results with surface treated TT-LGDLs under different temperatures (A) Polarization curve (B) EIS results at 1.6 A/cm^2.

The main ohmic loss comes from the resistance of the PEM and interface between each components [27]. With the increase in temperature, the conductivity of the PEM and CL will increase gradually, which will decrease the ohmic loss [59]. The electrical resistivity of titanium material doesn't change too much when the temperature varies between 23 to 80 ^{o}C, so the resistance of the LGDL will not vary, which will not affect the ohmic loss [60]. In addition, the contact between each component will become better at higher temperature, which will also reduce the ohmic loss of the PEMECs. It is known that the main polarization happens at the anode of PEMECs. This is due to the poor oxygen evolution reaction (OER) kinetics and limitations of proton transport in the catalyst layer. The performance can be improved with the higher temperature, which results from the better diffusion processes and electrode kinetics. The increase in temperature will obviously increase the exchange current density because of the intrinsic enhancement of the catalytic activity[53]. That is why the voltage of the polarization curve in Figure 23(A) becomes lower with increasing temperatures. In contrast, the second arc of the EIS in Figure 23 is becoming smaller with increasing temperature. This proves that the transport losses have been reduced as temperatures increase. As a result, the PEMEC performance improves significantly with increasing temperature due to the better diffusion processes, electrode kinetics and greatly reduced ohmic losses.

4.4.3 Short-term aging assessment of the surface treated TT-LGDLs

After the tests of each samples, the surface of the CCM was examined under SEM and EDS, as shown in Figure 24, including the fresh CCM without any tests. It can be found

that the fresh CCM has a flat surface and shows a uniformly distributed dark color as shown in Figure 24(A1). After the test with untreated titanium TT-LGDLs, the shape of the channel and LGDL is indented on the CCM, which is shown in Figure 24(B1). After the tests with the sputter coated TT-LGDLs, Au is clearly observed on the CCM surface, as shown in Figure 24(C1), which means the Au is partially peeled off from the TT-LGDL and adheres to the CCM after the tests and disassembly of the PEMECs. In Figure 24(C2), it can be found that there is a piece of material located on the surface of the catalyst and the catalyst has been indented with some deformation after the test with the sputter coated thin LGDL. The EDS mapping results (Not shown here) confirmed that the piece of the material is gold. While the CCM, examined after testing with the 180 nm Au electroplated LGDL, shows no peeled off Au. The surface of the CCM is also examined *ex situ* by EDS. It can be seen that the elements distributed uniformly after tests with both untreated thin LGDL and electroplated thin LGDL, as shown in Figure 24(B) and (D). The atomic percentage of elements, including Ir, Ru, F, O and C, are very close to one another. It can be concluded that the Au electroplated TT-LGDLs can not only achieve better performance, but also it is much more stable than the sputter coated Au layer.

Since the performance of the 180 nm Au electroplated TT-LGDL achieves better performance than the untreated and Au sputter coated TT-LGDLs, and the Au layer is stable during all the periods of the tests. The short-term stability test of the Au electroplated TT-LGDL was examined *in-situ* for 100 hours under the operation conditions of 0.2 A/cm^2 and 80 ^oC, and the result were shown in Figure 25.

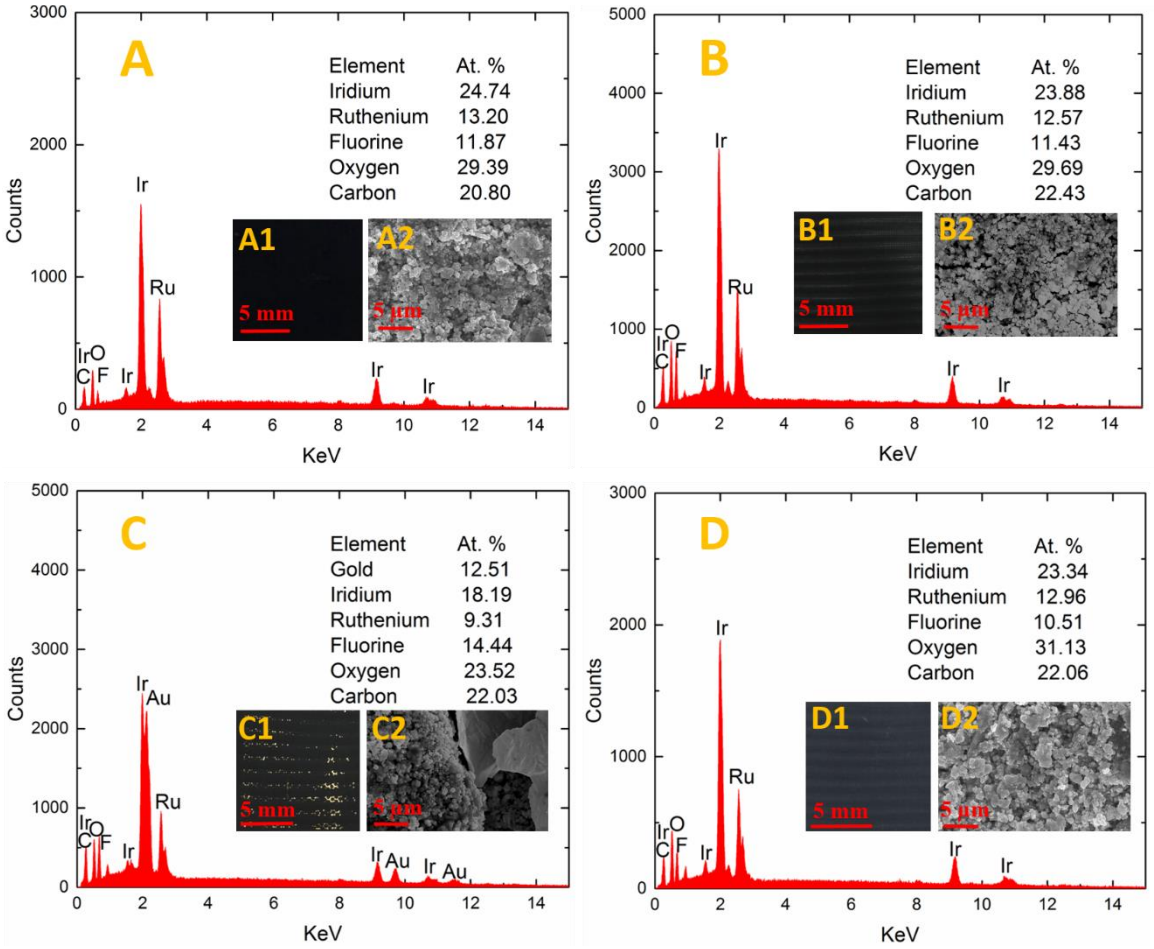

Figure 24. Surface characterizations (EDS, photographs and zoom-in SEMs) of the CCM (A) EDS results of fresh CCM with photograph (A1) and SEM (A2), (B) EDS results of CCM after test with untreated TT-LGDL with photograph (B1) and SEM (B2), (C) EDS results of CCM after test with sputter coated TT-LGDL with photograph (C1) and SEM (C2), (D) EDS results of CCM after test with electroplated TT-LGDL with photograph (D1) and SEM (D2).

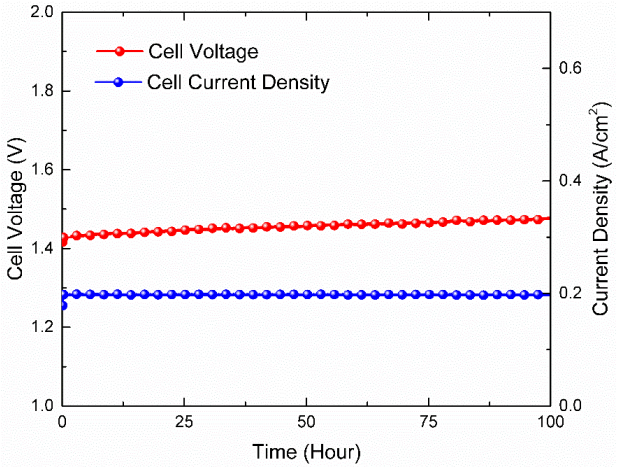

Figure 25. 100 hours water electrolysis test of the TT-LGDL with electroplating 180 nm Au at 80 ºC, 1 atm and 0.2 A/cm^2.

The cell voltage was recorded every 2 seconds during the test. It can be found that the cell voltage of the PEMECs with electroplated TT-LGDL was very stable and remains at ~1.45 V without any obvious cell voltage decay during the 100 hours test. This suggests that good short-term stability of the Au electroplated TT-LGDLs can be expected. The modest deterioration of the performance from 1.43 V to 1.47 V is likely due to the degradation of membrane electrode assembly (MEA) during the test [53, 61]. It can be concluded that the Au electroplated LGDLs have a good short-term stability and can be used as a promising method to enhance the PEMEC performance, due to its mature technology and ease to large scale manufacturing with low cost.

4.5 Conclusion

In this study, the novel TT-LGDLs with different gold surface treatments were investigated for the first time. The novel TT-LGDLs with 414 μm pore diameter and 0.62 porosity have

achieved a superior performance compared with conventional titanium LGDLs. The performance of the PEMECs was further improved by both Au sputter coating and electroplating surface treatments. The results show that, with electroplating a 180 nm Au thin film on the titanium-based TT-LGDLs, the PEMEC voltage can be decreased from 1.6849 V to 1.6328 V at 2.0 A/cm^2 and 80 ^{o}C. More importantly, the hydrogen/oxygen production rate can be greatly increased by 28.2% at 1.60 V and 80 ^{o}C compared with untreated TT-LGDL. The significantly improvement of hydrogen/oxygen production rate can help to reduce the cost of the catalyst layers, bipolar plates, membrane and PEMEC stack system as a whole, when a constant amount of hydrogen/oxygen are needed. In addition, the PEMEC performance was improved significantly with increasing temperature due to better diffusion processes, smaller OCV, lower electrode kinetics and greatly reduced ohmic losses. Furthermore, the CCM surface characterization after the tests demonstrate that the electroplated Au thin film is much more stable than sputter coated thin film that will peel off from the TT-LGDLs. It can be concluded that an ultra-thin Au layer that is electroplated on the TT-LGDLs will significantly improve the performance and efficiency of the PEMECs. The superior performance achieved by the TT-LGDLs with surface treatment make it a promising component in the PEMECs, which provide a route to improved efficiency of hydrogen/oxygen production from water splitting and help to industrialize PEMECs. The results obtained have also demonstrated the advantages of the gold electroplating as simple and reliable method for surface treatment of TT-LGDLs with cost effective for PEMEC application.

References

[1] Mo J, Kang Z, Yang G, Retterer ST, Cullen DA, Toops TJ, Green JB, Zhang F-Y. Thin liquid/gas diffusion layers for high-efficiency hydrogen production from water splitting. *Appl Energ*. 2016;177:817-22.

[2] Desideri U, Campana PE. Analysis and comparison between a concentrating solar and a photovoltaic power plant. *Appl Energ*. 2014;113:422-33.

[3] Liao Y-T, Huang C-W, Liao C-H, Wu JC-S, Wu KC-W. Synthesis of mesoporous titania thin films (MTTFs) with two different structures as photocatalysts for generating hydrogen from water splitting. *Appl Energ*. 2012;100:75-80.

[4] Mo J, Kang Z, Retterer ST, Cullen DA, Toops TJ, Green JB, Mench MM, Zhang F-Y. Discovery of true electrochemical reactions for ultrahigh catalyst mass activity in water splitting. *Science Advances*. 2016;2:e1600690.

[5] Chen H-C, Huang C-W, Wu JC, Lin S-T. Theoretical investigation of the metal-doped SrTiO3 photocatalysts for water splitting. *The Journal of Physical Chemistry C*. 2012;116:7897-903.

[6] Penchini D, Cinti G, Discepoli G, Desideri U. Theoretical study and performance evaluation of hydrogen production by 200 W solid oxide electrolyzer stack. *Int J Hydrogen Energ*. 2014;39:9457-66.

[7] Yan J, Shamim T, Chou S, Desideri U, Li H. Clean, efficient and affordable energy for a sustainable future. *Appl Energ*. 2017;185:953-62.

[8] Budt M, Wolf D, Span R, Yan J. A review on compressed air energy storage: Basic principles, past milestones and recent developments. *Appl Energ*. 2016;170:250-68.

[9] Duić N, Guzović Z, Kafarov V, Klemeš JJ, vad Mathiessen B, Yan J. Sustainable development of energy, water and environment systems. *Appl Energ*. 2013;101:3-5.

[10] Fall J, Humphreys D, Guo S. Design and testing of a unitized regenerative fuel cell. *J Fuel Cell Sci Tech*. 2009;6:031003.

[11] Park S, Shao Y, Liu J, Wang Y. Oxygen electrocatalysts for water electrolyzers and reversible fuel cells: status and perspective. *Energ Environ Sci*. 2012;5:9331-44.

[12] Turner JA. A realizable renewable energy future. *Science*. 1999;285:687-9.

[13] Briguglio N, Brunaccini G, Siracusano S, Randazzo N, Dispenza G, Ferraro M, Ornelas R, Arico A, Antonucci V. Design and testing of a compact PEM electrolyzer system. *Int J Hydrogen Energ*. 2013;38:11519-29.

[14] Liao C-H, Huang C-W, Wu J. Hydrogen production from semiconductor-based photocatalysis via water splitting. *Catalysts*. 2012;2:490-516.

[15] Wang J, Conejo AJ, Wang C, Yan J. Smart grids, renewable energy integration, and climate change mitigation–future electric energy systems. *Appl Energ*. 2012;96:1-3.

[16] Roskilly A, Taylor P, Yan J. Energy storage systems for a low carbon future–in need of an integrated approach. *Appl Energ*. 2015:463-6.

[17] Zhang Y, Lundblad A, Campana PE, Yan J. Comparative Study of Battery Storage and Hydrogen Storage to Increase Photovoltaic Self-sufficiency in a Residential Building of Sweden. *Energy Procedia*. 2016;103:268-73.

[18] Burhan M, Oh SJ, Chua KJE, Ng KC. Solar to hydrogen: Compact and cost effective CPV field for rooftop operation and hydrogen production. *Appl Energ*. 2016.

[19] Han B, Mo J, Kang Z, Zhang F-Y. Effects of membrane electrode assembly properties on two-phase transport and performance in proton exchange membrane electrolyzer cells. *Electrochim Acta*. 2016;188:317-26.

[20] Ehteshami SMM, Vignesh S, Rasheed R, Chan S. Numerical investigations on ethanol electrolysis for production of pure hydrogen from renewable sources. *Appl Energ*. 2016;170:388-93.

[21] Navasa M, Yuan J, Sundén B. Computational fluid dynamics approach for performance evaluation of a solid oxide electrolysis cell for hydrogen production. *Appl Energ*. 2015;137:867-76.

[22] Toops TJ, Brady MP, Zhang F-Y, Meyer HM, Ayers K, Roemer A, Dalton L. Evaluation of nitrided titanium separator plates for proton exchange membrane electrolyzer cells. *J Power Sources*. 2014;272:954-60.

[23] Siracusano S, Baglio V, Lufrano F, Staiti P, Arico A. Electrochemical characterization of a PEM water electrolyzer based on a sulfonated polysulfone membrane. *J Membrane Sci*. 2013;448:209-14.

[24] Yang G, Mo J, Kang Z, III FAL, Green J, Babu SS, Zhang F-Y. Additive manufactured bipolar plate for high-efficiency hydrogen production in proton exchange membrane electrolyzer cells. *Int J Hydrogen Energ*. 2017. 10.1016/j.ijhydene.2017.04.100.

[25] Siracusano S, Baglio V, Van Dijk N, Merlo L, Aricò AS. Enhanced performance and durability of low catalyst loading PEM water electrolyser based on a short-side chain perfluorosulfonic ionomer. *Appl Energ*. 2017;192:477-89.

[26] Dihrab SS, Sopian K, Alghoul M, Sulaiman MY. Review of the membrane and bipolar plates materials for conventional and unitized regenerative fuel cells. *Renewable and Sustainable Energy Reviews*. 2009;13:1663-8.

[27] Han B, Steen S, Mo J, Zhang F-Y. Modeling of interfacial resistance effects on the performance and efficiency for electrolyzer energy storage. 13th International Energy Conversion Engineering Conference2015. p. 3915.

[28] Hudkins JR, Wheeler DG, Peña B, Berlinguette CP. Rapid prototyping of electrolyzer flow field plates. *Energ Environ Sci*. 2016;9:3417-23.

[29] Han B, Mo J, Kang Z, Yang G, Barnhill W, Zhang F-Y. Modeling of two-phase transport in proton exchange membrane electrolyzer cells for hydrogen energy. *International Journal of Hydrogen Energy*. 2017. doi: 10.1016/j.ijhydene.2016.12.103.

[30] Brady MP, Weisbrod K, Paulauskas I, Buchanan R, More KL, Wang H, Wilson M, Garzon F, Walker LR. Preferential thermal nitridation to form pin-hole free Cr-

nitrides to protect proton exchange membrane fuel cell metallic bipolar plates. *Scripta Materialia*. 2004;50:1017-22.

[31] Brady MP, Yang B, Maziasz PJ. Iron-based alloy and nitridation treatment for PEM fuel cell bipolar plates. *Google Patents*; 2010.

[32] Wang J. System integration, durability and reliability of fuel cells: Challenges and solutions. *Appl Energ*. 2017;189:460-79.

[33] Gatto I, Stassi A, Baglio V, Carbone A, Passalacqua E, Aricò A, Schuster M, Bauer B. Optimization of perfluorosulphonic ionomer amount in gas diffusion electrodes for PEMFC operation under automotive conditions. *Electrochim Acta*. 2015;165:450-5.

[34] Medina P, Santarelli M. Analysis of water transport in a high pressure PEM electrolyzer. *Int J Hydrogen Energ*. 2010;35:5173-86.

[35] Görgün H. Dynamic modelling of a proton exchange membrane (PEM) electrolyzer. *Int J Hydrogen Energ*. 2006;31:29-38.

[36] Mo J, Dehoff RR, Peter WH, Toops TJ, Green JB, Zhang F-Y. Additive manufacturing of liquid/gas diffusion layers for low-cost and high-efficiency hydrogen production. *Int J Hydrogen Energ*. 2016;41:3128-35.

[37] Carmo M, Fritz DL, Mergel J, Stolten D. A comprehensive review on PEM water electrolysis. *Int J Hydrogen Energ*. 2013;38:4901-34.

[38] Mo J, Steen SM, Zhang F-Y, Toops TJ, Brady MP, Green JB. Electrochemical investigation of stainless steel corrosion in a proton exchange membrane electrolyzer cell. *Int J Hydrogen Energ*. 2015;40:12506-11.

[39] Steen III SM, Mo J, Kang Z, Yang G, Zhang F-Y. Investigation of Titanium Liquid/Gas Diffusion Layers in Proton Exchange Membrane Electrolyzer Cells. *International Journal of Green Energy*. 2016.

[40] Hwang CM, Ishida M, Ito H, Maeda T, Nakano A, Kato A, Yoshida T. Effect of titanium powder loading in gas diffusion layer of a polymer electrolyte unitized reversible fuel cell. *J Power Sources*. 2012;202:108-13.

[41] Ito H, Maeda T, Nakano A, Hwang CM, Ishida M, Kato A, Yoshida T. Experimental study on porous current collectors of PEM electrolyzers. *Int J Hydrogen Energ*. 2012;37:7418-28.

[42] Ito H, Maeda T, Nakano A, Kato A, Yoshida T. Influence of pore structural properties of current collectors on the performance of proton exchange membrane electrolyzer. *Electrochim Acta*. 2013;100:242-8.

[43] Hwang CM, Ishida M, Ito H, Maeda T, Nakano A, Hasegawa Y, Yokoi N, Kato A, Yoshida T. Influence of properties of gas diffusion layers on the performance of polymer electrolyte-based unitized reversible fuel cells. *Int J Hydrogen Energ*. 2011;36:1740-53.

[44] Grigoriev S, Millet P, Volobuev S, Fateev V. Optimization of porous current collectors for PEM water electrolysers. *Int J Hydrogen Energ*. 2009;34:4968-73.

[45] Ioroi T, Oku T, Yasuda K, Kumagai N, Miyazaki Y. Influence of PTFE coating on gas diffusion backing for unitized regenerative polymer electrolyte fuel cells. *J Power Sources*. 2003;124:385-9.

[46] Millet P, Dragoe D, Grigoriev S, Fateev V, Etievant C. GenHyPEM: a research program on PEM water electrolysis supported by the European Commission. *Int J Hydrogen Energ*. 2009;34:4974-82.

[47] Oh H, Park J, Min K, Lee E, Jyoung J-Y. Effects of pore size gradient in the substrate of a gas diffusion layer on the performance of a proton exchange membrane fuel cell. *Appl Energ*. 2015;149:186-93.

[48] Mo J, Steen SM, III BH, Kang Z, Terekhov A, Zhang F-Y, Retterer ST, Cullen DA. Investigation of titanium felt transport parameters for energy storage and hydrogen/oxygen production. 13th International Energy Conversion Engineering Conference. AIAA 2015-39142015. p. 3914.

[49] Mo J, Steen SM, Retterer S, Cullen DA, Terekhov A, Zhang F-Y. Mask-Patterned Wet Etching of Thin Titanium Liquid/Gas Diffusion Layers for a PEMEC. *Ecs Transactions*. 2015;66:3-10.

[50] Zhang F-Y, Advani SG, Prasad AK. Performance of a metallic gas diffusion layer for PEM fuel cells. *J Power Sources*. 2008;176:293-8.

[51] Zhang F-Y, Prasad AK, Advani SG. Investigation of a copper etching technique to fabricate metallic gas diffusion media. *J Micromech Microeng*. 2006;16:N23.

[52] Kang Z, Mo J, Yang G, Retterer ST, Cullen DA, Toops TJ, Green Jr JB, Mench MM, Zhang F-Y. Investigation of thin/well-tunable liquid/gas diffusion layers exhibiting superior multifunctional performance in low-temperature electrolytic water splitting. *Energ Environ Sci*. 2017;10:166-75.

[53] Su H, Linkov V, Bladergroen BJ. Membrane electrode assemblies with low noble metal loadings for hydrogen production from solid polymer electrolyte water electrolysis. *Int J Hydrogen Energ*. 2013;38:9601-8.

[54] Grigoriev S, Kalinnikov A. Mathematical modeling and experimental study of the performance of PEM water electrolysis cell with different loadings of platinum metals in electrocatalytic layers. *Int J Hydrogen Energ*. 2016.

[55] Spurgeon JM, Lewis NS. Proton exchange membrane electrolysis sustained by water vapor. *Energ Environ Sci*. 2011;4:2993-8.

[56] Zhang L, Shao Z-G, Yu H, Wang X, Yi B. IrO 2 coated TiO 2 nanopore arrays electrode for SPE HBr electrolysis. *J Electroanal Chem*. 2013;688:262-8.

[57] Rasheed RKA, Ehteshami SMM, Chan SH. Analytical modelling of boiling phase change phenomenon in high-temperature proton exchange membrane fuel cells during warm-up process. *Int J Hydrogen Energ*. 2014;39:2246-60.

[58] Sun S, Xiao Y, Liang D, Shao Z, Yu H, Hou M, Yi B. Behaviors of a proton exchange membrane electrolyzer under water starvation. *Rsc Adv*. 2015;5:14506-13.

[59] Mench MM. Fuel Cell Engines: *John Wiley & Sons*; 2008.

[60] Bel'skaya EA, Kulyamina EY. Electrical resistivity of titanium in the temperature range from 290 to 1800 K. *High Temperature*. 2007;45:785-96.

[61] Su H, Bladergroen BJ, Linkov V, Pasupathi S, Ji S. Study of catalyst sprayed membrane under irradiation method to prepare high performance membrane electrode assemblies for solid polymer electrolyte water electrolysis. *Int J Hydrogen Energ*. 2011;36:15081-8.

CHAPTER V

DEVELOPING TITANIUM MICRO/NANO POROUS LAYERS ON PLANAR THIN/TUNABLE LIQUID/GAS DIFFUSION LAYERS FOR HIGH-EFFICIENCY HYDROGEN PRODUCTION

This chapter will be further edited and revised based on the submitted publication in International Journal of Hydrogen Energy with the following authors and title:

Zhenye Kang, Gaoqiang Yang, Jingke Mo, Shule Yu, David A. Cullen, Scott T. Retterer, Todd J. Toops, Michael P. Brady, Guido Bender, Bryan S. Pivovar, Johney B. Green Jr, Feng-Yuan Zhang. "Developing titanium micro/nano porous layers on planar thin/tunable liquid/gas diffusion layers for high-efficiency hydrogen production."

I am fully responsible for the work submitted in this publication, contributions from co-authors will be added to submission for publication.

5.1 Graphical Abstract

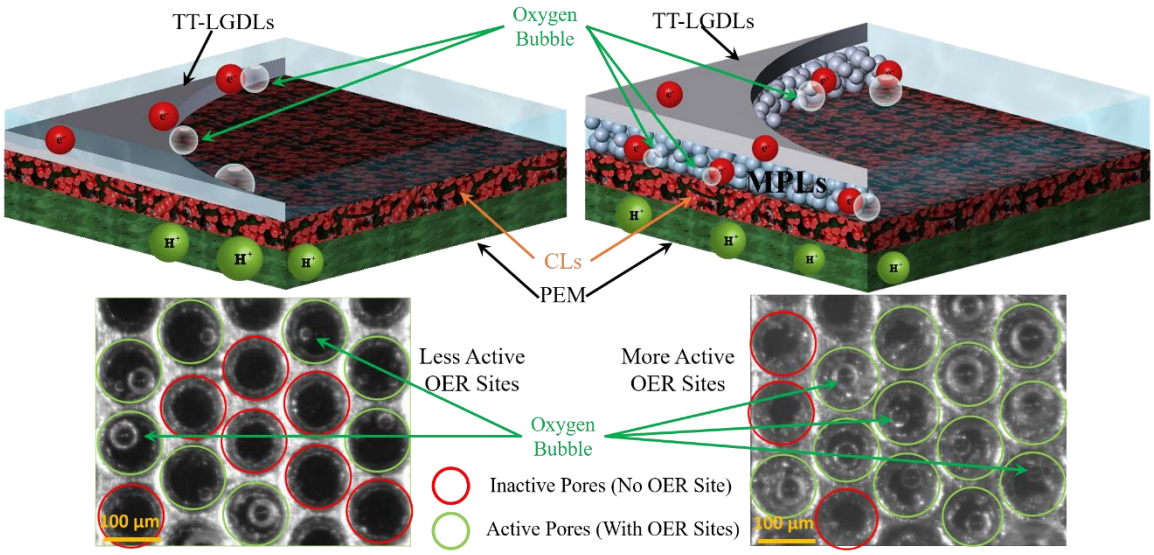

5.2 Abstract

Microporous layers (MPLs) have seen limited investigations in electrolysis and it can offer the potential to improve cell performance by allowing better reactant access and product removal to and from the catalyst layer. For exploring better proton exchange membrane electrolyzer cell (PEMEC) performance and catalyst utilization, MPLs, which have been widely used in fuel cells, are applied on novel thin/tunable liquid/gas diffusion layers (TT-LGDLs) in PEMECs. In this study, the MPLs are developed with both irregular micro (~5 μm) and sphere nano (30 – 50 nm) titanium particles by low temperature spraying method. The MPLs are investigated comprehensively both *in-situ* and *ex-situ*. The MPLs change the wettability of the TT-LGDLs and show super hydrophobic property. The results reveal that micro particle MPLs exhibit improved catalytic activity but increased ohmic resistances, and that nano particle MPLs do not impact catalytic activity meaningfully but exhibit even greater increases in ohmic resistance. The effects of the thickness of the MPLs are also investigated and the typical MPL is also studied by *in-situ* visualization in a transparent PEMEC with a high-speed and micro-scale visualization system (HMVS). It has been concluded that the MPLs offer some improved performance under specific conditions but may not be required for optimum TT-LGDLs in PEMECs. The results also indicate the strong feasibility of the TT-LGDLs with small pore size and large porosity for high efficiency and low cost PEMEC practical applications.

5.3 Introduction

Hydrogen is regarded as an ideal energy carrier, due to its high energy density and zero emission, either greenhouse gas or criteria pollutant during its usage [1-5]. The proton exchange membrane electrolyzer cell (PEMEC), which works in reverse of proton exchange membrane fuel cells (PEMFCs), is considered one of the most promising methods to store the sustainably-produced energy, especially for the electricity generated from intermittent energy sources, such as solar, wind, tide, or hydro [6-11]. PEMECs can mitigate the impact of electricity fluctuations from the intermittent sources and consumers' needs, and alleviate the energy waste within the current grid by storing the excess electricity during low demand and release the energy during high demand period. More importantly, it can be used to generate very high purity hydrogen/oxygen gas in an environmentally friendly way with high efficiency, which is beneficial for future storage and applications [12-15].

PEMECs mainly consist of a catalyst coated membrane (CCM) that is sandwiched by two electrodes. At each electrode, there is a catalyst layer (CL), liquid/gas diffusion layer (LGDL), bipolar plate (BP) with flow channels, and current distributor [7, 16]. The heart of the PEMECs is the membrane electrode assembly (MEA), which has a great impact on PEMEC performance. The LGDLs, which located between the CLs and BP, control the flow of reactants and products to and from the catalyst layer, and have to meet certain requirements, such as high corrosion resistance, good electrical conductivity, and small mass transport losses [17, 18]. Due to the high potential seen at the anode (~2V), the most

widely used LGDLs are titanium (Ti) based materials, such as Ti felt, Ti mesh, or sintered Ti particles [17, 19-21]. These LGDLs share similar properties, including random pore size and pore shape, large thickness, complex water/gas transport path, uneven surface, etc., which lead to large ohmic resistances, poor interfacial contact, large two-phase transport losses, all of which ultimately limit PEMEC performance. Much attention has been paid to reduce the interfacial contact resistance between the CLs and LGDLs, and different methods have been proposed and studied in both PEMFCs and PEMECs [22-24]. It is well known that introducing a micro-porous layer (MPL) between the nano-structured CLs and macro-structured gas diffusion layers (GDLs) at the cathode of PEMFCs can greatly improve its performance, durability, and stability. The MPL serves to decrease the interfacial contact resistance, protect the membrane from being punctured by GDL fibers, and promote water/gas transport [25].

Jin Hyun Nam et al. have proposed two effects of MPLs in water management in PEMFCs. They found that the MPLs can reduce the size and saturation level of the interfacial water droplets on CL surface, and reduce the number of water breakthroughs toward GDL in PEMFCs [24]. Guiyin Chen et al. developed MPLs in PEMFCs to examine its effects and mechanisms of water management under a wide range of operating conditions. They found that the effects and mechanisms of MPLs were closely related to humidity and temperature [25]. Su et al., on the contrary, eliminated the MPLs from the GDL in PEMFCs to achieve high performance under high temperature [22]. While very little has been reported on the role of MPLs in PEMECs. P. Lettenmeier et al. developed a MPL for PEMECs by

thermally spraying Ti particles on sintered Ti filters. They found that the MPL has a moderate impact on the PEMEC performance when the current density below 1.2 A/cm^2, while the MPL can greatly improve the performance under high current density ranges by reducing the interfacial contact resistance and mass transport limitations [23]. J. Polonsky et al. developed an MPL on Ti felt with antimony-doped tin oxide (ATO) mixed with Nafion solution, and improved performance was achieved in the voltage range dominated by charge transfer kinetics. They also concluded that a more conductive MPL could greatly enhance the PEMEC performance [26].

Recently, we reported a kind of novel thin/tunable LGDLs (TT-LGDLs), which has a thickness of only 25 μm, well controlled pore morphologies (including pore shape, pore size, and porosity), and planar surface with straight-through pores, as shown in Figure 26(A) [27, 28]. These TT-LGDLs can achieve superior PEMEC performance compared to the current state-of-the-art, and the cell voltage can be as low as 1.63 V at 2.0 A/cm^2 and 80 ^{o}C with a commercial Nafion 115 CCM (3.0 mg/cm^2 IrRuOx at anode and 3.0 mg/cm^2 Pt black at cathode and 5 cm^2 active area) [28, 29]. Based on our previous discoveries, the oxygen evolution reaction (OER) sites can be identified by the formation of oxygen bubble nucleation sites, which were found to occur at the rim of the TT-LGDL pores due to the large in-plane electrical resistance of the CL and the difficult two-phase transport under the TT-LGDL land area [27, 30]. Therefore, it seems that large amounts of catalyst located in the middle of the pore area and under the TT-LGDL land area is inactive or underutilized to some extent. By introducing the MPLs between the CLs and TT-LGDLs, as shown in

Figure 26(B), it is anticipated that more OER sites will be accessible and the PEMEC performance can be improved compared with TT-LGDLs without a MPL, as shown in Figure 26(A). The intent of applying a MPL provides an easy electrical conducting path with smaller resistance compared with the in-plane through CLs from the middle of the pore area to the TT-LGDLs, and it can offer the possibility of the water transport and oxygen removal between the under the TT-LGDL land area and the flow field. As can be seen in Figure 26, it is expected that more oxygen bubbles, which indicate the presence of active OER sites in both the middle of the pore area and the under land area, will appear, which represents that the improved catalyst utilization when the MPLs are added, resulting in improved PEMEC performance.

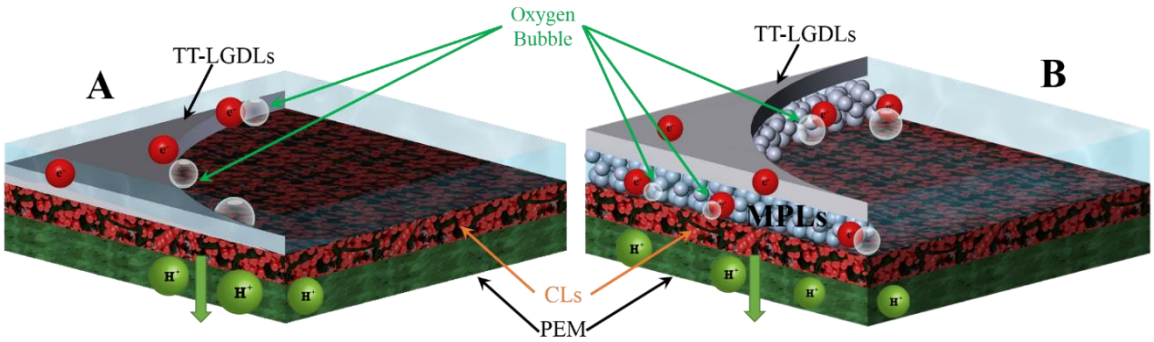

Figure 26. MEA schematic with TT-LGDLs. (A) Conventional MEAs; (B) MEAs with MPLs.

The effects of the MPLs on TT-LGDLs were comprehensively investigated in this study. MPLs were obtained by spraying both micro and nano Ti particles on TT-LGDLs. The

micro and nano MPLs with different thicknesses were characterized both *in-situ* and *ex-situ*. The thickness of the MPLs and the particle morphology of MPLs were examined under SEM. The wettability of the MPLs were also tested. The fresh TT-LGDL samples and TT-LGDL with different MPLs were characterized in a regular PEMEC, and both the polarization curve and electrochemical impedance spectroscopy (EIS) were obtained. In addition, the typical MPL on TT-LGDLs was *in-situ* visualized to further reveal its effects on the OER phenomenon, which were observed in a transparent PEMEC and captured by using the high-speed and micro-scale visualization system (HMVS). The results demonstrate that the MPLs offer some improved performance under specific conditions but may not be required for optimum TT-LGDLs in PEMECs, and also this study provides a direction of ideal TT-LGDL development for hydrogen/oxygen production in low temperature and high efficiency PEMECs.

5.4 Experimental Details

The MPLs were fabricated by a low temperature air spraying method. Before spraying the MPLs on TT-LGDLs, the MPL suspension was prepared from Ti particles, including the 99% 5 μm micro-particles or 99.9% 30-50 nm nano-particles (from US Research Nanomaterials, Inc.), Nafion (D1021 from Fuel Cell Store), and some certain solvents. First, 5.0 g Ti particles were weighted and stored in a glass bottle. Second, 5.0 g D1021 Nafion dispersion and 20.0 g isopropyl alcohol (IPA) were added into the bottle. The Nafion acted as the binder of the Ti particles in MPLs, and it can also aid water transport through the MPLs, which is intended to form a hydrophilic property of the MPLs [26].

Then, the mixture was ultrasonic blended for 15 mins. Third, 20.0 g ethylene glycol was added into the mixture and followed by another 1 hour of ultra-sonication to prepare the MPL suspension. Before spraying, all the samples were ultrasonic cleaned with acetone, methanol and ethanol in sequence for 15 mins, respectively, and lastly rinsed in DI water for 15 mins. All samples were dried in the air at room temperature for 24 hours before spraying. Two TT-LGDLs, as shown in Figure 27, were used as the substrate for MPLs. The TT-LGDLs had the same porosity of about 30%, and one of them had a large pore diameter about 800 μm and the other had a small pore diameter about 100 μm. The detailed fabrication process of the novel TT-LGDLs can be found in our previous research [31, 32]. The EDS analysis of the TT-LGDLs showed that it is pure Ti with the Al peak from the background stub. For the spraying tool, the medium head airbrush 150-1 (from WYN-WYN, Inc.) was used. The airbrush was connected to an air compressor with a pressure of 200 kPa and the flow rate was controlled manually by the valve on the airbrush. The dried fresh TT-LGDLs were mounted on a silicon wafer and then the wafer was fixed with an angle of ~60^{o} to the horizontal in a large fume hood before spraying. A constant volume of 1.5 ml MPL ink was added to the container of the airbrush and then sprayed on the surface of the TT-LGDLs. Then, the silicon wafer with sample on it, was moved to a hot stage with a temperature of 90 ^{o}C for 5 mins to evaporate the solvents (including IPA, alcohol and ethylene glycol). The thickness of the MPLs was controlled by the number of spray times, and three MPLs with different thickness were prepared with both micro and nano Ti particles. The detailed information on MPL samples are shown in Table 7.

Table 7. Detail parameters of TT-LGDLs and MPLs.

Sample	TT-LGDLs	Ti Particles	Particle Shape	MPL Thickness (μm)
A	~800 μm pore diameter; ~30% porosity	Null	Null	0
A1	A	5 μm microparticles	Irregular	~15
A2	A	5 μm microparticles	Irregular	~20
A3	A	5 μm microparticles	Irregular	~40
A4	A	30-50 nm nanoparticles	Sphere	~5
A5	A	30-50 nm nanoparticles	Sphere	~8
A6	A	30-50 nm nanoparticles	Sphere	~12
B	~100 μm pore diameter; ~30% porosity	Null	Null	0
B1	B	5 μm microparticles	Irregular	~20

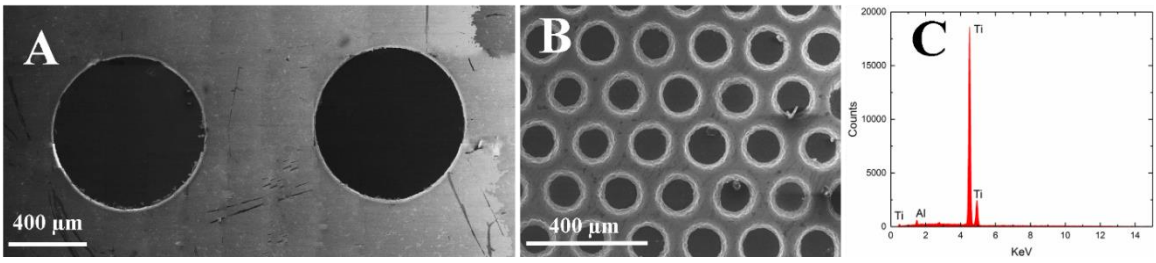

Figure 27. SEM images of TT-LGDLs. (A) Fresh A sample with a pore diameter of about 800 µm and a porosity of about 30%; (B) Fresh B sample with a pore diameter of about 100 µm and a porosity of about 30%; (C) EDS results of the TT-LGDLs.

For measuring the wettability of the samples, the sessile drop method was used to obtain the contact angle from an optical contact angle measuring device (Krüss Drop Shape Analyzer - DSA25E). All the samples were placed on the surface of the plastic substrate. During the measurements, a 2 µL droplet of deionized (DI) water was dropped from the tip of a microliter syringe to the surface of the samples which including titanium foil, typical TT-LGDLs, and TT-LGDLs with different MPLs. After a period of 5 seconds had elapsed, the image was collected and the contact angle between the drop and the sample was measured in the image by the software. Three measurements at different spots were obtained for each sample and the mean values were obtained accordingly. For the *ex-situ* characterizations, scanning electron microscopy (SEM) was conducted with a field emission SEM (JEOL JSM-6320F) and the energy-dispersive X-ray spectroscopy (EDS) was performed with an EDAX Octane plus Silicon Drift Detector in tandem, which is equipped with EDAX's TEAM EDS analyzing software.

For the *in-situ* tests, the Nafion 115 CCM (from FuelCellsEtc, EZ-CCM) with 3.0 mg/cm^2 IrRuOx at anode and 3.0 mg/cm^2 PtB at cathode was used. The regular PEMEC was

compressed to 4.52 N·m of torque by eight bolts at the two aluminum end plates. The carbon paper Toray 090 (from Fuel Cell Store) with a 280 μm thickness and 78% porosity was employed as cathode LGDL. The graphite bipolar plates with parallel flow channels were used at both anode and cathode. For the flow control, a pump (from KNF Neuberger) was employed to provide DI water at a flow rate of 20 ml/min to the anode. Water was heated in a water bath (WB10 from PolyScience) before entering the PEMEC. The exits of both anode and cathode were safely exhausted at air pressure. The temperature was controlled by a Multi-Zone controller (from OMEGA) coupled with heaters at both anode and cathode. For the testing equipment, the PEMEC was connected to the potentiostat with a booster VSP/VMP3B-100 (from Bio-Logic). The polarization curve and galvanostatic electrochemical impedance spectroscopy (GEIS) were measured during the tests for each sample. The sample B and B1 were chosen for *in-situ* visualization tests in a transparent PEMEC, and the detailed cell structure and set up can be found in our previous studies [33, 34]. For the test in the transparent PEMECs, the current density was maintained at a constant value and the cell voltage was recorded throughout the experiment. The visualization of the OER in PEMEC was captured under constant current density for each sample.

5.5 Results and Discussion

5.5.1 Ex-situ investigation of the MPLs

Both the cross-section and top view of the MPLs on TT-LGDLs were examined under SEM, and the results were shown in Figure 28 and Figure 29, respectively. Before doing

the SEM for the cross-section, the TT-LGDLs with MPLs were cut by a knife. Due to the good mechanical strength of Ti materials, the cross-section of the cutting area has been damaged and it is hard to observe the thickness of the MPLs. Therefore, all the cross-sections of TT-LGDLs with MPLs were examined in the pore area, which were not directly cut by the knife and reserve the original morphology. From Figure 28, it can be seen that the MPLs were mainly spread on the top surface of the TT-LGDLs. Very few micro particles adhered to the wall of the TT-LGDL pores, while a large amount of nano particles were located on the wall of the pores, especially when the MPL thickness is large as can be seen from Figure 28(E) and (F).

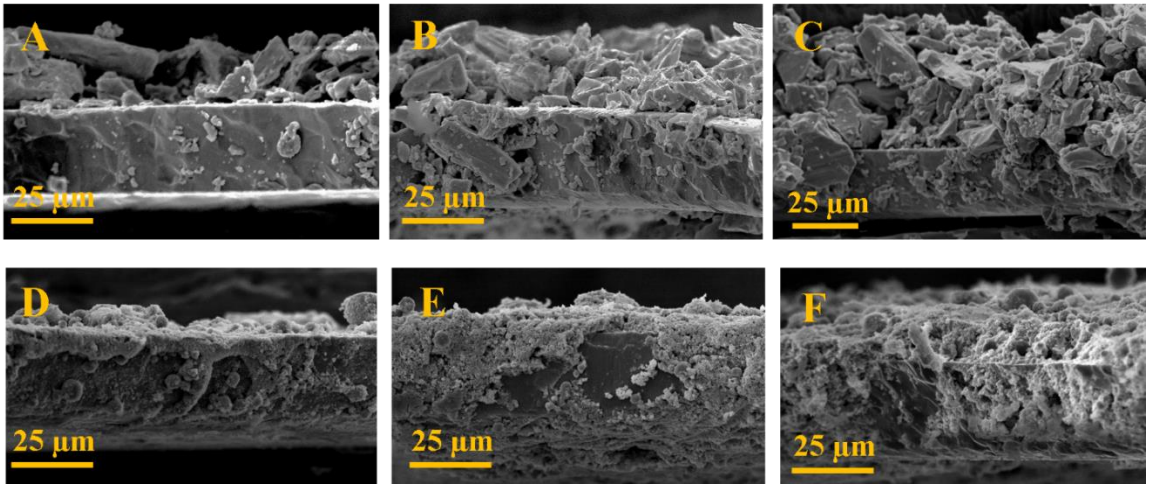

Figure 28. Cross-section SEM images of MPLs. (A) Sample A1; (B) Samples A2; (C) Sample A3; (D) Sample A4; (E) Sample A5; (F) Sample A6.

The thickness of the MPLs are shown in Table 7. It can be seen that the thickness of the micro particle MPLs is in the range of 15-40 µm, while the nano particle MPLs is about 5-

12 μm. One should note that the surface roughness of the MPLs is much worse than fresh TT-LGDL surface, which is different from MPLs on conventional LGDLs (such as Ti felt). Since Ti felt is made of Ti fibers and its surface is very rough, which has a poor interfacial contact, hence, a MPL spread on its surface could obviously enhance the contact with CLs. But for the MPLs on TT-LGDLs, this effect was not observed, since the fresh TT-LGDLs already exhibit a planar surface, and the Ti particles will damage this property, which may cause negative impact on PEMEC performance eventually.

Figure 29 shows the top view of the different MPLs on TT-LGDLs. It can be seen that the micro Ti particle exhibits a totally different morphology compared to the nano Ti particles. The nano Ti particle has a sphere shape, and the particle size is mainly in the range of 30-50 nm. But for the micro particles, the shape is irregular, and some of the particles can have a size larger than 20 μm. For the sample A1 and A4, it can be found that the MPLs cannot even cover all the TT-LGDLs, and the TT-LGDL surface can be observed through some areas of the MPLs. When increasing the thickness of the MPLs, both of the micro and nano particle MPLs can spread all over the TT-LGDL surface, which can be found for sample A2, A3, A5 and A6. It should be noted that when increasing the thickness of nano particle MPLs to 12 μm (Sample A6 as shown in Figure 29(G)), the surface will become much flatter than thinner MPLs, and the MPL exhibits a dense structure. From the EDS mapping results of both micro and nano Ti particle MPLs, it can be seen that the elements distributed more uniformly throughout the surface of the nano particle MPLs than the micro particle MPLs. For the micro particle MPLs, the micro pores were formed throughout the MPLs,

while the pores of the nano particle MPLs are much smaller. The C, S, F and O mainly come from the Nafion ionomer that acts as the particle binder in the MPLs.

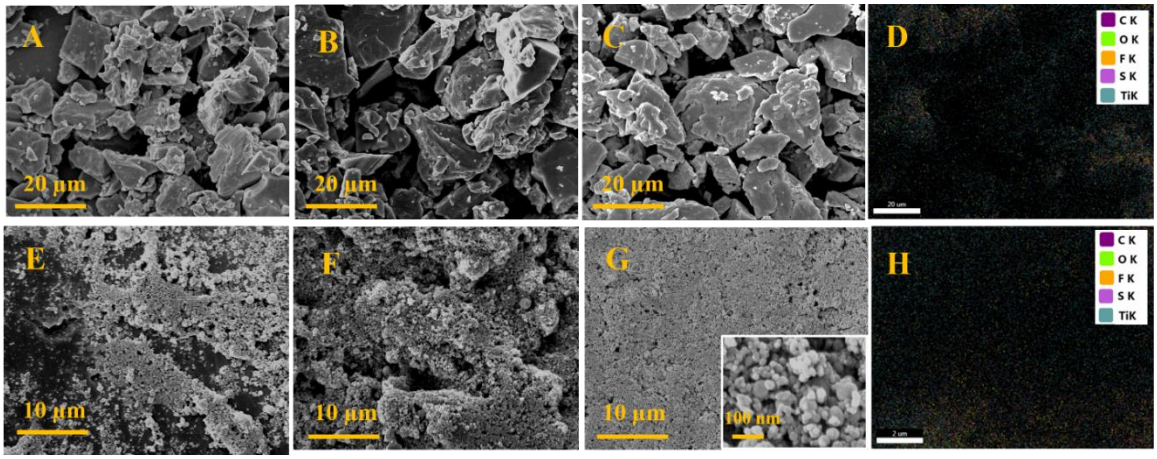

Figure 29. Typical SEM images of different MPL samples (A) Sample A1; (B) Sample A2; (C) Sample A3; (D) EDS mapping of micro particle MPLs; (E) SampleA4; (F) Sample A5; (G) Sample A6 with zoom-in Ti nano particles; (H) EDS mapping of nano particle MPLs.

Figure 30 shows the typical contact angle on different surface features, including titanium thin foil (no pores), sample A (TT-LGDLs with 800 µm pore diameter and 30% porosity), samples B (TT-LGDLs with 100 µm pore diameter and 30% porosity), sample A2 (sample A with micro-particle MPL), sample A5 (sample A with nano-particle MPL) and B1 (sample B with micro-particle MPL). Their contact angles are ~ 45^{o}, ~ 64^{o}, ~ 81^{o}, ~ 145^{o}, ~ 162^{o}, and ~ 150^{o}, respectively. The pores and MPLs have some effects on water contact angle of the dry LGDL samples. From the Figure 30(D), (E) and (F), the MPLs showed super hydrophobic wettability, which is not an ideal property of the MPLs in PEMECs since it may increase the water/gas transport resistance. Although the pores and MPLs

changed the wettability of Ti material, the fresh TT-LGDLs are still hydrophilic. It should be noticed that the LGDLs in the PEMECs are immersed in DI water which indicates that the samples are all wet during the operation. Therefore, we also measured our samples when a droplet was dropped on the LGDLs and the MPLs samples that are placed on the top of titanium foil substrate in wet conditions. As a comparison, a droplet on titanium foil is also captured during the same period. It has been found that the droplet on TT-LGDLs permeate to the bottom and the contact angle decreases gradually, while the droplet on the titanium foil nearly is unchanged besides the slight evaporation. The permeation rate of the droplet on different samples are different, but all the droplets permeate to the bottom and there is no more water exist on top surface of the MPLs at the end.

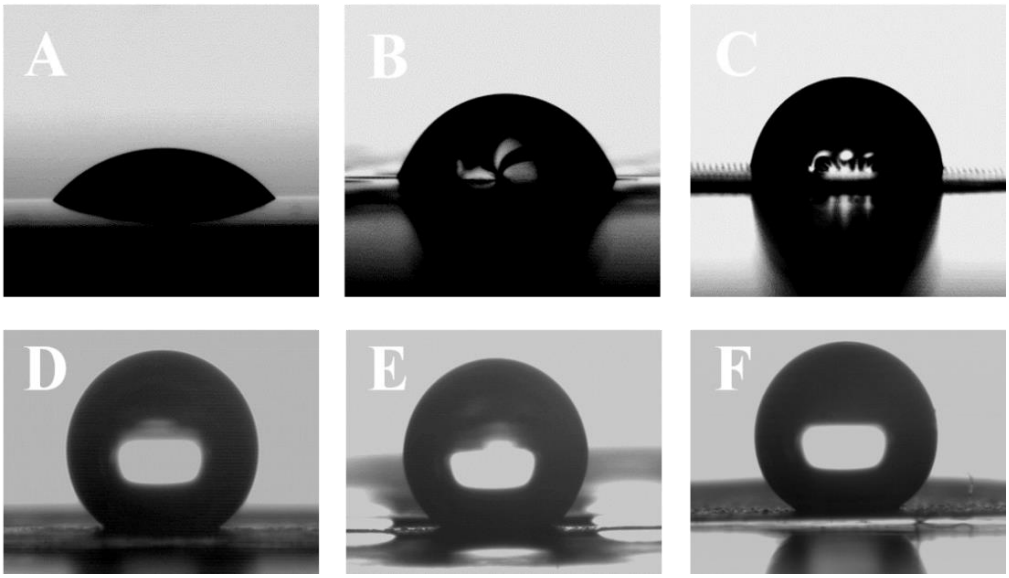

Figure 30. Contact angles of liquid water on different samples (A) Fresh Ti thin foil about 45°; (B) Fresh A about 64°; (C) Fresh B about 81°; (D) A2 about 145°; (E) A5 about 162°; (F) B1 about 150°.

5.5.2 Effects of the different MPLs

All the samples were *in-situ* characterized in a regular PEMEC and the results were shown in Figure 31. For the performance of PEMEC with micro particle MPLs, as shown in Figure 31(A), it can be seen that the performance of PEMEC can be slightly improved under the low current density range (<0.5 A/cm^2) where the activation overpotential is the main factor of the total cell voltage. But with the increase of the MPL thickness, it will have an inverse effect and results in higher cell voltage.

When the current density is increased, it can be seen that the performance of PEMEC with micro particle MPLs will approach the fresh TT-LGDL sample A. At 2.0 A/cm^2, the cell voltage of the fresh A TT-LGDLs is about 1.725 V, which is in accordance with our previous studies [27, 28, 35]. While the cell voltage for A1, A2 and A3 is about 1.722 V, 1.726 V and 1.752 V, respectively, which shows no improvement of PEMEC performance. The reason can be analyzed by the EIS results shown in Figure 31(B).

EIS is a very useful method to investigate PEMEC performance by measuring the impedance of a system at different frequencies. In this study, EIS is conducted at 80 ^{o}C and 0.2 A/cm^2. The scan frequency is set from 10 kHz to 20 mHz. The EIS curve has two intercepts with the x-axis: the left one indicates the ohmic resistance and the right one represents the total resistance, including ohmic, activation and mass transport resistances [36]. The distance between the two intercepts indicates the sum of activation and mass transport resistances. With the advantage of the TT-LGDLs, the mass transport resistance can be neglected, since there is only one arc of the EIS curve due to the easy path of the

mass transport in TT-LGDLs [27, 35]. Therefore, the diameter of the semicircle mainly indicates the activation resistance. The ohmic resistance of the fresh A, samples A1, A2 and A3 is about 83, 109, 110, and 120 mΩ*cm^2, respectively. It can be seen that the ohmic resistance of the PEMECs will be increased by adding the MPLs and the change of ohmic resistance will increase with the thicker MPLs. This may be caused by two reasons. First, MPLs have a relative roughness surface compared to the fresh TT-LGDLs, which may lead to larger interfacial contact resistance. Second, the micro particle MPLs are a mixture of micro Ti particles and Nafion ionomer, which are a porous medium and results in poor electrical conductivity. Therefore, when adding the micro particle MPLs, the ohmic resistance will be increased.

By examining the activation resistance, it can be found that the micro particle MPLs could have a smaller activation resistance. The activation resistance of the fresh A TT-LGDLs, sample A1, A2, and A3 is about 179, 126, 140 and 151 mΩ*cm^2, respectively. The activation resistance can be significantly reduced by the micro particle MPLs, as also can be seen from the IR-Free voltage in Figure 31(A). This is attributed to the more active OER sites due to the porous micro pores in the MPLs under the TT-LGDL land area, which can help to establish an easy path for water and oxygen transport within this area. By introducing the micro particle MPLs with fresh A TT-LGDLs, the previous inactive area where under the TT-LGDL land will participate in the OER, which enlarge the OER area and improve the utilization of catalyst. Thus, the activation of the OER can be reduced. But with the increase of the MPL thickness, the structure of the MPLs becomes more

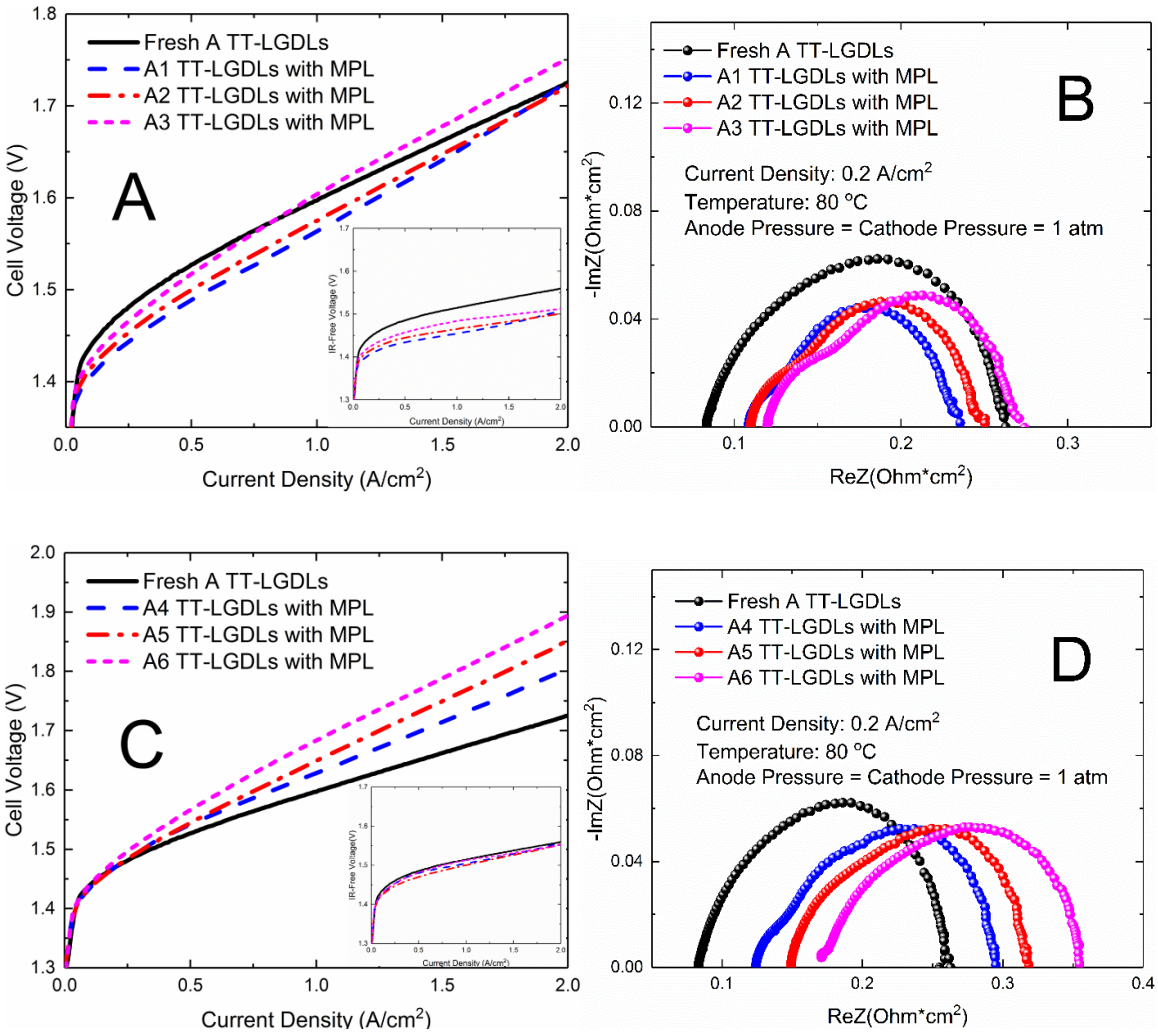

Figure 31. Performance and EIS results of A-group samples (A) Polarization curves of TT-LGDLs and micro MPLs; (B) EIS results of TT-LGDLs and micro MPLs; (C) Polarization curves of TT-LGDLs and nano MPLs; (D) EIS results of TT-LGDLs and nano MPLs.

complicated, as shown in Figure 28(A-C), which is not good for the water/oxygen transport in the MPLs. Therefore, the improvement of OER activation will decrease along with the increase of MPL thickness.

For the nano particle MPLs, as shown in Figure 31(C) and (D), different effects have been found. The PEMEC performance will be reduced by introducing the nano particle MPLs, and it will become worse with thicker nano particle MPLs. The cell voltage will increase to 1.804, 1.852, and 1.894 V for the sample A4, A5, and A6, respectively. This is mainly attributed to the increased ohmic resistance. From the EIS results, it can be seen that the ohmic resistance of fresh A TT-LGDLs, A4, A5 and A6 is about 83, 124, 149, and 171 $m\Omega*cm^2$, respectively. The ohmic resistance will be significantly increased by adding the nano particle MPLs, and it will increase with the thicker MPLs. As a result, the slope of the polarization curve will increase gradually with thicker MPLs, and leading to higher cell voltage. While the activation resistances between each sample are nearly the same as can be seen from the IR-Free voltage in Figure 31(C), which are due to the dense structure of the nano particle MPLs, as can be seen in Figure 28(D-F). This structure will prevent the possibility of increasing OER sites under the TT-LGDL land area. It is expected that the OER sites are not obviously affected, and the OER still mainly occurred at the rim of the pores. Therefore, the PEMEC performance will be reduced by the nano particle MPLs, which is due to the increased ohmic resistance.

Based on the above results and discussions, the effects of MPLs are expected to increase the OER sites, which will enhance the PEMEC performance by reducing the activation

loss. The TT-LGDLs used for sample A have a pore diameter of ~800 μm, and it is found that the micro and nano Ti particles will not block or bridge the pores. From our previous researches, it has been found that there is no OER sites in the middle of the pore area on the CLs, and the OER sites within this area will appear if adding some good electrical conductivity materials [30]. So sample B TT-LGDLs were employed. Since the micro particle MPLs exhibit a better performance than nano particle MPLs, and the 20 μm thickness MPLs show better uniformity of the Ti particles, it is used to prepare the sample B1. From Figure 32(A) and (B), it can be found that some Ti particles are located not only at the surface of TT-LGDL land but also in the pore area. The performance and EIS of fresh B TT-LGDLs and samples B1 were shown in Figure 32. It can be found that the ohmic resistance will increase from 81.9 to 93.8 $m\Omega*cm^2$ when adding the micro particle MPLs on sample B TT-LGDLs. In addition, the activation resistance can be significantly reduced from 165 to 114 $m\Omega*cm^2$. As a result, the cell voltage can be decreased from 1.707 V to 1.687 V at 2.0 A/cm^2. The effects of MPLs on fresh B TT-LGDLs will be *in-situ* visualized and discussed below.

5.5.3 In-situ visualization of MPL effects

In order to confirm the effects of MPLs on TT-LGDLs in PEMECs, the *in-situ* visualizations were obtained in a transparent PEMEC with the help of the HMVS. The detailed information on transparent PEMEC and HMVS can be found in our previous studies [33, 34]. The movies were captured at a speed of 3000 fps (frame per second), and slowly played at 30 fps. The fresh B TT-LGDLs and sample B1 were both *in-situ* visualized

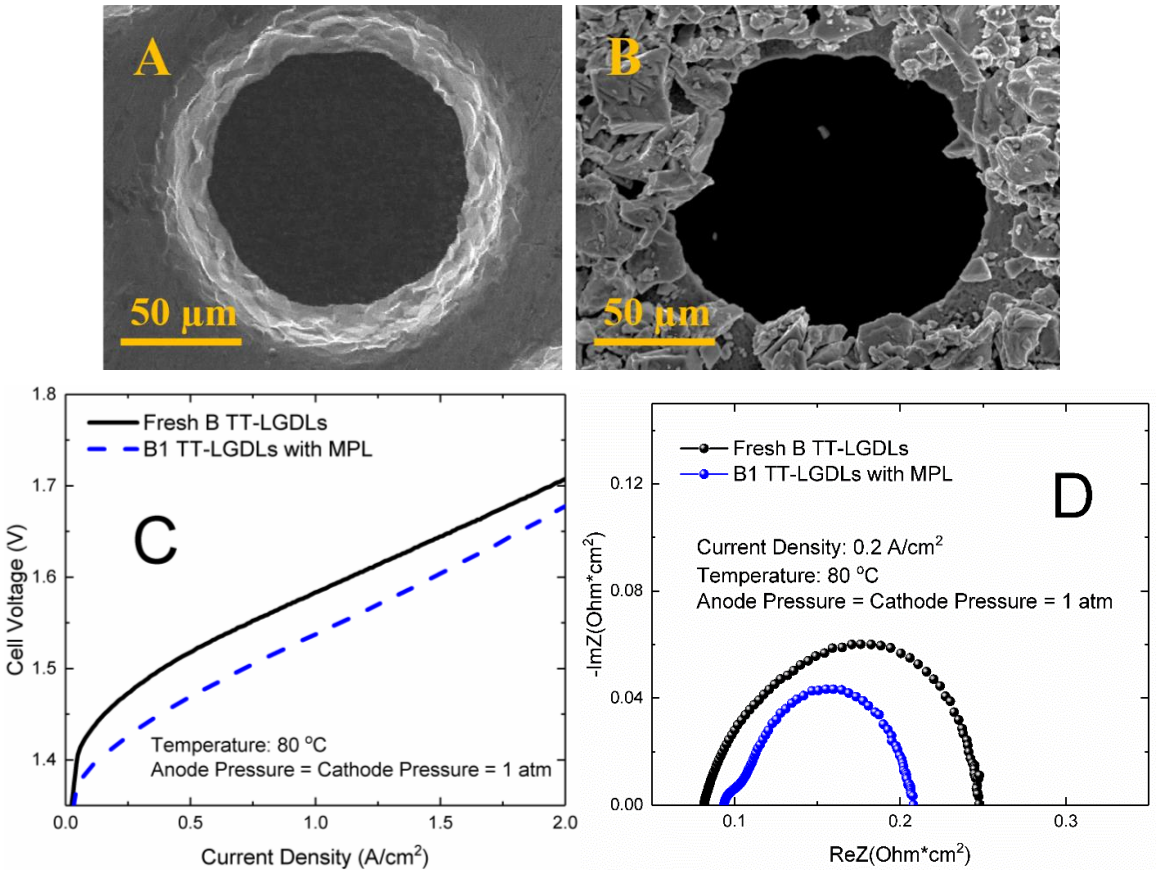

Figure 32. SEM images and *in-situ* characterization fresh B and B1 TT-LGDLs (A) Fresh B TT-LGDLs at pore-scale; (B) Sample B1 at pore-scale; (C) Polarization curves; (D) EIS results.

and the images shown in Figure 33 were captured from the supplementary movies.

Our previous studies have confirmed that the visualized bubble sites are the electrochemical reaction sites in PEMECs [30]. Due to the requirements of the electrochemical reactions at anode of PEMECs, the OER must meet the triple-phase boundary (TPB) [37, 38]. The porous complicated CL structures provide nonuniform active catalyst distribution throughout the CLs, which lead to unpredicted OER sites. But it can be found that due to the large in-plane electrical resistance, all the OER sites are mainly located at the rim of the TT-LGDL pores, and the OER sites are few within the field of view, as shown in Figure 33(A). The OER sites with fresh B TT-LGDLs varied in each pore, and some pores may have one to three OER sites, but a lot of pores have no active OER sites. From the movie, it can be seen that the oxygen bubble growth rate is slow, and the bubble detach diameter is small. When adding the micro particle MPLs, as shown in Figure 33(B), most of the pores have active OER sites. For comparison, the 15 pores are observed in the view, and it can be found that 7 pores of the fresh B TT-LGDLs are inactive, while there is only 3 inactive pores of the sample B1.

The more active pores indicate that more catalysts are participating in electrochemical reactions. That's the reason why the activation loss can be reduced when MPLs are applied. But the oxygen bubble detach diameter will increase, which is due to the wettability of the MPLs and it is not an ideal phenomenon in PEMECs. Therefore, the effects of MPLs can be summarized as follows. First, the micro porous structures of MPLs can increase the OER sites which help to reduce the activation loss of PEMEC to some extent. Second, the

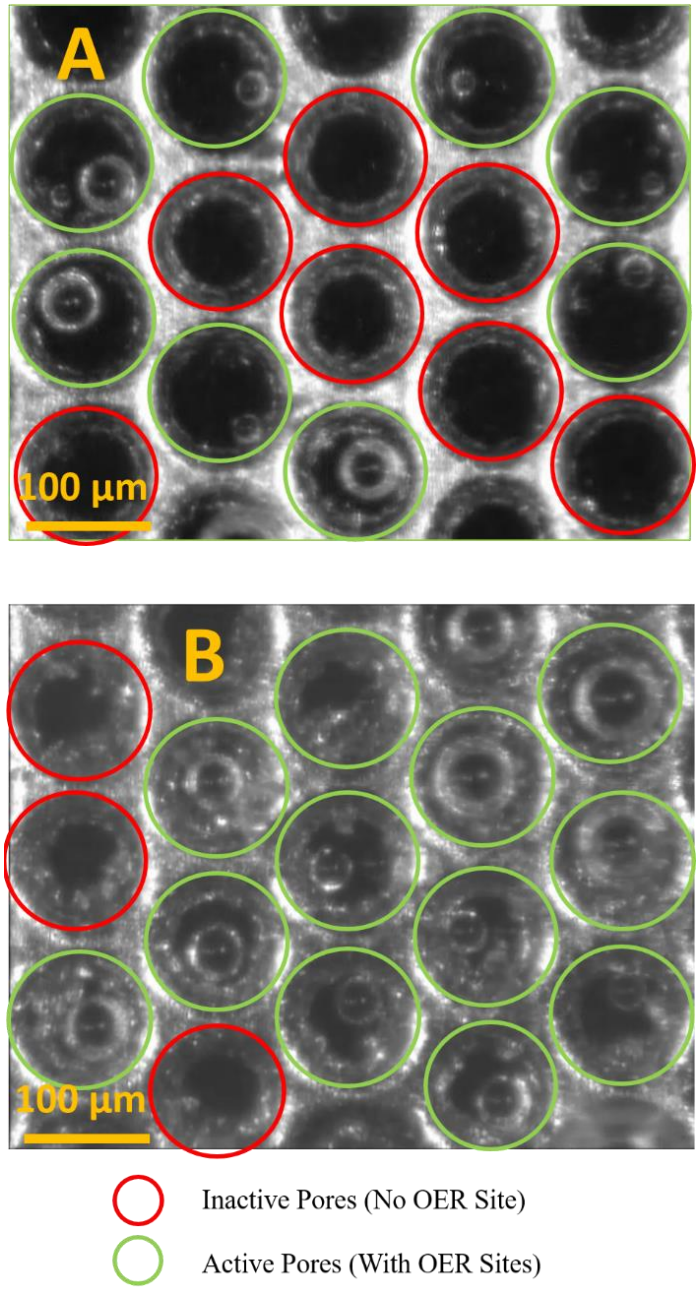

Figure 33. *In-situ* visualization of OER and oxygen bubble in PEMECs of different samples under 0.2 A/cm^2 (A) Fresh B; (B) B1.

super hydrophobic wettability of the MPLs leads to large oxygen bubble detach diameter and this may increase the mass transport loss especially at high current density ranges. Third, the additional layer between the TT-LGDLs and CLs at anode of PEMECs cannot significantly enhance the performance due to the increased ohmic loss that comes from the damaged interfacial contact and MPLs itself.

5.6 Conclusion

In this study, the MPLs in PEMECs were developed and fabricated on TT-LGDLs for the first time. The MPLs were fabricated with both micro Ti particles (~5 μm) and nano Ti particles (30-50 nm) by spraying method. The MPLs were *ex-situ* characterized and it was found that the nano particle MPLs formed a much denser structure than micro particle MPLs. Although the MPLs exhibit a super hydrophobic wettability during the measurements, the water can easily get through the TT-LGDL pores when the TT-LGDLs and MPLs are kept wet. Thus, it is anticipated that the water and oxygen can be transported within the MPLs. The nano particle MPLs exhibit a dense structure, which is not good for water/oxygen transport and lead to bad performance as a result. The *in-situ* characterization of the micro particle MPLs indicates that it has limited effects on PEMEC performance: the micro particle MPLs can slightly improve the PEMEC performance while the nano particle MPLs will degrade the PEMEC performance, which is due to the two contrary effects from the ohmic loss and activation loss. The activation loss can be reduced with the micro particle MPLs by increasing the OER sites under the TT-LGDL land area and in the pore area with some particle bridges formed, which has been confirmed by the *in-situ*

visualization results. On the other hand, the MPLs will increase the ohmic resistance because of the increased interfacial contact resistance and additional MPL resistance. Although the MPLs can reduce the activation loss by increasing OER sites, it will degrade the surface roughness and lead to large interfacial contact resistance, as the TT-LGDLs have the planar surface and thin thickness, which lead to good performance compared with conventional LGDLs in PEMECs, while the MPLs may degrade the interfacial contact. In addition, the MPLs will also increase the thickness of the MEAs, which also increase the ohmic resistance. By fabricating the TT-LGDLs with small pores and large porosities, the activation resistance is expected to be reduced, and it will not have much effect on ohmic resistance, which can lead to much better performance than TT-LGDLs with MPLs. Therefore, it is concluded that the MPLs offer some improved performance under specific conditions but may not be required for optimum TT-LGDLs in PEMECs. The results also indicate that the TT-LGDLs with small pore size and large porosity are a very promising component for high efficiency and low cost PEMEC.

References

[1] Burhan M, Oh SJ, Chua KJE, Ng KC. Solar to hydrogen: Compact and cost effective CPV field for rooftop operation and hydrogen production. *Appl Energ*. 2017;194:255-66.

[2] Ehteshami SMM, Vignesh S, Rasheed R, Chan S. Numerical investigations on ethanol electrolysis for production of pure hydrogen from renewable sources. *Appl Energ*. 2016;170:388-93.

[3] Yang J, Yu X, An L, Tu S-T, Yan J. CO2 capture with the absorbent of a mixed ionic liquid and amine solution considering the effects of SO2 and O2. *Applied energy*. 2017;194:9-18.

[4] Ruth MF, Jadun P, Pivovar BS. H2@ Scale: Technical and Economic Potential of Hydrogen as an Energy Intermediate. *National Renewable Energy Lab.(NREL), Golden, CO (United States)*; 2017.

[5] Pivovar B, Rustagi N, Satyapal S. Hydrogen at Scale (H2@Scale) Key to a Clean, Economic, and Sustainable Energy System. *The Electrochemical Society Interface*. 2018;27:67-72.

[6] Yuan X, Ding X-L, Wang C-Y, Ma Z-F. Use of polypyrrole in catalysts for low temperature fuel cells. *Energ Environ Sci*. 2013;6:1105-24.

[7] Carmo M, Fritz DL, Mergel J, Stolten D. A comprehensive review on PEM water electrolysis. *Int J Hydrogen Energ*. 2013;38:4901-34.

[8] Kotaka T, Tabuchi Y, Pasaogullari U, Wang C-Y. Impact of interfacial water transport in PEMFCs on cell performance. *Electrochim Acta*. 2014;146:618-29.

[9] Siracusano S, Baglio V, Van Dijk N, Merlo L, Aricò AS. Enhanced performance and durability of low catalyst loading PEM water electrolyser based on a short-side chain perfluorosulfonic ionomer. *Appl Energ*. 2017;192:477-89.

[10] Yan J, Shamim T, Chou S, Desideri U, Li H. Clean, efficient and affordable energy for a sustainable future. *Appl Energ*. 2017;185:953-62.

[11] Budt M, Wolf D, Span R, Yan J. A review on compressed air energy storage: Basic principles, past milestones and recent developments. *Appl Energ*. 2016;170:250-68.

[12] Ma L, Sui S, Zhai Y. Investigations on high performance proton exchange membrane water electrolyzer. *Int J Hydrogen Energ*. 2009;34:678-84.

[13] Spurgeon JM, Lewis NS. Proton exchange membrane electrolysis sustained by water vapor. *Energ Environ Sci*. 2011;4:2993-8.

[14] Hou Y, Lohe MR, Zhang J, Liu S, Zhuang X, Feng X. Vertically oriented cobalt selenide/NiFe layered-double-hydroxide nanosheets supported on exfoliated graphene foil: an efficient 3D electrode for overall water splitting. *Energy & Environmental Science*. 2016;9:478-83.

[15] Gatto I, Stassi A, Baglio V, Carbone A, Passalacqua E, Aricò A, Schuster M, Bauer B. Optimization of perfluorosulphonic ionomer amount in gas diffusion electrodes

for PEMFC operation under automotive conditions. *Electrochim Acta*. 2015;165:450-5.

[16] Han B, Mo J, Kang Z, Yang G, Barnhill W, Zhang F-Y. Modeling of two-phase transport in proton exchange membrane electrolyzer cells for hydrogen energy. *Int J Hydrogen Energ*. 2017;42:4478-89. doi: 10.1016/j.ijhydene.2016.12.103.

[17] Ito H, Maeda T, Nakano A, Kato A, Yoshida T. Influence of pore structural properties of current collectors on the performance of proton exchange membrane electrolyzer. *Electrochim Acta*. 2013;100:242-8.

[18] Mo J, Steen S, Kang Z, Yang G, Taylor DA, Li Y, Toops TJ, Brady MP, Retterer ST, Cullen DA. Study on corrosion migrations within catalyst-coated membranes of proton exchange membrane electrolyzer cells. *Int J Hydrogen Energ*. 2017. DOI: 10.1016/j.ijhydene.2017.09.020.

[19] Steen III SM, Mo J, Kang Z, Yang G, Zhang F-Y. Investigation of titanium liquid/gas diffusion layers in proton exchange membrane electrolyzer cells. *International Journal of Green Energy*. 2017;14:162-70.

[20] Mo J, Steen SM, III BH, Kang Z, Terekhov A, Zhang F-Y, Retterer ST, Cullen DA. Investigation of titanium felt transport parameters for energy storage and hydrogen/oxygen production. 13th International Energy Conversion Engineering Conference2015. p. 27-9.

[21] Ito H, Maeda T, Nakano A, Hwang CM, Ishida M, Kato A, Yoshida T. Experimental study on porous current collectors of PEM electrolyzers. *Int J Hydrogen Energ*. 2012;37:7418-28.

[22] Su H, Xu Q, Chong J, Li H, Sita C, Pasupathi S. Eliminating micro-porous layer from gas diffusion electrode for use in high temperature polymer electrolyte membrane fuel cell. *J Power Sources*. 2017;341:302-8.

[23] Lettenmeier P, Kolb S, Burggraf F, Gago A, Friedrich KA. Towards developing a backing layer for proton exchange membrane electrolyzers. *J Power Sources*. 2016;311:153-8.

[24] Nam JH, Lee K-J, Hwang G-S, Kim C-J, Kaviany M. Microporous layer for water morphology control in PEMFC. *Int J Heat Mass Tran*. 2009;52:2779-91.

[25] Chen G, Zhang G, Guo L, Liu H. Systematic study on the functions and mechanisms of micro porous layer on water transport in proton exchange membrane fuel cells. *Int J Hydrogen Energ*. 2016;41:5063-73.

[26] Polonský J, Kodým R, Vágner P, Paidar M, Bensmann B, Bouzek K. Anodic microporous layer for polymer electrolyte membrane water electrolysers. *J Appl Electrochem*.1-10.

[27] Kang Z, Mo J, Yang G, Retterer ST, Cullen DA, Toops TJ, Green Jr JB, Mench MM, Zhang F-Y. Investigation of thin/well-tunable liquid/gas diffusion layers exhibiting superior multifunctional performance in low-temperature electrolytic water splitting. *Energ Environ Sci*. 2017;10:166-75.

[28] Kang Z, Mo J, Yang G, Li Y, Zhang F-Y, Retterer ST, Cullen DA. Investigation of Novel Thin LGDLs for High-Efficiency Hydrogen/Oxygen Generation and Energy Storage. 15th International Energy Conversion Engineering Conference2017. p. 4873.

[29] Kang Z, Mo J, Yang G, Li Y, Talley DA, Retterer ST, Cullen DA, Toops TJ, Brady MP, Bender G, Pivovar BS, Green Jr JB, Zhang F-Y. Thin film surface modifications of thin/tunable liquid/gas diffusion layers for high-efficiency proton exchange membrane electrolyzer cells. *Appl Energ*. 2017;206:983-90.

[30] Mo J, Kang Z, Retterer ST, Cullen DA, Toops TJ, Green JB, Mench MM, Zhang F-Y. Discovery of true electrochemical reactions for ultrahigh catalyst mass activity in water splitting. *Science Advances*. 2016;2:e1600690.

[31] Kang Z, Mo J, Yang G, Zhang F-Y, Reterer ST, Cullen DA. Micro/nano manufacturing of novel multifunctional layers for hydrogen production from water splitting. Nano/Micro Engineered and Molecular Systems (NEMS), 2017 IEEE 12th International Conference on: *IEEE*; 2017. p. 126-30.

[32] Mo J, Kang Z, Yang G, Retterer ST, Cullen DA, Toops TJ, Green JB, Zhang F-Y. Thin liquid/gas diffusion layers for high-efficiency hydrogen production from water splitting. *Appl Energ*. 2016;177:817-22.

[33] Mo J, Kang Z, Yang G, Li Y, Retterer ST, Cullen DA, Toops TJ, Bender G, Pivovar B, Green J. In-situ investigation on ultrafast oxygen evolution reactions of water

splitting in proton exchange membrane electrolyzer cells. *J Mater Chem A*. 2017;5:18469-75.

[34] Mo J, Kang Z, Yang G, Barnhill W, Zhang F-Y, Talley D. Visualization on rapid and micro-scale dynamics of oxygen bubble evolution in PEMECs. Nano/Micro Engineered and Molecular Systems (NEMS), 2017 IEEE 12th International Conference on: *IEEE*; 2017. p. 101-5.

[35] Kang Z, Mo J, Yang G, Li Y, Talley DA, Han B, Zhang F-Y. Performance Modeling and Current Mapping of Proton Exchange Membrane Electrolyzer Cells with Novel Thin/Tunable Liquid/Gas Diffusion Layers. *Electrochim Acta*. 2017;255:405-16. DOI: 10.1016/j.electacta.2017.09.170.

[36] Sun S, Xiao Y, Liang D, Shao Z, Yu H, Hou M, Yi B. Behaviors of a proton exchange membrane electrolyzer under water starvation. *Rsc Adv*. 2015;5:14506-13.

[37] Mench MM. Fuel Cell Engines: *John Wiley & Sons*; 2008.

[38] Hong WT, Risch M, Stoerzinger KA, Grimaud A, Suntivich J, Shao-Horn Y. Toward the rational design of non-precious transition metal oxides for oxygen electrocatalysis. *Energ Environ Sci*. 2015;8:1404-27.

CHAPTER VI

NOVEL THIN/TUNABLE GAS DIFFUSION ELECTRODES WITH ULTRA-LOW CATALYST LOADING FOR HYDROGEN EVOLUTION REACTION IN PROTON EXCHANGE MEMBRANE ELECTROLYZER CELLS

A version of this chapter was originally published by Zhenye Kang:

Zhenye Kang, Jingke Mo, Gaoqiang Yang, Yifan Li, Scott T. Retterer, David A. Cullen, Todd J. Toops, Guido Bender, Bryan S. Pivovar, Johney B. Green Jr, Feng-Yuan Zhang. "Novel Thin/Tunable Gas Diffusion Electrodes with Ultra-Low Catalyst Loading for Hydrogen Evolution Reaction in Proton Exchange Membrane Electrolyzer Cells." *Nano Energy*, 47, (2018): 434-441.

I am fully responsible for the work submitted in this publication.

6.1 Graphical Abstract

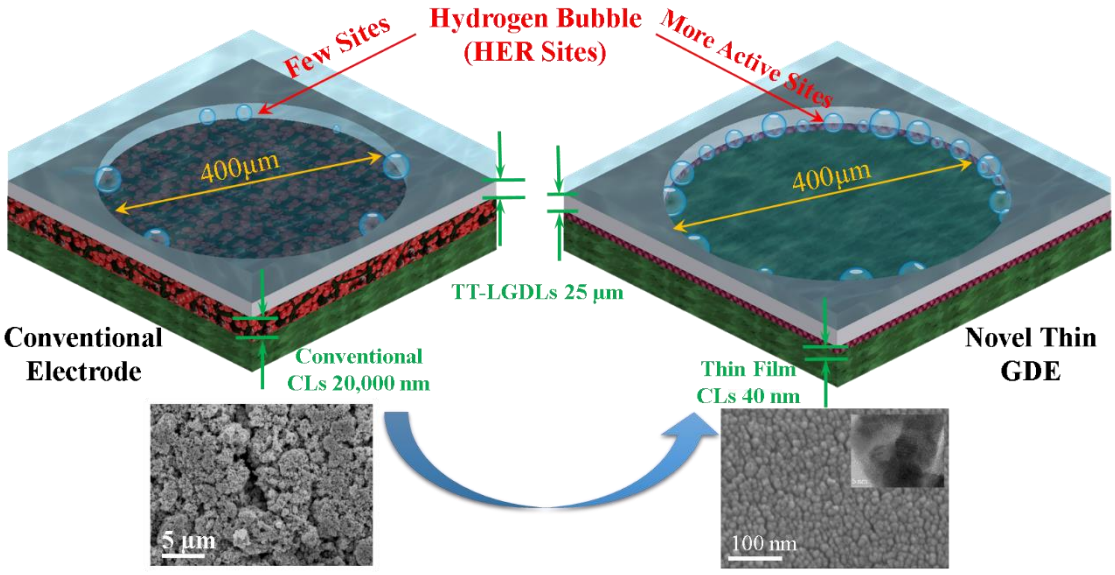

6.2 Abstract

Proton exchange membrane electrolyzer cells (PEMECs) have received great attention for hydrogen/oxygen production due to their high efficiencies even at low-temperature operations. Because of the high cost of noble platinum-group metals (PGM) catalysts (Ir, Ru, Pt, etc.) that are widely used in water splitting, a PEMEC with low catalyst loadings and high catalyst utilizations is strongly desired for its wide commercialization In this study, the ultrafast and multiscale hydrogen evolution reaction (HER) phenomena in an operating PEMEC is *in-situ* observed for the first time. The visualization results reveal that the HER and hydrogen bubble nucleation mainly occur on catalyst layers at the rim of the pores of the thin/tunable liquid/gas diffusion layers (TT-LGDLs). This indicates that the catalyst material of the conventional catalyst-coated membrane (CCM) that is located in the middle area of the LGDL pore is underutilized/inactive. Based on this discovery, a novel thin and tunable gas diffusion electrode (GDE) with a Pt catalyst thickness of 15 nm and a total thickness of about 25 μm has been proposed and developed by taking advantage of advanced micro/nano manufacturing. The novel thin GDEs are comprehensively characterized both *ex-situ* and *in-situ*, and exhibit excellent PEMEC performance. More importantly, they achieve much higher catalyst mass activity of up to 58 times higher than conventional CCM at 1.6 V under the operating conditions of 80 ^{o}C and 1 atm. This study points out a promising concept for PEMEC anode electrode development, and provides a direction of future catalyst design and fabrication for electrochemical devices.

6.3 Introduction

Hydrogen is considered to be very attractive energy carrier, as it offers high energy density and non-pollutant emissions. When coupled with renewable energy resources, proton exchange membrane electrolyzer cells (PEMECs) are capable of hydrogen/oxygen production for sustainable energy system with high efficiency and low cost [1-12]. Water can be split into oxygen and hydrogen through catalyst-driven electrochemical reactions at low temperatures. Catalysts are typically iridium-ruthenium oxides ($IrRuO_x$) at the anode and platinum black (PtB) at the cathode [11-13]. All three metals are very scarce, which means it is critical to maximize utilization and to reduce precious metal loadings [14, 15]. Challenges regarding catalyst cost and availability will only worsen as hydrogen production begins to scale up, making this issue even more critical [16-22].

In PEMECs, the hydrogen generated at the cathode via the hydrogen evolution reaction (HER), usually includes three steps: Volmer, Heyrovsky and Tafel steps [23-25]. The HER rate is greatly influenced by hydrogen adsorption free energy (HAFE). The optimal HER catalysts should have the HAFE close to zero, and also have appropriate properties in order to provide the best catalytic activity [23]. Platinum offers a high catalytic activity for the HER in acidic media and a conversion efficiency > 80% and it is the most commonly used catalyst for the HER [26]. Typical and conventional methods of manufacturing the catalyst layer in membrane electrode assemblies (MEAs) include painting, spraying, and printing of catalyst inks, which contain polymer electrolyte and carbon supported catalysts, onto the Nafion membrane [27-30]. Many new fabrication techniques have been used to produce

electrodes with extremely low catalyst loadings. Production methods include sputter deposition, reactive spray deposition techniques (RSDT), core-shell catalyst structure fabrication, platinum nanocages or nanowires. Most of these novel catalysts were characterized and analyzed with *ex-situ* methods, lacking any *in-situ* PEMEC performance characterization [14, 19, 31-33]. Sputter deposition, with its advantages of low cost and ease of operation, has been investigated to fabricate electrodes in different types of fuel cells (FCs). In many cases, these electrodes improved catalyst utilization over conventional catalyst-coated membrane (CCM) [32-35]. In particular, it has been found that catalysts that are deposited directly on gas diffusion layers (GDLs) show good potential to improve FC performance. The mechanisms for these results remained unclear and the *in-situ* HER in a PEMEC has never been explored partially because it occurs very rapidly and inside the PEMEC device [33, 36-38]. To our best knowledge, there is no public literature that has *in-situ* visualized the HER in an operating PEMEC. We recently developed the thin and tunable liquid/gas diffusion layers (TT-LGDLs) with straight-through pores and well-controlled pore morphologies. These TT-LGDLs have demonstrated superior multifunctional performance with voltages as low as 1.66 V at 2.0 A/cm^2 and 80 ^{o}C [39]. By taking advantages of the TT-LGDL unique features with the straight-through pores, the oxygen evolution reaction (OER) at the PEMEC anode has been successful captured [11].

In this study, the ultrafast and multiscale HER, and hydrogen bubble dynamics in an operating PEMEC was *in-situ* observed for the first time. Based on the micro pore-scale visualization results, a novel thin GDE with a catalyst thickness of 15~90 nm and a total

thickness of only 25 μm was developed using TT-LGDLs. The impact of catalyst loading on thin GDE morphology was examined by scanning electron microscopy (SEM) and scanning transmission electron microscopy (STEM). The *in-situ* performances of samples with different catalyst loadings were investigated and compared to PEMEC with conventional CCMs. It has been found that the novel thin GDEs could not only obtain an excellent performance, but also achieve superior catalyst mass activity of up to 58 times more than conventional CCM.

6.4 Experimental Details

For the testing system, the PEMEC was compressed by eight evenly distributed bolts, which were tightened to 4.52 N·m of torque. Two end-plates were made from commercial grade Al and provided even compression on the PEMEC. The bipolar plates made from graphite (AXF-5Q) had the parallel flow channels. The PEMEC had an active area of 5 cm^2. The tests were operated under atmosphere pressure at 80 ^oC. The PEMEC was attached to an electrolyzer control system with current range up to 100 A and a voltage range up to 5 V (Potentiostat VSP/VMP3B-100 from Bio-Logic). The hardware was connected to EC-Lab, an electrochemical analysis software from Bio-Logic, which was used to test and evaluate performance. The polarization curve of performance and high-frequency resistance (HFR) were measured during the tests.

To catch the phenomena of the electrochemical reactions in an operating PEMEC, a high-speed and micro-scale visualization system (HMVS) was built and coupled with a

transparent PEMEC cathode [11]. In order to visualize the HER and hydrogen bubble formation at the cathode side, DI water was circulated at both anode and cathode of the transparent PEMEC. The flow of DI water at anode and cathode was controlled by two separate diaphragm liquid pumps with a flow rate of 20 ml/min (about 5.86 cm/s in each flow channel). The HMVS contained a high-speed camera (Phantom V711) and long working distance optical system (Infinity K2 DistaMax). With the help of the HMVS, local hydrogen formation can be observed and analyzed based on micro-scale bubble generation in the transparent/operational PEMECs.

A conventional CCM (Nafion 115 from FuelCellEtc) with 3.0 mg/cm^2 $IrRuO_x$ at the anode and 3.0 mg/cm^2 Pt black at the cathode was used as a baseline. Nafion 115 membranes coated on a single side with 3.0 mg/cm^2 $IrRuO_x$ at the anode were used as membranes in this study. A fresh carbon paper with 280 µm thickness and 78% porosity was used as the anode LGDLs for each test [39, 40]. Titanium TT-LGDLs with a circular pore diameter of 400 µm and porosity of approximate 50% were used as cathode LGDLs, and also acted as substrates for platinum sputter deposition. Plasma modifications and sputter deposition augmentations were both completed using a BIO-RAD Polaron Division SEM Coating System E5150. A potential of 2.4 kV and a current of 20 mA was maintained to control the deposition rate for platinum. The thickness of the coating was controlled by the sputtering time. A titanium foil sample was sputter deposited *in-situ* with each TT-LGDL. The sputter coated Pt was examined under SEM to determine the surface characteristics of the platinum thin film. The loadings of Pt and thickness were calculated by weighing the TT-LGDLs

and the *in-situ* deposited Ti foil, respectively, and the results are shown in Table 8. When estimating the thickness of the Pt thin film, the bulk density of Pt was used, and the thickness was also examined under STEM. It should be noted that the catalyst loading of the CCM is 15 to 93 times that of the catalyst deposited on the TT-LGDLs as shown in Table 8.

The Pt morphologies were identified by using a field emission SEM JEOL JSM-6320F with an accelerating voltage of 0.5 – 30 kV, a magnification of 130 x~650,000 x and a 5-axis specimen mount. Thin cross section samples were prepared for STEM analysis by diamond-knife ultramicrotomy. Aberration-corrected bright-field STEM images were acquired in the JEOL JEM 2200FS TEM/STEM and energy dispersive X-ray spectroscopy (EDS) was performed in the Hitachi HF3300 TEM/STEM.

Table 8. Parameters of the platinum thin film coated on the TT-LGDLs.

Sample	Thickness [nm]	Effective Pt Loading [mg/cm^2]	Loading Ratio of CCM Pt over Sputter Deposited Pt
A1	15	0.032	93.75
A2	24	0.051	58.82
A3	40	0.086	34.88
A4	90	0.193	15.54

6.5 Results and Discussion

The catalysts morphology of the conventional CCM is examined under SEM and the results are shown in Figure 34(a) and (b). It can be seen that the CL of the conventional CCM is a porous media which forms non-uniformly distributed agglomerates on the membrane surface [39]. This will likely cause locally changing physical properties and catalytic activities at the conventional CL. The conventional CLs have a thickness of 20 μm. It conducts both protons and electrons: protons from the PEM will be transported through the ionomer in the CLs to the HER sites, while the electrons are conducted by the Ti felt LGDL or TT-LGDLs and the Pt in the CLs to the HER sites. HER occurred hydrogen bubbles are generated across the entire CL, as shown in Figure 34(g) and (h), since the protons and electrons can be transported in the CL. For the LGDLs, the conventional LGDLs made from Ti fibers or carbon fibers, are porous media and have a random pore morphology, including pore shape, pore size and pore distribution. The complex structures of Ti felt hinder the possibility of *in-situ* visualization of HER and hydrogen bubble in PEMECs. In order to visualize the ultrafast and microscale HER, the novel TT-LGDLs with straight-through pores and planar surface are designed and fabricated. The typical manufacturing process includes photo-lithography and chemical wet-etching. The thickness of the TT-LGDLs is only 25 μm, which is much thinner than conventional Ti felt of about 350 μm in thickness. The PEMECs with TT-LGDLs can obtain a superior performance due to the remarkably reduced mass transport, ohmic and activation losses [39, 41, 42] compared with the conventional Ti LGDL at anode side [40, 43].

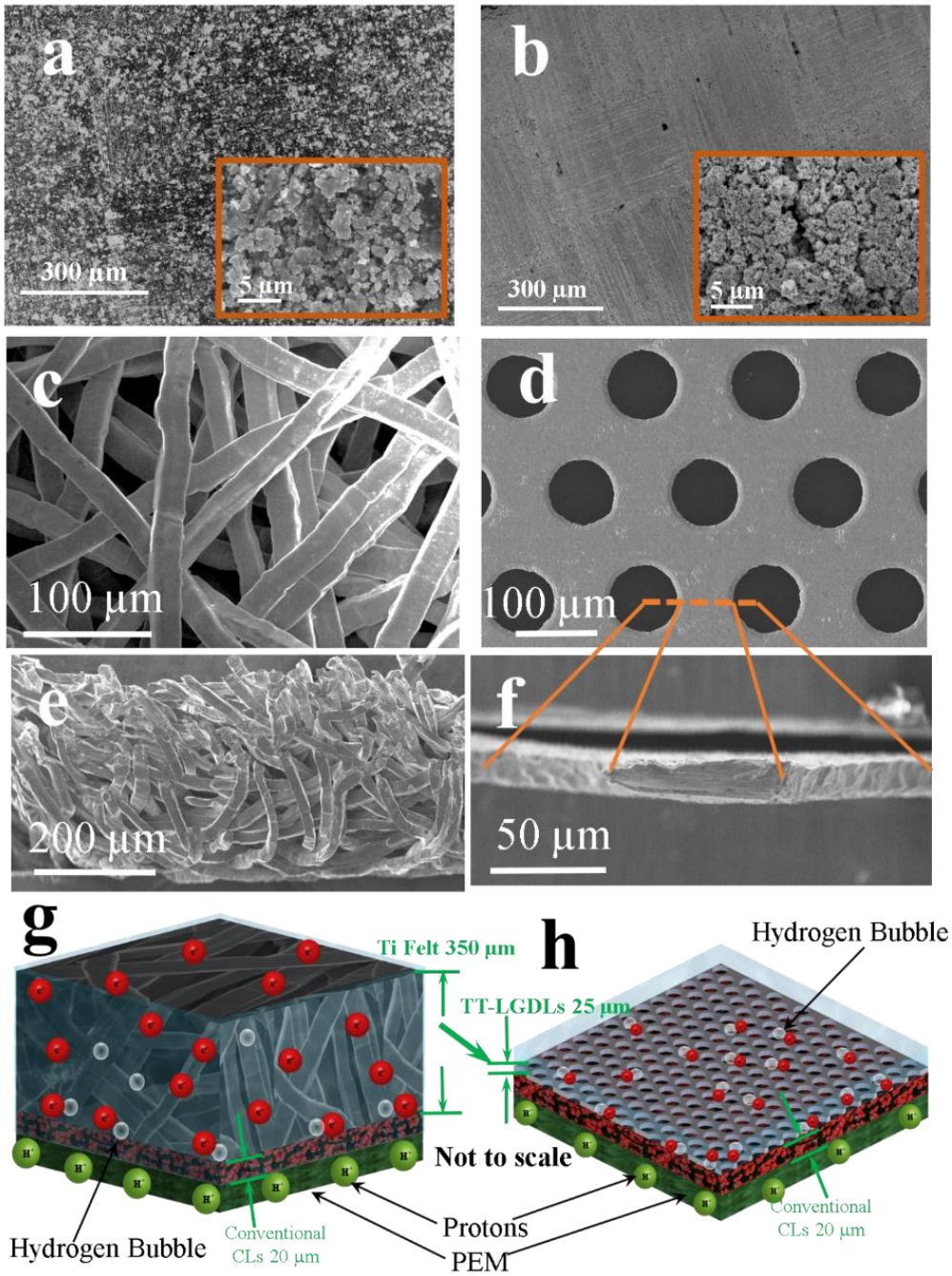

Figure 34. SEM images and schematics of different MEAs. (a) Anode CL ($IrRuO_x$) of CCM. (b) Cathode CL (PtB) of CCM. (c) Top-view of conventional Ti felt LGDLs. (d) Top-view of TT-LGDLs. (e) Cross-section of conventional Ti felt LGDLs. (f) Cross-section of TT-LGDLs. (g) Schematic of HER and hydrogen bubble generation in conventional LGDLs. (h) Schematic of conventional perception of hydrogen bubble generation with novel TT-LGDLs.

The conventional CCM with TT-LGDLs is assembled in a transparent PEMEC and tested *in-situ*. The *in-situ* ultrafast and microscale HER is captured and observed using the HMVS system. Results are shown in Figure 35(b) and (c), which are from the movies. The visualization movie is captured under the frame rate of 3000 fps and replayed at 15 fps in order to analyze the ultrafast HER phenomenon. The flow channels and pores of the TT-LGDLs are filled with water with exception of hydrogen bubbles from the HER. The shiny part is the novel TT-LGDLs and the dark grey part in the circular pore is the cathode catalyst layer (Pt black) of the CCM. The pattern of the CCM cathode catalyst layer is similar to that of the sample in Figure 34(b), which is due to the CCM fabrication process. It is well known that the electrochemical reaction happens at triple-phase boundaries (TPBs) representing the locations with electron/proton conductors, active catalysts, and pathways for reactants/products [11]. At the cathode, there are no reactants besides the protons from the Nafion membrane and electrons from the external circuit, and the only product is hydrogen. Hydrogen will generate at the sites that satisfy the TPB requirements. During the visualization experiment, the hydrogen bubbles form mainly at the rim of the pore. Our previous research has verified that the bubble generation sites are the same as the electrochemical reaction sites, which means the bubble will be eventually observed whenever and wherever there is electrochemical reaction on the CLs [11]. Due to the fabrication of the CCM, the catalyst in the CL may not distribute uniformly and the complex structure of the CL will lead to nonuniform TPB sites [39]. That is why only a few sites on the rim of the pore can be active as shown in Figure 35(b) and (c).

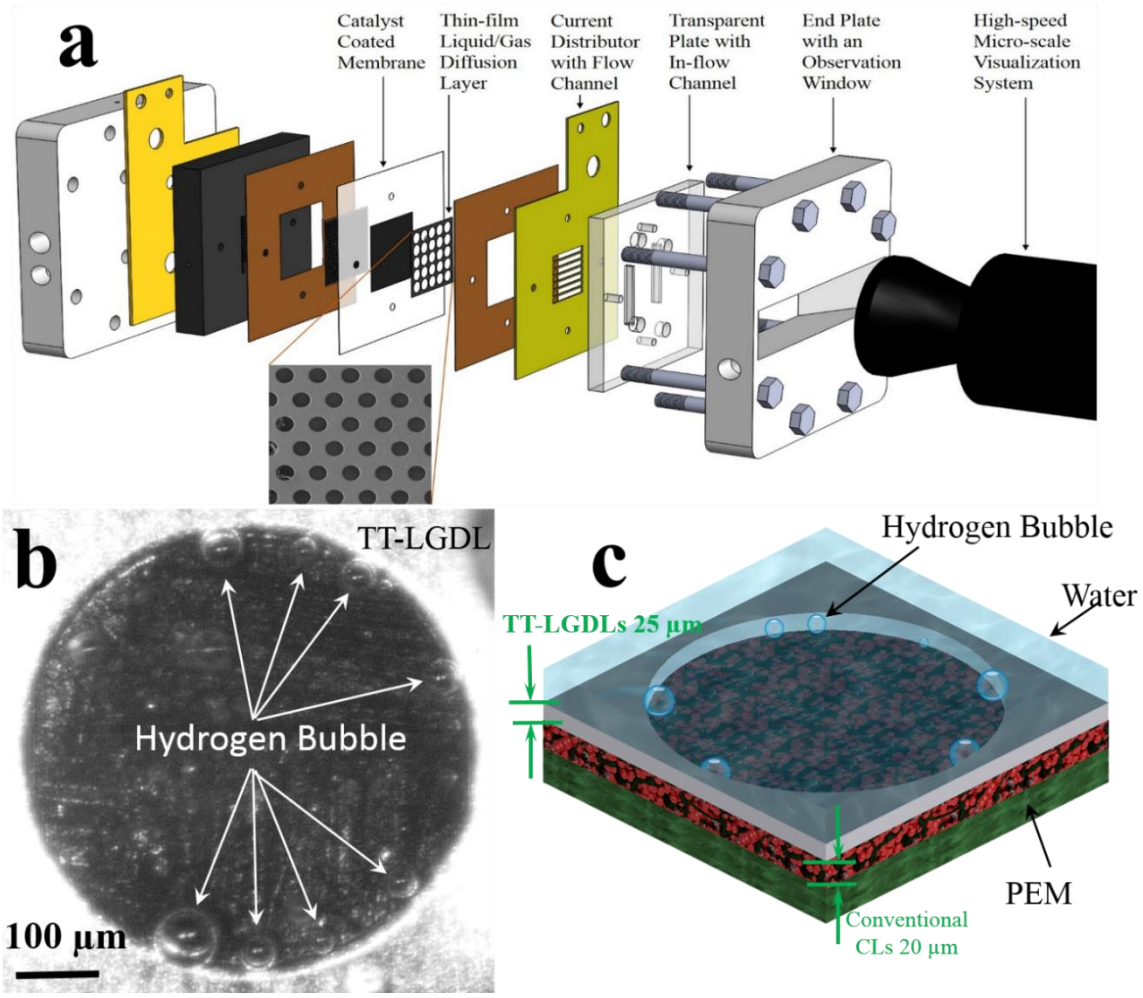

Figure 35. High-speed and micro-scale visualization system (HMVS) and high-speed/pore-scale visualization results with conventional MEAs. (a) Schematic of HMVS and transparent PEMECs with novel TT-LGDLs. (b) and (c) Image and schematic of HER phenomena within pore area under the operating conditions of 80 ^{o}C at 0.4 A/cm^{2}.

It is believed that due to the large electrical resistance in conventional CLs, the hydrogen bubbles are mainly generated at the rim of the pore. This observation is similar to the observation of the bubble formation during the OER at the anode of PEMECs [11, 39]. From the above *in-situ* HER and hydrogen bubble generation observations, it can be assumed that a large amount of catalyst located in the middle of the pore area is inactive. This would cause low catalyst mass activity. Based on the above assumptions, a novel thin GDE with ultra-low catalyst loadings is designed, as shown in Figure 36(a) and (b). The design features the lack of catalyst in the pore area, reducing the CL thickness (from ~20 μm to only 15-90 nm) and using ionomer free CL design (thin film Pt layer). It is expected to increase catalyst utilization and achieve a higher Pt catalyst mass activity. For the novel thin GDEs, the protons can be transported from the PEM directly to the HER sites, while the electrons can be transported from the TT-LGDLs through the thin film CLs to the HER sites. With the design of the novel thin GDEs, it is expected that the HER and hydrogen bubble generation will only occur at the rim of the pore, due to the TPB requirements.

The novel thin GDEs are tested in the transparent PEMECs and the visualization results are shown in Figure 36(c) and (d). For the GDEs, the nano-film Pt is deposited on the surface of the TT-LGDLs and in direct contact with the Nafion of the membrane. The dark black area in Figure 36(c) shows the anode catalyst layer on the membrane backside since the Nafion membrane is almost transparent. For the novel thin GDE shown in Figure 36(c) and (d), the reaction sites are distributed along the rim of the pore as well, which is similar to the HERs occurred in the PEMEC with conventional CCMs.

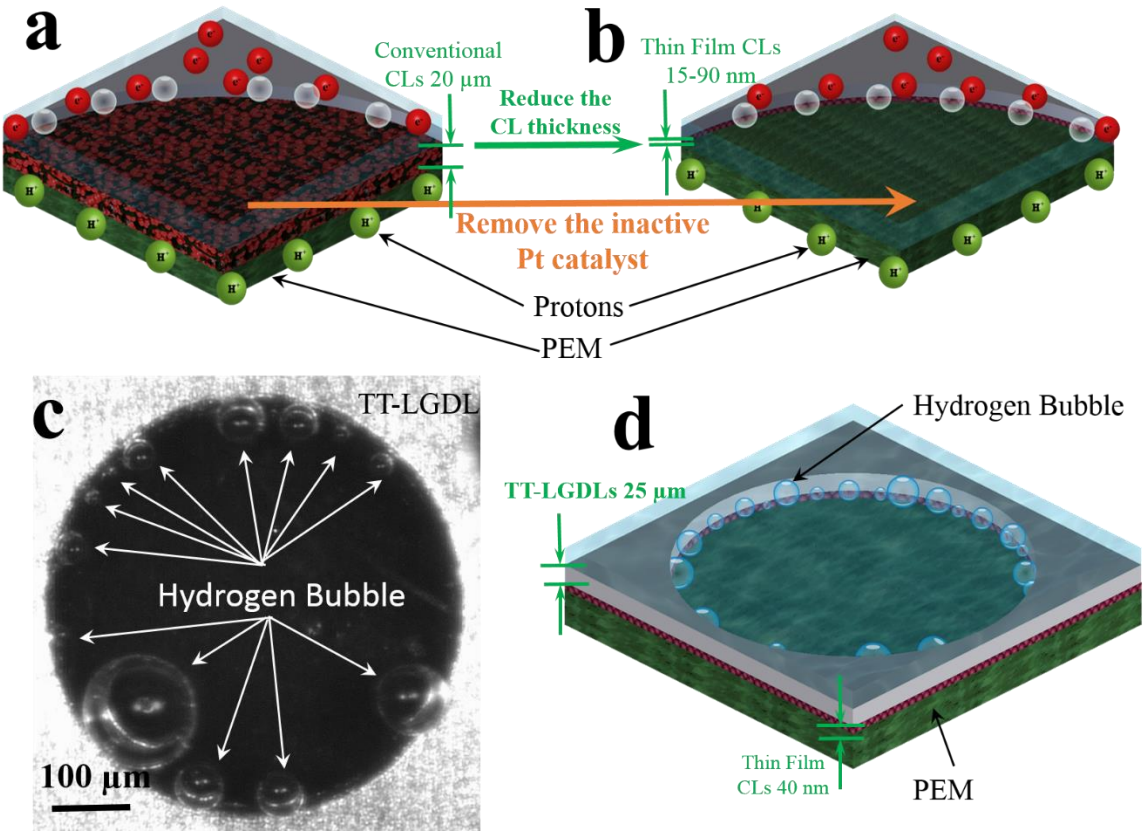

Figure 36. Schematics and high-speed/pore-scale visualization results with novel thin GDEs. (a) HER and hydrogen bubble generation with conventional MEAs and TT-LGDLs. (b) Novel thin GDEs – nano-film catalyst-coated TT-LGDLs. (c) Image of HER phenomena within pore area with the novel thin GDE under the operating conditions of 80 ^{o}C at 0.4 A/cm^2. (d) Schematic of HER and hydrogen bubble generation.

The novel thin GDEs Pt nano-film catalysts are *ex-situ* characterized and *in-situ* test in a standard PEMEC. As shown in Figure 37(a), (b) and (c), the morphologies of the sputter coated catalyst and conventional CCM (as shown in Figure 34(b)) are very different. The catalyst of the CCM has a porous morphology while the sputtered catalyst is obviously much denser just with some cracks on the surface. The grain size, lattice fringe and thickness of the thin film Pt layer are examined under BF-STEM and STEM-EDS, as shown in Figure 37(b) and (c). It can be seen that the thickness of the CL (Sample A3) is around 40 nm with individual crystalline grains of about 5 nm, and the platinum distributed uniformly on the surface of the Ti substrate.

Both conventional CCM with TT-LGDLs and Ti Felt, and novel thin GDEs are tested in a regular PEMEC and the results for the conventional CCM and GDE A3 (40 nm Pt thin film layer) are shown in Figure 37.

It can be seen that the performance of the CCM with Ti felt achieves similar performance compared with our novel thin GDE, but worse than CCM with TT-LGDLs. The cell voltage of the CCM with TT-LGDLs, Ti Felt, and GDE A3 is about 1.72 V, 1.85 V, and 1.84 V at 2.0 A/cm^2, respectively. The HFR of the Ti felt is about 0.034 Ω, which is much larger than CCM with TT-LGDLs (0.015 Ω) and GDE-A3 (0.022 Ω), and it will lead to higher cell voltage at high current density ranges (> 1.0 A/cm^2). It has been proofed that the TT-LGDLs can significantly reduce the ohmic losses due to its planar surface, thin thickness and good conductivity, and that is why the CCM with TT-LGDLs can achieve smaller HFR than CCM with Ti Felt [39, 40].

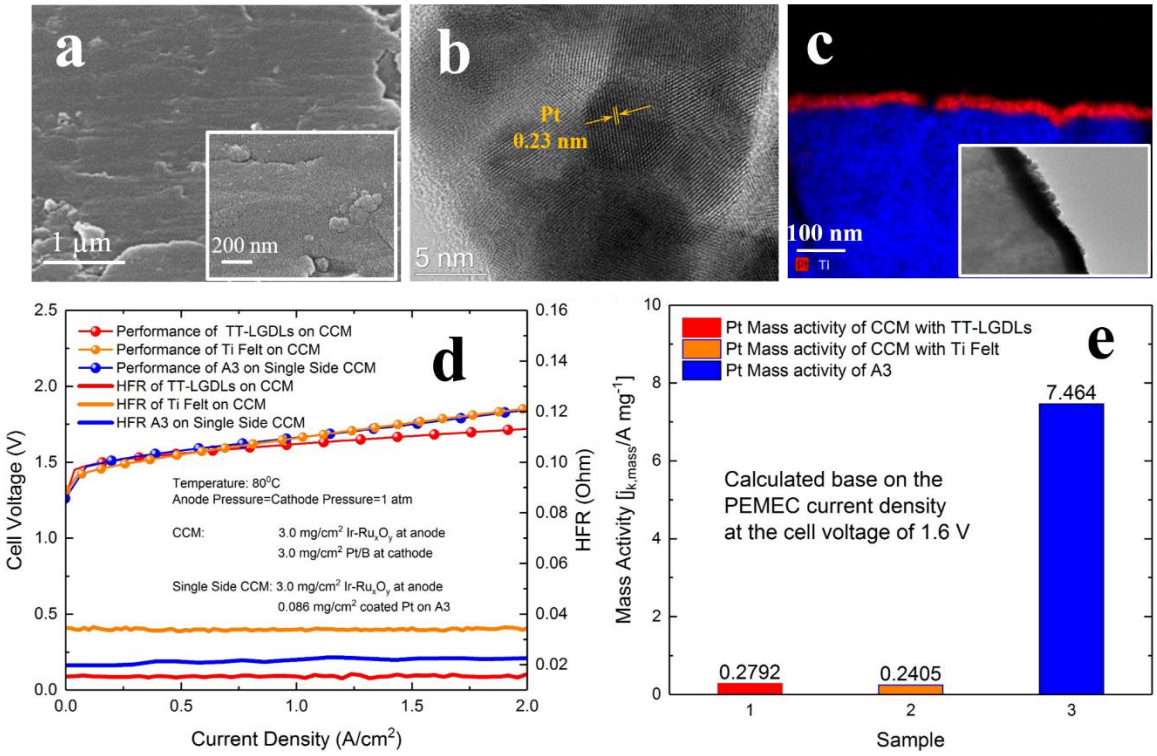

Figure 37. SEM/STEM results and performance comparison. (a) SEM images of the Pt CL on GDE. (b) BF-STEM images of Pt CL on GDE showing crystallite size and Pt lattice spacing. (c) Cross-sectional STEM-EDS spectrum image of Pt CL on GDE with a thickness of about 40 nm. (d) Polarization curves between conventional MEA and the novel thin GDE. (e) Catalyst mass activity comparisons at 1.6 V.

It is known that the interfacial contact resistance in the PEMEC contributes to a large part of ohmic resistance [44]. For the novel thin GDEs, an increased HFR may be expected from the proton transport resistance at the CL/PEM interface. The Pt mass activity is about 0.24, 0.28 A/mg for the CCM with TT-LGDLs and Ti Felt, respectively, which means that the TT-LGDLs can slightly improve the catalytic activity. Therefore, the CCM with TT-LGDLs can achieve better performance due to the improved catalyst mass activity and reduced ohmic loss. While the novel thin GDEs can greatly improve the Pt mass activity to 7.4 A/mg, almost 31 folds than CCM with Ti felt, and 26 folds than CCM with TT-LGDLs. Although the GDE A3 cannot achieve better performance than CCM with TT-LGDLs, it should be noted that the Pt loading of the GDE A3 is small. The utilization of the catalyst has been greatly enhanced and improved. On the other hand, the similar performances of the conventional CCM with TT-LGDLs and the novel thin GDE, as shown in Figure 37(d), may demonstrate that most of the catalyst that located in the middle of the pore area is inactive and does not contribute to the cell performance. Therefore, the novel thin GDEs are able to achieve good performance although no catalyst is present in the pore area of the TT-LGDLs, which is almost 50% of the geometric area. The ultra-thin GDEs consequently achieve much higher utilization and higher catalyst mass activity.

Figure 38 and Figure 39 show *ex-situ* and *in-situ* results of novel thin GDEs with different thicknesses of catalyst thin films. The *ex-situ* experiments indicate that the platinum did not form continuous films on the titanium TT-LGDLs, but rather agglomerated, which is consistent with the literatures [33, 45].

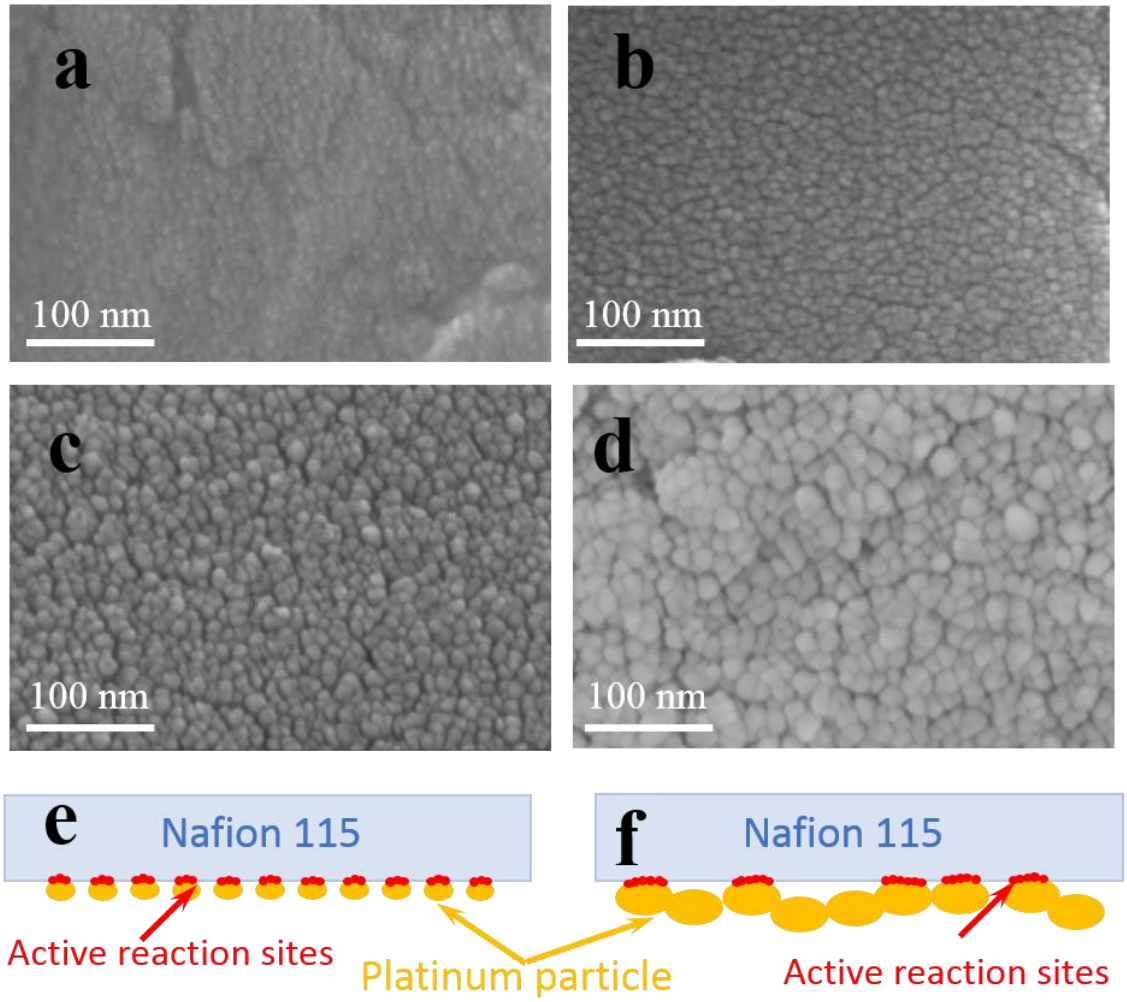

Figure 38. High resolution SEM images and schematic images of novel thin GDEs with different thicknesses of Pt CLs. Top view of SEM images of samples A1 (a), A2 (b), A3 (c), and A4 (d). Schematics of the contact and active reaction sites for the flat surface with smaller particle size (e) and rough surface with larger particle size (f).

The grain size of the platinum particles increases with the increase of deposition thickness, as shown in Figure 38. The particle size is under 10 nm when the thickness is less than 25 nm, and it increases to about 15 nm at 40 nm thickness and 20 nm at 90 nm thickness, respectively. The increase of the particle size indicates that the platinum agglomerates gradually during the deposition process. From the Figure 38(d), it can be seen that some bulges formed at the catalyst surface and the surface is not as flat as the other samples, which may result in deterioration of interfacial contacts and lead to reduced performance.

The effects of platinum loading on PEMEC performance and catalyst mass activity are shown in Figure 39. At a certain catalyst loading, or a certain catalyst layer thickness, the PEMEC shows the best performance, while at lower or higher loadings, the performance decreases. For example, at a current of 2.0 A/cm^2 the sample with the lowest loading sample A1 requires a cell voltage of 1.897 V, the best performing sample A3 requires 1.845 V and the highest loaded sample A4 requires 1.867 V. This may indicate that the amount of active reaction sites in this electrode is also a function of electrode thickness.

The electrochemical reaction occurs only at TPBs (solid/liquid/gas phase), where there are good conductors for protons (ionomer) and electrons (TT-LGDLs and Pt), paths for product (hydrogen gas), and also active catalysts [33, 46]. The Pt particles are distributed uniformly on the TT-LGDL surface. When the Pt thin film thickness increases from 15 nm to 40 nm (A1, A2 and A3), the particle size increases, which may reduce the active reaction sites and the PEMEC performance. But it has been known that the protons, which have high mobility and small size, mostly can permeate into the ionomer-free Pt thin film within tens

of nanometer scale that can increase the active reaction sites [47, 48]. Therefore, the real active reaction sites should be increased when the thickness of Pt thin film increases from 15 nm (A1) to 40 nm (A3). But this effect is limited to a threshold thickness due to the proton transport in the ionomer-free Pt thin film. When the particle size of A4 (as shown in Figure 38(f)) is larger and the surface is rougher than sample A3 (as shown in Figure 38(e)), the reaction sites will likely be reduced due to the bulges and large particle size, resulting in decreased TPB sites. The performance of the sample A2, A3 and A4 are very close, and they all achieve relatively good performance compared to the literature [28, 31, 49]. From Figure 39(b), it can be seen that the catalyst mass activity at 1.6 V decreases with increasing catalyst loading. A1 achieves the largest mass activity at 16.175 A/mg, which is almost 58 times higher than the one measured for the conventional CCM with TT-LGDLs and the value is very high when compared to the literature [11, 50]. The significant increase of catalyst mass activity demonstrated that the novel thin GDEs are an effective approach to improving the catalyst utilization. EIS is a very useful *in situ* method for analyzing PEMEC performance, ohmic resistance, activation resistance and diffusion resistance. Usually, there are two x-intercepts of the Nyquist EIS plot: the left one (high frequency) indicates the ohmic resistance and the right one (low frequency) is the sum of the resistance [51]. The EIS results of the four GDEs are tested at 0.2 A/cm^2, as shown in Figure 39(c). It can be seen that GDE-A1 has the largest ohmic loss than the others, while the differences between them are very small, which means that the ohmic resistances are almost the same, and these results can be also found as the HFR in Figure 39(a).

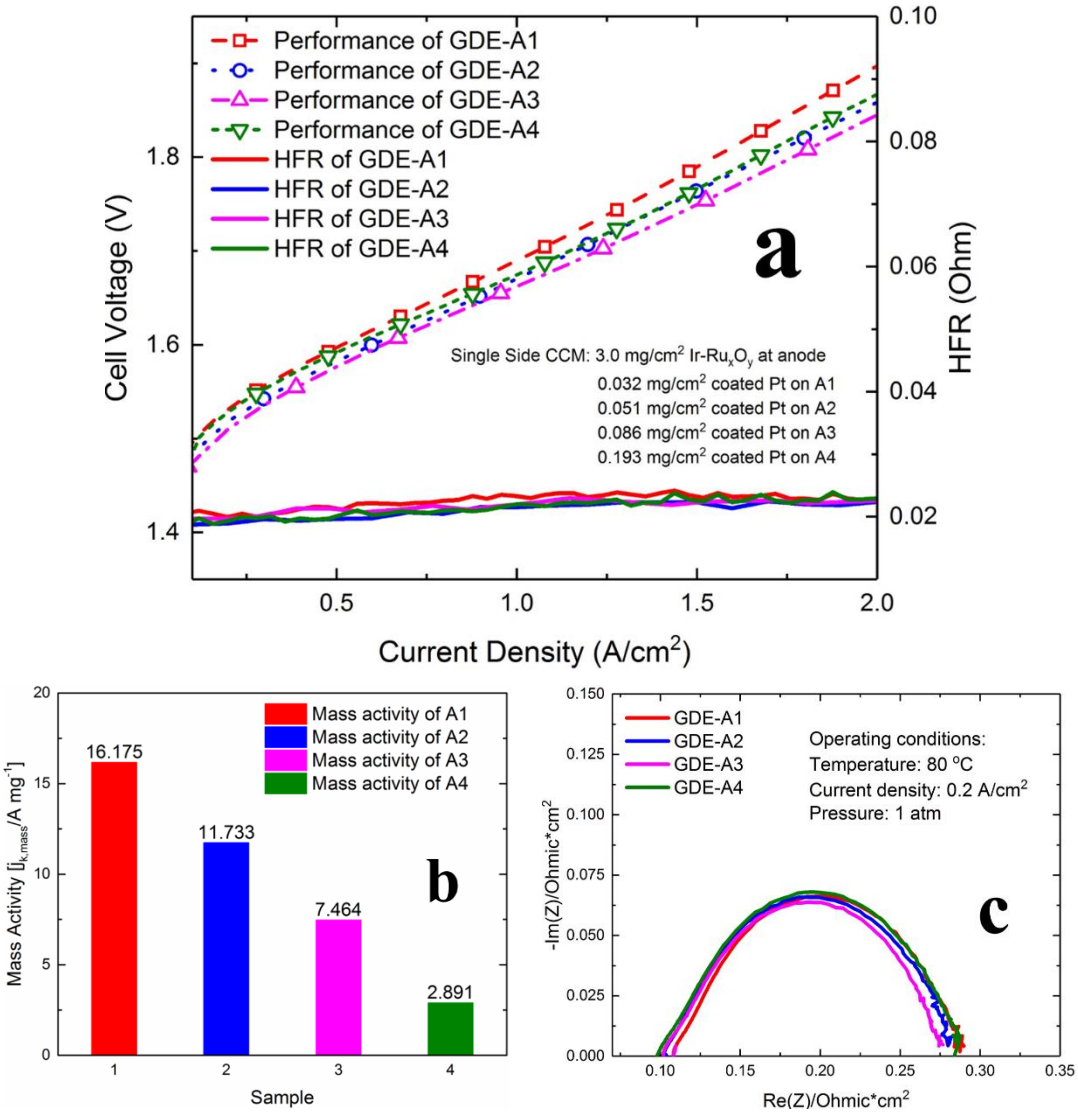

Figure 39. The effect of the nano-film catalyst thickness. (a) Polarization curves. (b) Mass activity comparisons at 1.6 V. (c) EIS.

The distance between the two x-intercepts mainly represents the activation loss [51], and it shows that the GDE-A2 and A3 have the smaller activation losses than the GDE-A1 and A4, which is in accordance with the performance results. The EIS results confirm that the Pt catalytic activity is enhanced when the Pt thin film thickness increases from 15 nm to 40 nm, while it cannot be further improved by increasing the thickness from 40 nm to 90 nm, which may be attributed to the rougher and large particle size of the GDE-A4.

6.6 Conclusion

In this study, the ultrafast and multiscale hydrogen evolution reaction (HER) and hydrogen bubble formation in an operating PEMEC are observed *in-situ* using a specially designed high-speed and micro-scale visualization system and a transparent PEMEC for the first time. The visualization results show that the hydrogen bubbles are mainly generated at the pore rim of TT-LGDLs and indicate that most catalysts located within the pore area are underutilized/inactive. Based on the findings, novel thin/tunable GDEs coupled with TT-LGDLs are developed to improve the catalyst mass activity and reduce the catalyst loading in a PEMEC. The novel thin GDEs are *ex-situ* characterized and *in-situ* tested. The novel thin GDEs achieve similar performance to conventional CCMs even at a small fraction of the catalyst loading. Superior catalyst mass activities up to 16.175 A/mg $_{Pt}$ are demonstrated. Improvements of mass activity are as high as 58 times that of conventional CCMs at 1.6 V and 80 ^{o}C. Furthermore, the effects of the catalyst loadings are investigated and an optimized thickness of GDE catalyst layer (40 nm or 0.086 mg/cm^2) is found. The successful development of the novel thin GDEs points out a promising concept and method

for the OER electrode, which has more impact on PEMEC performance and cost. This study provides a direction of future catalyst design and fabrication in future electrochemical devices.

References

[1] Chandrasekaran S, Nann T, Voelcker NH. Nanostructured silicon photoelectrodes for solar water electrolysis. *Nano Energy*. 2015;17:308-22.

[2] Escapa A, Gil-Carrera L, García V, Morán A. Performance of a continuous flow microbial electrolysis cell (MEC) fed with domestic wastewater. *Bioresource Technol*. 2012;117:55-62.

[3] Zhou X, Yang X, Hedhili MN, Li H, Min S, Ming J, Huang K-W, Zhang W, Li L-J. Symmetrical synergy of hybrid Co 9 S 8-MoS x electrocatalysts for hydrogen evolution reaction. *Nano Energy*. 2017;32:470-8. DOI: 10.1016/j.nanoen.2017.01.011.

[4] Han B, Mo J, Kang Z, Yang G, Barnhill W, Zhang F-Y. Modeling of two-phase transport in proton exchange membrane electrolyzer cells for hydrogen energy. *International Journal of Hydrogen Energy*. 2017. DOI: 10.1016/j.ijhydene.2016.12.103.

[5] Yang G, Mo J, Kang Z, III FAL, Green J, Babu SS, Zhang F-Y. Additive manufactured bipolar plate for high-efficiency hydrogen production in proton exchange membrane electrolyzer cells. *Int J Hydrogen Energ*. 2017. 10.1016/j.ijhydene.2017.04.100.

[6] Qin Y, Wang X, Wang ZL. Microfibre-nanowire hybrid structure for energy scavenging. *Nature*. 2008;451:809.

[7] Yang Y, Zhang H, Zhu G, Lee S, Lin Z-H, Wang ZL. Flexible hybrid energy cell for simultaneously harvesting thermal, mechanical, and solar energies. *Acs Nano*. 2012;7:785-90.

[8] Hansen BJ, Liu Y, Yang R, Wang ZL. Hybrid nanogenerator for concurrently harvesting biomechanical and biochemical energy. *Acs Nano*. 2010;4:3647-52.

[9] Wang ZL, Wu W. Nanotechnology-enabled energy harvesting for self-powered micro-/nanosystems. *Angewandte Chemie International Edition*. 2012;51:11700-21.

[10] Kang Z, Mo J, Yang G, Li Y, Talley DA, Han B, Zhang F-Y. Performance Modeling and Current Mapping of Proton Exchange Membrane Electrolyzer Cells with Novel Thin/Tunable Liquid/Gas Diffusion Layers. *Electrochimica Acta*. 2017;255:405-16.

[11] Mo J, Kang Z, Retterer ST, Cullen DA, Toops TJ, Green JB, Mench MM, Zhang F-Y. Discovery of true electrochemical reactions for ultrahigh catalyst mass activity in water splitting. *Science Advances*. 2016;2:e1600690.

[12] Park S, Shao Y, Liu J, Wang Y. Oxygen electrocatalysts for water electrolyzers and reversible fuel cells: status and perspective. *Energ Environ Sci*. 2012;5:9331-44.

[13] Song S, Zhang H, Ma X, Shao Z, Baker RT, Yi B. Electrochemical investigation of electrocatalysts for the oxygen evolution reaction in PEM water electrolyzers. *Int J Hydrogen Energ*. 2008;33:4955-61.

[14] Cheng N, Shao Y, Liu J, Sun X. Electrocatalysts by Atomic Layer Deposition for Fuel Cell Applications. *Nano Energy*. 2016;29:220-42. DOI: 10.1016/j.nanoen.2016.01.016.

[15] Chang YH, Lin CT, Chen TY, Hsu CL, Lee YH, Zhang W, Wei KH, Li LJ. Highly Efficient Electrocatalytic Hydrogen Production by MoSx Grown on Graphene-Protected 3D Ni Foams. *Adv Mater*. 2013;25:756-60.

[16] Ayers KE, Renner JN, Danilovic N, Wang JX, Zhang Y, Maric R, Yu H. Pathways to ultra-low platinum group metal catalyst loading in proton exchange membrane electrolyzers. *Catalysis Today*. 2016;262:121-32.

[17] Yang X, Lu A-Y, Zhu Y, Hedhili MN, Min S, Huang K-W, Han Y, Li L-J. CoP nanosheet assembly grown on carbon cloth: A highly efficient electrocatalyst for hydrogen generation. *Nano Energy*. 2015;15:634-41.

[18] Cheng N, Banis MN, Liu J, Riese A, Li X, Li R, Ye S, Knights S, Sun X. Extremely stable platinum nanoparticles encapsulated in a zirconia nanocage by area-selective atomic layer deposition for the oxygen reduction reaction. *Adv Mater*. 2015;27:277-81.

[19] Mo J, Dehoff RR, Peter WH, Toops TJ, Green JB, Zhang F-Y. Additive manufacturing of liquid/gas diffusion layers for low-cost and high-efficiency hydrogen production. *Int J Hydrogen Energ*. 2016;41:3128-35.

[20] Wang Z, Huang H, Liu H, Zhou X. Self-sustained electrochemical promotion catalysts for partial oxidation reforming of heavy hydrocarbons. *Int J Hydrogen Energ*. 2012;37:17928-35.

[21] Jia F, Guo L, Liu H. Dynamic characteristics and mitigations of hydrogen starvations in proton exchange membrane fuel cells during start-ups. *Int J Hydrogen Energ*. 2014;39:12835-41.

[22] Xu N, Zhu T, Qiao J, Zhang F, Chen Z. Nitrogen and sulfur co-doped mesoporous carbon as cathode catalyst for H 2/O 2 alkaline membrane fuel cell–effect of catalyst/bonding layer loading. *Int J Hydrogen Energ*. 2016;41:9159-66.

[23] Benck JD, Hellstern TR, Kibsgaard J, Chakthranont P, Jaramillo TF. Catalyzing the hydrogen evolution reaction (HER) with molybdenum sulfide nanomaterials. *Acs Catal*. 2014;4:3957-71.

[24] Kibler LA. Hydrogen electrocatalysis. *ChemPhysChem*. 2006;7:985-91.

[25] Han B, Steen SM, Mo J, Zhang F-Y. Electrochemical performance modeling of a proton exchange membrane electrolyzer cell for hydrogen energy. *Int J Hydrogen Energ*. 2015;40:7006-16.

[26] Grigoriev S, Millet P, Fateev V. Evaluation of carbon-supported Pt and Pd nanoparticles for the hydrogen evolution reaction in PEM water electrolysers. *J Power Sources*. 2008;177:281-5.

[27] Du L, Shao Y, Sun J, Yin G, Liu J, Wang Y. Advanced catalyst supports for PEM fuel cell cathodes. *Nano Energy*. 2016;29:314-22. DOI: 10.1016/j.nanoen.2016.03.016.

[28] Carmo M, Fritz DL, Mergel J, Stolten D. A comprehensive review on PEM water electrolysis. *Int J Hydrogen Energ*. 2013;38:4901-34.

[29] Yano H, Watanabe M, Iiyama A, Uchida H. Particle-size effect of Pt cathode catalysts on durability in fuel cells. *Nano Energy*. 2016;29:323-33. DOI: 10.1016/j.nanoen.2016.02.016.

[30] Litster S, McLean G. PEM fuel cell electrodes. *J Power Sources*. 2004;130:61-76.

[31] Mo J, Steen SM, III BH, Kang Z, Terekhov A, Zhang F-Y, Retterer ST, Cullen DA. Investigation of titanium felt transport parameters for energy storage and hydrogen/oxygen production. 13th International Energy Conversion Engineering Conference. AIAA 2015-39142015. p. 3914.

[32] Witham C, Chun W, Valdez T, Narayanan S. Performance of Direct Methanol Fuel Cells with Sputter-Deposited Anode Catalyst Layers. *Electrochemical and solid-state letters*. 2000;3:497-500.

[33] Haug AT, White RE, Weidner JW, Huang W, Shi S, Rana N, Grunow S, Stoner TC, Kaloyeros AE. Using sputter deposition to increase CO tolerance in a proton-exchange membrane fuel cell. *J Electrochem Soc*. 2002;149:A868-A72.

[34] Fang S-Y, Teoh LG, Huang R-H, Hsueh K-L, Yang K-H, Chao W-K, Shieu F-S. Enhancement of proton exchange membrane fuel cell performance by titanium-coated anode gas diffusion layer. *Int J Hydrogen Energ*. 2014;39:21177-84.

[35] Debe MK, Schmoeckel AK, Vernstrom GD, Atanasoski R. High voltage stability of nanostructured thin film catalysts for PEM fuel cells. *J Power Sources*. 2006;161:1002-11.

[36] O'Hayre R, Lee S-J, Cha S-W, Prinz FB. A sharp peak in the performance of sputtered platinum fuel cells at ultra-low platinum loading. *J Power Sources*. 2002;109:483-93.

[37] Gustavsson M, Ekström H, Hanarp P, Eurenius L, Lindbergh G, Olsson E, Kasemo B. Thin film Pt/TiO 2 catalysts for the polymer electrolyte fuel cell. *J Power Sources*. 2007;163:671-8.

[38] Xiu YK, Nakagawa N. Performance of a DMFC with a Sputtered Pt Layer on the Electrode/Electrolyte Interface of the Anode. *J Electrochem Soc*. 2004;151:A1483-A8.

[39] Kang Z, Mo J, Yang G, Retterer ST, Cullen DA, Toops TJ, Green Jr JB, Mench MM, Zhang F-Y. Investigation of thin/well-tunable liquid/gas diffusion layers exhibiting superior multifunctional performance in low-temperature electrolytic water splitting. *Energ Environ Sci*. 2017;10:166-75.

[40] Mo J, Kang Z, Yang G, Retterer ST, Cullen DA, Toops TJ, Green JB, Zhang F-Y. Thin liquid/gas diffusion layers for high-efficiency hydrogen production from water splitting. *Appl Energ*. 2016;177:817-22.

[41] Kang Z, Mo J, Yang G, Retterer ST, Cullen DA, Zhang F-Y. Micro/Nano Manufacturing of Novel Multifunctional Layers for Hydrogen Production from Water Splitting. IEEE 12th Annual International Conference on Nano/Micro Engineered and Molecular Systems (NEMS). UCLA, Los Angeles, USA2017. p. 126-30.

[42] Kang Z, Mo J, Yang G, Li Y, Talley DA, Retterer ST, Cullen DA, Toops TJ, Brady MP, Bender G, Pivovar BS, Green Jr JB, Zhang F-Y. Thin film surface modifications of thin/tunable liquid/gas diffusion layers for high-efficiency proton exchange membrane electrolyzer cells. *Appl Energ*. 2017;206:983-90.

[43] Steen III SM, Mo J, Kang Z, Yang G, Zhang F-Y. Investigation of titanium liquid/gas diffusion layers in proton exchange membrane electrolyzer cells. *International Journal of Green Energy*. 2017;14:162-70.

[44] Kalidindi A, Taspinar R, Litster S, Kumbur E. A two-phase model for studying the role of microporous layer and catalyst layer interface on polymer electrolyte fuel cell performance. *Int J Hydrogen Energ*. 2013;38:9297-309.

[45] Poirier JA, Stoner GE. Microstructural Effects on Electrocatalytic Oxygen Reduction Activity of Nano-Grained Thin-film Platinum in Acid Media. *J Electrochem Soc*. 1994;141:425-30.

[46] Mench MM. Fuel Cell Engines: *John Wiley & Sons*; 2008.

[47] Wang Y, Narayanan S, Wu W. Field-Assisted Splitting of Pure Water Based on Deep-Sub-Debye-Length Nanogap Electrochemical Cells. *Acs Nano*. 2017;11:8421-8.

[48] Slavcheva E, Ganske G, Topalov G, Mokwa W, Schnakenberg U. Effect of sputtering parameters on surface morphology and catalytic efficiency of thin platinum films. *Appl Surf Sci*. 2009;255:6479-86.

[49] Li H, Inada A, Nakajima H, Ito K. Impact of Cathode Current Collector on High Temperature PEM Water Electrolysis. *Ecs Transactions*. 2015;69:3-12.

[50] Li M, Zhao Z, Cheng T, Fortunelli A, Chen C-Y, Yu R, Zhang Q, Gu L, Merinov BV, Lin Z. Ultrafine jagged platinum nanowires enable ultrahigh mass activity for the oxygen reduction reaction. *Science*. 2016;354:1414-9.

[51] Sun S, Xiao Y, Liang D, Shao Z, Yu H, Hou M, Yi B. Behaviors of a proton exchange membrane electrolyzer under water starvation. *Rsc Adv*. 2015;5:14506-13.

CHAPTER VII

PERFORMANCE MODELING AND CURRENT MAPPING OF PROTON EXCHANGE MEMBRANE ELECTROLYZER CELLS WITH NOVEL THIN/TUNABLE LIQUID/GAS DIFFUSION LAYERS

A version of this chapter was originally published by Zhenye Kang:

Zhenye Kang, Jingke Mo, Gaoqiang Yang, Yifan Li, Derrick A. Talley, Bo Han, Feng-Yuan Zhang. "Performance Modeling and Current Mapping of Proton Exchange Membrane Electrolyzer Cells with Novel Thin/Tunable Liquid/Gas Diffusion Layers." *Electrochimica Acta* 255 (2017): 405-416.

I am fully responsible for the work submitted in this publication.

7.1 Abstract

The novel titanium thin/tunable liquid/gas diffusion layers (TT-LGDLs) with precisely controllable pore morphologies have achieved superior multifunctional performance in proton exchange membrane electrolyzer cells (PEMECs) with its advantages of ultra-thin thickness (25 μm), planar surface, and straight-through pores. Since the conventional PEMEC models cannot effectively simulate the effects of pore morphologies of TT-LGDLs on PEMEC performance, a comprehensive computational model is developed in MATLAB/Simulink platform to simulate its electrochemical performance. By taking advantage of the precisely controlled pore morphology of TT-LGDLs, the model regarding the interfacial contact resistance between the TT-LGDLs and catalyst layers (CLs) is closely correlated to the pore diameter and porosity of the TT-LGDLs. In addition, the roughness factor, which is a critical coefficient in simulating the activation overpotential in Butler-Volmer equation, is also modeled as a function of TT-LGDL morphologies. More

importantly, a novel two-dimensional (2D) CL resistance model that consists of both in-plane and through-plane resistances is also developed to predict the current distribution on the CLs. The present model can precisely match the experimental results and effectively calculate the PEMEC performance with different TT-LGDL morphologies and operating temperatures. The optimized morphology of TT-LGDLs is the larger porosity and smaller pore diameter, which can offer better PEMEC performance. Results obtained from the present model will provide a deep understanding of the functions of TT-LGDL morphology, and also help to optimize the design and fabrication of both the TT-LGDLs and CLs.

7.2 Introduction

Proton exchange membrane electrolyzer cells (PEMECs), which work as the reverse PEM fuel cells (PEMFCs), have been considered as one of the most attractive and popular methods for hydrogen and oxygen generation from water splitting, especially when coupled with the renewable energy sources such as wind, solar, hydro, tide, etc. [1-7]. PEMECs can produce very pure hydrogen/oxygen with few contaminants and have many advantages, including high energy efficiency, fast charging/discharging, and compact design [8-11]. In addition, PEMECs provide a completely environmentally friendly approach to produce hydrogen compared with the conventional methods, such as alkaline water electrolysis and fossil fuel reforming, and it can be operated effectively under low temperatures [12-16].

Figure 40 shows the main components in a typical PEMEC, which is similar to the structure of PEMFCs [17]. It consists of two electrodes, including anode and cathode, which are separated by a proton exchange membrane (PEM). At each electrode, there are a bipolar plate (BP) with flow channels (FCs) on it, a liquid/gas diffusion layer (LGDL), and a catalyst layer (CL).

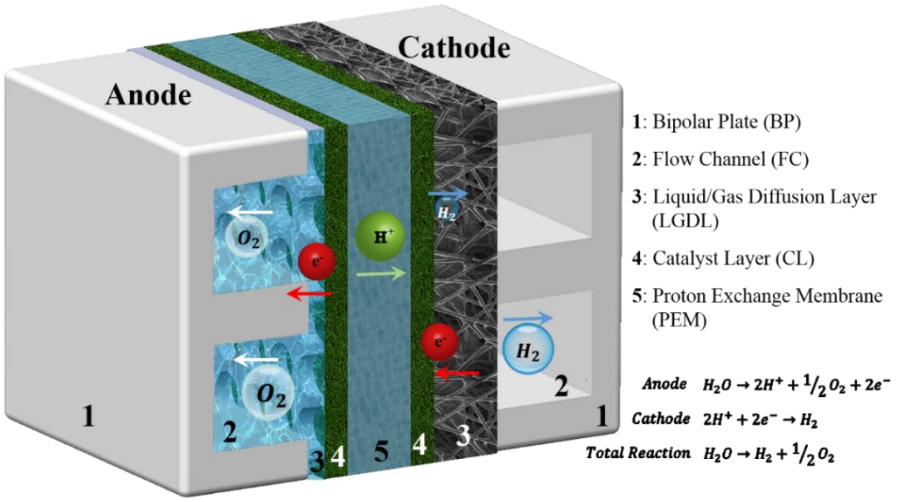

Figure 40. Three-dimensional geometrical schematic of a PEMEC with TT-LGDLs.

Liquid water at the anode is continuously supplied and it flows from the BP/FCs through the LGDLs to the surface of the CLs, where water is electrochemically split into oxygen molecules, protons, and electrons after the electricity is applied to the PEMECs. Protons, generated at anode, transport from the electrochemical reaction sites through the PEM to the cathode to form hydrogen gas. The electrochemical performance of the PEMECs is influenced by many factors, including operating conditions, PEM physical parameters, CL properties, LGDL pore morphologies and so on [18]. Modeling is one of the promising

methods to optimize PEMEC designs and operations due to its precisely predicting results, time saving, and low cost.

Choi et al. developed a simple mathematical model that calculated the cell voltage of solid polymer electrolyte water electrolysis, including interfacial contact ohmic overpotential. They also used simplified Butler-Volmer equation to calculate the activation overpotential [19]. Gorgun's model focused on studying water transport phenomenon through the membrane in PEMECs with Simulink[20]. Z. Abdin et al. also used Simulink to model and simulate the PEMEC performance, which is a powerful tool for exploring the effects of each component [21]. Grigoriev et al. introduced a model to evaluate PEMEC performance under atmosphere and high pressure. The effects of different operating pressure, temperature, and current density were also discussed comprehensively [22, 23]. Marangio et al. also developed a theoretical model especially for high pressure PEMECs, which used Gibbs free energy to calculate the open circuit voltage. The water transport in PEMECs were also comprehensively investigated by considering the concentration difference, electroosmotic drag, pressure difference, and so on. The interfacial contact resistances was also considered in the model which had a great influence on PEMEC performance [24]. David et al. established a three-dimensional (3D) model of CLs in PEMFCs by taking into account the detailed composition and structure of the CLs using a multiple thin-film agglomerate model [25]. Our group also established a electrochemical performance model of a PEMEC which fully considered the effects of various operating conditions and design parameters on the cell performance based on the porous conventional LGDLs [26, 27]. The

two-phase transport model was developed to investigate the transport properties in the anode porous LGDL and to analyze their effects on the PEMEC performance and efficiency [28-31].

By taking advantage of advanced micro/nano manufacturing [32], a novel thin planar titanium LGDL with tunable pore morphologies has achieved superior performance with a large porosity and small circular pore diameter, as shown in Figure 41, and this kind of thin/tunable LGDLs (TT-LGDLs) can significantly reduce the ohmic and activation losses [33-35]. Although a lot of models have been established for PEMECs and PEMFCs, they all use conventional porous media as their LGDLs, such as Ti felts as shown in Figure 41 [19, 36-38]. It has been found that the structures of the TT-LGDLs are significantly different from conventional porous Ti felt LGDLs, and the thickness of the novel TT-LGDLs is only 25μm, which is much thinner than conventional Ti felt (350 μm). The planar surface of the TT-LGDLs can greatly enhance the interfacial contact characteristics, while the Ti felt is made of fibers and the interface is impacted by compression conditions. An impressive phenomenon has shown that the oxygen bubbles only generate at the rim of the pores along the CL surface, which has been captured by a high-speed micro-scale visualization system [34, 39]. The conventional models cannot successfully simulate the PEMECs with TT-LGDLs by simply changing some parameters in the codes because they are used for the conventional LGDLs, such as Ti felt, sintered Ti powders, which are always considered as a thick porous media. These conventional LGDLs are simplified in the model and some of the models even consider the LGDL and CL as a whole [21, 24, 27].

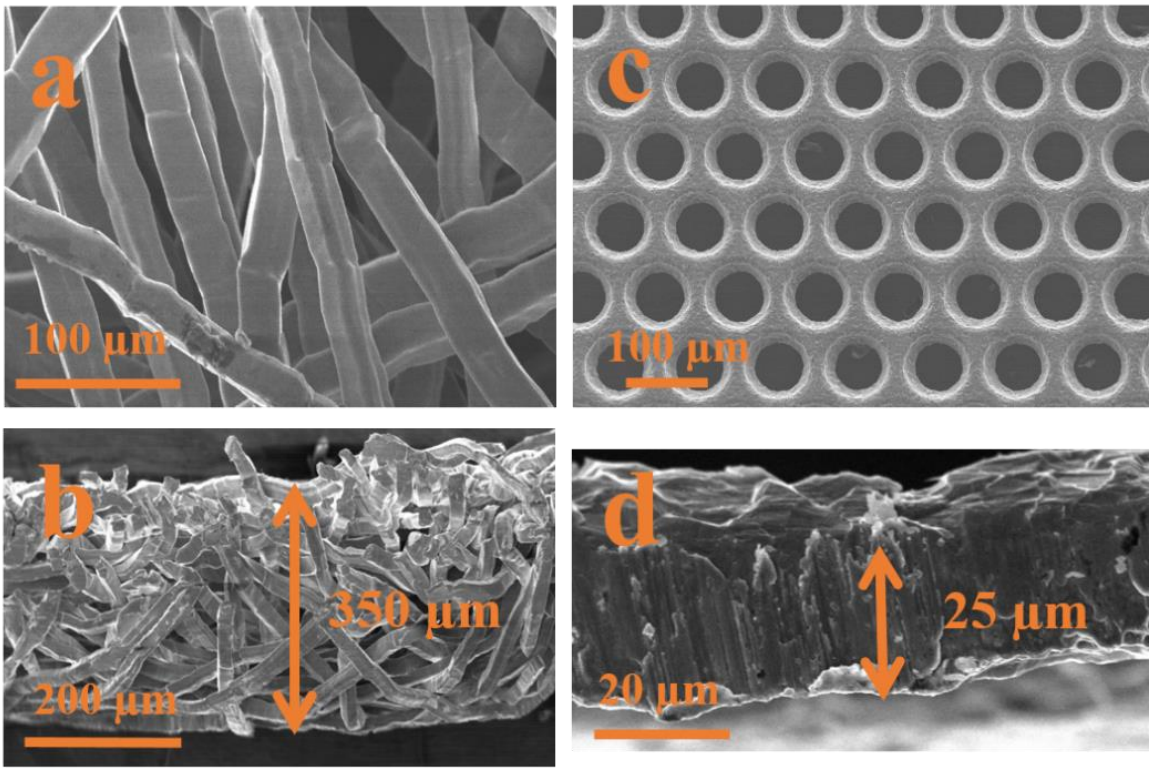

Figure 41. SEM images of TT-LGDLs and conventional titanium felt LGDLs. (a) Top view of Ti felt LGDLs. (b) Cross-section of Ti felt LGDLs. (c) Top view of TT-LGDLs. (d) Cross-section of TT-LGDLs.

Therefore, the conventional PEMEC models cannot precisely predict the effects of the pore diameter and porosity of TT-LGDLs, and the current mapping cannot be effectively modeled and validated. At present, a comprehensive model for better correlating the effects of both design parameters and operating conditions with TT-LGDLs is strongly desired. Therefore, some new modules and equations should be added into the conventional models, to establish a comprehensive model for precisely assessing the impacts of TT-LGDL morphologies on the PEMEC performance.

In this study, a comprehensive computational model for the PEMECs with TT-LGDLs at anode side is established based on the previous PEMEC model [30]. MATLAB/Simulink is adopted to develop this novel model due to its user-friendliness, modular programming, very good interactivity and portability [40]. A new ohmic loss model for PEMECs, including the interfacial contact resistances between the CLs and TT-LGDLs, has been developed. Furthermore, the roughness factor in the Butler-Volmer equation, which is used to calculate the activation overpotential, can greatly influence the PEMEC performance by pore morphology of the TT-LGDLs, and its relation has been embedded in the comprehensive computational model. The influence of operating conditions and TT-LGDL pore diameter and porosity on PEMEC performance can be investigated precisely. More importantly, a novel two-dimensional (2D) CL resistance model, which consists of both in-plane and through-plane resistance models, is also developed to predict the current distribution on the CLs.

7.3 Model Development

7.3.1 Electrochemical performance

The electrochemical performance of a PEMEC can be expressed by the polarization curve, which is the relation between the current density and cell voltage. The cell voltage of a PEMEC consists of open circuit voltage (OCV), ohmic overpotential, activation overpotential, and diffusion overpotential, which is shown as [36]:

$$\boldsymbol{V = V_{OCV} + V_{Ohm} + V_{act} + V_{diff}} \qquad \textbf{Equation 7}$$

Where V_{OCV} is OCV, V_{Ohm} is ohmic overpotential, V_{act} is activation overpotential, and V_{diff} is diffusion overpotential.

It is obvious that the lower cell voltage at a constant current density represents a better performance of PEMECs. During the experiments, the PEMEC voltage can be measured and recorded by any potentiostat systems, while it is difficult to distinguish each part of the overpotentials. Therefore, the mathematical modeling is employed to calculate each of the overpotentials and obtain the PEMEC performance. The following sections will discuss about the calculation of each overpotential.

7.3.2 Open circuit voltage

The open circuit voltage of a PEMEC, which is also called the reversible voltage, can be calculated from the Nernst equation and expressed as follows [36].

$$\boldsymbol{V_{OCV} = V_0 + \frac{RT}{2F} ln\left(\frac{\alpha_{H_2}\alpha_{O_2}^{0.5}}{\alpha_{H_2O}}\right)} \quad \textbf{Equation 8}$$

V_0 is the reversible voltage under standard pressure condition, which can be expressed by:

$$\boldsymbol{V_0 = 1.229 - 0.9 \times 10^{-3}(T - 298.0)} \quad \textbf{Equation 9}$$

Where R is the gas constant that is 8.314 J/mol K, T is the operating temperature in the unit of K, α_{H_2} and α_{O_2} is the activity of ideal hydrogen and oxygen gas, respectively, which can be calculated by:

$$\boldsymbol{\alpha_{H_2} = \frac{P_{H_2}}{P_0}, \alpha_{O_2} = \frac{P_{O_2}}{P_0},} \quad \textbf{Equation 10}$$

P_{H_2} and P_{O_2} are the partial pressure of hydrogen and oxygen, respectively, P_0 is the standard atmosphere pressure. α_{H_2O} equals to 1.0 for the liquid water.

7.3.3 Ohmic overpotential

The ohmic overpotential is due to the ohmic resistances of BPs, LGDLs, CLs, PEM, and the interfaces between components. The total ohmic overpotential can be expressed as:

$$\boldsymbol{V_{ohm} = (R_{BP} + R_{LGDL} + R_{CL} + R_{PEM} + R_{in})iA} \quad \textbf{Equation 11}$$

Where the PEM resistance contributes to the most of the total ohmic loss, which can be calculated as [31, 41]:

$$R_{PEM} = \frac{\delta_m}{A\sigma_m} \qquad \textbf{Equation 12}$$

Where δ_m is the PEM thickness and σ_m is the PEM conductivity in the unit of *S/cm*, which is related to the humidification degree λ and operating temperature T in the unit of *K*, and can be expressed as [41]:

$$\sigma_m = (0.005139\lambda - 0.00326)exp\left[1268\left(\frac{1}{303} - \frac{1}{T}\right)\right] \qquad \textbf{Equation 13}$$

Figure 42 shows the equivalent circuit model with each resistance for a PEMEC with the TT-LGDLs at anode of PEMECs. The calculation of the BP resistance and LGDL resistance has been studied and can be easily found in the previous publications [21, 24, 27]. The LGDL/CL interfacial contact resistance and the CL resistance will be comprehensively investigated in the present study.

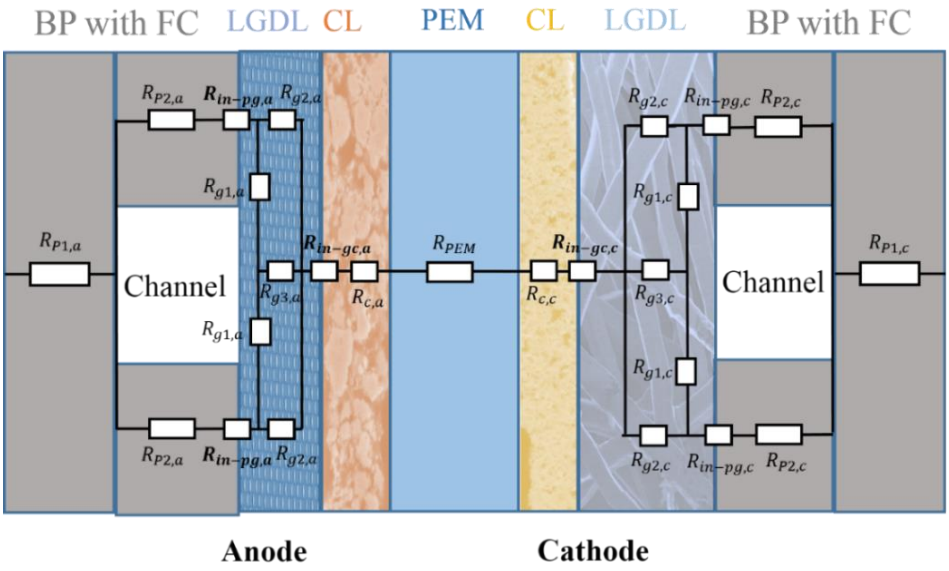

Figure 42. Equivalent resistance model of the PEMECs with TT-LGDLs.

7.3.3.1 LGDL/CL interfacial contact resistance

From the analysis of experimental results in our previous researches, it can been concluded that the number of reaction sites has great influence on the PEMEC performance [34]. Based on our previous discovery, the electrochemical reaction in an operating PEMEC only occurs on the CLs at the rim of the TT-LGDL pores, and there is no bubble generated on CLs in the open area of the TT-LGDL pores. It has been concluded that the large electrical resistance of the CL hindered the electron transport in the CL, and the electrochemical reaction happened at the interface between the CL and TT-LGDL [34]. This effect can be considered as interfacial contact resistance between the anode LGDL and anode CL. It has been already derived that the reaction sites is proportional to porosity over pore diameter that is shown below [34].

$$\boldsymbol{S = 4A_t \times \frac{x}{l} \times \frac{\varepsilon}{D}} \qquad \textbf{Equation 14}$$

Where S is the number of total reaction sites, A_t is the total reaction area of the PEMECs, x is the number of reaction sites on each length l on the rim of the pore, D and ε are the pore diameter and porosity of the TT-LGDLs, respectively. It is assumed that all the reaction sites are in electric parallel with each other, so the total interfacial contact resistance would be inversely proportional to reaction sites. Therefore, the interfacial contact resistance between the anode LGDL and CL is derived from Equation 14 and can be represented by:

$$R_{in,gc,a} = K \times d_0/\varepsilon_0 \qquad \textbf{Equation 15}$$

Where *K* represents the interfacial contact resistance coefficient and it is a constant (equals to 1.4×10^{-2} Ω), which comes from the PEMEC performance experimental data fitting. ε_0 and d_0 are defined as dimensionless relative porosity and pore diameter, respectively, which is used to eliminate their unit and make them easier for future calculations:

$$\varepsilon_0 = \varepsilon/0.1 \qquad \textbf{Equation 16}$$

$$d_0 = D/1000 \qquad \textbf{Equation 17}$$

It can also be found that with larger pore diameter, a large amount of catalyst sites located away from the rim will not behave normally due to the large in-plane resistance, which will result in worse performance and catalyst underutilization [34]. By increasing the porosity or decreasing the pore diameter, the number of reaction sites can be increased, and more catalysts are active.

7.3.3.2 CL resistance

It is known that the conventional CL is often the mixture of noble metal catalyst particles and the binder of ionomer, which are used to conduct electrons and protons, respectively. In a PEMEC, the electrochemical reaction takes place at triple-phase boundary (TPB) where there are electron/proton conductors, active catalysts, and pathways for reactants/products. The real equivalent circuit is very complex due to the complicated conducting pathway. To estimate the ohmic overpotential and obtain the current distribution within the CLs, a simplified CL equivalent resistance model is established to

calculate CL resistance, as shown in Figure 43.It has been concluded that the larger porosity under the same pore diameter will result in more reaction sites, which will contribute to better PEMEC performance [34]. When the porosity increases at a fixed pore diameter, the area under the land will decrease. If the similar electrochemical reaction happens under the TT-LGDL land, the land-area reduction will result in less reaction sites, which should cause worse PEMEC performance. From the present results and conclusions, the larger porosity will lead to more reaction sites and better performance. On the other hand, the transports of reactant and product to and from the under the land area of TT-LGDL are more difficult than the pore area, which may also hinder the reaction under the land. Therefore, it can be assumed that the reactions under the TT-LGDL land are limited. All the currents will go through the CLs within pore area and their directions are from the TT-LGDLs through the CLs to the active reaction sites, which is shown in Figure 43. In order to analyze each resistance, the pore area of the CLs is divided into *n* tori. At the rim of the pore, the electrochemical reaction site within the first torus is marked as *1*, and it is marked as *n* at the center of the pore. For instance, if the reaction site is located at the *m* torus, electrons will go from the $(m-1)^{th}$ torus through the CL to the 1^{st} torus. While protons will diffuse directly through m^{th} torus of the CLs to the PEM under the CLs. Hence, there exist two types of resistances: in-plane resistance due to the electron conduct and through-plane resistance due to the proton conduct. The equivalent circuit of CLs is between point A and B, and other resistances of the PEMECs besides the CLs is represent by R_x and R_y.

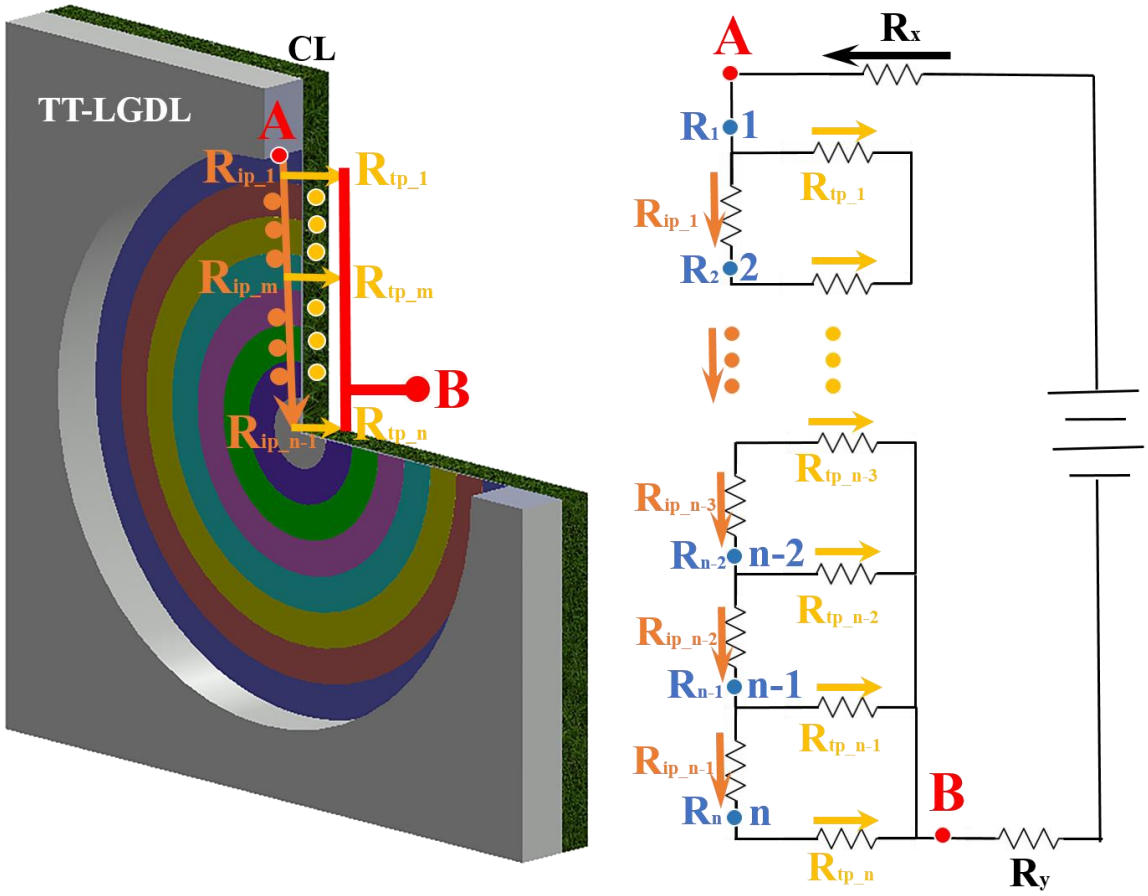

Figure 43. Equivalent resistance model of the CLs within one pore of the TT-LGDLs at anode of PEMECs (Arrows in the figure represents the current flow direction).

Because the parameter of each torus is very small (just few microns in dimension), the in-plane electron transport is considered as a 1D thin film. Therefore, the in-plane resistance of the CLs can be simplified and expressed by [41]:

$$\boldsymbol{R_{ip\_m} = \rho_{in} \frac{l}{A_m}} \qquad \textbf{Equation 18}$$

Where ρ_{in} is the resistivity of the CLs, and it is calculated from the sheet resistance of the CLs:

$$\boldsymbol{\rho_{in} = R_{sheet} \times \delta} \qquad \textbf{Equation 19}$$

The sheet resistance R_{sheet} equals to 1011.85 Ω/□ for the anode CL ($IrRuO_x$), which is measured by the four-point probe. The thickness of the CLs δ is 15 μm. l is the length of the electron transport distance in each torus which is assumed to be the width of each torus and can be calculated by:

$$\boldsymbol{l = \frac{D}{2n}} \qquad \textbf{Equation 20}$$

The area A_m is the lateral area of each CL torus:

$$\boldsymbol{A_m = \pi d_m \delta} \qquad \textbf{Equation 21}$$

Where d_m is the diameter of the m^{th} torus.

For the through-plane resistance, it can be expressed as below:

$$\boldsymbol{R_{tp\_m} = \rho_{tp} \frac{\delta}{A'_m}} \qquad \textbf{Equation 22}$$

Where ρ_{tp} is the through-plane resistivity, which can be calculated from the ionic conductivity of the Nafion membrane. A'_m is the proton conducting area which is the torus area of CL as shown in Figure 43.

After acquiring the in-plane and through-plane resistances of each torus, the total resistance of the CLs R_{CL} can be obtained based on the fundamental knowledge of electrical circuit.

$$\boldsymbol{R_{CL} = \frac{R_1}{N}} \qquad \textbf{Equation 23}$$

Where R_1 and N are the CL resistance of each pore and number of pores in the TT-LGDLs, respectively, and they can be expressed by:

$$\boldsymbol{R_m = \frac{1}{\frac{1}{R_{ip\_m}+R_{m+1}}+\frac{1}{R_{tp\_m}}}} \ \boldsymbol{(m = 1, 2 \ldots \ldots n-1)} \qquad \textbf{Equation 24}$$

$$\boldsymbol{N = \frac{A\varepsilon}{\pi(D/2)^2}} \qquad \textbf{Equation 25}$$

R_m is the resistance between point *m* and point B as shown in Figure 43. The current of each resistances can be also obtained by the equivalent circuit. The in-plane and through-plane currents of each torus can be calculated by:

$$\begin{cases} \boldsymbol{I_{tp\_m} = I_{ip\_m-1} \times \frac{R_{ip\_m}+R_{m+1}}{R_{ip\_m}+R_{m+1}+R_{tp\_m}}} \\ \boldsymbol{I_{ip\_m} = I_{ip\_m-1} - I_{tp\_m}} \qquad (\boldsymbol{m = 1, 2 \ldots \ldots n}) \\ \boldsymbol{I_{ip\_0} = \frac{iA}{N}} \end{cases} \qquad \textbf{Equation 26}$$

Based on the above equations, the current distribution can be obtained and used to further analyze the electrochemical reaction mechanism.

7.3.4 Activation and diffusion overpotential

The activation overpotential and the diffusion overpotential can be expressed as [31, 36, 41]:

$$\boldsymbol{V_{act} = \frac{RT_a}{\alpha_a F} sinh^{-1}\left(\frac{i}{2a_{r,an}si_{0,a}}\right) + \frac{RT_c}{\alpha_c F} sinh^{-1}\left(\frac{i}{2a_{r,cat}si_{0,c}}\right)} \qquad \textbf{Equation 27}$$

$$\boldsymbol{V_{diff} = \frac{RT_a}{4F} \ln\left(\frac{C_{O_2,m}}{C_{O_2,m0}}\right) + \frac{RT_c}{2F} \ln\left(\frac{C_{H_2,m}}{C_{H_2,m0}}\right)} \qquad \textbf{Equation 28}$$

Where R is the gas constant, T is the operating temperature, α_a and α_c is the charge transfer coefficients at the anode and cathode, which are 2.0 and 0.5, respectively [36], F is the Faraday constant, i is current density, i_0 is the exchange current density on the anode and cathode electrode, $a_{r,an}$ and $a_{r,cat}$ is the roughness factor of the anode and cathode, respectively, s is the interfacial liquid saturation between the anode LGDL and CL, $C_{O_2,m}$ and $C_{H_2,m}$are the oxygen and hydrogen concentrations at the interface of CL and PEM, respectively. $C_{O_2,m0}$ and $C_{H_2,m0}$ indicate the reference values, which are calculated from the equations in the reference [27], and the values are 11.4 mol/m^3 and 28.4 mol/m^3, respectively.

In the Butler-Volmer model of kinetics, the activation potential is related to many factors, such as reaction mechanism, catalyst morphology, operating parameters, species concentrations and so on [41]. Different morphologies of TT-LGDLs will affect the number of active catalysts and species concentrations at the reaction sites, where meet TPB requirements. The species concentrations on the reaction sites at the rim of the pore will change with different TT-LGDL pore diameters and porosities. Based on our previous studies, the morphology of TT-LGDLs will affect the activation overpotential, which is inversely proportional to porosity and proportional to pore diameter [34]. Therefore, this effect is assumed as the roughness factor in Butler-Volmer model. By analyzing the experimental data, it has been found that this relation is not linear. Therefore, the anode roughness factor ($a_{r,an}$) is influenced by the TT-LGDL pore diameter (d_0), and porosity (ε_0), which can be expressed as:

$$\boldsymbol{a_{r,an} = c * \varepsilon_0^u / d_0^v} \qquad \textbf{Equation 29}$$

The constant and exponentials in this equation are the coefficients that obtained by the experimental fitting. Where *c* equals to 10, *u* and *v* equal to 2.5 and 0.5, respectively. For the cathode LGDL is carbon paper (Toray 090), which has been widely used in PEMEC modeling, and the roughness factor. Therefore, it is assumed equal to 1.0 [21].

In the present model, several assumptions for simplification are needed. First, the steady state and isothermal conditions are incorporated into the two-phase model of LGDL, since the titanium LGDL thickness is relatively small and its thermal conductivity of the Ti materials is high. Second, the electrochemical reaction only occurs at the interface between

the LGDL and CL. Since a typical oxygen-liquid water two-phase flow occurs at the anode of PEMEC that contributes to most of the diffusion losses, the present model will only focus on the mass transport process inside the anode LGDLs without considering the transport effects in the CL and PEM. At the anode side of a PEMEC, liquid water enters through the channel and then diffuses through the porous LGDL to the reaction site in the CL, where liquid water is decomposed into electrons, protons, and oxygen. Oxygen and liquid water two-phase transport equations inside the anode LGDL can be rewritten in the following form (for a hydrophilic LGDL) [31]:

$$\begin{cases} \nabla \cdot \left(-\frac{k(1-s)^3}{\mu_{O_2}/\rho_{O_2}} \nabla p_{O_2} \right) = 0 \\ \nabla \cdot \left[\left(-\frac{ks^3}{\mu_{H_2O}/\rho_{H_2O}} \right) \nabla p_{O_2} \right] + \nabla \cdot \left\{ \left(-\frac{ks^3}{\mu_{H_2O}/\rho_{H_2O}} \right) \left[-\left(\frac{\varepsilon}{k}\right)^{0.5} \sigma cos\theta \right] \nabla \left(1.417(1-s) - 2.120(1-s)^2 + 1.263(1-s)^3 \right) \right\} = 0 \end{cases}$$

Equation 30

In the present model, in addition to the diffusion overpotential, the activation overpotential is also closely related to the liquid water transport (the interfacial saturation), as shown in Equation 27 and Equation 28.

7.4 Results and Discussions

7.4.1 Model validation

A self-written computational program, which is developed in MATLAB/Simulink platform, is performed to numerically solve the present mathematical model. Figure 44 shows the full Simulink model of the PEMECs with TT-LGDLs, which includes the

operation module, TT-LGDL parameter module, ohmic resistance module, and voltage calculation module. When the operation conditions are kept the same, the effects of the pore diameter and porosity of the TT-LGDL can be calculated. To validate the present model, the experimental data of PEMEC performance with TT-LGDLs, which were performed in our previous study [34], are chosen to compare with the present modeling results. The operating temperature is varied, and the operating pressure is 1 atm at both the anode and cathode. Table 9 shows the basic geometrical and physicochemical parameters used in present model.

Figure 45 (a) and (b) show the comparison of the present PEMEC model and experimental data of the PEMEC polarization curves with four different TT-LGDLs and one of them under different temperatures, respectively. In Figure 45(a), three TT-LGDLs with different pore diameters and porosities under 80^{o}C are used to determine the critical fitting parameters in the model, including the exchange current density, the interfacial contact resistance coefficient, and the constants in Equation 15. By adjusting the exchange current density and the constants in Equation 15, the modeling polarization curves would gradually fit the experimental data under low current density range. The differences between the modeling results and the experimental data were calculated, and the optimized parameters were obtained. After determining these parameters, the interfacial contact resistance coefficient is adjusted and optimized to better fit the experimental data, especially under medium and high current density ranges.

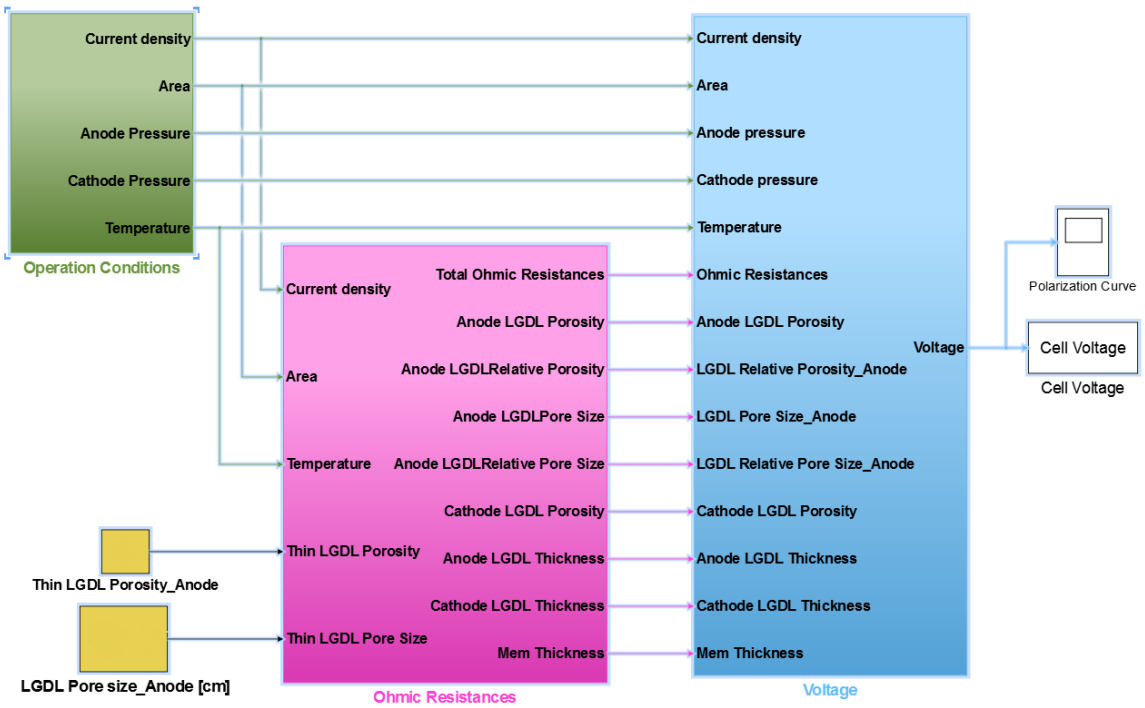

Figure 44. MATLAB/Simulink model schematic of the PEMECs with TT-LGDLs.

Table 9. Basic parameters for the comprehensive PEMEC modeling.

Description, symbol	Value, unit
MEA active area	5.0 cm^2
PEM	Nafion 115 with 125 μm thickness
Operating pressure, P	Anode: 1 atm, cathode: 1atm
Operating temperature, T	20, 40, 60, and 80^0C
Anode LGDL	Ti thin LGDL with 25.4 μm thickness
Cathode LGDL	Carbon paper with 280 μm thickness
LGDL porosity, ε	Anode: Varied from 0.1 to 0.9; Cathode: 0.78
CL thickness, δ	15 μm
Titanium electrical resistivity	5.4×10^{-5} Ω cm
Carbon paper (Toray 090) electrical resistivity	8.0×10^{-2} Ω cm [30]
Graphite (AXF-5Q) electrical resistivity	1.5×10^{-3} Ω cm [42]
Anode CL electrical resistivity (catalyst: $Ir_xRu_{1-x}O_2$) Through plane	5×10^{-2} Ω cm [30]
Cathode CL electrical resistivity (catalyst: Pt/C) Through plane	1.4×10^{-3} Ω cm [30]

Table 9. Continued.

Description, symbol	Value, unit
Liquid water dynamic viscosity, μ_{H_2O}	3.55×10^{-4} N s/m^2 [30]
Liquid water density, ρ_{H_2O}	1000 kg/m^3
Charge transfer coefficient, $\alpha_a$and α_c	Anode: 2.0, Cathode: 0.5
Reference value of oxygen concentrations, $C_{O_2,m0}$	11.4 mol/m^3
Reference value of hydrogen concentrations, $C_{H_2,m0}$	28.4 mol/m^3
Membrane humidification degree (Fitted)	24 [21, 43]
Exchange current density (A/cm^2) (Fitted)	Anode: 6.0×10^{-10}, Cathode: 3.4×10^{-1}
Interfacial contact resistance coefficient, *K* (Fitted)	1.4×10^{-2} **Ω**
Constant and coefficient, *c*, *u*, and *v* (Fitted)	10, 2.5, 0.5

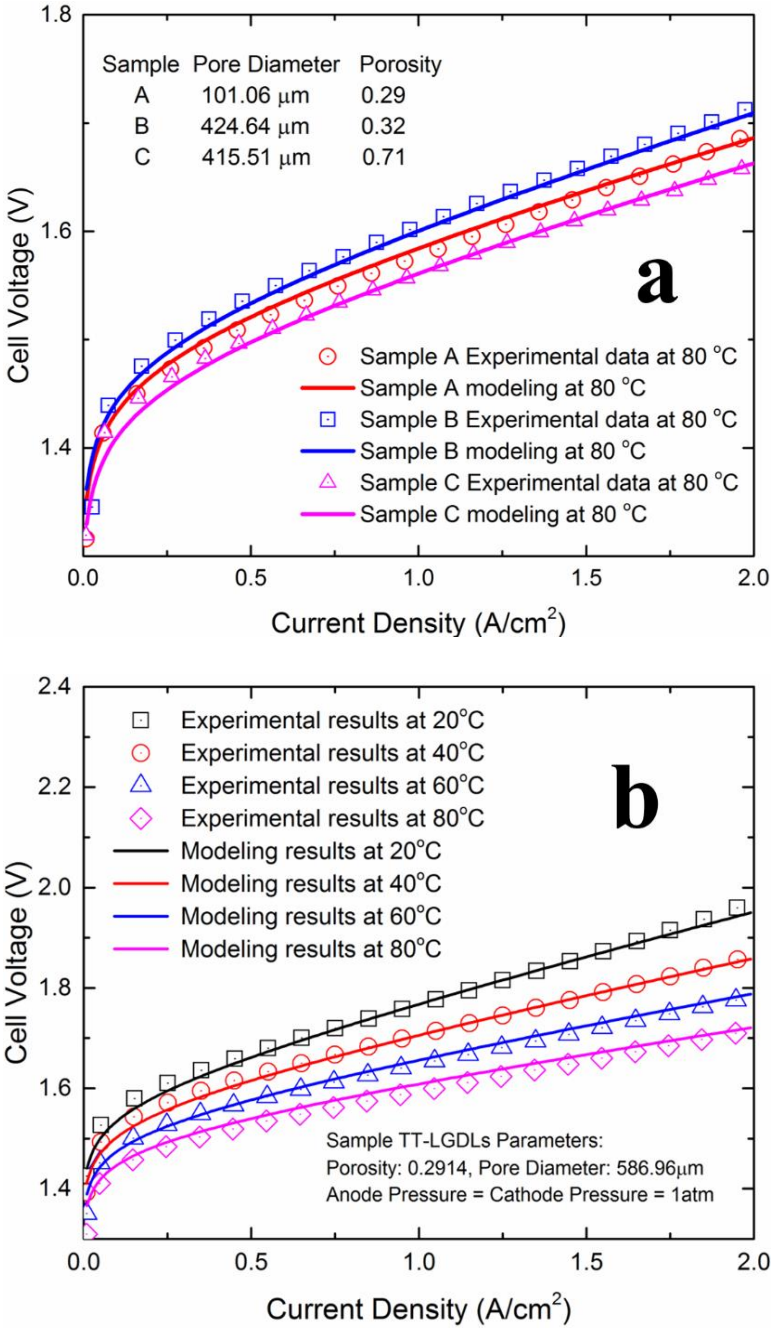

Figure 45. Comparison and validation between the PEMEC modeling and experimental data. (a) Three TT-LGDLs with different pore diameters and porosities. (b) TT-LGDL tested under different temperatures.

The modeling results show very good agreement with experimental results for all the current density range for the above three TT-LGDLs. In Figure 45(b), one TT-LGDL sample are used in order to validate the model under different temperatures, and the results on temperature are in good agreement as well. Moreover, we checked the reliability of the model without changing any fitting parameters by using other experimental data. After the validation, the effective model is then used to calculate and analyze the current mapping around the CL surface, ohmic resistances effects, and TT-LGDL parameters and operating conditions effects on electrochemical performance and optimization of the PEMECs.

7.4.2 Effects of LGDL pore diameter and porosity

Pore diameter and porosity are two main parameters of the TT-LGDLs and they can be well-controlled during the fabrication process. It has been found that the larger porosity and smaller pore diameter could achieve better performance, and a superior performance of only 1.66 V at 2.0 A/cm^2 and 80 ^{o}C has been obtained from the experimental study [34]. In order to further analyze the effects of the pore diameter and porosity, a wide range of pore diameters and porosities are chosen to model the performance of the PEMECs with TT-LGDLs. Figure 46 shows the cell voltage of PEMECs at 2.0 A/cm^2 with different TT-LGDL parameters. It can be seen that with the pore diameter of 50 μm and porosity of 0.9, the cell voltage is as low as 1.626 V. Under the same porosity, the cell voltage gradually increases to 1.6325 V, 1.6340 V, 1.648 V, 1.656 V, and 1.663 V with the increase of the pore diameter from 100 μm, 200 μm, 400 μm, 600 μm, to 800 μm. On the other hand, under the same pore diameter of 50 μm, with the decrease of porosity, the cell voltage will

be increased to 1.640 V, 1.656 V, 1.677 V, and 1.743 V for a porosity of 0.7, 0.5, 0.3 and 0.1, respectively. When the porosity is 0.1, it can be found that the cell voltage is very high that is larger than 1.743 V, and it will reach 1.913 V with 800 μm pore diameter. It is obviously that the large porosity and small pore diameter TT-LGDLs have better PEMEC performance, which agrees with the experimental results [34].

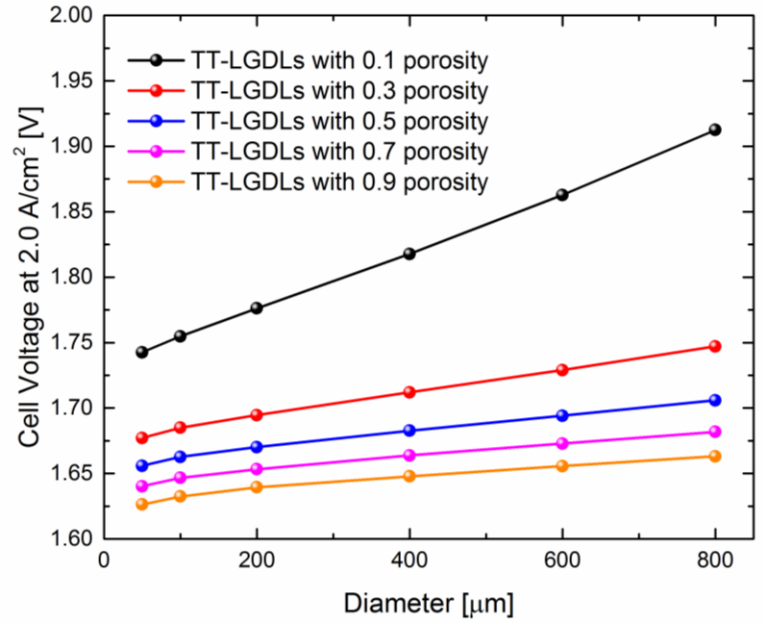

Figure 46. Cell voltage of the PEMECs with TT-LGDLs with different pore porosities under a temperature of 80 ºC at a current density of 2.0 A/cm^2.

Figure 47 shows the contribution of each overpotential to polarization curve of the PEMECs under 80 ºC temperature and 1 atm pressure. Regarding the four parts of overpotential, the diffusion overpotential contributes much less than the other three overpotentials. OCV occupies a large portion of the total cell voltage, and it equals to

1.1794 V under the 80 ºC. Under low current density range, the ohmic overpotential is very small and activation overpotential dominates the polarization curve. In addition, the activation overpotential is relatively stable and it changes very small throughout the high current density range. The ohmic overpotential increases gradually with the increase of current density, but it still has less effect than activation overpotential.

The ohmic resistance of the PEMECs comprises many parts, including PEM, CLs, LGDL, BP, interfacial contact and so on. The present comprehensive model can distinguish each of these resistances and the resistance of each component is shown in Table 10. It can be seen that the PEM resistance is the main contribution of the ohmic resistance which is a constant under a defined temperature and membrane humidification. Interfacial contact resistances are also larger than CL resistances, and it is greatly influenced by pore diameter and porosity of the TT-LGDLs. It can be seen that the total resistance decreased with the increase of porosity, and the CL and interfacial contact resistance have the same trend. While the ohmic resistance of the TT-LGDLs will increase with the increase of porosity. It should be noted that the ohmic resistance of the TT-LGDLs is relatively small compared with other resistances, such as PEM and interfacial contact. Therefore, it has limited effects on total resistance. Each overpotential of PEMECs with different TT-LGDLs was summarized in Table 11. It can be found that activation and ohmic overpotentials are the two main contributions of the total cell voltage besides the OCV. Both the LGDL pore sizes and porosities have important impacts on PEMEC overpotentials. The effects of pore diameter and porosity can be observed from Table 11.

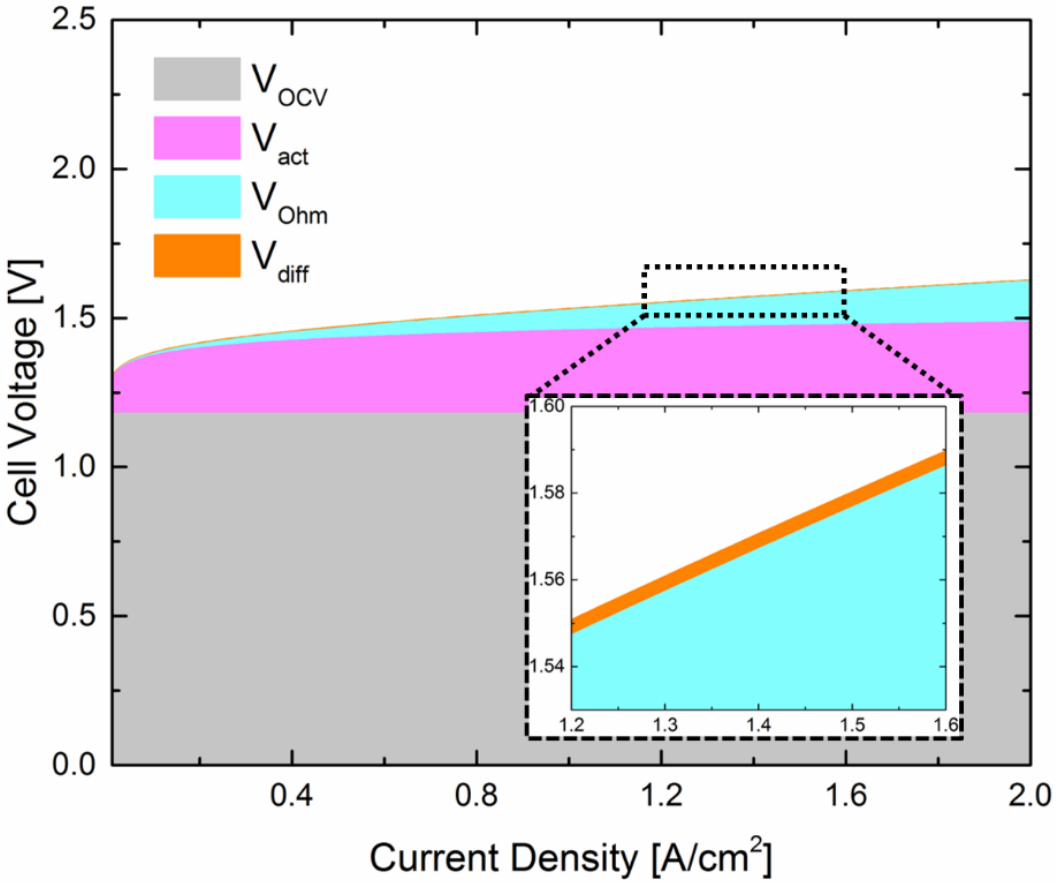

Figure 47. Contributions of each overpotential to polarization curve of the PEMECs with TT-LGDLs.

Table 10. Relationship between resistance and anode LGDL with different pore diameters and porosities at 80ºC.

Pore Diameter [µm]	Porosity	Total Resistance [mΩ]	TT-LGDL Resistance [mΩ]	CL Resistance [mΩ]	PEM Resistance [mΩ]	Interfacial contact Resistance [mΩ]
50	0.1	15.17	0.000024	0.01802	11.49	1.497
50	0.3	14.66	0.000031	0.00624	11.49	1.002
50	0.5	14.46	0.000043	0.00389	11.49	0.8012
50	0.7	14.18	0.000072	0.00288	11.49	0.5225
50	0.9	13.73	0.000216	0.00231	11.49	0.0778

Table 11. Overpotential of PEMECs with different pore morphologies at 2.0 A/cm^2 and 80 ºC.

Pore Diameter [μm]	Porosity	Total Cell Voltage [V]	OCV [V]	Activation Overpotential [V]	Ohmic Overpotential [V]	Diffusion Overpotential [V]
50	0.1	1.7427	1.1794	0.3899	0.1517	0.0218
	0.3	1.6772	1.1794	0.3480	0.1466	0.0032
	0.5	1.6559	1.1794	0.3286	0.1446	0.0034
	0.7	1.6403	1.1794	0.3158	0.1418	0.0034
	0.9	1.6264	1.1794	0.3062	0.1373	0.0034
100	0.1	1.7549	1.1794	0.3949	0.1584	0.0222
	0.3	1.6850	1.1794	0.3533	0.1491	0.0032
	0.5	1.6627	1.1794	0.3338	0.1461	0.0034
	0.7	1.6467	1.1794	0.3210	0.1429	0.0034
	0.9	1.6325	1.1794	0.3115	0.1382	0.0034
200	0.1	1.7762	1.1794	0.4001	0.1745	0.0222
	0.3	1.6946	1.1794	0.3583	0.1537	0.0032
	0.5	1.6702	1.1794	0.3389	0.1486	0.0034
	0.7	1.6533	1.1794	0.3261	0.1444	0.0034
	0.9	1.6395	1.1794	0.3167	0.1400	0.0034

For the TT-LGDLs with same 50 μm pore diameter but different porosities, the activation and ohmic overpotential will decrease about 83.7 mV and 14.4 mV, respectively, when the porosity is increased from 0.1 to 0.9. For the other pore diameter TT-LGDLs, the similar trend can be obtained. When the porosity is kept the same at 0.9, the activation and ohmic overpotential will increase about 10.5 mV and 2.7 mV, respectively, when the pore diameter increased from 50 μm to 200 μm. The results showed that the activation overpotentials have more contribution for the performance improvement than ohmic overpotentials and the diffusion overpotentials are very small under the present conditions.

7.4.3 Effects of temperature

For the present comprehensive model, it can be found that the OCV, activation overpotential, membrane conductivity, etc. are closely related to the operation temperature. This model has been effectively validated to calculate the polarization curve under different temperatures and it has been seen that the performance of the PEMECs is greatly influenced by the temperature. Therefore, the temperature effects are investigated under a wide range with the 50 μm pore diameter and varied porosity TT-LGDLs and the modeling results are shown in Figure 48.

It has been found that OCV occupies a large portion of the cell voltage from Fig.8, and its relation with temperature is shown in Table 12. OCV decreases gradually with the temperature increasing, which will help to obtain a lower cell voltage at higher temperature. For the ohmic overpotential, the largest ohmic resistance is from the PEM, and it will decrease significantly with the increase of temperature, as shown in Table 12.

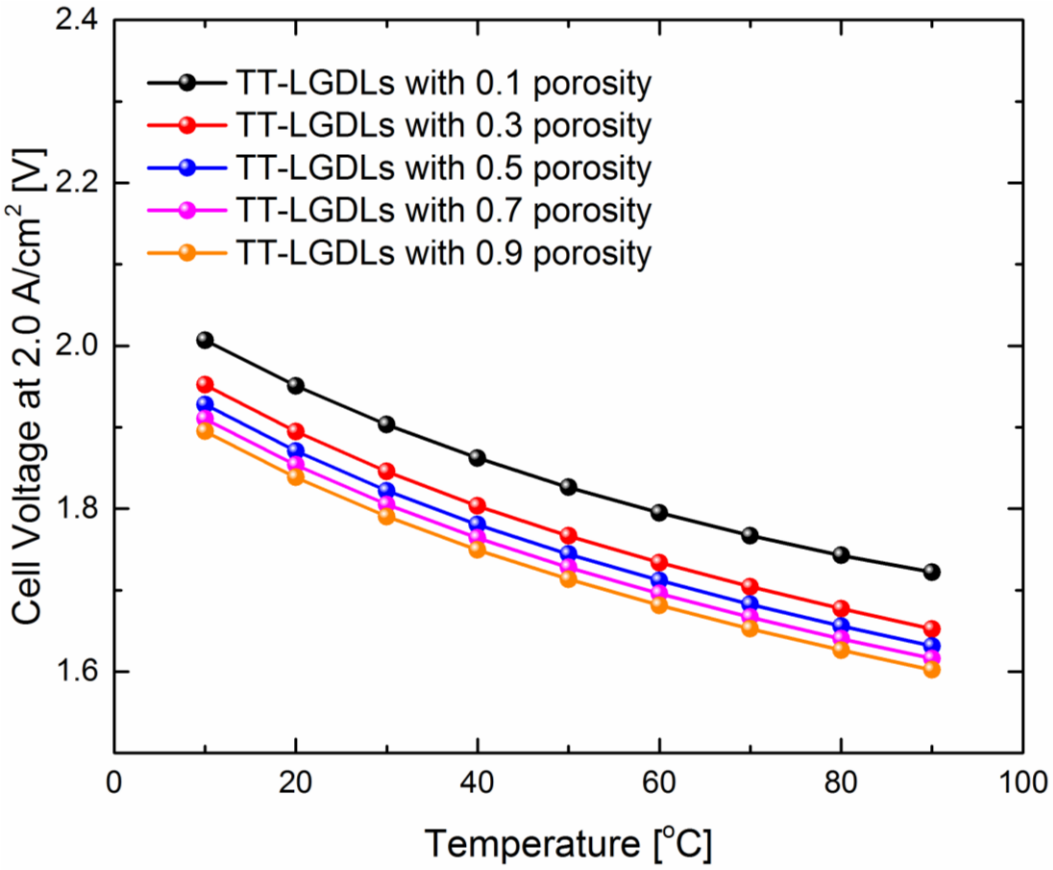

Figure 48. Cell voltage of the PEMECs with a pore diameter of 50 µm TT-LGDLs under different temperatures at a current density of 2.0 A/cm^2.

When the temperature increases from 10 to 90 ^{o}C, the OCV has a decrease of 72 mV, and the ohmic overpotential has a decrease of 175.1 mV due to the PEM. The activation and diffusion overpotential also has a closely relation with temperature, which will also impact the cell voltage of the PEMECs. Base on the calculation, it can be seen that the cell voltage will be reduced significantly with the increasing temperature and its effects are higher than TT-LGDL porosity. The results of the cell voltage confirm that the performance of PEMECs with TT-LGDLs could be improved by using larger porosity and applying higher temperature.

7.4.4 Current mapping

For the validation of the CL resistance model, the previous *in-situ* visualization results were used [18, 34]. The rapid microbubble dynamics, including its nucleation, growth and detachment, can be observed clearly. Even under the current density of 2.0 A/cm^2, the bubble detaches rapidly within the pore in a few milliseconds, and its detachment diameter is much smaller than the pore sizes. In our previous study, the bubble nucleation sites have been verified to be same at electrochemical reaction sites [39]. Therefore, all bubbles nucleate along the rim of each pore, which also indicate the electrochemical reactions only occur at the triple-phase boundary (TPB) sites achieved at the rim zone of the pore. The CL sites that don't satisfy TPB conditions will not have electrochemical reaction, and the bubble will not nucleate and grow [39]. The large in-plane ohmic losses in catalyst layers prevent the electrochemical reactions from occurring in the middle region of pores and act as an open circuit [34].

Table 12. OCV and PEM resistance under different temperatures.

Temperature (°C)	OCV (V)	PEM Resistance (mΩ)
10	1.2424	27.92
20	1.2334	23.96
30	1.2244	20.78
40	1.2154	18.18
50	1.2064	16.04
60	1.1974	14.26
70	1.1884	12.76
80	1.1794	11.49
90	1.1704	10.41

Based on the modeling of the CL in-plane and through-plane electrical resistances, the current distribution along the radius direction can be obtained and the results are shown in Figure 49. The TT-LGDLs with a pore diameter of 50 μm and a porosity of 0.9 is chosen to map the current distribution.

From the Figure 49(a), it can be found that the current will drop to less than 1% of current flow into this pore when the distance from the rim of the pore is over 3 μm, which implies that 99% of the in-plane current flow within a narrow torus at the rim area of the pore due to the large CL in-plane electrical resistivity. This phenomenon is confirmed by the *in-situ* visualization of oxygen bubble generation in PEMECs from our previous researches [18, 34] and can explain why there is no electrochemical reaction at the middle of the pore. Therefore, it can be concluded that the utilization of the catalyst is highly controlled by electron transport within the CLs. It is expected that the utilization of catalyst can be improved by reducing the CL in-plane electrical resistivity and the results are also shown in Figure 49. It can be found that the current will go through the CLs within a wider torus, and the current will occupy larger area of the pore with the decreasing CL in-plane electrical resistivity. The current will distribute more uniformly when the CL in-plane electrical resistivity is reduced, as shown in Figure 49(e). The CL in-plane electrical resistivity is about $1.52*10^{-2}$ Ω*m, and the measured sheet resistance is about 1011.85 Ω/□ . For the TT-LGDLs, the resistivity is $5.4*10^{-7}$ Ω*m and the calculated sheet resistance is about 0.0213 Ω/□ , which is much smaller than anode CL. It can be found that the present CL in-plane electrical resistivity is over 10,000 times than the electrical

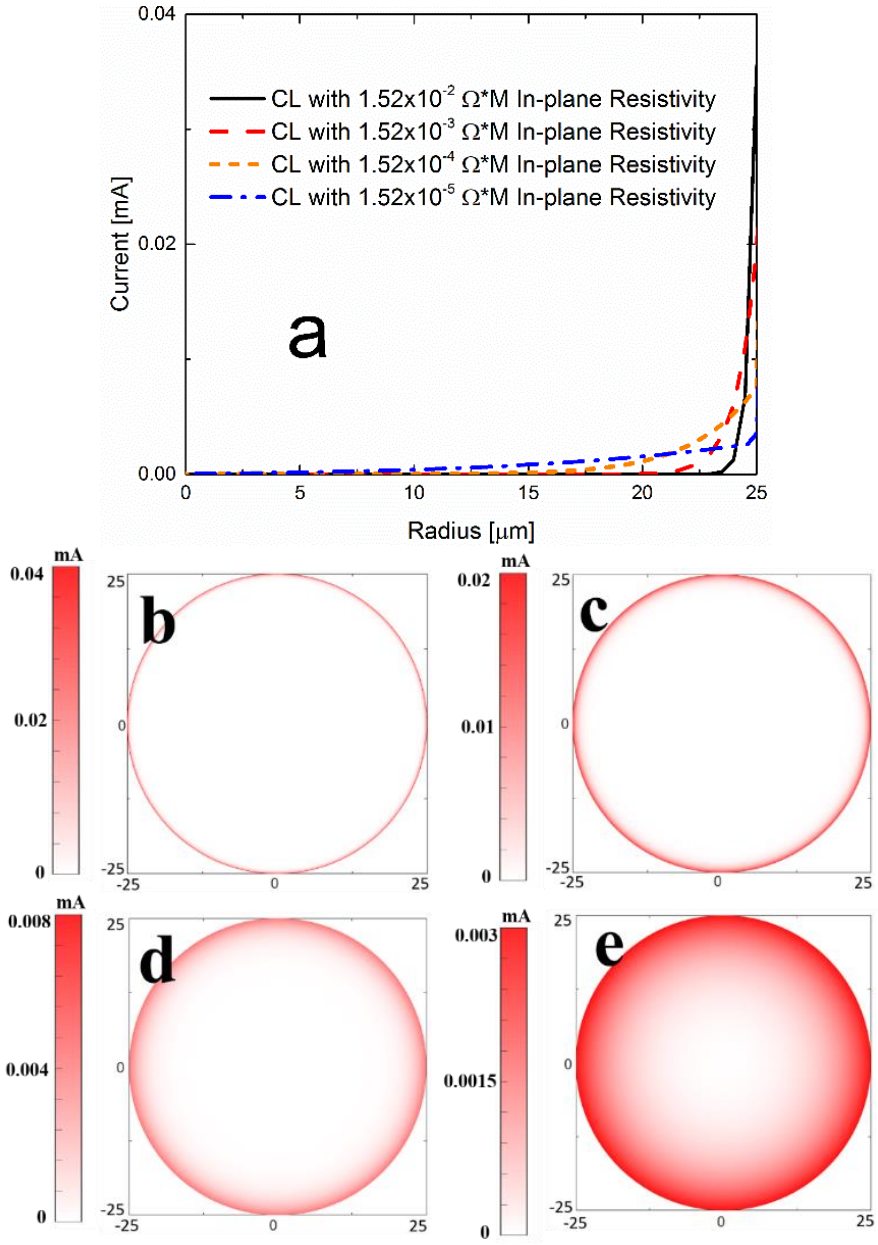

Figure 49. Current mapping of the anode CLs in one pore area of TT-LGDLs (50 μm pore diameter and 0.9 porosity) under 80 °C and 2.0 A/cm². (a) Current distribution from the center to the rim of the pore with different CL in-plane resistivities. (b) Current mapping with 1.52*10^{-2} Ω*m CL in-plane resistivity. (c) Current mapping with 1.52*10^{-3} Ω*m CL in-plane resistivity. (d) Current mapping with 1.52*10^{-4} Ω*m CL in-plane resistivity. (e) Current mapping with 1.52*10^{-5} Ω*m CL in-plane resistivity.

resistivity of TT-LGDLs. The pore diameter and porosity of the TT-LGDLs have great effects on PEMEC performance due to the electrochemical reaction mainly occurred at the rim of the pores and a large part of the CLs is not active. If the CL in-plane electrical resistivity is improved, it can be seen that the catalyst located at the middle of the pore will be activated, and the catalyst utilization rate will be greatly improved. The results of the current mapping clearly introduce a new direction of CL design and fabrication, which can greatly increase the catalyst utilization rate by preparing the CLs with smaller in-plane electrical resistivity.

7.5 Conclusions

In this study, a comprehensive PEMEC model for simulating the interfacial contact resistance, CL current distribution, and electrochemical performance coupled with thin/tunable liquid/gas diffusion layers (TT-LGDLs) at anode is developed and validated. This model takes advantage of the highly controlled pore morphology of TT-LGDLs and precisely simulate the effects of TT-LGDL pore diameter and porosity on resistances and overpotentials in PEMECs. The results exhibit that with a larger porosity and/or smaller pore diameter of TT-LGDLs, both CL in-plane resistances and CL/LGDL interfacial contact resistances will be reduced, and a better PEMEC performance will be obtained. In addition, a small pore diameter and/or a large porosity will lead to greater roughness factors, thus resulting in smaller activation overpotential. The temperature also has a great impact on PEMEC performance, especially on the OCV, ohmic resistance, and activation overpotential. The voltage of the PEMECs will increase significantly with the decreasing

of temperature, and the better performance will be achieved under higher temperature. More importantly, the present comprehensive model can be used to calculate the current distribution on the CL surface, which is confirmed and validated by previous experimental visualization results. The utilization of the catalyst and electrochemical reaction are highly controlled by in-plane electron conductivities within the CLs. The current mainly flow through the rim with narrow width of the pores and the catalyst in the middle of the pores is inactive, which will decrease the catalyst utilization, due to the large CL in-plane electrical resistivity of the conventional catalyst-coated membrane. It can be concluded that the catalyst utilization can be improved by reducing the pore diameter, increasing porosity, or reducing the CL in-plane electrical resistivity, which provide a new insight and direction for TT-LGDL and CL design and fabrication.

References

[1] Ito H, Maeda T, Nakano A, Kato A, Yoshida T. Influence of pore structural properties of current collectors on the performance of proton exchange membrane electrolyzer. *Electrochim Acta*. 2013;100:242-8.

[2] Turner JA. A realizable renewable energy future. *Science*. 1999;285:687-9.

[3] Song G-H, Meng H. Numerical modeling and simulation of PEM fuel cells: Progress and perspective. *Acta Mechanica Sinica*. 2013;29:318-34.

[4] Meng H. Numerical studies of liquid water behaviors in PEM fuel cell cathode considering transport across different porous layers. *Int J Hydrogen Energ*. 2010;35:5569-79.

[5] Jia F, Guo L, Liu H. Dynamic characteristics and mitigations of hydrogen starvations in proton exchange membrane fuel cells during start-ups. *Int J Hydrogen Energ*. 2014;39:12835-41.

[6] Wang Y, Chen KS, Mishler J, Cho SC, Adroher XC. A review of polymer electrolyte membrane fuel cells: technology, applications, and needs on fundamental research. *Appl Energ*. 2011;88:981-1007.

[7] Kotaka T, Tabuchi Y, Pasaogullari U, Wang C-Y. Impact of interfacial water transport in PEMFCs on cell performance. *Electrochim Acta*. 2014;146:618-29.

[8] Steen III SM, Mo J, Kang Z, Yang G, Zhang F-Y. Investigation of Titanium Liquid/Gas Diffusion Layers in Proton Exchange Membrane Electrolyzer Cells. *International Journal of Green Energy*. 2016;14:162-70.

[9] Mo J, Steen S, Han B, Kang Z, Terekhov A, Zhang F-Y, Retterer ST, Cullen DA. Investigation of titanium felt transport parameters for energy storage and hydrogen/oxygen production. 13th International Energy Conversion Engineering Conference2015. p. 3914.

[10] Trincado M, Banerjee D, Grützmacher H. Molecular catalysts for hydrogen production from alcohols. *Energ Environ Sci*. 2014;7:2464-503.

[11] Kang Z, Mo J, Yang G, Li Y, Zhang F-Y, Retterer ST, Cullen DA. Investigation of Novel Thin LGDLs for High-Efficiency Hydrogen/Oxygen Generation and Energy Storage. 15th International Energy Conversion Engineering Conference2017. p. 4873.

[12] Spurgeon JM, Lewis NS. Proton exchange membrane electrolysis sustained by water vapor. *Energ Environ Sci*. 2011;4:2993-8.

[13] Matar S, Liu H. Effect of cathode catalyst layer thickness on methanol cross-over in a DMFC. *Electrochim Acta*. 2010;56:600-6.

[14] Wang Z, Huang H, Liu H, Zhou X. Self-sustained electrochemical promotion catalysts for partial oxidation reforming of heavy hydrocarbons. *Int J Hydrogen Energ*. 2012;37:17928-35.

[15] Yang G, Mo J, Kang Z, List FA, Green JB, Babu SS, Zhang F-Y. Additive manufactured bipolar plate for high-efficiency hydrogen production in proton exchange membrane electrolyzer cells. *Int J Hydrogen Energ*. 2017;42:14734-40.

[16] Kang Z, Mo J, Yang G, Li Y, Talley DA, Retterer ST, Cullen DA, Toops TJ, Brady MP, Bender G, Pivovar BS, Green Jr JB, Zhang F-Y. Thin film surface modifications of thin/tunable liquid/gas diffusion layers for high-efficiency proton exchange membrane electrolyzer cells. *Appl Energ*. 2017;206:983-90.

[17] Mishler J, Wang Y, Mukundan R, Spendelow J, Hussey DS, Jacobson DL, Borup RL. Probing the water content in polymer electrolyte fuel cells using neutron radiography. *Electrochim Acta*. 2012;75:1-10.

[18] Mo J, Kang Z, Yang G, Li Y, Retterer ST, Cullen DA, Toops TJ, Bender G, Pivovar B, Green J. In-situ investigation on ultrafast oxygen evolution reactions of water splitting in proton exchange membrane electrolyzer cells. *J Mater Chem A*. 2017;5:18469-75.

[19] Choi P, Bessarabov DG, Datta R. A simple model for solid polymer electrolyte (SPE) water electrolysis. *Solid State Ionics*. 2004;175:535-9.

[20] Görgün H. Dynamic modelling of a proton exchange membrane (PEM) electrolyzer. *Int J Hydrogen Energ*. 2006;31:29-38.

[21] Abdin Z, Webb C, Gray EM. Modelling and simulation of a proton exchange membrane (PEM) electrolyser cell. *Int J Hydrogen Energ*. 2015;40:13243-57.

[22] Grigoriev S, Kalinnikov A, Millet P, Porembsky V, Fateev V. Mathematical modeling of high-pressure PEM water electrolysis. *J Appl Electrochem*. 2010;40:921-32.

[23] Grigoriev S, Millet P, Volobuev S, Fateev V. Optimization of porous current collectors for PEM water electrolysers. *Int J Hydrogen Energ*. 2009;34:4968-73.

[24] Marangio F, Santarelli M, Cali M. Theoretical model and experimental analysis of a high pressure PEM water electrolyser for hydrogen production. *Int J Hydrogen Energ*. 2009;34:1143-58.

[25] Schwarz DH, Djilali N. 3D Modeling of Catalyst Layers in PEM Fuel Cells Effects of Transport Limitations. *J Electrochem Soc*. 2007;154:B1167-B78.

[26] Han B, Steen S, Mo J, Zhang F. Modeling of interfacial resistance effects on the performance and efficiency for electrolyzer energy storage. 13th International Energy Conversion Engineering Conference2015. p. 3915.

[27] Han B, Steen SM, Mo J, Zhang F-Y. Electrochemical performance modeling of a proton exchange membrane electrolyzer cell for hydrogen energy. *Int J Hydrogen Energ*. 2015;40:7006-16.

[28] Han B, Ni M, Meng H. Three-dimensional lattice boltzmann simulation of liquid water transport in porous layer of PEMFC. *Entropy*. 2015;18:17.

[29] Adroher XC, Wang Y. Ex situ and modeling study of two-phase flow in a single channel of polymer electrolyte membrane fuel cells. *J Power Sources*. 2011;196:9544-51.

[30] Han B, Mo J, Kang Z, Zhang F-Y. Effects of membrane electrode assembly properties on two-phase transport and performance in proton exchange membrane electrolyzer cells. *Electrochim Acta*. 2016;188:317-26.

[31] Han B, Mo J, Kang Z, Yang G, Barnhill W, Zhang F-Y. Modeling of two-phase transport in proton exchange membrane electrolyzer cells for hydrogen energy. *Int J Hydrogen Energ*. 2017;42:4478-89. doi: 10.1016/j.ijhydene.2016.12.103.

[32] Kang Z, Mo J, Yang G, Zhang F-Y, Reterer ST, Cullen DA. Micro/nano manufacturing of novel multifunctional layers for hydrogen production from water splitting. Nano/Micro Engineered and Molecular Systems (NEMS), 2017 IEEE 12th International Conference on: *IEEE*; 2017. p. 126-30.

[33] Mo J, Kang Z, Yang G, Retterer ST, Cullen DA, Toops TJ, Green JB, Zhang F-Y. Thin liquid/gas diffusion layers for high-efficiency hydrogen production from water splitting. *Appl Energ*. 2016;177:817-22.

[34] Kang Z, Mo J, Yang G, Retterer ST, Cullen DA, Toops TJ, Green Jr JB, Mench MM, Zhang F-Y. Investigation of thin/well-tunable liquid/gas diffusion layers exhibiting superior multifunctional performance in low-temperature electrolytic water splitting. *Energ Environ Sci*. 2017;10:166-75.

[35] Mo J, Steen SM, Retterer S, Cullen DA, Terekhov A, Zhang F-Y. Mask-Patterned Wet Etching of Thin Titanium Liquid/Gas Diffusion Layers for a PEMEC. *Ecs Transactions*. 2015;66:3-10.

[36] Carmo M, Fritz DL, Mergel J, Stolten D. A comprehensive review on PEM water electrolysis. *Int J Hydrogen Energ*. 2013;38:4901-34.

[37] Berning T, Lu DM, Djilali N. Three-dimensional computational analysis of transport phenomena in a PEM fuel cell. *J Power Sources*. 2002;106:284-94.

[38] Singh D, Lu D, Djilali N. A two-dimensional analysis of mass transport in proton exchange membrane fuel cells. *International Journal of Engineering Science*. 1999;37:431-52.

[39] Mo J, Kang Z, Retterer ST, Cullen DA, Toops TJ, Green JB, Mench MM, Zhang F-Y. Discovery of true electrochemical reactions for ultrahigh catalyst mass activity in water splitting. *Science Advances*. 2016;2:e1600690.

[40] KANG Z-y, LIU Z-x, REN G-z, LV Y-g. Simulation and Calculation of Fuel Temperature in Aircraft Fuel Tank Based on MATLAB/Simulink. *Journal of Propulsion Technology*. 2014;1:010.

[41] Mench MM. Fuel Cell Engines: *John Wiley & Sons*; 2008.

[42] Poco Graphite I. http://poco.com/MaterialsandServices/Graphite/IndustrialGrades/AXF5Q.aspx. 2017.

[43] Ojong ET, Kwan JTH, Nouri-Khorasani A, Bonakdarpour A, Wilkinson DP, Smolinka T. Development of an experimentally validated semi-empirical fully-coupled performance model of a PEM electrolysis cell with a 3-D structured porous transport layer. *Int J Hydrogen Energ*. 2017. DOI: 10.1016/j.ijhydene.2017.08.183.

Appendix

List of symbols

A	Reaction area, cm^2
a_0	Empirical coefficient to estimate the interfacial saturation
$a_{\mathrm{r,an}}$	Roughness factor of anode in Bulter-Volmer equation
$a_{\mathrm{r,cat}}$	Roughness factor of cathode in Bulter-Volmer equation
$C_{O_2,m}$	Oxygen concentration at the interface of electrode and membrane, mol/cm^3
$C_{H_2,m}$	Hydrogen concentration at the interface of electrode and membrane, mol/cm^3
D	The pore diameter of the TT-LGDLs, μm
d_0	Dimensionless relative pore diameter
i	Current density, A/cm^2
i_0	Exchange current density, A/cm^2
k	Permeability, m^2
N	The total number of pores in the TT-LGDLs
p	Pressure, atm
R_{in}	Interfacial contact resistance, Ω
R_{ip_m}	In-plane resistance of the CLs at the *m* torus, Ω
R_{tp_m}	Through-plane resistance of the CLs at the *m* torus, Ω
R_{LGDL}	LGDL resistance, Ω

R_{PEM}	PEM resistance, Ω
R_{BP}	Bipolar plate resistance, Ω
S	The number of total reaction sites
s	Liquid saturation
t	Time, s
T	Temperature, K
V	Voltage or overpotential, V
V_0	Reversible voltage, V
z	Mole number of electrons

Greek

α_a	Anode charge transfer coefficient
α_c	Cathode charge transfer coefficient
ε	Porosity
ε_0	Dimensionless relative porosity
θ	Contact angle of TT-LGDLs, degree (°)
μ	Fluid dynamic viscosity, N s/cm^2
ρ	Resistivity, Ω cm or Fluid density, kg/cm^3
σ	Surface tension, N/cm
σ_m	PEM conductivity, S/cm
δ_m	PEM thickness, micron (μm)
λ	PEM humidification degree

Constants

ρ_{H_2O}	Water density, 1.0 g/cm^3
μ_{H_2O}	Water dynamic viscosity, 3.5×10^{-7} N S/cm^2
F	Faraday constant, 96485.0 C/mol
K	K coefficient, 1.4×10^{-2} Ω
M_{H_2}	Hydrogen molar mass, 2.0 g/mol
M_{H_2O}	Water molar mass, 18.0 g/mol
M_{O_2}	Oxygen molar mass, 32.0 g/mol
R	Gas constant, 8.314 J/mol K

CHAPTER VIII

CONCLUSIONS AND SUGGESTIONS FOR FUTURE WORKS

In this research, a set of thin titanium LGDLs with well-tunable pore morphologies have been developed to promote PEMEC performance, and to precisely investigate the impacts of the LGDL pore size, porosity and pore shape. The TT-LGDLs exhibit exceptional performance: at a current density of 2.0 A/cm^2 with a porosity of 0.7 and a pore size of 400 μm, the required voltage reaches only 1.661 V. It has been revealed that the PEMEC has a better performance with a larger porosity under a fixed pore size. It also can be found that the PEMEC performance decreases gradually with the increase of pore size from 100 to 800 μm, but pore-size impacts are not significant compared to porosity. The effect of pore size and porosity explained by the electrochemical reaction mechanism is also introduced in this study. Larger porosity and smaller pore size can increase the reaction sites in the PEMEC which could help to decrease the total ohmic losses and activation loss which are two dominant factors of PEMEC performance. The superior performance (1.639 V at 2.0 A/cm^2 and 80 ^{o}C) has been achieved by a square TT-LGDLs with 418 μm pore size and 0.70 porosity, which is the lowest value that has been publicly reported so far. In addition, it has been found that the square is the best and the circular is the worst pore shape among the three different designs. The TT-LGDLs with square pore shape can achieve better PEMEC performance than triangle and circular TT-LGDLs with a similar pore morphology. Due to the thin features of the novel TT-LGDLs, not only the thickness/volume/weight of the PEMEC stack can be reduced greatly, but also the materials

used for LGDLs can be decreased which helps to reduce the cost. Since all the TT-LGDLs in this study have a better performance than the conventional LGDLs, such as titanium felt and woven mesh, they are expected to have many potential applications in energy and environmental engineering.

However, resistance to corrosion in such systems is achieved by surface oxide formation, which can increase surface electrical resistivity and detrimentally impact cell performance. In this research, different gold surface treatment methods were applied to TT-LGDLs in order to gauge the potential to improve the PEMEC performance. By applying a 180 nm thick Au thin film on the titanium based TT-LGDLs, the PEMEC voltage can be decreased from 1.6849 V to 1.6328 V at 2.0 A/cm^2 and 80 °C. More importantly, the hydrogen/oxygen production rate can be greatly increased by 28.2% at 1.60 V and 80 °C compared to untreated TT-LGDLs, which will greatly save the feedstock cost and energy. Furthermore, the 100 hour short term stability test of the surface treated TT-LGDLs showed no obvious degradation, which demonstrated that the electroplated Au thin film has a good stability. The superior performance achieved by the TT-LGDLs with surface treatments makes them a promising component in the PEMECs and helps to industrialize PEMECs, which provide a route to improve efficiency of hydrogen/oxygen production from water splitting. The results obtained have also demonstrated the advantages of the gold electroplating as a simple and reliable method for TT-LGDL surface treatments for enhancing the PEMEC application and titanium material protection.

The ultrafast and multiscale HER and hydrogen bubble dynamic phenomena in an operating PEMEC was also *in-situ* observed for the first time in this study. Based on the visualization results, the novel thin GDE was introduced and characterized. This work introduces a novel thin GDE formed by the deposition of platinum directly onto TT-LGDLs. These novel TT-LGDLs have been shown to deliver superior performance in PEMECs over conventional CCMs. The impact of Pt loading on thin film morphology was examined by SEM and STEM. The performance of different loadings was *in-situ* investigated in a PEMEC and the results were compared to those performed in CCMs. Although the performance of the deposited GDE was not better than conventional CCM, the GDE achieved satisfactory performance with much higher mass activity, most importantly with the significantly reduced platinum catalyst loadings by removing the inactive catalyst in the middle of the pore area, which provide a direction of future CL design and fabrication. It is likely that by decreasing the resistance of the novel thin GDEs, the mass activity and performance of the PEMEC can be further improved, which will be a promising method of novel GDE fabrication.

The well-tunable pore morphologies are extremely valuable to advance numerical modeling of electrochemical reactions and associated multiphase flow as well. This research for the first time presents a comprehensive computational model for the PEMECs with TT-LGDLs, which have attracted more attention for renewable energy storage and hydrogen production. A new ohmic loss model for PEMECs has been developed and the influence of operating conditions and physical design parameters on its performance has

also been investigated. The interfacial contact resistances between the CLs and LGDLs have been found to play an important role in electrolyzer performance, and the present mathematical model can precisely simulate and calculate the contact resistance. Furthermore, the roughness factor in the Butler-Volmer equation, which is used to calculate the activation overpotential, can greatly influence the PEMEC performance by pore morphology of the TT-LGDLs, and its relation has been embedded in the comprehensive computational model. More importantly, a novel two-dimensional (2D) CL resistance model, which consists of both in-plane and through-plane resistance models, is also developed to predict the current distribution on the CLs. The present model can precisely match the experimental results and effectively calculate the PEMEC performance with different TT-LGDL morphologies and operating temperatures. It is obviously that the large porosity and small pore size TT-LGDLs have better PEMEC performance, which agrees with the experimental results. The pore size and porosity of the TT-LGDLs have great effects on PEMEC performance due to the electrochemical reaction mainly occurred at the rim of the pores and a large part of the CLs is not active. If the CL in-plane electrical resistivity is improved, it can be seen that more catalyst located at the middle of the pore will be activated, and the catalyst utilization rate will be greatly improved. The results of the current mapping clearly introduce a new direction of CL design and fabrication, which can greatly increase the catalyst utilization rate by preparing the CLs with smaller in-plane electrical resistivity. Results obtained from the present model will provide a deep

understanding of the functions of TT-LGDL morphology, and also help to optimize the design and fabrication of both the TT-LGDLs and CLs.

It has been found that TT-LGDLs with smaller pore size and large porosity can help to enhance the PEMEC performance. But, by using the above mentioned technologies, it is impossible to fabricate the TT-LGDLs with pore size smaller than 100 μm and very large porosity. In the future, it is also very attractive to develop laser machined thin titanium-LGDLs (LMTT-LGDLs) with nano/micro pores by using advanced laser machining technology, which can fabricate pores with a size of less than 10 μm and a high porosity. In addition, the TT-LGDLs with smaller pore size can be made from dry-etching. These two methods can be investigated which will help to fully understand the effects of TT-LGDL parameters, and the improved performance is also expected with smaller pores.

Another novel thin dual layer TT-LGDLs (DTT-LGDLs) are also a promising component for PEMEC performance enhancement. This DTT_LGDLs can be designed with a thickness of 50 μm, and have a gradient pore size along its thickness, as shown in Figure 50. The upside of the DTT-LGDLs has the large pores and it is connected with BP, while the bottom has much smaller pores and connect to CL. Because the in-plane transport is not allowed in TT-LGDLs, lots of pores will be blocked by the land of the flow field on the BPs if the pore is fully covered by the BP land, and this effect can be significant especially when the pore size is much smaller than the land width. Here, the DTT-LGDLs are proposed and it can perfectly deal with this problem by introducing a gradient pore size. At the BP side, a large pore (with 150 to 400 μm pore size) can be manufactured by the

chemical wet-etching with about 25 μm thickness. Then, the bottom of the pore will be further fabricated with much smaller pores (with 10 to 50 μm pore size) by advanced micro/nano manufacturing methods, such as dry etching and laser machining. It is expected that much more active reaction sites will be available when applying the DTT-LGDLs, which is due to the smaller pore size on the CL surface and elimination of BP land blocked pores.

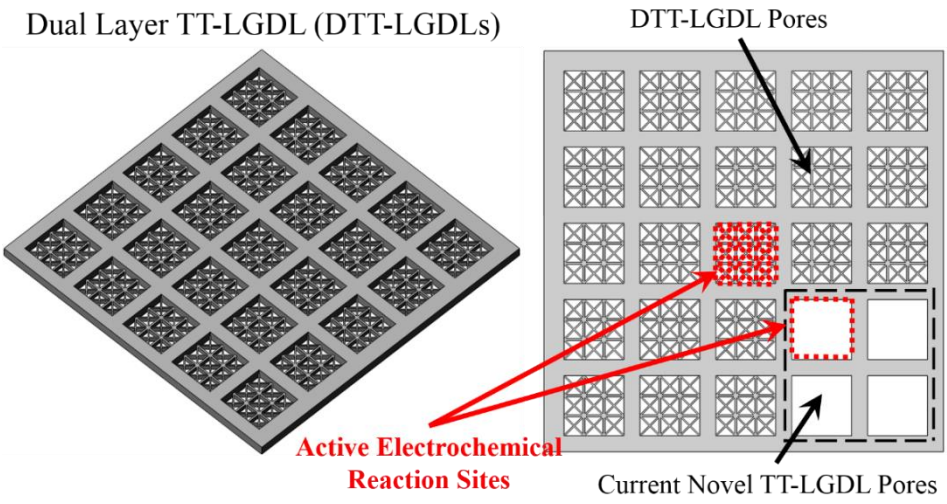

Figure 50. Schematic of the novel DTT-LGDLs.

More importantly, the idea of TT-LGDLs will lead to a manufacturing solution to combine the LGDL with the metallic bipolar plates, since they can be easily integrated together by top-down and bottom-up manufacturing process. For example, by utilizing the additive manufacturing (AM) methods, four conventional components (LGDL, BP, CD, and Gasket) in a PEMEC can be integrated into one multifunctional AM plate without

committing to tools or molds. In addition, since the interfacial contact resistances between those parts were eliminated, the PEMEC performance and efficiency are expected to be greatly improved.

The OER is the main source of irreversibility, and the anode electrocatalysts have much more effects on the overall PEMEC performance than the cathode. The novel thin GDEs as cathode electrode have achieved much higher catalyst mass activity and good performance, therefore, this method is also anticipated to be effective when applied at anode. In state-of-the-art technology, Ir oxide is generally used as anode catalyst with a typical loading of few mg/cm^2. The Ir can be deposited on TT-LGDLs by sputter coating or electroplating, and the deposited TT-LGDLs can work as anode GDEs. The Ir deposited GDEs are expected to achieve good performance and high catalyst mass activity. This is also a promising method for future GDE design and development.

The other proposed methods for CL fabrication including the spraying and 3D ink-jet printing. It has been found that the sputter deposited Pt thin film is an ionomer free CL, which leads to a large interfacial contact resistance between the CL and PEM. This research proposes to fabricate the CLs using the advanced 3D ink-jet printing method, which can print the CLs layer by layer with different patterns, desired catalyst loadings, thickness and ionomer content. The catalyst inks will be prepared by ethylene glycol, DI water, catalyst nano particles, and ionomer solution to reach a satisfied viscosity, concentration and etc. for 3D printing. It is expected that there will be more HER/OER sites occurred in the pore area than conventional CCM due to the desired CL patterns and improved in-plane

electrical conductivity of the CLs, which will lead to better performance than conventional CCM.

The work will lead to a new guide for future researches and developments towards high-efficiency and low-cost energy storage, which could help to make PEMECs widely applied in industry and let hydrogen goes into our daily life.

VITA

Zhenye Kang was born in Xianyang, Shaanxi, P. R. China. He graduated from Xianyang Caihong Middle School in 2007 and studied at Nanjing University of Aeronautics and Astronautics (NUAA) from 2007 to 2011 for the B. S. degree in major of Aircraft Power Engineering. He continued to study at Northwestern Polytechnical University (NPU) with exemption from the entry exam and got his M. S. degree in major of Propulsion Theory and Engineering of Aeronautics and Astronautics in April 2014. He also studied some Ph.D. courses during the study at NPU from 2013 to 2015, and attended or leaded several projects during that time under Dr. Zhenxia Liu's guidance. He began to pursue his Ph.D. at the University of Tennessee, Knoxville (UTK) since June 2015 in Mechanical Engineering under the supervision of Dr. Feng-Yuan Zhang.